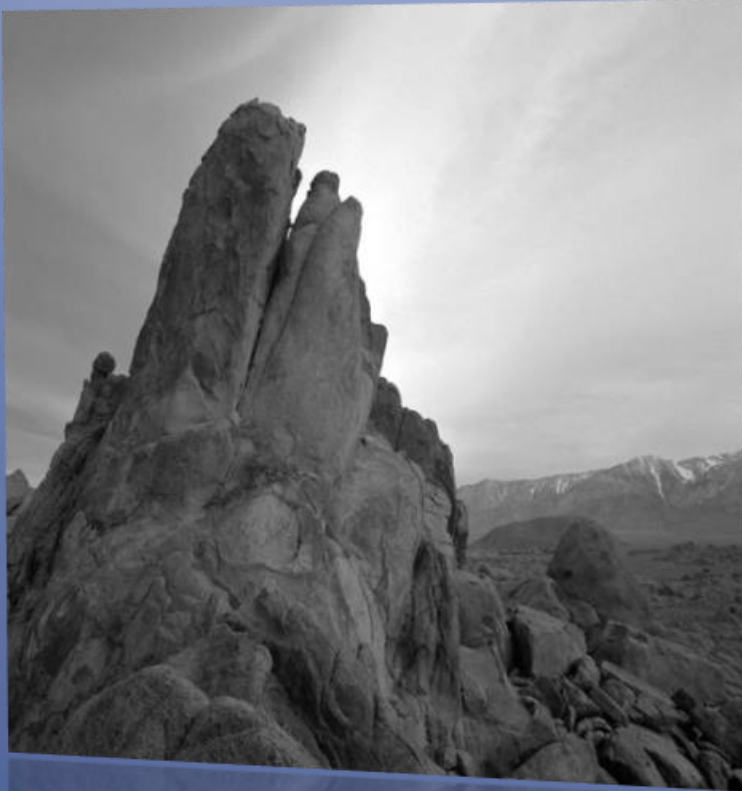




Utrecht University



Submitted to the
Faculty of Geosciences
Of
Utrecht University

In partial fulfillment of
the requirements for
the degree of
Master of
energy Science

Supervisor
Dr. C. A. Ramirez

Assessing the joint potential for CO₂-enhanced oil recovery and CO₂-plume geothermal energy production

Energy science thesis – Roland Vernooij

Acknowledgements

This thesis is the final the conclusion of the Natural Science track of the energy science master Program at the Copernicus Institute, Utrecht University. The text is original, unpublished independent work by the author, R. Vernooij.

This Master thesis would not have been possible without the support and guidance from my thesis supervisor, Dr. ir. Adrea Ramirez, throughout the course of research. I am indebted to her distinctive knowledge and ability to challenge me while providing the essential supervision to ensure the fruition of this research.

I would want to extend my gratitude to all the people working at Accenture for giving me a place to perform the research. Special thanks go out to my internship supervisors Michal Svoboda and Richard Bilby, their confidence in my ability to conduct this research has always inspired me to rise to the challenge. My sincere thanks also go out to Kris Welkenhuysen from the Royal Belgian Institute of Natural Sciences for his critical feedback, significant input, and mentorship during this journey. As well I would like to express my sincere appreciation to Aleks Athrens from Queensland University, Australia. His very bright and friendly advice helped me greatly with this research. Last but not least I would like to thank all my coworkers at Accenture for the many coffees and contributions to this report, most notably Juliette van Hessen and Liselotte Den Ouden.

Since the start of this research six months ago, I have spent countless hours struggling with the methodology to tackle the novelty of the challenge. This paper is the report of this long process. It cannot express the long days spent battling Matlab's unforgiving error messages, shoulder to shoulder with my fellow scientists and friends, the joy for the model to work, the hope for good results and the sadness and tiredness with each failed attempt. Although I am looking forward to a holiday, I might miss waking up to the lovely voice of Rick Astley every night, who was summoned by Matlab to inform me that the it had ended its run (bottom Appendix I). All in all, I feel like I have learned a great deal from writing this thesis, and it has inspired me to further develop myself in this field.

Roland Vernooij

30 April, 2015

Abstract

Many currently producing oil fields are depleting in the near future, leading to abandonment. In the meantime, the demand for oil is still projected to rise. Oil companies are searching for new ways to produce more oil from existing fields. To achieve the 2050 climate goals, the IEA allocates 14 percent of the projected global emission abatements to CCS, making it a potentially huge market in the near future. Using CO₂ as a working fluid, geothermal energy extraction from medium temperature, naturally porous reservoirs becomes feasible while CO₂ is stored in the formation. Mature CO₂-EOR fields may be transformed into efficient CPG fields in a mutually beneficial way, leading to extended EOR time and reduced start-up time for CPG energy production. If this transition is viable, oil reservoirs could be transformed to CPG reservoirs that store CO₂ and produce sustainable energy and heat while making smart use of energy market fluctuations.

This research focusses on the technical feasibility of the transition from CO₂-EOR to CPG and the parameters that affect the reservoir suitability for both technologies. The parameters that affect both techniques are discussed from literature and an uncertainty analysis was performed for the most relevant parameters. The most important benefits and pitfalls were discussed for three different configurations in which CO₂-EOR and CPG might be combined. Based on the literature research, parameters were chosen for a fictional reservoir where both miscible CO₂-EOR and CPG would be technically feasible. A model was created in Matlab to calculate the potential of both technologies in a case reservoir, and calculate the costs of the entire operation.

The same reservoirs that can be used for CO₂-enhanced oil recovery could be used for CO₂-plume geothermal. For deeper and hotter reservoirs, enough pressure difference can be generated to successfully operate a direct supercritical CO₂ turbine. Based on the model, assuming a closed system with minimal mixing in the reservoir, a 99% dry stream of supercritical CO₂ can be achieved in a relatively short period of time. Additional research is required on the effect of the presence of heavy oil fractions on CPG operation in a reservoir. The power generated by a CPG system was found to maximize at low depths or depths of 4 – 4.5 km. For the reference case, an injection rate of 140 kg s⁻¹ was found to have the best performance. At higher flow rates, the additional friction in the wellbore will reduce the efficiency of the system. Due to the high mobility of supercritical CO₂ these injection rates would not lead to high pressure drops (<10MPa), as long as there is single phase flow, even at very low permeability (10⁻¹⁵ m²). However, if the multi-phase flow is taken into account, injection rates, may have to be reduced.

The transition from miscible CO₂-EOR to CPG appears to be feasible for a range of reservoir parameters. Although without the use of the heat the electricity price is not competitive with large scale electricity generation methods, additional power produced from the heat and income generated from storing CO₂, may make the technology economically viable. In the future, if taxation on CO₂ emissions become more rigorous, this technology provides a cost effective way of storing CO₂.

Table of Contents

Acknowledgements	i
Abstract	ii
<i>List of figures</i>	v
<i>List of tables</i>	vi
1. Introduction.....	- 7 -
Road to sustainability	- 8 -
Aim and research question	- 8 -
Research question:	- 9 -
2. Theoretical Background.....	- 10 -
2.1 properties of CO ₂	- 10 -
2.2 CO ₂ -enhanced oil recovery.....	- 12 -
2.3 CO ₂ enhanced geothermal energy production (CO ₂ -EGS).....	- 17 -
2.4 CO ₂ -storage in porous reservoirs	- 25 -
3. Parameter and configuration assessment (Part I &II)	- 30 -
3.1 Parameter analysis	- 30 -
3.2 Correlation.....	- 30 -
3.3 Reservoir criteria for CO ₂ -EOR.....	- 31 -
3.4 Reservoir criteria for CPG	- 36 -
3.5 CO ₂ -plume geothermal enhanced oil recovery (CPG-EOR)	- 41 -
4. Modeling in Matlab.....	- 45 -
4.1 Site selection	- 45 -
4.2 Modelling assumptions	- 46 -
4.3 The CO ₂ -EOR phase	- 47 -
4.4 Drying time to start CPG operation.....	- 50 -
4.5 CO ₂ -plume geothermal energy recovery.....	- 54 -
4.6 Economic analysis of the CPG-EOR system	- 58 -
5. Modelling results.....	- 64 -
5.1 CO ₂ -EOR.....	- 64 -
5.2 Drying the reservoir.....	- 67 -
5.3 CO ₂ -plume geothermal.....	- 71 -
5.4 Costs analysis.....	76
5.5 Technical sensitivity analysis.....	81
5.6 Sensitivity analysis for the costs.....	83

6. Discussion	84
6.1 limitations of the model	84
6.2 Comparison with literature	85
6.3 Knowledge gaps.....	88
7. Conclusion	89
8 Future research	93
8.1 3D-Modelling for the drying and EOR	93
8.2 CPG-EGR	93
8.3 The effect of viscosity enhancers and WAG-Operation on CPG	93
8.4 The effect of economic and policy parameters.....	94
8.5 Reactive transport modelling	94
8.6 The option of skipping secondary oil recovery.....	94
<i>Nomenclature</i>	95
Bibliography.....	- 96 -
Appendix I: main Matlab script	- 108 -
Appendix II: CO ₂ -calibration	- 117 -
Appendix III: CO ₂ (thermodynamics).....	- 117 -
Appendix IV: reservoir miscibility.....	- 119 -
Appendix V: CO ₂ -EOR	- 120 -
Appendix VI: Capital costs EOR.....	- 122 -
Appendix VII: Drying.....	- 123 -
Appendix VIII: Downhole (injection well).....	- 124 -
Appendix IX: reservoir flow	- 125 -
Appendix X: CO ₂ viscosity	- 127 -
Appendix XI: Uphole (production well)	- 128 -
Appendix XII: CO ₂ turbine.....	- 129 -
Appendix XIII: Hemholz free energy CO ₂ Equation of state	- 130 -
Appendix XIV: Capital costs of the CPG system.....	- 134 -
Appendix XV: LCE CO ₂ plume geothermal.....	- 135 -
Appendix XVI: LCE CO ₂ -EOR.....	- 136 -
Appendix XVII: Injectivity reduction through salt precipitation.....	- 136 -
Appendix XIX: Properties of CO ₂	- 137 -

List of figures

Figure 2.3: schematic view of a CO ₂ -EOR operation using antropogenic CO ₂ [6].	Pg. 10
Figure 2.4: contact angle in brine-supercritical CO ₂ systems [134].	Pg. 10
Figure 2.5: positioning of the oil and brine phases in the pore space [27].	Pg. 11
Figure 2.6: Potential for CO ₂ -EOR in the world's top 52 oil basins [25].	Pg. 13
Figure 2.7: Mobility of CO ₂ versus mobility of H ₂ O [37].	Pg. 15
Figure 1.8: Static pressure profiles within a well [12].	Pg. 16
Figure 2.9: Effective pumping power generated by a CO ₂ vs brine based thermosiphon.	Pg. 16
Figure 2.10 Effect of the CO ₂ dissolution on convective [41].	Pg. 17
Figure 2.11: Geothermal heat replenishment map with current CO ₂ -EOR projects [43].	Pg. 18
Figure 2.12: Different configurations for CO ₂ -plume geothermal energy extraction [19].	Pg. 19
Figure 2.13: VPC and ORC temperature profile comparison [51].	Pg. 20
Figure 2.14: Flow rate flexibility to match heat demand over the year [53].	Pg. 21
Figure 2.15: Dependence of solubility on the brine composition [58].	Pg. 22
Figure 2.16: different saturation zones of CO ₂ in hot fractured rock [45].	Pg. 23
Figure 2.17: geo-mechanical risks that are associated with CO ₂ injection [135].	Pg. 26
Figure 3.1: °API to MW C5+ relation.	Pg. 28
Figure 3.2: Correlation between temperature and the minimum miscibility pressure [101].	Pg. 29
Figure 3.3: Sensitivity analysis of the new CO ₂ -oil MMP model [97].	Pg. 29
Figure 3.4: The relationship between reservoir porosity and depth (A) [103].	Pg. 31
Figure 3.5: Heat extraction cycle change with rejection temperature.	Pg. 34
Figure 3.6: salinity increase in hydrocarbon reservoirs with depth [141].	Pg. 35
Figure 3.7: Temperature and pressure profiles over the lifetimes of the CPG system [79].	Pg. 37
Figure 3.8: Results of numerical simulations of electricity production efficiency [139].	Pg. 38
Figure 3.9: Reservoir heat profile for CPG ([37].	Pg. 39
Figure 3.10: The consecutive configuration for CO ₂ -EOR and CPG.	Pg. 40
Figure 3.11: The parallel configuration for CO ₂ -EOR and CPG.	Pg. 41
Figure 4.1: 5-spot well configuration as used in the modelling.	Pg. 43
Figure 4.2: Schematic presentation of the box model used for the EOR part of the system.	Pg. 44
Figure 4.3: Different phases in the reservoir during the drying.	Pg. 49
Figure 4.4: Schematic representation of the CPG system.	Pg. 52
Figure 5.1: Minimum miscibility pressure vs depth for different geothermal gradients.	Pg. 60
Figure 5.2: Costs and revenue profiles for the CO ₂ -EOR phase vs time.	Pg. 61
Figure 5.3: CO ₂ -price for the CO ₂ project over the years.	Pg. 66
Figure 5.4: Dew lines for a CO ₂ -H ₂ O [85].	Pg. 68
Figure 5.5: Bubble point lines for a CO ₂ -H ₂ O mixture [80].	Pg. 69
Figure 5.6: Volumetric pore fraction of CO ₂ during the CO ₂ -EOR phase and the drying phase.	Pg. 70
Figure 5.7: Pressure drop over the drying front during the drying phase.	Pg. 70
Figure 5.8: Phase diagram for the CO ₂ in different phases in the CPG system.	Pg. 71
Figure 5.9: Pressure profile for the CO ₂ as it moves through the subsurface.	Pg. 72
Figure 5.10: Moliers chart for CO ₂ at the various phases of the system.	Pg. 73
Figure 5.11: performance of the direct turbine for different depths.	Pg. 74
Figure 5.12: performance of the binary turbine for different depths.	Pg. 74
Figure 5.13: output of the direct turbine, binary turbine and Net Work vs injection rate.	Pg. 75
Figure 5.14: Reservoir temperature depletion over the lifetime of the CPG system.	Pg. 76
Figure 5.15: Cost buildup of the CO ₂ -EOR phase.	Pg. 77
Figure 3.16: Cost buildup of the CPG phase.	Pg. 77
Figure 5.17: Oil production during the drying phase.	Pg. 78
Figure 5.18: Relation between the Levelised costs oil production with depth.	Pg. 79
Figure 5.19: Relation between the Levelized costs of electricity with depth.	Pg. 80

Figure 5.20: U.S. average levelized costs for plants entering service in 2019 [131].	Pg. 81
Figure 5.21: thermosiphon performance vs. permeability.	Pg. 82
Figure 5.22: Effect of increasing wellbore diameter on performance of the CPG system.	Pg. 82
Figure 5.23: difference in well costs calculations.	Pg. 83
Figure 5.24: Cost of the drying phase and drying time vs. CO ₂ – purity threshold.	Pg. 83
Figure 6.1: lifting costs (2008) for various oil producing regions [137].	Pg. 85
Figure 6.2: Performance of the CPG system [137].	Pg. 87

List of tables

Table 3.1: list of assessed parameters, and their respective correlations.	Pg. 27
Table 3.2: Compositions of CO ₂ captured from anthropogenic sources [87].	Pg. 30
Table 3.3: Well configurations for the six largest EOR projects in 1999 [90].	Pg. 32
Table 3.4 reservoir screening criteria for miscible CO ₂ -enhanced oil recovery.	Pg. 33
Table 3.5: Thermal conductivity of different reservoir formation types [114].	Pg. 37
Table 4.1: Input parameters for the reference case modelling study in Matlab.	Pg. 43
Table 4.2: Composition of crude oil and CO ₂ .	Pg. 46
Table 5.1: The effect of static CO ₂ price on the performance of the CO ₂ -EOR phase	Pg. 65
Table 5.2: The effect of the recovery factor on the performance of CO ₂ -EOR	Pg. 65
Table 5.3: The effect of the average oil/CO ₂ ratio on the performance CO ₂ -EOR	Pg. 66
Table 5.5: Costs/Benefits of CO ₂ storage	Pg. 79
Table 6.1: Comparison of the input parameters from different modeling studies	Pg. 84

1. Introduction

Anthropogenic emissions of CO₂, mainly caused by the combustion of fossil fuels have increased the level of atmospheric CO₂ from 280 ppmv in pre-industrial times to about 400 ppmv in 2014 [1]. If unabated, this level is projected to increase to 1100 ppmv by 2100 [2]. In order to achieve the Copenhagen target of no more than 2°C average global temperature increase, the International Panel on Climate Change (IPCC) recommended that atmospheric CO₂ levels should stabilize around 450 ppm. This goal would mean an emission reduction of between 50% and 85% from 2000 levels by 2050 [3].

Fossil fuels supply about 86% of the current global energy demand and account for 75% of current CO₂ emissions. One of the most cost effective solutions to reduce CO₂ emissions at large scale is CO₂ capture and geological storage (CCS) [3]. Geological formations, such as deep saline aquifers, deep coal seams and mature and depleted petroleum fields form the reservoirs in which CO₂ captured from large stationary sources may be safely injected. The occurrences of natural CO₂ fields such as the Mc Elmo Dome and Sheep Mountain in Colorado, and the Bravo Dome in New Mexico [4] demonstrate that hydrodynamic traps can safely store large quantities of CO₂ for millions of years [5]. The major barriers for large scale implementation of CO₂ storage in geological media are the high costs of capture, transport and injection, and the public opposition towards geological storage of CO₂.

Although CO₂ is regarded as an atmospheric pollutant, there are various ways in which CO₂ can be put to use. With CO₂-enhanced oil recovery (CO₂-EOR) it is possible to both re-stimulate field production and reduce CO₂ emissions from large stationary sources such as power plants and chemical factories. New generation CO₂-EOR technologies like foam injection enable an additional production of up to 22% of the original oil in place (OOIP) with the potential to sequester 40-60% of the initial CO₂ injected [6] [7]. A typical barrel of crude oil contains 0.42 tonne of releasable CO₂. As such, netting the injection and storage of 0.26 to 0.32 tonne of CO₂ emissions against the 0.42 tonne of CO₂ in the produced oil, makes the domestic oil produced by CO₂-EOR about 70% “carbon free” [8]. The CO₂ that is produced alongside the oil is separated, using subsequent depressurization (flashing) and solvent (scrubbing) or membrane processes [9]. Easily accessible resources are becoming more scarce and increasingly in control of national oil companies (NOC's). To keep up energy production and maintain energy security, international oil companies (IOC's) have shift their focus increasingly towards hard to produce and environmentally risky plays using unconventional production methods as well as to remote locations like the Arctic and deep water fields.

With the call for sustainability and improving energy security becoming increasingly more urgent, harnessing the significant potential for geothermal energy has gained interest and political support [10]. Although current projects mainly focus on hotspots like those found in Iceland and Italy, the predominant part of the global geothermal potential is found in the form of low temperature (100°C-200°C) reservoirs [11]. Using supercritical CO₂ as a working fluid, it is possible to utilize this potential while storing CO₂ in the subsurface. Supercritical CO₂ has certain advantages that make it more favorable to be used in deep reservoir heat mining than water [12]. Supercritical CO₂ is a poor solvent for most rock elements, has a higher mobility and higher compressibility than water, making production more efficient [13]. Using a CO₂-based trans-critical Rankine cycle, electricity production can be realized, even from low temperature (80°C-

120°C) reservoirs [14]. Currently, CO₂-Enhanced geothermal systems (CO₂-EGS) are not yet being applied on a wide scale, some pilot plants have been constructed in Soultz (France), Ogasaki (Japan) [15] and Basel (Switzerland) [16].

Road to sustainability

This thesis explores a combined deployment of various technologies. For oil companies, this may be an opportunity to optimise the use of their reservoir knowledge, infrastructure and well systems by prolonging their oil production. Furthermore, this would mean a fluent transition towards an environmentally friendly energy source while storing significant amounts of CO₂, answering both the call for energy security and sustainability.



Injection of either anthropogenic CO₂ or CO₂ from natural sources can take place when energy supply is higher than demand, and the electricity price is low. Because of the thermosiphon effect¹, high-temperature CO₂ can be produced efficiently and on-demand when the energy price is high. Using well-managed CPG, depleted reservoirs can be used as highly efficient storage options. This could have a buffering effect on electricity markets allowing higher market potentials for other renewables like wind and solar energy.

Aim and research question

This research focusses on the feasibility and viability for a transition from CO₂-EOR to CPG. Apart from the costs of CO₂, the most important investments and energy consumption in both CO₂-EOR and CO₂-EGS systems are associated with capture facilities, compression, monitoring equipment, infrastructure and wells [11]. During the lifetime of a CO₂-enhanced oil recovery project, the portion of CO₂ that is produced alongside oil will gradually increase until a point where the production is no longer economically viable, and injection is terminated. As the produced CO₂ is recycled, the demand for new CO₂ declines while the supply captured from the emitter remains the same. By combining these technologies to be used in either consecutive phases or as complementary systems sharing important infrastructure, investment costs may theoretically be reduced, and the facilities may be used longer and more efficiently. Depending on the temperature in the reservoir (quality of the heat) and the heat demand in the vicinity of the field, the produced heat may, for instance, be used for:

- Electricity production
- Residential heating or heating of nearby facilities
- Industrial (pre)heating processes for e.g. carbon capture

¹ CO₂ expands much more with heat than water, creating a strong buoyancy force and pressure gradient between the production and injection well. This eliminates the need for power intensive pumps. This will be further explained in section two.

An additional opportunity, proposed by heat and possibly electricity production using CO₂-EGS is that due to the significant expansion of the geothermally heated CO₂, heat can be produced efficiently and on demand. The main energy inputs on the site, for the compression and injection of the CO₂, can take place when the energy supply is high. This makes it well compatible with energy production methods that have large fluctuations like wind and solar or very low flexibility like nuclear, during periods of low demand.

For oil companies, making the transition to geothermal heat production might be an opportunity to optimise the use of their reservoir knowledge, infrastructure and well systems while prolonging their oil production. Furthermore, this means a fluent transition towards an environmentally friendly energy source while storing significant amounts of CO₂, answering both the call for energy security and sustainability. There are articles that mention combined heat and oil production by means of CO₂ injection in the reservoir [17] [18]. However, to the knowledge of the author, no studies exist that specify the configuration or reservoir type required for this combined deployment.

The goal of this thesis is to provide an exploratory assessment of the technical feasibility of a transition from CO₂-EOR and CPG. Three different configurations are proposed for a combined deployment of CO₂-EOR and CO₂-EGS. For the proposed configurations the technologies share the same CO₂ capture plant, infrastructure and monitoring equipment: 1) combined heat and oil production 2) consecutive oil and heat production 3) parallel heat and oil production.

For the configuration that shows the best technical feasibility, the storage potential, cost of energy and capacity are modelled for a case study.

Research question:

Could CO₂-enhanced oil recovery CO₂-plume geothermal heat extraction be used in a complementary way to allow more efficient use of reservoirs, infrastructure and monitoring equipment?

Sub-questions:

- What parameters affect the feasibility of CO₂-EOR and CPG?
- What is the importance of these parameters and how are they related?
- What configuration would be best for CPG-EOR and what are the most important bottlenecks?
- What is the estimated potential for CO₂ storage and heat and oil production in the case reservoir?

2. Theoretical Background

In this section, the current state of research will be discussed starting with the properties of CO₂, its capture and its behavior in the subsurface. In section 2.2 and 2.3, the basic principles, state of technology and configuration will be elaborated upon for CO₂-EOR and CPG respectively. The final part of this chapter will assess the risks of CO₂ injection into the subsurface and the storage mechanisms.

2.1 properties of CO₂

Before discussing the technology for CO₂ utilization in the subsurface, let us elaborate on the properties of CO₂. In the atmosphere, CO₂ absorbs and re-emits electromagnetic radiation in the infrared part of the spectrum. This way it impedes a part of the earth's long-wave radiation to reach out to space while letting most of the short-wave solar radiation through. The dramatic rise in atmospheric CO₂ since the industrial revolution is the main driver behind global warming [19]. To abate the harmful effects of atmospheric CO₂, much research has focussed on the capture of CO₂ from flue gases thus limiting emissions. This CO₂ can then subsequently be stored in the subsurface or utilized for energy extraction using e.g. CO₂-EOR or CPG.

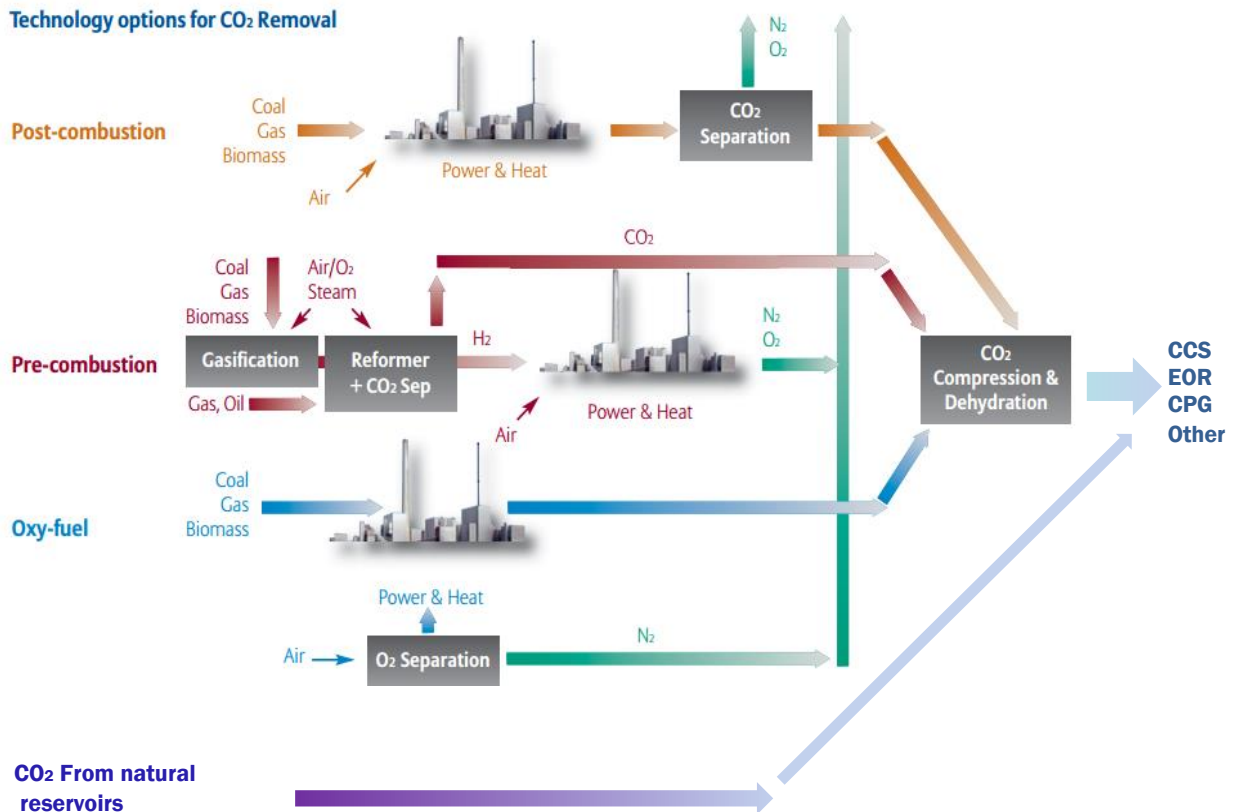


Figure 2.2: Various sources of CO₂ to be used for CCS, EOR or CPG operations. (Modified from [157]).

Besides anthropogenic CO₂, natural reservoirs can be a source of CO₂ for EOR and CPG. The occurrence of natural CO₂ reservoirs like the Mc Elmo Dome and Sheep Mountain Dome in Colorado and the Bravo Dome in New Mexico [4] prove that stratigraphic traps can safely store CO₂ for long periods of time. It is from these fields that current CO₂-EOR projects are feeding their needs for CO₂ [20]. Figure 2.1 provides an overview of various mechanisms to capture CO₂ from flue gases. Since this research focusses on methods to prevent CO₂ from reaching the

atmosphere by means of underground utilization and storage, the remainder of this section will focus on the thermodynamic behaviour of CO₂ in the subsurface.

2.1.2 Properties of CO₂

Under atmospheric conditions, CO₂ is a gas, slightly heavier than air with a density of 1.892 Kg/m³. The density of CO₂ is strongly dependent on temperature and pressure conditions. The critical point of CO₂ lies at T_c= 31.1°C and P_c = 7.38MPa that is the equivalent of a 738m hydrostatic column of water. Figure 2.2 represents the pressure-enthalpy diagram for CO₂ with its respective phase.

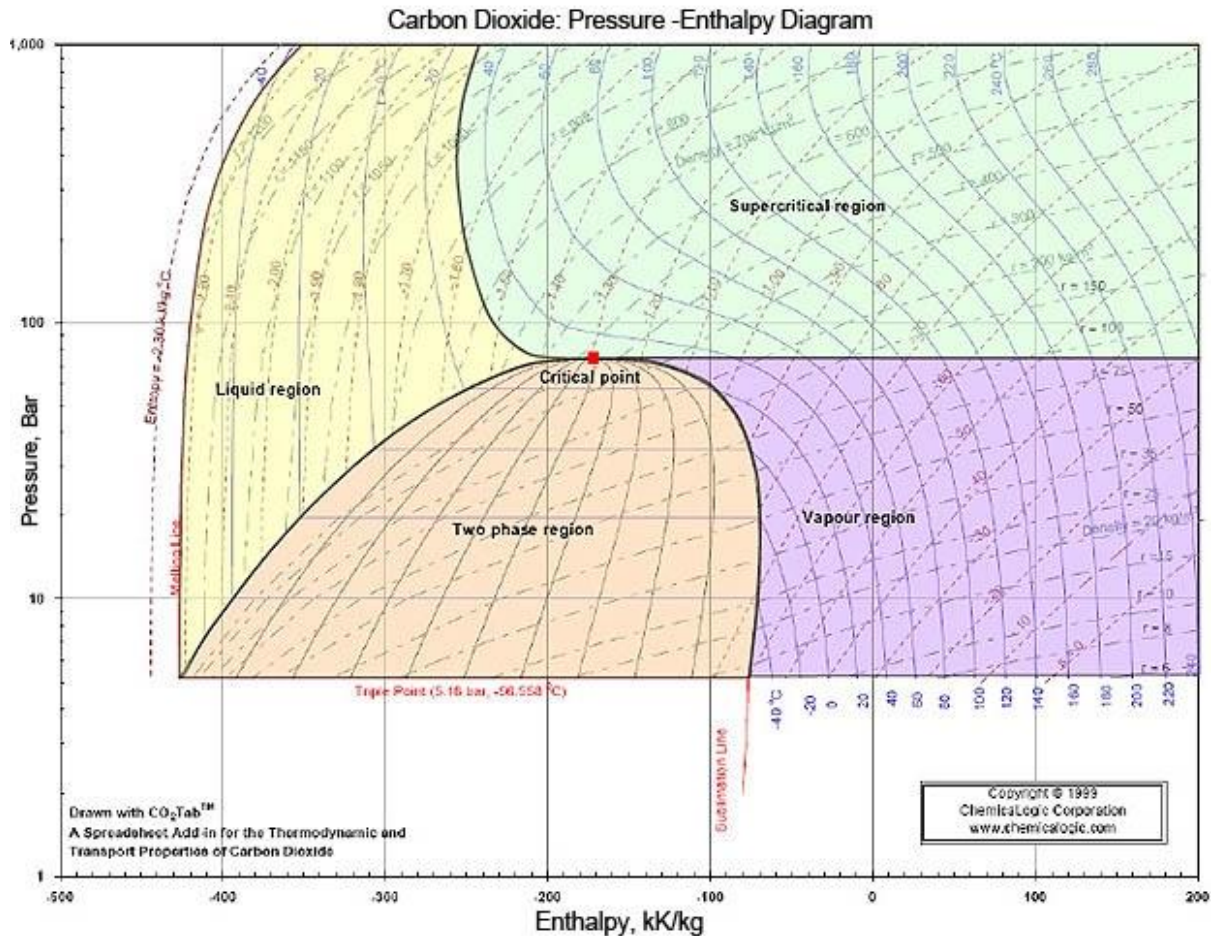


Figure 2.2: Pressure-enthalpy diagram for carbon dioxide [158].

At pressure and temperature conditions that are common for oil reservoirs (around 100-200°C and a few hundred bars) CO₂ will be in supercritical phase. As a supercritical fluid, CO₂ (sc) has high densities (ranging from 200–900 kg/m³, depending on pressure and temperature) similar to a liquid, and it has a low viscosity like a gas. This property makes CO₂(sc) favorable for efficient compression, transportation and injection. Furthermore, the high mobility of supercritical CO₂ is favorable for extracting heat from the reservoir. Pressure and temperature generally increase with depth and have opposite effects on CO₂ density [21]. CO₂ (sc) has a lower density than water and will, therefore, rise to the top of the reservoir. Depending on the type of oil and the reservoir conditions, CO₂ may have a higher or lower density than oil [22].

2.2 CO₂-enhanced oil recovery

During primary oil recovery, oil production is driven by the natural pressure difference between the reservoir and the well. As the reservoir pressure drops over time, the rate at which oil is produced declines. In order to re-stimulate production, a substance (generally water) is injected in a process called water flooding to increase the pressure of the reservoir. This phase is called secondary production. During the primary phase, typically 25% and 5% OOIP is produced for light oils and heavy oils respectively. The secondary oil phase will produce about 30% of the OOIP for light oils, and 5% in the case of heavy oils [23]. This still leaves a significant part of the OOIP trapped in the reservoir. Leaving still a significant potential of 45-90% of the OOIP as a target for enhanced oil recovery.

Oil that is left behind after water flooding is there because of two reasons: Either it has not been contacted by the injected fluid, or because of the capillary forces that exist between oil, water and the porous rock are too high for the pressure difference to displace it [20]. One of the most promising technologies developed to enhance oil production in this stage is based on the use of CO₂ to reduce these capillary forces. Currently, the majority of CO₂ injection into the subsurface is dedicated to enhanced oil recovery [6]. This section provides an overview on CO₂-EOR, the principles that govern oil displacement by CO₂ and the current state of technology.

2.1.1. Principles

There are two main processes that govern the enhanced production of oil by CO₂ injection, miscible and immiscible displacement. Immiscible Displacement occurs at reservoir pressures below the minimum miscibility pressure (MMP) for the specific crude oil type. In this case, the injected gas is mainly used to maintain the pressure and allow gravity stabilized drainage [7] to push additional oil out. Although Immiscible CO₂ enhanced oil recovery is less effective, it still recovers more oil than water flooding [24]. Crude oil is a cocktail of hundreds of different hydrocarbon components, many of them containing more than 30 carbon atoms. Under typical conditions, it is miscible with individual, short chain alkanes containing fewer than 13 carbon atoms. In thermodynamic equilibrium, a mixture of the reservoir oil and carbon dioxide forms two phases; One is a phase rich in CO₂ and light hydrocarbons, while the other phase contains a preponderance of heavier molecules [22]. If CO₂ is injected into an oil reservoir under miscible conditions, the CO₂ vaporizes the lighter oil fractions causing this fraction of the oil to dissolve into the dense supercritical CO₂. At the same time, CO₂ condenses into the reservoirs oil phase creating two fluids that become miscible [25]. A narrow transition zone (mixing zone) develops between the dry supercritical CO₂ and the reservoir oil, inducing a piston-like displacement. Figure 2.3 shows a schematic subsection of a CO₂-EOR reservoir with the miscible zone in which both CO₂-saturated oil and oil-saturated CO₂ are present. The factors that determine whether displacement takes place according miscible or immiscible principles will be further discussed in this section.

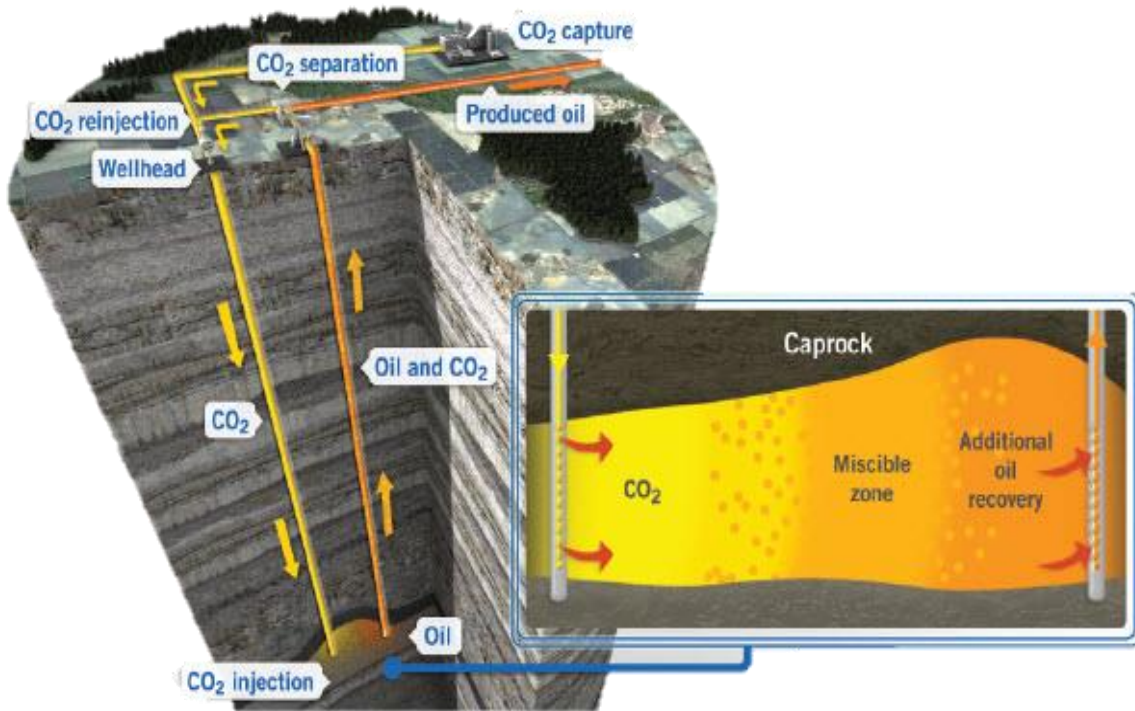


Figure 2.3: schematic view of a CO₂-EOR operation using anthropogenic CO₂ [6].

Wettability

In the case of multiple phases being present in a porous medium, wettability is defined as the tendency of one fluid to adhere to a the solid surface in the presence of other immiscible fluids. In the case of CO₂-EOR, the interactions between brine, oil, CO₂ and the rock minerals decide the location of the phases in the porous medium. The adhesive electrostatic forces between the rock and the fluid depend on rock mineralogy and fluid composition. The fluid that is attracted to the surface the strongest and, therefore, occupies the edges of the pore is called the wetting fluid and will disperse over the solid covering much of the mineral surface. Wettability preference is measured by the contact angle of the meniscus between the two fluids and the mineral surface (θ) [26].

Before coming in contact with oil, reservoirs are water-wet. However, as polar components in the oil interact with the mineral surface, this interaction can cause wettability to shift more towards oil-wet. This process only happens in those pores where the oil is in contact with the mineral surface, and thus depends on pore geometry and mineralogy. Figure 2.4 shows the positioning of the phases in the pore space with their respective classification.

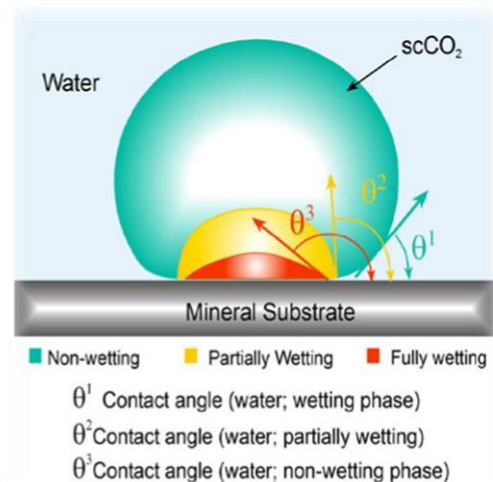


Figure 2.4: contact angle in brine-supercritical CO₂ systems [155].

Wettability is of high importance in reservoir physics as it determines flow and saturation within the formation. After primary and secondary oil production, typically around one-third of the original oil in place (OOIP) is produced [27]. Much of the remaining oil is trapped by capillary forces as disconnected blobs, surrounded by water, or as a continuous phase at low saturation with gas or brine occupying the larger fraction of the pore space. Figure 2.5 is a schematic representation of the positioning of oil and brine in the pore space with its classification.

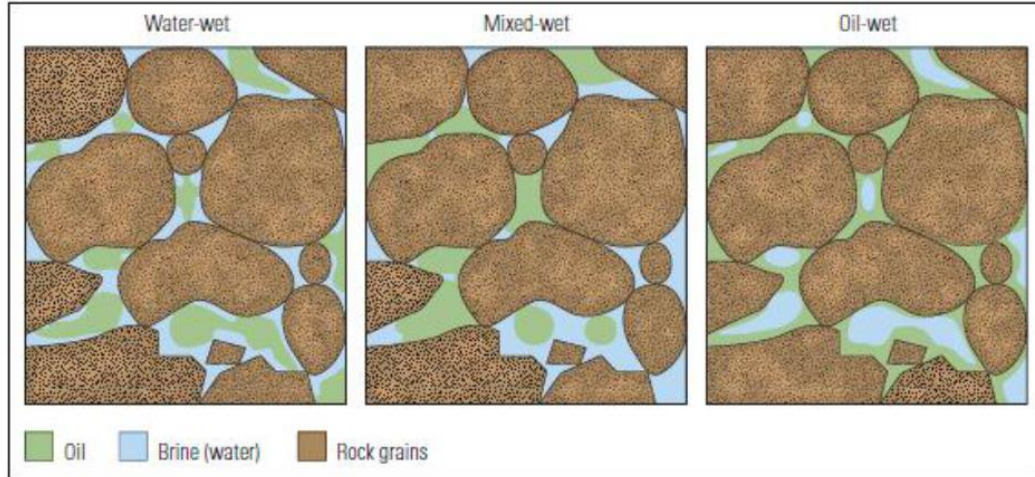


Figure 2.5: positioning of the oil and brine phases in the pore space depending on the mineralogy of the formation and the composition of the oil and brine phases [27].

As the oil travels upward due to buoyancy forces, it has to pass through a network of pores varying in size, shape, mineral composition and fluid saturation. In order for the oil to flow through a passageway, the oil pressure must exceed the capillary pressure that can be calculated using formula 2.1

(Eq. 2.1)
$$P_c = \frac{2\sigma_{nw,w} \cos \theta}{r}$$

In which P_c is the capillary pressure, $\sigma_{nw,w}$ is the interfacial tension between the oil and the brine, θ is the contact angle and r is the pore radius.

The interfacial tension is probably the most important factor causing one-third of the OOIP to be unrecoverable by using either gas or water flooding alone [28]. Enhanced oil production through CO₂-flooding works according to two mechanisms. The mobility is enhanced through a reduction in oil viscosity and changes occur in the interfacial tension lowering the capillary pressure via equation 2.1.

CO₂ miscibility with crude oil and the MMP

Miscibility is defined as the property of substances to mix in all proportions and form a homogeneous solution. Miscibility depends on the cohesion between the individual molecules, also known as Van der Waals forces. The strength of the intermolecular cohesion will determine the interfacial tension between the different phases. If the cohesive forces are stronger towards molecules of their own kind, the interfacial tension has a positive value. In this case, the fluids are immiscible and will remain separated by a membrane-like surface [29]. If the interfacial

tension is close to zero, or negative; in time, diffusion will cause chemical interactions between the phases. In time, the phases to become fully miscible creating a new fluid. Miscibility can occur either at first contact (SCM) or after multiple contacts (MCM).

Miscibility is not a fixed property but depends on the purity of the CO₂, oil gravity, reservoir pressure and temperature [27]. Under isothermal conditions, immiscible substances can become miscible with an increase in pressure. Different types of crude oil, based on their °API gravity² have different MMP's. The advantage of CO₂ over other gasses is that it can become miscible with oil at lower pressures compared to for instance CH₄ or N₂ [7].

Miscibility causes the oil to swell slightly and become less viscous so that it flows through the reservoir pores more easily. In addition, interfacial tension is reduced to zero in miscible flooding. Therefore, the capillary number theoretically becomes infinity, and displacement efficiency approaches one if the mobility ratio is favorable ($M < 1$) [23]. Laboratory studies using slim tube tests have shown that miscible CO₂ secondary flooding can reach an oil recovery factor (RF) of 90% [30].

2.2.2. Configuration

After CO₂ is obtained from either natural or anthropogenic sources (figure 1.1) it is compressed and injected into the oil holding formation. Residual and dissolution trapping mean that a significant part of the injected CO₂ ($\pm 40\%$ [6]) remains trapped in the reservoir after injection for CO₂-EOR. At the surface, the CO₂ that is produced alongside oil is recycled as this is cheaper and more environmentally friendly than to buy new CO₂.

In a typical CO₂-EOR project, surface processing takes place in three steps; The first step is to separate the gasses from the liquids. This is done using a technique called 'Flashing' in which the pressure of the production stream is dropped using valves. This depressurization often takes place in multiple steps (secondary, tertiary flashing) to avoid high energy losses due to recompression of the gasses later in the system. Depending on the pressure of each step, volatile molecules like N₂, CO₂, H₂O, CH₄ and some C₂H₆ and C₃H₁₀ evaporate and are separated from the heavier oil fractions. The heavier hydrocarbons are then transported to the refinery for the further separation.

The second step is to separate the organic compounds and impurities from the gas. This step is often difficult and very costly. Various different methods exist for this separation; Amine-based capture or 'amine scrubbing' uses the reversible equilibrium with amines and CO₂ forming soluble salts. The flue gas is circulated through an aqueous amine solution where CO₂ dissolves into the amine solvent. Using high temperatures, the CO₂ can be retrieved from the solvent by heating the solvent. Retrieving the CO₂ from the solvent requires high additional energy inputs making the technology unsuitable for energy recovery. Cryogenic capture is based on the deposition of solid CO₂ from the flue gas at low temperatures. The solid CO₂ can then sublime again if the cooling is stopped and be injected. A third way to separate gasses is with the use of membranes. The membranes have holes that are permeable to small molecules like methane and N₂ while being impermeable to larger molecules like CO₂. To successfully overcome the higher partial pressure of methane and N₂ on the other side of the membrane, the flue gas has to be

² The American Petroleum Institute gravity, or °API gravity, is a measure of how heavy or light a petroleum liquid is compared to water: if °API > 10, the oil floats on water; if °API < 10, it is heavier and sinks.

compressed. The separation technology that is most suitable for the technology depends on the configuration to be used.

The last step is dehydration of the flue CO₂-water mixture. This step is mainly required to reduce the material costs of pipes, compressors, and turbines. Regional pressure differences cause water to condense in the system that is then saturated with CO₂. The presence of multiple phases is challenging for turbines and compressors, especially due to the corrosive nature of CO₂-saturated water. Two methods for dehydration of CO₂ are using triethylene glycol (TEG) and a solid bed desiccant. TEG based systems have been widely used for the drying of methane. In this technology, the wet gas is circulated through glycol, adsorbing the H₂O from the stream. In a second step, the glycol is heated to 180°C, this boils out the water to close the loop. The H₂O (g) is vented out. Because CO₂ has a higher affinity to glycol than methane, some of the CO₂ will be co-adsorbed and vented in the process [31]. In solid bed desiccant dehydration, the wet CO₂ is circulated through a bed of fine-grained solid desiccant adsorbing the water fraction from the gas. When the bed is water-saturated, variations in temperature and pressure are used to desorb the water and regenerate the desiccant. Continuous operation requires a setup of multiple parallel dehydration cells [32]. After dehydration, the recycled CO₂ is replenished with newly purchased CO₂, compressed and re-injected into the reservoir.

2.2.3. Current state of technology

CO₂-enhanced oil recovery is a proven technology and potentially profitable, Commercial scale CO₂-EOR has been ongoing for over 40 years in the United States. In 2012, there was a total of 114 miscible and nine immiscible ongoing CO₂-EOR projects and the total oil production volume from the miscible CO₂-EOR projects was 308 564 barrels per day in the U.S.A. [33]. In 2009, the IEA performed a screening to assess the global potential for CO₂-EOR in the world’s top 52 oil basins. Figure 2.6 shows the potential for miscible displacement found by this study [25].

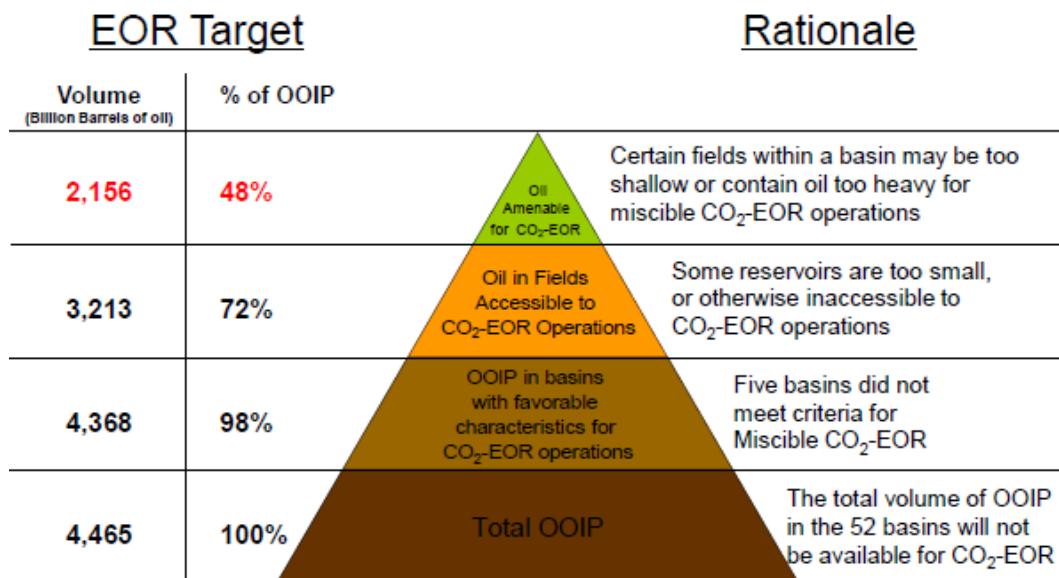


Figure 2.6: Potential for CO₂-EOR in the world’s top 52 oil basins as assessed by the IEA, 2009 [25].

Apart from the Permian Basin and the Rocky Mountains, wide-scale development of CO₂-EOR has not yet occurred. Furthermore, the majority of the CO₂-EOR projects that have been constructed to this point have not been designed with CO₂ storage as a co-objective. Due to the relatively high costs of carbon capture, most of the current projects use CO₂ from natural sources

instead of relatively expensive anthropogenic CO₂. Besides the high energy penalties associated with capturing the CO₂ from flue gasses, an additional problem is the low pressure. After the various stages of purification, CO₂ exits the facility at low pressure. This means that additional energy consuming compression is required before the anthropogenic CO₂ can be injected. In the case of natural CO₂ sources, CO₂ is often produced from deep (high pressure) reservoirs (± 100 bar at plant gate for CO₂ from the Sheep Mountain field [20]), limiting the need for additional compression. Although natural CO₂ projects do not address the climate issue, they have proven the potential of the technology and advances in this field drive down operation costs via technological learning, thereby paving the way for CCS.

EOR in offshore fields is not only constrained by reservoir lithology, but also by surface facilities and environmental regulations, among other factors. Therefore, EOR applicability in offshore fields is limited compared to onshore fields [34]. The majority of the CO₂ flood projects are situated in the U.S. and use nearby natural CO₂-sources at a price of around \$19/Metric tonne. However, modelling studies have shown that the larger North Sea reservoirs are also a promising target for CO₂ injection, because they contain light oil and are relatively permeable and homogeneous [22].

Trends

Much of the current research in the field of CO₂-EOR focusses on improving the sweep efficiency and improving miscibility. Under reservoir conditions, the viscosity of CO₂ is at least one order of magnitude lower than the viscosity of water [35]. Due to its low viscosity, supercritical CO₂ easily flows through the subsurface compared to other reservoir fluids. This high flow ability causes spatial variances in reservoir permeability to create a finger-like penetration pattern called "viscous fingering". The CO₂ flows faster in preferential flow paths in the reservoir blocking off pockets of brine and oil leading to an inefficient sweep of the formation. Also, buoyancy causes gravity segregation in the reservoir; this effect is stronger with a higher CO₂ mobility. The injected gas overrides the displaced formation liquids and breaks through in the production well without contacting most of the trapped oil. Another method to increase the sweep efficiency of CO₂ in the reservoir is to use horizontal injection wells [36]. Various methods have been developed to increase the viscosity of the injected CO₂ and thereby improve the sweep efficiency. One of these methods is the addition of surfactants to injection water creating foam. Foam reduces the gas mobility by immobilizing or trapping a large fraction of the gas without compromising its efficiency. The CO₂ holding foam moves slower and over a broad front. This delays the initial oil production, but in the end improves the effective sweep of the reservoir [27].

2.3 CO₂ enhanced geothermal energy production (CO₂-EGS)

In the search for sustainable energy sources, the vast potential of geothermal energy has been intensively studied. The majority of this potential occurs in the form of moderate temperature reservoirs ranging (100°C-200°C) [11]. Conventional geothermal systems use water or brine to extract heat from an often engineered (fracked) reservoir and then use a binary system to generate electricity. Because of the efficiency losses in the heat exchanger, these systems require high-temperature hotspots and are unsuited to harness the majority of the geothermal potential. CO₂ based systems can generate electricity from moderate-temperature reservoirs while storing CO₂ in the subsurface. This section elaborates on the principles, the current state of technology and configuration of such systems.

2.3.1 Principles

Under most conventional hydrocarbon-reservoir pressure and temperature conditions, CO₂ is in supercritical phase. Supercritical CO₂ has some advantages over water as a working fluid for geothermal heat recovery. CO₂ has a strong tendency to expand with increased temperature creating a density difference between the cold CO₂ at the injection well and the hot CO₂ at the production well. This generates a natural convection flow (thermosiphon) eliminating the necessity for energy consuming pumps [13]. Furthermore, because of its non-polar nature, most mineral species that are abundant in reservoirs like salts do not dissolve in supercritical CO₂ as they do in H₂O. This reduces the maintenance costs for piping, heat exchangers, turbines and compressors [13]. As the viscosity of CO₂ (sc) is only 40% of the viscosity of H₂O, the reservoir flow potential is higher. Figure 2.7 shows the dependency of CO₂ and H₂O mobility on temperature and pressure.

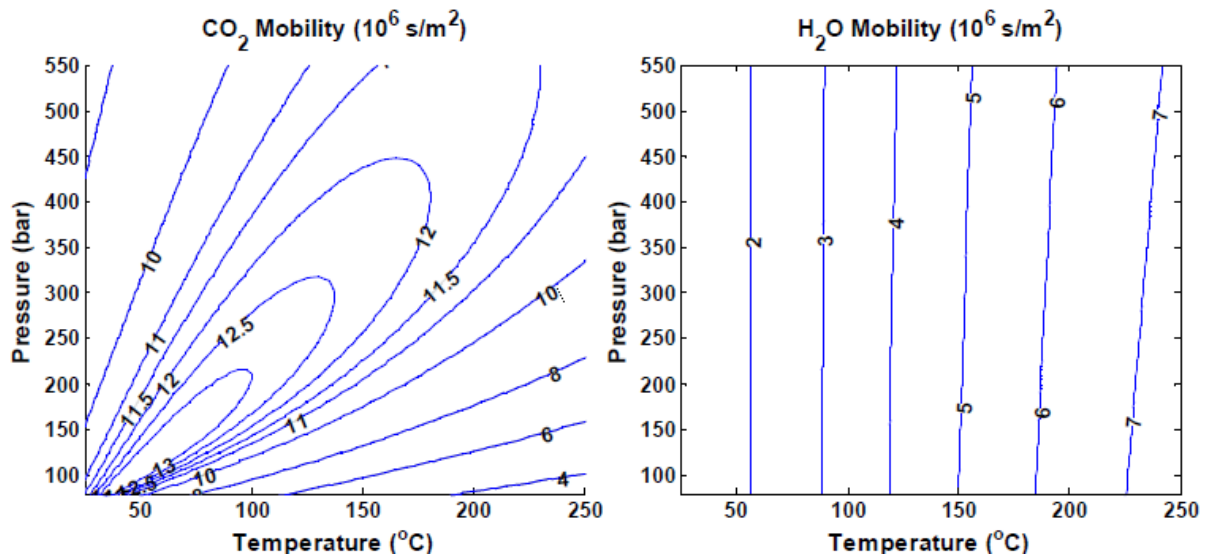


Figure 2.7: Mobility of CO₂ versus mobility of H₂O under common hydrocarbon reservoir conditions [37].

The heat capacity of CO₂ is lower than the heat capacity of water or brine (2.20 versus 4.16 kJ/kg/K at 100 °C and 250 bar) [37]. Therefore, higher CO₂ flow rates are required than in a water or brine based system. This is more than compensated for by the greater mobility and, all in all; the advantages may lead to higher heat extraction rates than brine based systems for the first few decades of production [38]. Two principles that are relatively insignificant for conventional water and brine systems due to their low compressibility are Joules Thompson cooling and the thermosiphon effect. However, because CO₂ is relatively close to its critical conditions and is highly compressible, these principles cannot be neglected in this case. These principles will therefore be further elaborated upon in this section.

Thermosiphon effect

Supercritical CO₂ has high compressibility compared to other working fluids like water or Brine. As a fluid comes up the well, the pressure decreases due to the reduced hydrostatic column and friction losses with the wellbore. For a static fluid, the pressure difference can be calculated using Bernoulli's equation:

(Eq 2.2)
$$\int_1^2 \frac{\Delta P}{\rho} = g(z_1 - z_2)$$

In systems using water or brine as a working fluid, density changes due to temperature and pressure changes are minor, leading to similar pressure profiles for the injection and the production well. As the pressure difference between the wellheads is small, the water or brine will be stagnant unless actively pumped [18]. In systems using CO₂ as a working fluid, pressure profiles are highly affected by temperature and density variation.

Pruess and Azarual calculated the static pressure profile for a 5000m deep injection well [12]. For both water and CO₂, they start from an injection wellhead pressure of 57.4 bar, slightly in excess of the CO₂ saturation pressure at injection temperature (57.36 bar at T = 20 °C). Corresponding static downhole pressures at a depth of 5000m are 528.7bar for CO₂ and 553.4 bar for water. At a production well the temperature of 200°C they calculated that the pressure at the production wellhead would be 288.1bar for CO₂ and 118.6bar for water. This corresponds to a wellhead pressure difference of 230.7 bar for CO₂ and 61.2 bar for water.

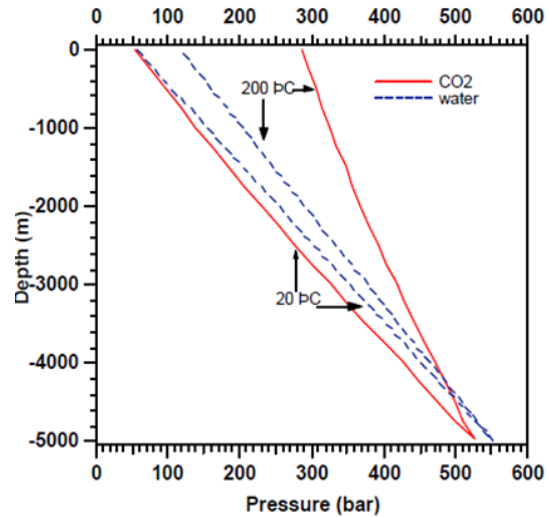


Figure 3.8: Static pressure profiles within a well for constant temperatures of 20°C and 200°C [12].

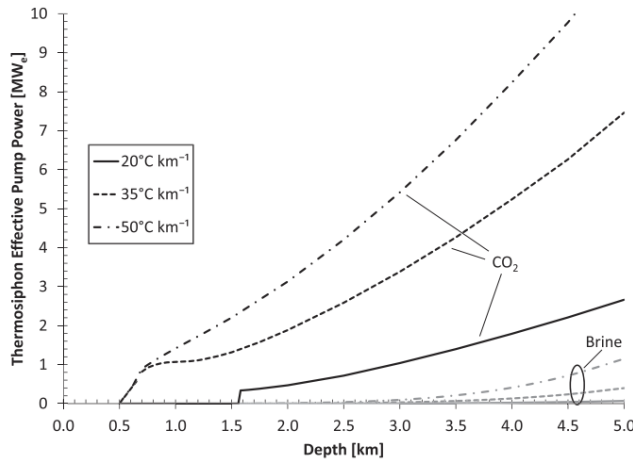


Figure 2.9: Effective pumping power generated by a CO₂ vs brine based thermosiphon for different geothermal gradients [18].

This density related pressure difference at the surface can be utilized to minimize the power needed for pumping or, by means of a direct CO₂ turbine, for electricity generation. The electricity that is saved by this natural thermosiphon compared to an isentropic pump is called the effective pumping power and was calculated by Adams et al. (2014) [18]. Figure 2.9 represents the effective pumping power related to reservoir depth for different thermal systems, for CO₂ and brine based systems.

Joules-Thompson effect

The temperature difference in a gas caused by its expansion is called the Joules-Thompson effect. In oil and gas exploration, this effect is commonly associated with permeability losses through the formation of hydrates in under-pressurized reservoirs near the injection well. However, in geothermal systems using CO₂ as a working fluid, this effect could also substantially reduce the production temperature at the wellhead leading to a reduced efficiency [39]. As CO₂ moves up the production well, the reduction in the overlying gas column leads to a reduction in pressure. For a Van der Waals or ‘ideal’ gas, adiabatic depressurization of the gas leads to a reduction in temperature [39].

Enhanced convective heat transport

As CO₂ is injected into the reservoir, it forms a plume displacing other reservoir fluids. At the edge of the CO₂ plume where the CO₂ is in contact with the formation brine, spatial diversification in dissolved CO₂ and gravity-driven flow accelerate the dissolution of CO₂ through convective transport. The mass density driven upward flow of CO₂ can be quantified by the bond number (B) given by equation 2.3 [40] and depends on the density difference ($\rho_w - \rho_{CO_2}$) divided by capillary forces ($T_s - \cos \theta$). In equation 2.3, k is the permeability and k_{rCO_2} is the relative permeability with respect to CO₂.

$$(Eq. 2.3) \quad B = \frac{(\rho_w - \rho_{CO_2})gk k_{rCO_2}}{(T_s - \cos \theta)}$$

As more CO₂ dissolves in the brine, the density of the formation brine (ρ_w) slightly increases. This causes CO₂-saturated brine to migrate downwards and unsaturated water to rise towards the CO₂ plume [35]. The chemically induced convection flow, combined with the thermally induced convection flow of hot water towards the CO₂-brine interface, favors the heat transport within the reservoir towards the CO₂ at the top. The effect of CO₂ dissolution into brine on the thermal productivity of geothermal reservoirs was studied by Yousefi et al., (2014) [41]. They found that depending on the mass fraction of dissolved CO₂, dissolution led to an increase in the Nusselt number³ by a factor 10 and the normalized stream function by a factor 2.67. Figure 2.10 shows the relation between the mass fraction of dissolved CO₂ and the Nusselt number for various temperature differences [41].

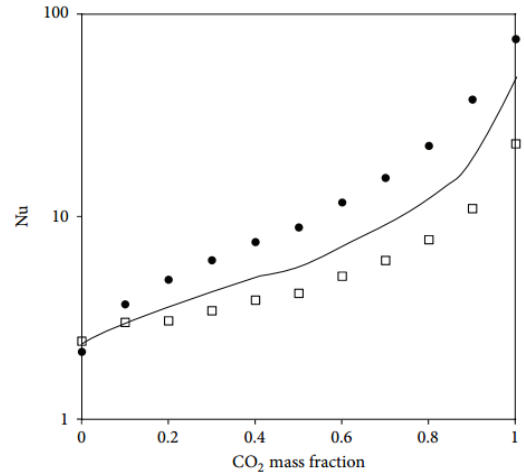


Figure 2.10 Effect of the CO₂ dissolution on convective flow possibly leading to enhanced reservoir productivity and longevity for $\Delta T=85^\circ\text{C}$ at differ temperatures [41].

2.3.2 Current state of technology

The potential of geothermal heat is large if it can be efficiently extracted. For the U.S., the inventory down to drilling-accessible depths of 6,500m was estimated to be over 600,000 EJ, corresponding to 6,000 times the countries annual primary energy use [42]. Although reservoir heat gets depleted depending on the heat extraction and replenishment rates, geothermal heat gets replenished on a human timescale rather than a geological timescale and can, therefore, be considered renewable. Figure 2.11 shows a map of the geothermal replenishment rates of the United States. Unlike most other renewable energy sources, geothermal energy is continuously available. Furthermore, the start-up time for electricity productions is relatively fast allowing geothermal energy to serve as a base-load, as well as a peak-load energy resource [18].

³ The Nusselt number (Nu) is the ratio of convective to conductive heat transfer across a boundary.

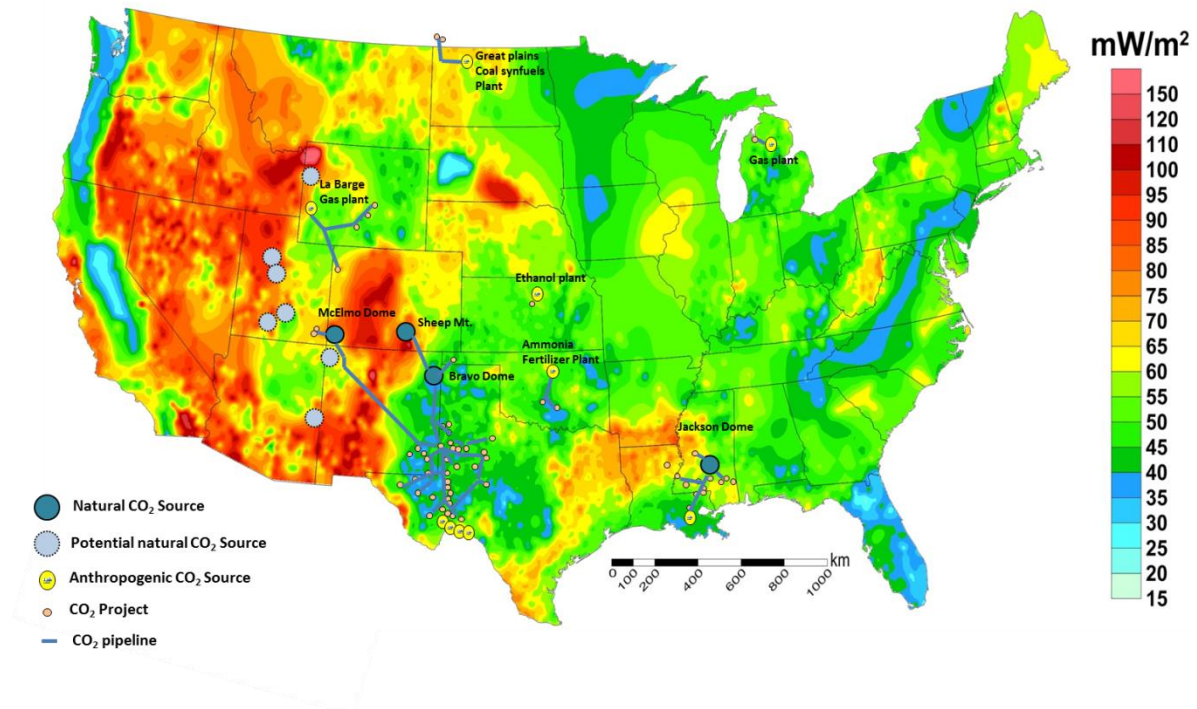


Figure 2.11: Geothermal heat replenishment map with current CO₂-EOR projects and sources of CO₂ for the United States. Modified from [43].

Currently, geothermal energy extraction using CO₂ as a working fluid is still in the proof of concept phase, and no commercial applications are operational yet. However, some pilot plants have been constructed in Soultz (France) and Ogashi (Japan) [15]. Furthermore, there are construction plans for a pilot site in Basel (Switzerland) [16].

So far, the majority of the research into CO₂-EGS systems has focused on artificially fractured reservoirs [44] [13] [45]. A numerical modelling study performed using TOUGH2 reservoir modelling software [46], shows that CO₂ enhanced geothermal energy mining in naturally porous reservoirs, like abandoned conventional hydrocarbon fields, had higher commercial potential. They found that even at relatively low reservoir temperatures of 100°C, utilization of the CO₂ mined heat could completely offset the costs of carbon capture [19]. This technique is called CO₂-plume geothermal heat recovery (CPG) and has the advantage that, through the use of naturally porous reservoirs, it does not require fracturing. Fracking can lead to induced seismicity and pollution by fracking fluids and must overcome significant socio-political resistance, as became clear during the termination of EGS projects in Switzerland in 2009 [47]. Another advantage of CPG over fracked systems is that the reservoirs are typically much larger. Therefore, the CO₂ storage potential is much higher. Because of the favorable heat extraction properties of CO₂, a larger percentage of the low to medium temperature reservoirs becomes viable for geothermal energy production [37].

In 2011, Randolph and Saar [19] performed a modeling study comparing CPG Systems with H₂O based geothermal systems. In their calculations, they only took into account the heat mining and flow properties, operational advantages were not included. They found average heat extraction rates for CPG over 25 years that were 1.8 times higher than an engineered CO₂-EGS system and 2.9 times H₂O-based system.

The first field demonstration for CPG combined with CCS is proposed for the SECARB Cranfield site in Mississippi [48]. The target reservoir is the Tuscaloosa formation at a depth of 3km and an initial reservoir temperature of 127°C. As the site is already an existing CO₂ storage project, infrastructure is already in place, including a CO₂ injection well and various monitoring wells of which one will now be used as a producer. For this field, the goal is to achieve a 3.3 kg/s CO₂ injection rate, and the designed generator electricity output will be 100kW.

2.3.3 Configuration

Subsurface configuration strongly depends on the properties and geometry of the reservoir. In naturally porous reservoirs, the subsurface configuration is very similar to CO₂-EOR without the use of viscosity enhancers. Gravity segregation will lead to the formation of a top layer of relatively high mobile supercritical CO₂ forming a preferential pathway from the injection well to the production well.

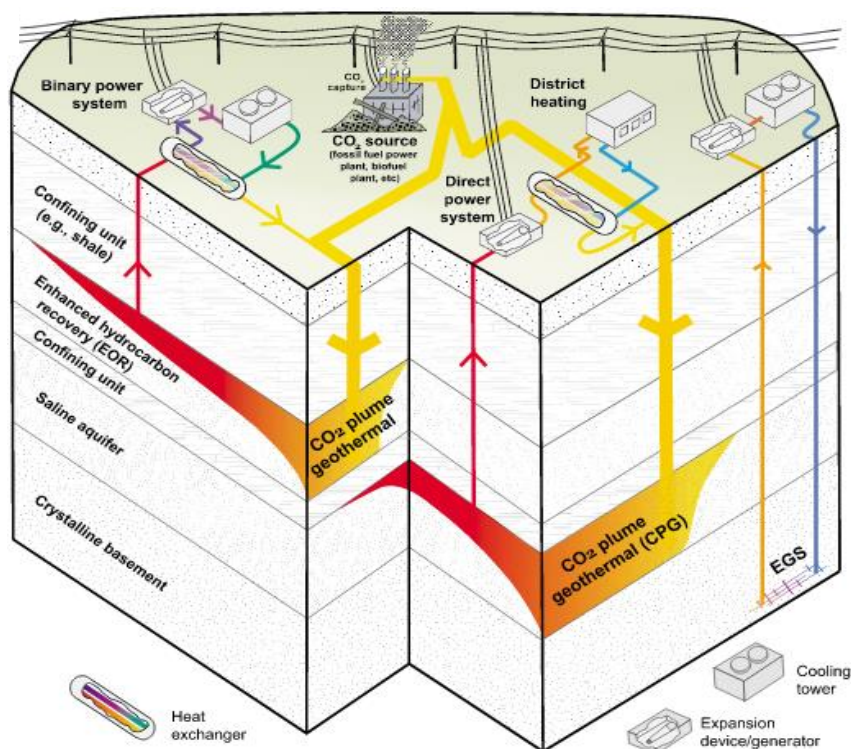


Figure 2.12: Different configurations for CO₂-plume geothermal energy extraction as proposed by Randolph and Saar [19].

The heat that is produced using CO₂-CPG, depending on the temperature, can be used in various processes including residential heating, (pre)heating for industrial processes like carbon capture, and electricity production. Direct utilization of heat is relatively straightforward. The heat can be utilized either in a direct CO₂-turbine or via a binary system in which another fluid is used to transport the heat. Figure 2.12 presents various configurations in which CPG can be used [19].

Heating demand often fluctuates with the ambient temperature and the transport of heat is often inefficient resulting in high energy losses. Therefore, transformation to work, and specifically into electricity is often favored [49]. Using a CO₂-based trans-critical Rankine cycle, power production can be realized, even from low temperature (80°C-120°C) reservoirs [14].

Depending on the purity of the output stream, power production can take place using either a direct or an indirect system.

Direct CO₂ turbine for electricity production

Unlike conventional geothermal systems using steam, brine or water as a working fluid, a CO₂-based geothermal system generates a significant pressure gradient between the hot production- and cold injection wellheads. If this pressure gradient is large enough and the well distance is not too large, this pressure gradient can be directly utilized for electricity production.

For the produced CO₂ stream to be used in a direct turbine, eliminating heat exchanger efficiency losses, the CO₂ needs to be undersaturated with respect to H₂O. Therefore, the amount of dissolved H₂O needs to be small enough to not be precipitated even in the low pressure and temperature phases of the system.

Binary system for electricity production

If the CO₂-stream is not pure enough (< ±94% CO₂) for utilization in a direct system, an alternative is to use a binary system in which a secondary fluid is used as a transmission fluid. These systems, however, suffer from heat exchanger efficiency losses and are therefore considered less desirable [50]. A typical binary cycle that is used to transform the produced heat into electricity is an Organic Rankine Cycle (ORC). This cycle uses a binary system, implying that an operating fluid is boiled in the vaporizer using the heat from the CO₂ stream. The vapor is subsequently superheated and expanded through a turbine. A cooling tower is used to condense and sub-cool the refrigerant, closing the cycle. Typical isentropic efficiencies⁴ for the state of the art ORC based turbines at relatively low temperatures are around 50% [51].

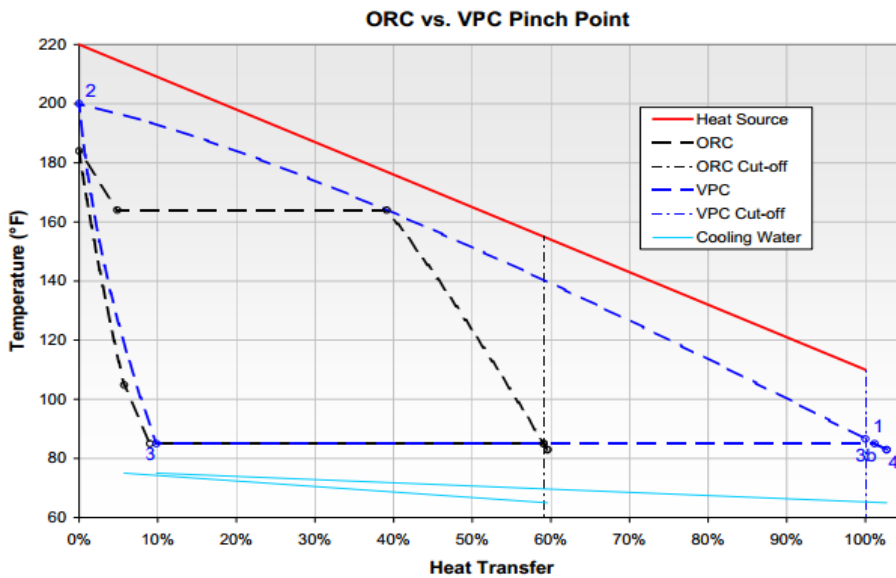


Figure 2.13: VPC and ORC temperature profile comparison [51].

Advances in turbines that specialize in the utilization of relatively low-temperature heat streams like geothermal heat or industrial waste heat include the Euler turbine and the variable phase

⁴ The isentropic efficiency of a turbine is a comparison of the actual power output with the isentropic case, so assuming no entropy increase throughout the cycle.

turbine (VPC). The Euler turbine works with the Kalina cycle. This cycle is an improvement of the organic Rankine cycle that works with multiple component fluids. The difference in boiling points causes a slide effect during the boiling process reducing the pinch point allowing the Euler turbine an electrical efficiency of 75,3% [51]. The variable phase turbine makes use of various individual nozzles by which enthalpy is converted to two-phase kinetic energy in a near isentropic expansion. The inlet flow (liquid, vapor, supercritical or two-phase) breaks up leaving the nozzles, as it expands into smaller droplets and gas. The small diameter of the droplets results in a close coupling of the gas and liquid, producing an efficient acceleration of both phases. This aspect eliminates the boiling pinch point restriction leading to more efficient heat profile (Figure 2.13). Both these turbines claim to increase system efficiency significantly and reduce maintenance and installation costs [51].

Transitions from heat to work are affected by the Carnot efficiency limiting the possible electricity to be produced (Eq 2.4) [52]. As CO₂ is only deposited at temperatures significantly below 0°C, the heat rejection temperature in cold climates can be much lower than in H₂O-based systems leading to a higher Carnot efficiency.

(Eq. 2.4)
$$\eta_{Carnot} = 1 - \frac{T_{Sink}}{T_{Production\ wellhead}}$$

On demand power supply

One of the major barriers for the large scale implementation of renewables is to match the energy supply and demand. As energy is difficult and costly to store, generated electricity has to be immediately consumed. Especially with wind and solar energy, matching the electricity supply and demand curves often creates the necessity for high overcapacity, backup plants, and expensive flexible load power solutions.

The primary power input in a CPG system is associated with the separation and compression of CO₂. Depending on the availability of storage, these processes can be done at times when the energy demand and price, are low. Through the strong thermosiphon effect, power inputs in the production are minor allowing for efficient electricity use. Production can be increased in - or limited to peak hours when the demand for heat or electricity is high.

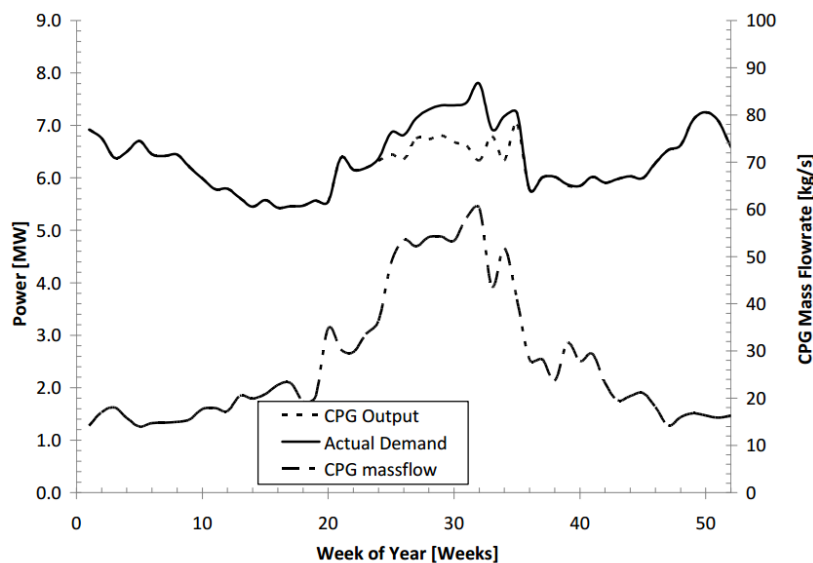


Figure 2.14: Flow rate flexibility to match heat demand over the year [53].

Figure 2.14 shows how the turbine output can be adjusted to match the power demand fluctuations over the year by adjusting the injection flow rate [53].

2.4 CO₂-storage in porous reservoirs

Leakage of CO₂ from geological reservoirs into overlying potable aquifers can lead to acidification of aquifers, mobilization of bitumen and heavy metals and reduced plant growth. Therefore, a complete assessment of the risks of potential subsurface utilization of CO₂ requires a multi-disciplinary approach including geomechanics, geochemistry, and fluid dynamics. In this section, possible risks caused by mechanical and chemical changes induced by CO₂-injection will be discussed.

2.4.1 CO₂ storage in conventional oil reservoirs

Due to the high capacity and the use of existing technology, carbon capture, and geological storage is considered a promising and cost-effective option to reduce CO₂ emissions from large stationary sources [54]. In their optimized strategy for realizing a maximum average global temperature rise of 2°C by the year 2050, the International Energy Agency (IEA) allocates a cumulative contribution to CO₂ emission reductions of 14% to carbon capture and storage [55]. ETS levels are projected to rise dramatically in the coming decennia [55], making CO₂-storage a potentially large industry in the coming decennia. Various geological formation types, such as deep saline aquifers, deep coal seams and mature and depleted hydrocarbon fields are identified as possible sinks for safely storing CO₂ [21]. Since the aim of this research is to explore the joint potential with CO₂-EOR, the focus lies on conventional hydrocarbon reservoirs.

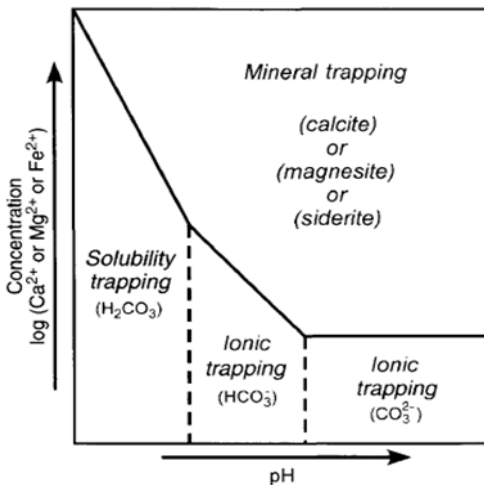


Figure 2.15: Dependence of solubility, ionic and mineral trapping mechanisms on the brine composition [58].

Within the reservoir, different trapping mechanisms, operating at different time scales, hold the CO₂ in place [56]. The so-called “primary trapping mechanisms”: The potential for primary trapping depends on the porosity and geometry of the reservoir and the presence of other immiscible phases. Stratigraphic trapping is the static trapping of buoyant, mobile CO₂ by stratigraphic and structural traps, in the same way, that hydrocarbons are trapped within a conventional reservoir. Upward and lateral flow of CO₂ are impeded by low-permeability rocks keeping the CO₂ in a confined space. If a pathway is found, buoyancy forces may cause CO₂ to escape from the reservoir. Structural traps are caused by crustal movement while stratigraphic traps are the result of depositional or diagenetic processes [56].

During injection, CO₂ saturation increases and water is drained from the pores. CO₂ moves laterally away from the injection wells due to the pressure gradient and upwards due buoyancy forces. Supercritical CO₂ and brine are not miscible. Therefore, pathways can be blocked off by the wetting phase during imbibition. Some residual, discontinuous CO₂ remains in the pore space when the wetting fluid reaches maximum saturation during the imbibition cycle. The path dependence of relative permeability and capillary pressures on the saturation path cause CO₂ to

remain trapped within the pore space [57]. This process is called residual trapping and will be further explained in section.

Dissolution trapping is an undesirable mechanism when it comes to CO₂ utilization. Once the CO₂ is dissolved in brine or oil, it will no longer migrate upwards as a separate phase but instead travel at the same rates the in-situ fluids. Even if subsurface flow is present, the CO₂ may remain underground for millions of years before discharging. Figure 2.15 shows the dependence of solubility, ionic and mineral trapping of CO₂ on the chemical composition of the host rock formation brine at equilibrium. The solid line represents the phase boundary along which minerals precipitate and may vertically shift up or down depending on temperature, pressure and the total concentration of carbonate species. Below this boundary only the aqueous phase is present containing various coexisting carbonate species. The dotted lines represent the dominant species over the depicted pH range [58]. Solubility of CO₂ in the formation decreases with salinity due to the salting out effect [59]. Simulation studies on the injection of CO₂ in the limestone Dogger Aquifer (Paris basin) show an evolution in pH due to concomitant processes that proceed at different kinetic rates. At the interface between the supercritical CO₂ bubble and the aqueous solution, an exchange zone resides where CO₂ continuously diffuses [60].

The long-term behavior of this outermost zone of the plume will be crucial for sustaining energy recovery, for estimating CO₂ storage rates, and for figuring tradeoffs between power generation and geologic storage of CO₂ [45]. CO₂-dissolution into the formation brine and subsequent mineralization in carbonate minerals are desirable from an environmental perspective. However, with the current environmental policies, costs for CO₂ still are a significant expense in both CO₂-EOR and CPG projects. Therefore, from an economic perspective, high CO₂-losses (to geological storage) negatively affect the viability of a project. The rate at which this dissolution takes place depends on various factors like the salinity of the brine and the convection flow within the reservoir.

After the initial hydrostatic, residual and solubility trapping, aqueous CO₂ can react with other aqueous species present in the formation brine. The amount of carbon mineralization is proportional to the bulk concentration of carbonate forming elements, principally Fe, Mg, Ca, Na and Al in the formation brine [61]. In most conventional reservoirs, the availability of free reactive elements is not very high, and most of the CO₂ will remain in liquid or supercritical phase [62].

2.4.1 CO₂ mineral interactions

The development of a new and unused reservoir for CPG will consist of three stages. First, the pore water in place has to be displaced by CO₂ using continuous injection, and primarily brine will be produced. In the second stage, a two-phase brine-CO₂ mixture will be produced with an increasingly higher percentage of CO₂. It can take up to several years before a single CO₂ phase production is reached [63]. Even then, in the third stage, significant levels of dissolved water will be present in the CO₂ stream for many years. However, the effects of the dissolved water during this final single-phase production on mass flow and heat transfer are found to be negligible [42]. If however, the reservoir has been previously used in CO₂-EOR, saturation of the reservoir might be quicker.

In a fully developed CPG field, three zones will occur based on their CO₂ saturation Figure 2.16. In the center of the plume, a zone of supercritical CO₂ with some dissolved water (wet CO₂) will be established (Zone 1) [45]. Followed by a mixed zone that contains both supercritical CO₂ and CO₂-saturated brine. On the edge of the plume, a halo of formation brine or hydrocarbons forms with a decreasing portion of dissolved CO₂. Geochemical reactions in these three different zones are expected to be very different [64].

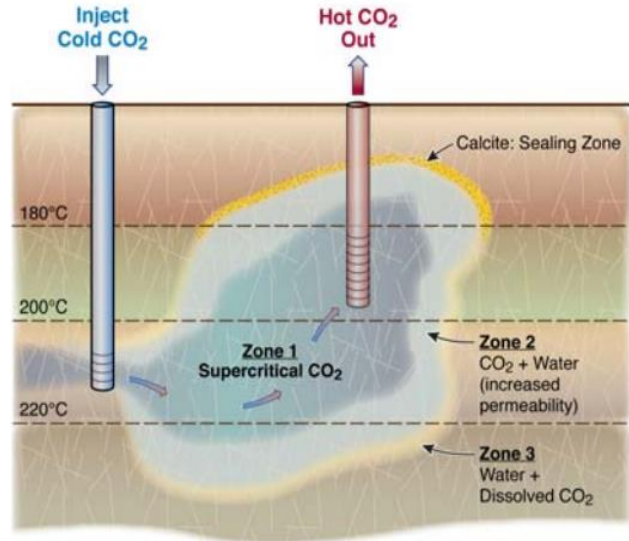


Figure 2.16: different saturation zones of CO₂ in hot fractured rock [45].

In the first zone, the lack of water is expected to reduce the mineral interactions in this zone. Dry CO₂ is not an ionic solvent and, therefore, mineral reactions within the inner zone are expected to be much less than in the case of geothermal heat extraction using water or brine as a working fluid. Rock minerals exist chemical stable in the water-free supercritical CO₂ system [65]. Lower mineral dissolution and subsequent precipitation rates mean lower risks of clogging in the formation or the subsequent utilization phase [13]. As dry CO₂ flows through the reservoir formation for prolonged production periods, it extracts weakly bound H₂O from the reservoir minerals. This CO₂ drying of the rock causes volume reduction, leading to an increase in porosity and permeability. Therefore, over time, the flow of relatively dry CO₂ through a porous reservoir is a self-enhancing process [66].

In the second and third zones, CO₂ will be in contact with the formation brine. As the CO₂ dissolves in the formation fluids, it forms carbonic acids leading to brine acidification following reaction 2.1



Shortly after injection, 10-20% of the CO₂ will dissolve into the formation brine [67]. Even long after injection, dissolution will take place as a result of diffusion and convection driven by small density differences caused by the dissolution of CO₂. Depending on the availability of hydroxide atoms, reaction 2.2 and 2.3 will occur.



The dissolution of CO₂ within the formation brine and acidification of the brine allow the aqueous CO₂ to react with other aqueous species present in the brine. These other aqueous species primarily originate from the reservoir formation.

Some concerns are expressed on the possibility of mineral dissolution affecting the sealing capability of cap rocks [68] [69]. However, due to the extremely low porosity and permeability in cap rocks, reactive surface areas are very small. Also, the infiltration and flow rate within the

infiltrated area are very low, limiting reactions between the brine and the caprock. Along flow pathways, acidified brine dissolves minerals and increases porosity. Even small porosity increases may cause the hydraulic conductivity to increase by a factor 10-100 [70]. Without the existence of a preferred flow path, reactions with most cap rocks are negligible [71] [72]. Depending on the brine saturation, with respect to carbonates, calcite and magnesite cementation (figure 2.13) may even reduce the permeability of the formation. This process may enhance the sealing capacity of the cap rock [69] [73]. Furthermore, it should be noted that pure supercritical CO₂ is a poor solvent. Leakage from a CPG-reservoir would, therefore, have a lower self-enhancing effect as leakage of a brine based geothermal reservoir.

A geochemical modeling study was performed for CO₂-EGS in the granite formation at the Roosevelt Hot Springs, Utah using Tough2 modeling software [38]. The primary minerals are quartz, oligoclase, albite, k-feldspar, annite, and phlogopite and the brine composition was equilibrated with the initial reservoir mineralogy. They found some leakage would take place after a period of several decades. However, the small amounts of CO₂ will most likely be trapped, dissolved and mineralized by the mechanisms discussed, long before it reaches potable aquifers [38]. It is important to note that this is a fractured engineered reservoir and not a hydrostatic trap like conventional oil fields. They find that some quartz dissolution may take place in the un-acidified area causing subsequent precipitation in the CO₂ affected area. They furthermore find that, after one year of CO₂ injection there is illite and carbonate precipitation in the areas of the reservoir that have a high gas saturation. These results match with previously performed batch experiments and depending on the location of precipitation, might affect permeability [72]. Most precipitation was found to take place at the top of the reservoir like in figure 2.14, not in the injection/production layer [38].

2.4.3 Geomechanics

CO₂ injection into the storage formation causes the pore pressure first to increase locally. The injection acts as a piston, pushing the formation fluids laterally away from the injection well [60]. Two shocks are formed; one shock between the single-phase gas region and two-phase gas and the liquid region is called the trailing shock. The second shock is called the leading shock and is between the two-phase region and the single phase liquid/brine region [74]. As the reservoir pressure increases, this leads to vertical expansion of the reservoir lifting up the overburden. At the surface, these effects can be monitored as surface heave. The amount of heave and spreading of the heave depend on the geometry and mechanical properties of the reservoir and the overburden [75]. How quickly the increased pressure disperses over the reservoir depends on the permeability and capillary forces, hence mineralogy and presence of other immiscible phases [76]. Drying of the reservoir may be accompanied by precipitation of salts in the reservoir. In the case of high CO₂ fluxes, brine concentration may lead to the subsequent precipitation of carbonates, sulfates and evaporates [77]. Reductions in porosity and permeability caused by mineral precipitation in flow paths might negatively affect the reservoirs injectivity. Also, the higher density in the concentrated brines will lead to vertical flow, and different brine-rock interactions might take place as a consequence of the increased ionic strength [78]. This effect will be stronger for more concentrated brines.

High (local) pore fluid pressures may result in substantial and irreversible mechanical changes such as creation of new fractures, strain in the well assembly and reactivation of larger pre-existing faults. These pressure induced changes may open flow paths causing buoyant CO₂ to leak from the reservoir. Because of the high mobility of supercritical CO₂, pressure gradients within the reservoir are most likely lower in CO₂-flooding than in water flooding reducing the risk of local high pore pressures [37].

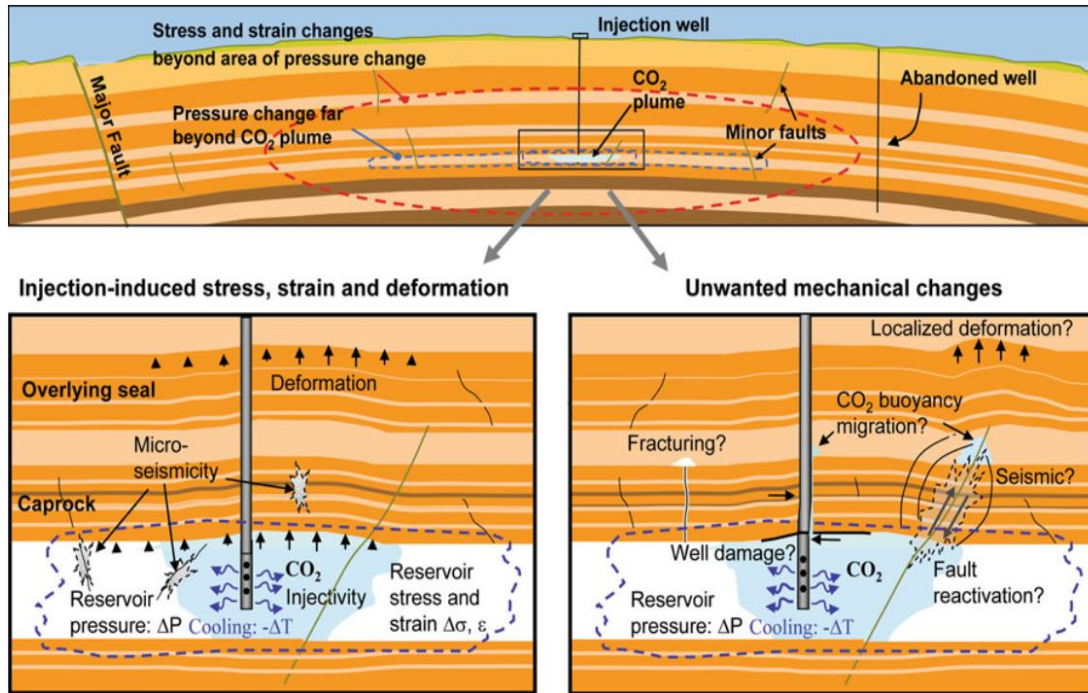
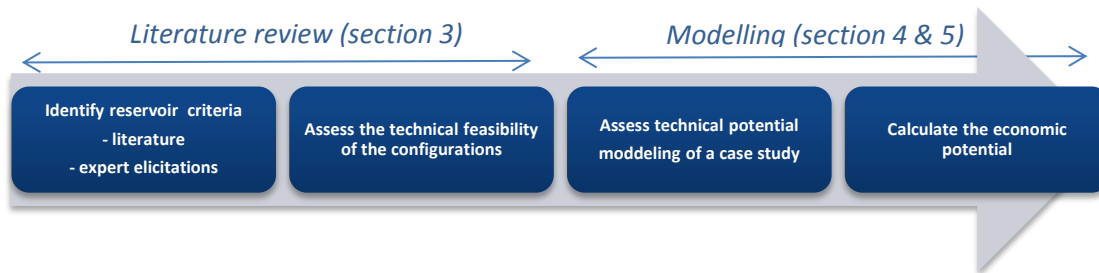


Figure 2.17: geo-mechanical risks that are associated with CO₂ injection in geological formations [156].

Figure 2.17 only takes into account the mechanics of storage and therefore pressure buildup. In the case of production of hot CO₂ from the reservoir, however, pressure depletion may come with additional risks. At the production well, hot CO₂ is extracted from the reservoir that is replaced by colder denser CO₂ at the injection well. This injection is accompanied by a reduction in overall CO₂ volume in the formation leading to a reservoir pressure reduction over time. Especially with high CO₂-flow regimes, this reduction can amount to several MPa's over 30 years [79].

3. Parameter and configuration assessment (Part I &II)

This thesis is an explorative study into the possibility of performing CO₂-EOR and CPG in the same reservoir. The research consists of three consecutive phases. The first phase aims to determine the reservoir criteria for CO₂-EOR and CPG separately based on literature. The second



step focusses on the configuration for CPG-EOR based on the criteria found in the previous step. In the final step, the potential of the technology for a reservoir that meets the requirements found in step 1 and the configuration from step 2 was roughly assessed using simulations in Matlab. This section explains the methodology and intermediate results of the literature study.

3.1 Parameter analysis

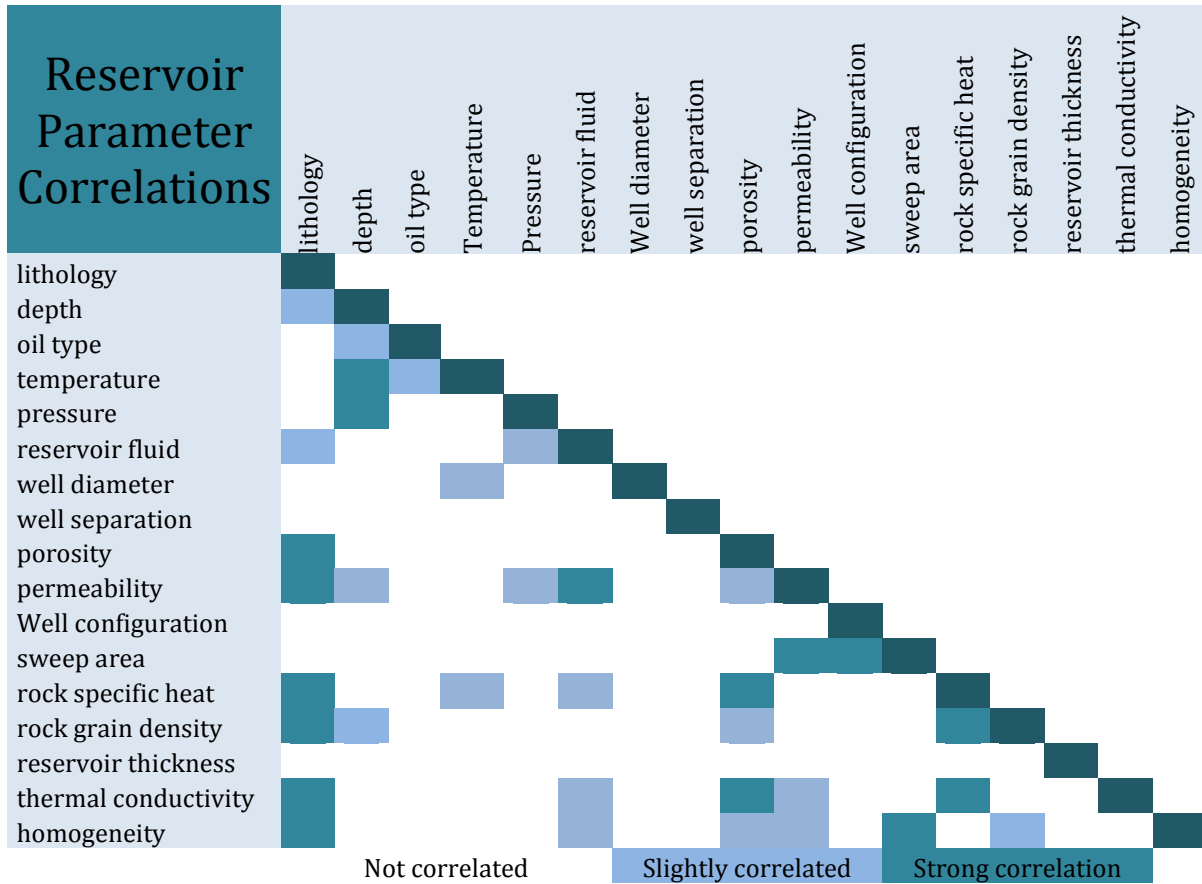
The first step to assess the possibility of CO₂-EOR and CPG to take place in the same reservoir is to identify the reservoir criteria for the separate technologies. A literature study was performed into the effects of various parameters on the performance and applicability of the technology. The study looked at different models to determine the most relevant parameters affecting CPG and EOR. To avoid double counting, correlations between parameters were identified.

Parameters were assessed based on their potential effect on technical feasibility economic viability. From literature and open interviews, the ranges within which CPG-EOR is technically feasible were determined. This research focusses on the technical parameters.

3.2 Correlation

This section elaborates on the most relevant parameters and their effect on reservoir suitability. Many parameters that affect reservoir suitability are correlated (Table 3.1). The correlations that were identified were incorporated in the input reservoir parameters to make sure that the parameters chosen for the fictional reservoir would be realistic. High correlations were found for parameters like lithology and permeability, and homogeneity and porosity and rock specific heat.

Table 3.1: list of assessed parameters, and their respective correlations.



3.3 Reservoir criteria for CO₂-EOR

Oil displacement by CO₂ injection can take place via two pathways. Fully miscible displacement requires higher reservoir pressures but also leads to greater oil recoveries. Immiscible CO₂ recovery is less effective but still recovers more oil than water flooding [24]. The effects of reservoir characteristics on the success of CO₂ flooding are primarily through their effects on miscibility, surface tension, and sweep efficiency. The reservoir criteria discussed below are based on miscible oil displacement. Since immiscible displacement uses the CO₂ to physically push the hydrocarbons out, criteria for this technique will be far less strict. The most important parameters in assessing field suitability for CO₂-EOR are the oil characteristics and specifically gravity, temperature, pressure, CO₂ purity, permeability, sweep efficiency and the configuration of the system.

Oil type and gravity

The specific gravity of the hydrocarbons in the formation is based on the molar composition and strongly affects the miscibility with CO₂(sc). Light oils contain a relatively small fraction hydrocarbon chains

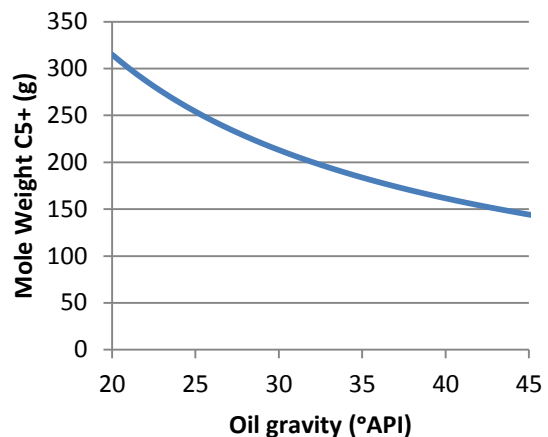


Figure 3.4: °API to MW C₅₊ relation.

of more than five consecutive carbon atoms (C₅₊ fraction), have a high °API gravity and are miscible with CO₂ at relatively low pressures. Heavier oils have longer chains, higher viscosity and require much higher pressures to achieve miscibility making them harder to displace. Since oil viscosity is directly affected by the gravity of the oil, it is not separately evaluated in this analysis. Figure 3.1 shows the relation between the gravity and the molecular weight of the C₅₊ fraction. Oil with a gravity higher than 45°API is volatile and therefore not suitable for miscible displacement [80].

Temperature

The temperature has the highest impact on the CO₂-oil MMP with calculated correlations ranging from 0,73 [81] to 0,925 [82]. High reservoir temperatures mean that a higher pressure is required, to achieve miscibility. Yelling and Metcalfe (1980) performed slim-tube tests to determine the correlation between the MMP and temperature experimentally. They found that for the range of 35-89°C, increased temperature led to an increase of 57 kPa/°C [83]. Most current CO₂-EOR projects take place in the region with low geothermal gradients [84] [81]. For this reason, research into the effects of temperature on the MMP remains limited to relatively low-temperature ranges. Additional research is required to assess the effect of higher temperatures on the potential for CO₂-EOR.

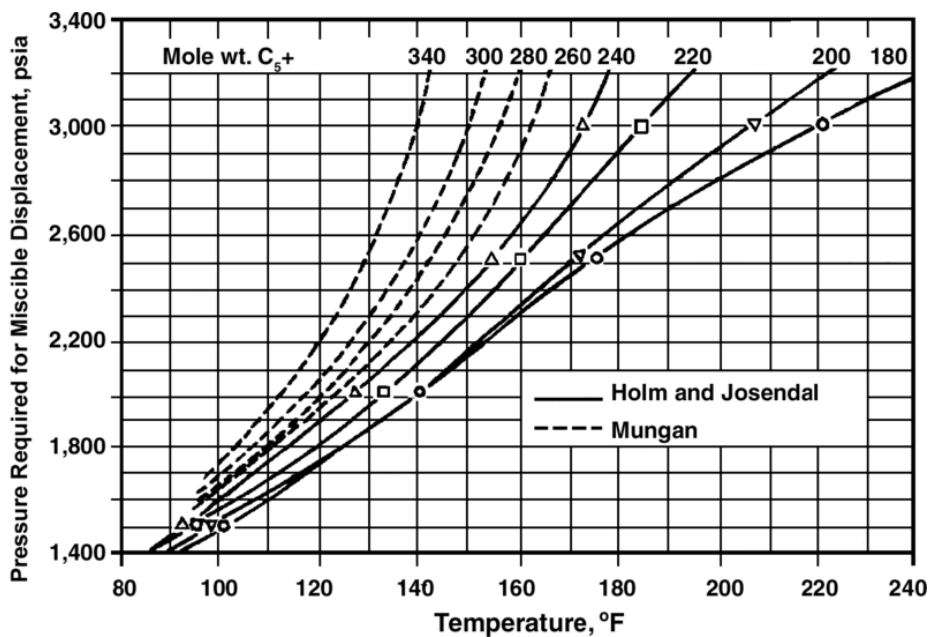


Figure 3.5: Correlation between temperature and the minimum miscibility pressure for oil with Various mole weight for the C₅₊ fraction [85].

Figure 3.2 shows the correlation between temperature and the MMP for oils with varying C₅₊ molar weight fractions. The graph shows that, for light oils, a reservoir of 100°C (212°F) and a pressure of 250 bar as proposed in the dissertation of Randolph [37], would be suitable for miscible displacement. This temperature-MMP corresponds to regions with a low to moderate thermal gradient of 30-35°C/km. For regions with higher geothermal gradients this might mean that the reservoir either has to be over-pressurized, additives have to be added to decrease the MMP. Displacement might also place according to an immiscible or partially miscible regime.

CO₂ purity

The purity of the CO₂ stream that is injected into the subsurface is one of the main factors that determines the miscibility. The presence of impurities (e.g., methane, H₂S and N₂) or intermediate hydrocarbons components (such as ethane, propane, and butane) in the injected gas strongly affects the MMP. Depending on the type of component their presence either raises or lowers it [81].

The presence of H₂S, as well as intermediate

hydrocarbons, generally reduces the MMP whereas the presence of methane and nitrogen can severely increase the CO₂-oil MMP [86]. Nitrogen is often present in the flue gas after the burning of fossil fuels and methane is often co-produced with oil production. Both these substances are difficult and costly to separate. Figure 3.3 presents the sensitivity of various factors that affect the MMP. In this figure, *TR* is the temperature of the reservoir, *Vol., %* is the mole percentage of volatiles (CH₄ and N₂), *C1*, is the mole percentage of methane, *MWC₅₊*, is the Molar weight of C₅₊ fraction and *interm., %* is the mole fraction of Intermediates components (C₂H₆, C₃H₈, C₄H₁₀, H₂S and CO₂). Table 3.2 shows the compositions of CO₂ captured from various anthropogenic sources.

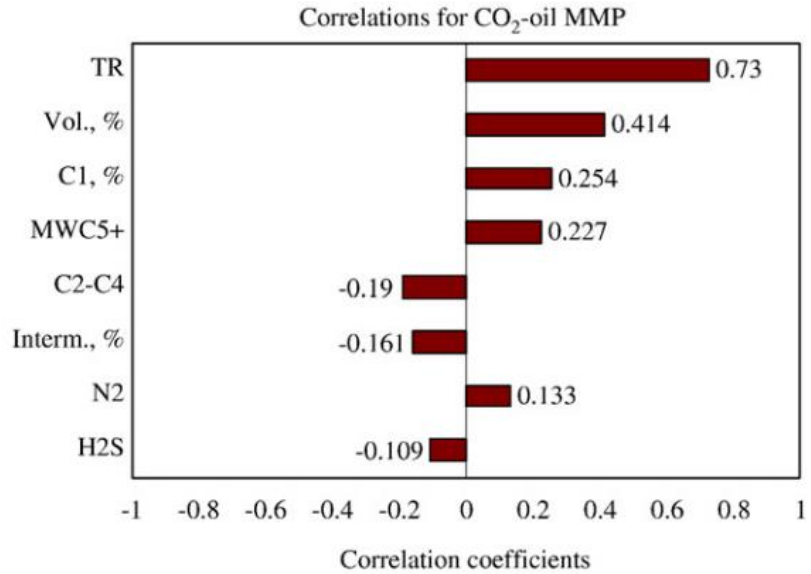


Figure 3.3: Sensitivity analysis of the new CO₂-oil MMP model and the dependence of CO₂-oil MMP on each of the independent variables [81].

Table 3.2: Compositions of CO₂ captured from anthropogenic sources [87].

Component	Natural gas combustion	Coal-fired ⁵	Coke production	Portland cement	Lime production
CO ₂	99,7000%	99,8000%	99,4000%	99,0000%	99,5200%
CO	0,0814%		0,0701%	0,1620%	0,2000%
N ₂ O	0,0018%				
NO ₂		0,0019%			
NO _x	0,2330%		0,1690%	0,3330%	0,1100%
HCl		0,0006%	0,0027%	0,0066%	
SO ₂	0,0500%	0,1258%		0,4410%	0,1700%
SO ₃		0,0154%			0,0100%
SO _x			0,3030%		
CH ₄	0,0019%		0,0206%		

⁵ Relative Proportions in Separated CO₂ Stream with Low NO_x Burners, Selective Catalytic Reduction, and Wet Flue Gas Desulfurization Scrubber (%[w])

Pressure

Pressure differences are the driving force behind oil production. Large enough pressure differences are necessary to drive the oil towards the production well. In the case of CO₂-flooding, the pressure furthermore is a critical factor in determining miscibility and therefore oil mobility. Although the theoretical minimum (Pressure/MMP) ratio is 1, in reality, miscible displacement can still occur at a ratio of 0.95 [84].

Permeability

The average permeability is not considered to be a limiting factor for CO₂-EOR projects since EOR is a consecutive step to primary and secondary oil recovery. Reservoirs that inhibit permeability that is too low (tight reservoirs) for CO₂-injection will have been deemed unsuitable for these previous recovery steps. CO₂(sc) has a higher mobility than water or oil, sufficient injection rates can easily be maintained while keeping safe pressure differences, due to the low surface tension [24] [84]. The spatial variance of the permeability of the reservoir, however, is more relevant. High permeability pathways through the reservoir cause viscous fingering limiting the sweep efficiency.

In 2005, Ehrenberg and Nadeau compared the average porosity vs. depth for 30,122 siliciclastic petroleum reservoirs and 10,481 carbonate oil reservoirs covering all petroleum-producing countries except Canada [88]. They also looked at the porosity and permeability relations for the two reservoir types. Figure 3.4a and b represent the trends for porosity decrease with depth and the porosity-permeability relations respectively.

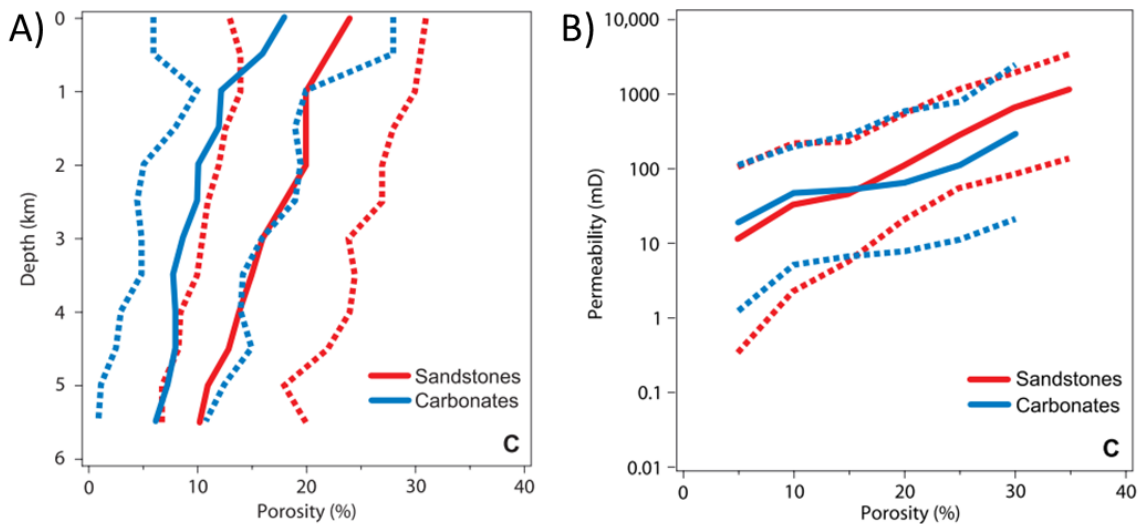


Figure 3.4: The relationship between reservoir porosity and depth (A) and reservoir porosity and reservoir permeability for carbonate (blue) and sandstone (red) reservoirs. The dotted lines represent the 10% and the 90% boundaries. Hence, 80% of the reservoirs falls within these boundaries [88].

Swept area

The swept area is the part of the reservoir that is touched by the supercritical CO₂. A simple volume estimation can be made for the bulk volume that will be affected by CO₂ injection using equation 3.1 [35].

(Eq. 3.1)
$$V_{bulk} = \frac{1}{\psi} \frac{V_{CO_2(inj-pro)}}{\phi}$$

In this formula the affected reservoir volume (V_{bulk}) depends on the injected volume (V_{CO_2}), the average formation porosity (ϕ) and the displacement efficiency coefficient (ψ). This later term can be extremely low in the case of closed hydraulic boundary conditions and multiple injection wells. The displacement efficiency is mainly affected by the mobility ratio (relative permeability/viscosity) of CO₂, brine and the oil, the gravity segregation and the reservoir heterogeneity [84].

Lithology and formation type

Although formation type and thickness have not been found to have significant effects on CO₂-EOR performance [89]. CO₂-EOR can take place in both carbonate and sandstone reservoirs, the latter are slightly preferred because of the flow properties. Carbonate reservoirs are often highly fractured and, therefore, inhibit a network of preferential flow paths. This causes the CO₂ to pass large parts of the reservoir reducing the sweep efficiency. In sandstone reservoirs, the pore space is spread more homogeneously over the reservoir, reducing the risk of preferential flow through just some pathways.

Well configuration

Depending upon the previous well setting, CO₂-EOR injection wells may be either drilled as new wells or re-completed by converting an existing producing well or a water injection well to a CO₂ injector [20]. The well density needed for efficient extraction strongly depends on the reservoir morphology and flow characteristics.

The ratio between injection and production wells in a CO₂-EOR project strongly depends on whether WAG injection or continuous CO₂ injection is used. For WAG injection, the ‘rule of thumb’ is that there be a rough balance between producers and injectors. Hence, the maturity of the field and the choice of injection strategy together determine whether or not extra wells are needed [90]. Wells can be drilled vertically, as is the case in most current EOR projects or horizontally, to enhance the sweep efficiency [91]. Table 3.3 shows the injection production well ratio and well density for the six largest EOR projects (in 1999) [90].

Table 3.3: Well configurations for the six largest EOR projects in 1999 modified from [90].

Operator	Field	Injection strategy	Area (km2)	Production wells	injection wells	I/P	density (pro)	density (inj)
Altura	Wasson	WAG	113	735	385	1,9	6,5	3,4
Amerada Hess	Seminole	continuous	64	408	160	2,6	6,4	2,5
Chevron	Rangely Weber Sand	WAG	61	341	209	1,6	5,6	3,4
Exxon Mobil	Salt Creek	WAG	49	137	100	1,4	2,8	2,0
Devon Energy	SACROC	continuous	202	325	57	5,7	1,6	0,3
Altura	Wasson (ODC)	WAG	32	293	290	1	9,2	9,1

Screening criteria EOR

CO₂-EOR experience over past projects performed in the US shows that successful CO₂-EOR operation depends on the following criteria [25]:

- The technical criteria for achieving miscibility (primarily depth and oil composition) must be met.
- The reservoir must contain sufficient unrecovered oil after primary and secondary recovery (water flooding).
- The project must have access to reliable sources of high purity CO₂ at affordable costs.
- The oil price must be adequate.
- Have operators with the necessary capital, technical expertise and also corporate culture to accept the inherent uncertainties associated with designing and executing CO₂-EOR projects.

This study focusses on the first of these criteria. Various studies have focused on predicting the potential for miscible CO₂-EOR in reservoirs. Table 3.4 provides an overview of the most relevant screening criteria that affect the potential for miscible oil displacement. Although the effects of impurities in the injected CO₂ are significant, it is not included in the table since the effects vary per species and can be limited by surface separation.

Table 3.4 reservoir screening criteria for miscible CO₂-enhanced oil recovery.

Source	Depth (meter)	Temperature (°C)	Pressure (Bar)	Permeability (mD) ⁶	Oil gravity (°API)	Viscosity (cP)	Saturation % PV
[92]			> 75		>30	< 3	> 25%
[93]	> 914		> 103		>30	< 12	> 25%
[94]	> 701	< 121			>27	< 10	
[95]	> 609			> 5	>35	< 5	> 25%
[80]	> 762			> 10	30-45	< 10	> 25%
[96]	> 762				> 27	< 12	
[97]	> 2987	< 90	> 83	> 1	>40	< 2	> 30%
[98]	> 609				>26	< 15	> 30%
[24]	> 762				>22	< 10	> 20%
[82]	> 762	< 130	> 75	> 10	>27	< 10	20-50%
[99]	609 - 3000	<121 ('not critical')	>83	>1/5	>27	<10	>25%

3.4 Reservoir criteria for CPG

CO₂-plume geothermal is a new concept. Therefore, no extensive research has been done yet on the reservoir criteria that affect its deployment. No commercial or pilot reservoirs exist yet from which data can be acquired. The most important parameters affecting the reservoir suitability for CPG are temperature, pressure, depth, lithology, and configuration of the system. This section will elaborate on each of these parameters individually.

Temperature

The temperature of the produced CO₂ is very important as it determines the Carnot efficiency according to equation 2.4. Compression in a pump or compressor and expansion over a turbine are isentropic processes. At low temperatures isentropic profiles in a Mollier diagram are steeper, meaning a lower enthalpy difference for a change in pressure. Since less energy has to be added, this is the P-T region that is commonly used for compression in geothermal systems.

⁶ One milli-Darcy (mD) is equivalent to $9.869233 \times 10^{-16} \text{ m}^2$

Especially in regions with a low ambient rejection temperature, the use of CO₂ as a working fluid can be highly efficient. Figure 3.5 shows the Mollier diagram for a rejection temperature of 20°C compared to a rejection temperature of 10°C for a reservoir of 100°C, 100 bar.

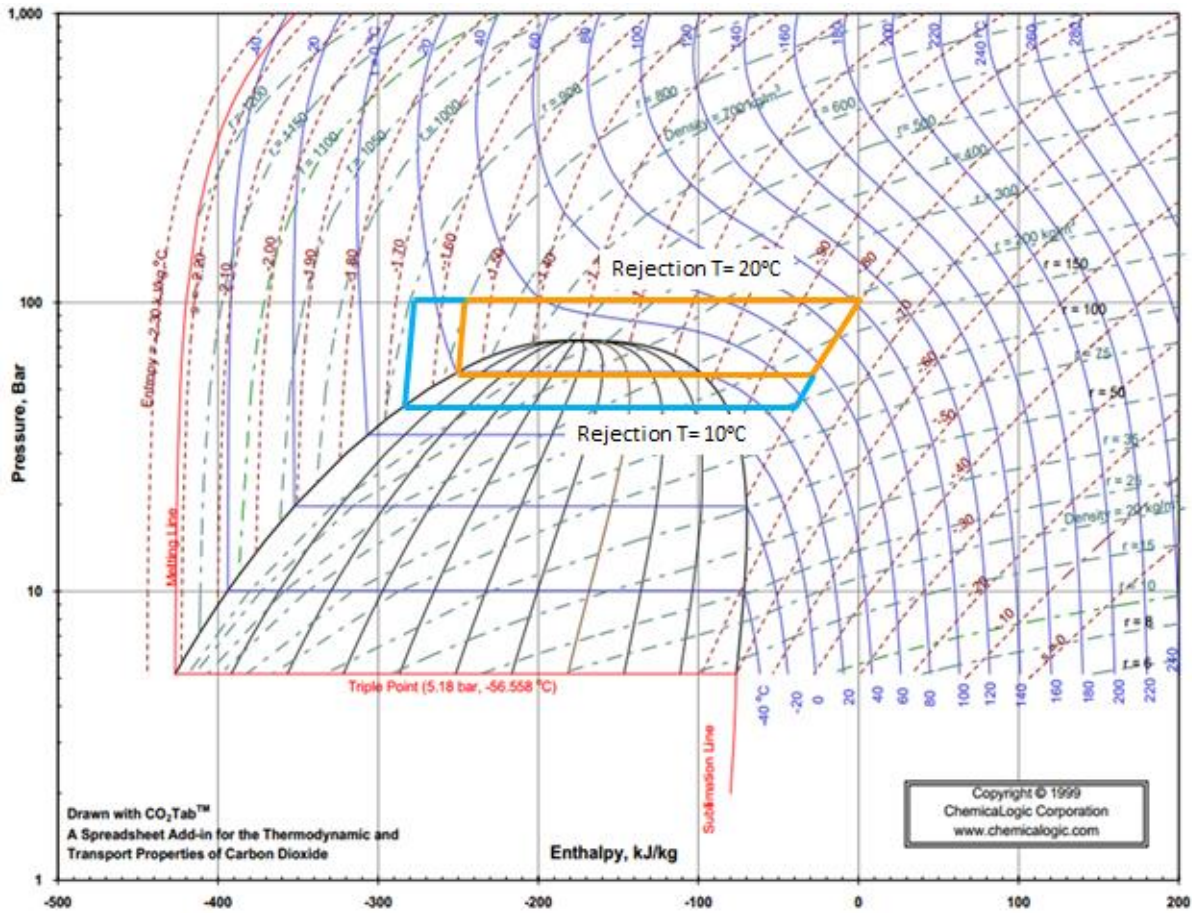


Figure 3.5: Heat extraction cycle with a rejection temperature of 20°C (orange) vs. a rejection temperature of 10°C (blue).

Pressure

For efficient pumping, it is important that a single dense phase is present. This requirement calls for a minimum pressure at the injection wellhead. High reservoir pressures lead to a reduction in overall enthalpy gain caused by the heating of the CO₂ in the reservoir. Hence, the rate of energy extraction is much lower in high-pressure reservoirs.

The pressure drop over the reservoir determines the flow rate through the reservoir and, therefore, the heat extraction rate of the system. If the pressure drop over the reservoir is too high, this might lead to induced seismicity and leakage of CO₂ from the reservoir. Because of the low viscosity/density ratio of CO₂ pressure drops in CO₂ systems are typically much lower than in water or brine based systems.

Depth

The depth of the reservoir determines the magnitude of the static and friction induced pressure reduction over the production well. High static pressure drop over the well leads to a high-temperature reduction due to Joules Thompson cooling. Furthermore, the depth strongly affects the costs for wells as this exponentially increases with depth [100].

Salinity

As was shown in figure 2.15, the salinity of the brine in the system affects the amount of mineralization that will take place. Depending on the amount of dissolved salts, CO₂ dissolution might lead to dissolution (permeability enhancing) or precipitation (clogging) of reservoir minerals [73].

Furthermore, during the drying phase, H₂O dissolution into the supercritical CO₂ stream will mean the concentration of the brine will become higher leading to the precipitation of solid salts. This salting-out effects may block flow paths and thus reduce porosity and permeability. Higher salinity brines will, therefore, lead to higher permeability reductions during the drying phase. In general, the salinity of brines in hydrocarbon reservoirs increases with depth [101]. Figure 3.6 shows the salinity vs. depth relation for several reservoir formations in the U.S. and one in Russia.

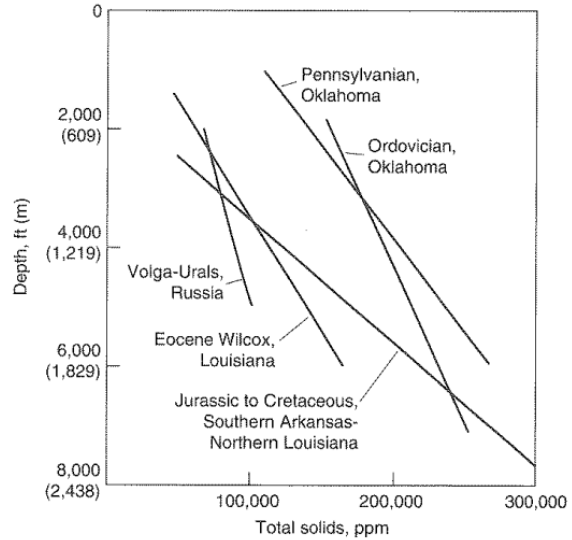


Figure 3.6: salinity increase in hydrocarbon reservoirs with depth [101].

Flow rate

Inconsistencies in the literature exist on the effect of flow rate on the temperature at the wellhead of the production well. A comparative modelling study was performed by Athrens et al. (2010) into the performance of CO₂ and H₂O based thermosiphon systems. They found that for their reference case, a CO₂ based system produces less exergy⁷ than an H₂O based system [102]. This is mainly due to the lower heat capacity of CO₂ and the high temperature decrease in the production well due to Joule-Thompson cooling. CO₂ systems primarily perform better in the case of high impedance reservoirs and shallow engineered reservoirs. The exergy losses due to reductions in pressure and temperature occurring in the production wellbore are strongly increased at higher flow rates through the friction component. This effect is much stronger for CO₂ than for water due to its high compressibility. To reduce this effect, CO₂ based systems would benefit from larger diameter production wellbores and a higher production well to injection well ratio.

A different modelling study performed by Pan et al. (2014), looked at the pressure and temperature profiles in the production and injection wells [79]. They state that flow through the wellbore cannot be considered isenthalpic as heat exchange takes place with the surrounding formations. For a duration of 30 years, for a 152,2°C, 29.15 Mpa reservoir at low (5kg/s) and high (25kg/s) Flow rates, they have modeled pressure, density and temperature changes in the wellbores. Figure 4.7 shows the profiles for the production- (a and c) and injection (b and d) well. In contrast to Athrens et al. (2010) [102], they find significantly higher wellhead temperatures at higher flow rates.

⁷ The exergy is the potential of a system to cause a change as it achieves equilibrium with its environment.

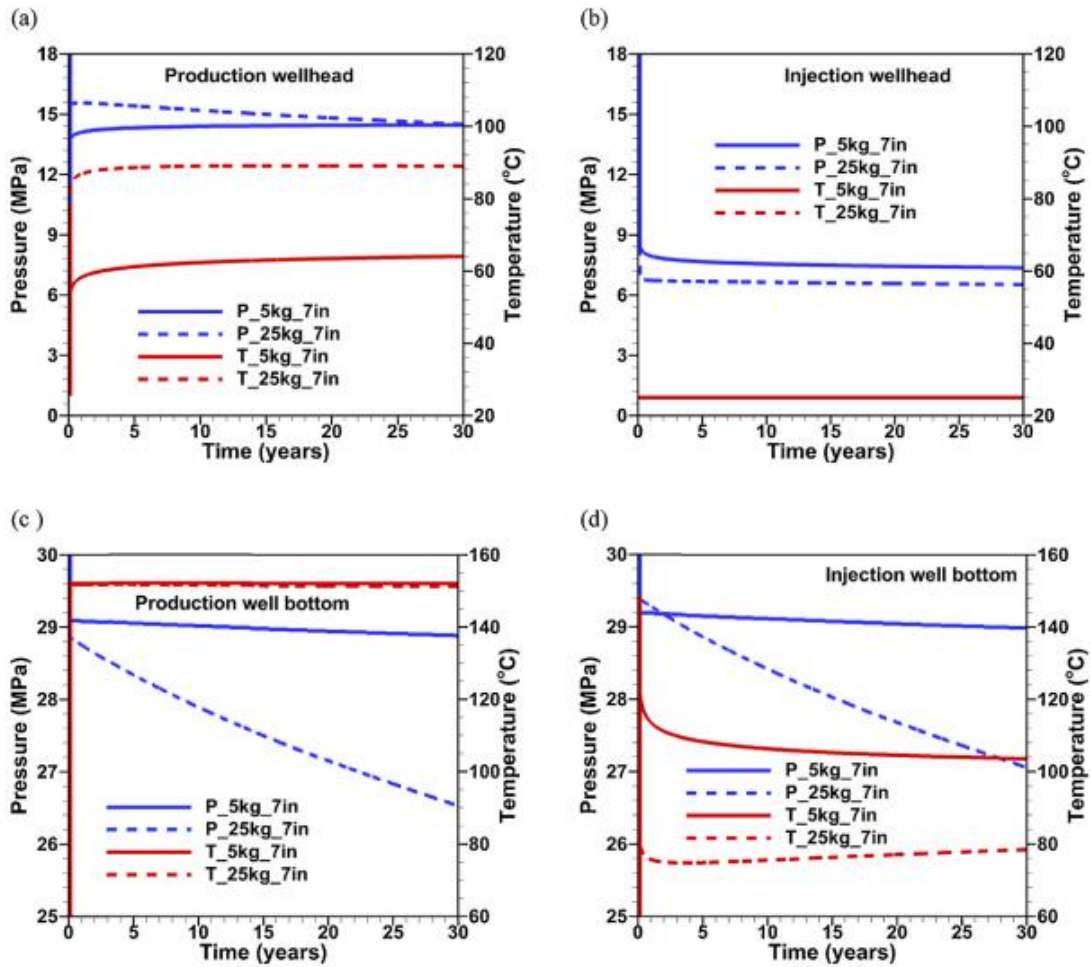


Figure 3.7: Temperature and pressure profiles over the lifetimes of the CPG system for (a) the production wellhead (b) the injection wellhead (c) the production well bottom and (d) the injection well bottom [79].

Lithology

The importance of lithology lies in its effect on various properties. First of all it influences important factors like permeability via the density, size distribution and geometry of the grains. Secondly, the mineralogy effects the available reactive species in the formation brine as explained in section 2.4.1.

In the case of geothermal heat extraction, the rock type has an additional importance. The amount of heat that can be extracted from a formation can be calculated from its size, rock grain density, temperature, rock specific heat, thermal conductivity and replenishment heat flux. Most of these parameters are rock specific. These parameters will be shortly discussed for the two most commonly used reservoir formations, sandstone and limestone reservoirs.

Thermal conductivity (K)

Thermal conductivity of a reservoir formation is not constant but depends on temperature, presence of fluids or gasses in the pores and mineral presence. For both sandstone and limestone, temperature has a negative effect on thermal conductivity. Within the temperature range associated with CPG, this effect is a slightly stronger for sandstone reservoirs.

Table 3.5 shows the thermal conductivity range of sandstones and limestone's, depending on porosity at 27°C, 5Mpa. The uncertainty range in sandstones is based on quartz content of the formation varying from 30% (min) - 90% (max). The data was calculated from the USGS report on thermal properties of rock types [103]. The conductivities presented in the table are based on water in the pores ($K_{H_2O} = 1.46$).

Table 3.5: Thermal conductivity of different reservoir formation types [103].

Thermal conductivity in (10^{-3} W/cm °C)					
Porosity (ϕ)	10%	15%	20%	25%	30%
Limestone	25,54	24,28	21,35	18,84	17,17
Sandstone (min) ⁸	20,93	21,35	23,03	24,70	29,31
Sandstone (max) ⁸	40,61	43,54	46,89	50,24	61,96

Rock specific heat (C_p)

The Rock specific heat of a formation depends on the mineral composition of the rock. The specific heat of a mineral increases with temperature. For sandstone, typical specific heat is 0.92 kJ/kg °C. For limestone, this is 0.908 kJ/kg °C [104].

Bulk density (ρ)

The bulk density of a reservoir depends on the porosity of the formation, its mineral composition, whether it is saturated and the pore fluid and the level of consolidation. Typical Bulk densities for sandstone reservoirs vary from 0.22 g/cm³ to 0.27 g/cm³ ($\phi=0.007$). For limestone reservoirs these values range from 2.6 g/cm³ ($\phi=0.05$) to 2.7 g/cm³ ($\phi=0.005$) [103].

Permeability (k)

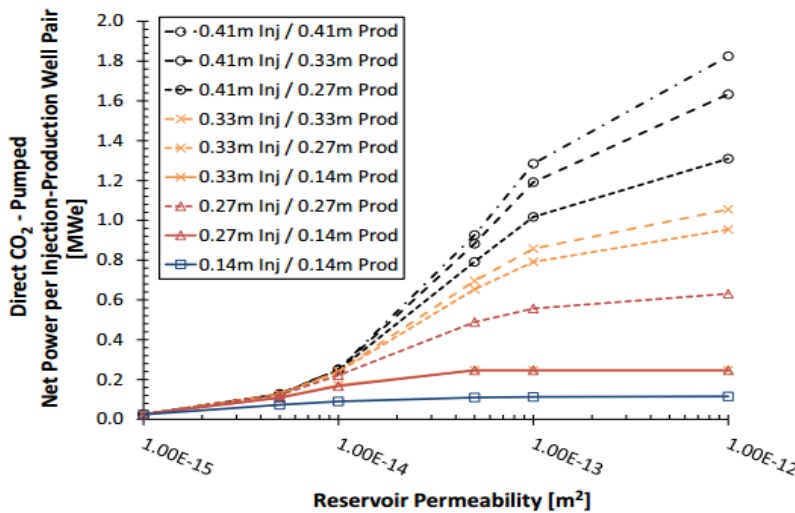


Figure 3.8: Results of numerical simulations of electricity production efficiency (net electricity production divided by thermal energy extracted from the reservoir) versus reservoir permeability (k) and well diameter [138].

Because of the high mobility of supercritical CO₂ compared to water or brine, CO₂ based systems have a clear advantage when it comes to low permeability reservoirs. Figure 3.8 shows the production power correlation with the reservoir permeability and well diameter for a direct-CO₂ system in a 100°C, 250bar reservoir. In permeability's that are often present in hydrocarbon reservoirs, CO₂ performs significantly better than water or brine based systems [105].

⁸ The minimal and maximal conductivities are based on a quartz content range of 30% (min) to 90% (max).

Well configuration

Besides the static losses due to pressure reduction and Joules-Thompson cooling, efficiency losses in the wellbore are caused by conductive heat transfer and friction with the pipe. Figure 3.8 illustrates the importance of wellbore diameter on the production efficiency of the geothermal system. The friction component of these losses is significantly higher than in water or brine based systems due to the gaseous nature of CO₂. Besides the wellbore diameter, the roughness of the pipes is an important parameter determining the pressure and temperature losses over the wellbore [106]. Especially at higher pressures, the effect of doubling the well diameter could weigh up against the additional costs [106].

The majority of the friction induced energy losses in a CO₂ thermosiphon take place in the production well. To reduce the flow rate over the production well would mean a significant reduction of these friction losses. Therefore, especially at higher pressures, it would be beneficial to have larger number of production wells than injection wells. Figure 4.9 presents the temperature profile of supercritical CO₂ through the reservoir. A well distance of 600 meters is sufficient to obtain the maximum temperature at a heat extraction rate of 50MW over the first ten years of production.

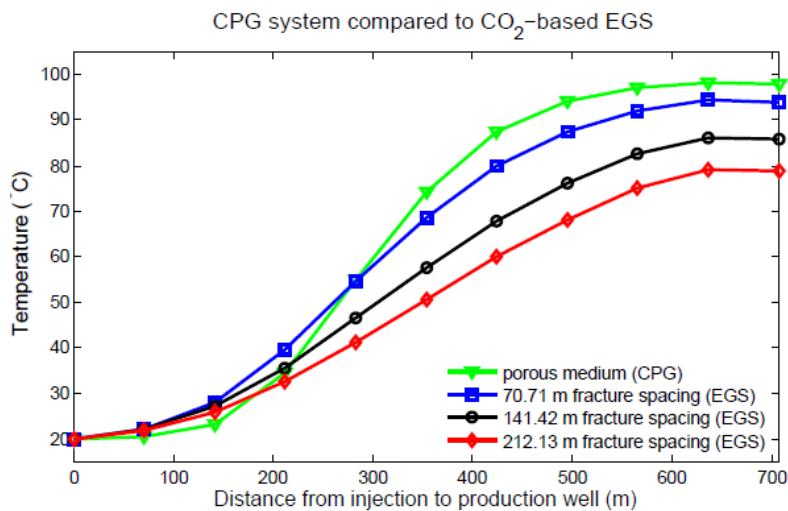


Figure 3.9: Reservoir heat profile for CPG ($k = 5 \times 10^{-14} \text{ m}^2$) and fractured geothermal energy recovery after ten years of production at a heat extraction rate of 50 MW [37].

3.5 CO₂-Plume Geothermal - Enhanced Oil Recovery (CPG-EOR)

This section covers the advantages and pitfalls of the different proposed configurations and motivates the choice for the chosen configuration for the modelling phase of the research. Three different configurations are proposed sharing the same CO₂ capture plant, infrastructure and monitoring equipment: 1) consecutive oil and heat production 2) parallel heat and oil production 3) combined heat and oil production. Appendix I shows a schematic view of each of the configurations with their respective production and sequestration profiles over time. For each of the configurations, the benefits and barriers will be assessed based on the parameters identified from the first step. The third phase models the CPG in the reservoir.

The consecutive configuration exists of a first phase of just EOR. After oil production is no longer economically viable, the reservoir is flushed with supercritical CO₂. The flushing stops at a point where the level of impurities (hydrocarbons and water) is low enough to not impose problems for CPG heat extraction using a binary or direct system. This is very similar to the current methodology of starting up a CPG project in a formation containing just brine.

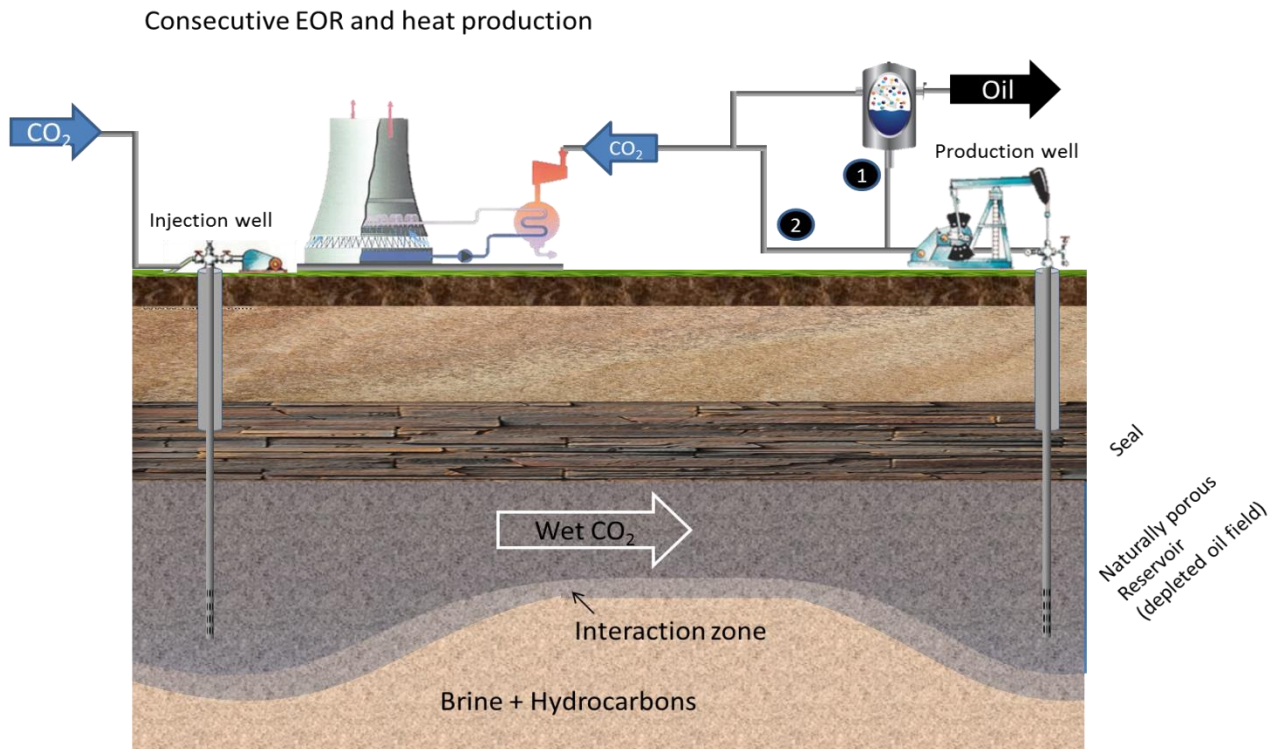


Figure 3.10: The consecutive configuration for CO₂-EOR and CPG. During the EOR stage, CO₂ will pass the recycling plant and be re-injected, when the stream is pure enough, the CO₂ will be passed through the turbine and then be re-injected.

Advantages of the consecutive deployment are that, because the same reservoir is used, reservoir knowledge, monitoring equipment and infrastructure can be reused. The fact that the reservoir successfully contained hydrocarbons for long periods of time is a strong indicator that there is a quality seal present.

From a CPG perspective, the previous injection of CO₂(SC) in the formation is favorable as this might limit the startup time before the CO₂ stream is pure enough to be utilized in a turbine. Furthermore, as the surface infrastructure is already in place, hydrocarbons that are produced alongside CO₂ during this phase can still be separated and sold. However, at some point the stream of CO₂ may become too big for the existing surface infrastructure to separate. On a field scale, EOR and CPG might happen simultaneously as sections of a field are often separately exploited.

The most important barrier for this configuration is that the MMP of oil with CO₂ increases with an increase in temperature. For this reason, CO₂-EOR either has to take place in deep reservoirs or at relatively low-temperature reservoirs limiting the amount of energy that can be extracted. Another option is that CO₂ takes place under immiscible conditions limiting the efficiency of the EOR. Possible additional barriers for this configuration are that previous production methods in

the reservoir might have affected the reservoirs suitability for CPG. Although most oil recovery mechanisms aim to enhance permeability and are, therefore, beneficial for CPG, the use of viscosity enhancers during EOR to improve sweep efficiency might negatively affect the mobility of CO₂ during the CPG phase. More research is necessary on the effects of viscosity enhancers in later stages of reservoir utilization. Unless WAG injection is used, this preliminary efficient sweep might even enhance the flow potential of CO₂ through the reservoir through a reduction of immiscible multi-phase flow.

Another possible barrier for the consecutive configuration is that the reservoir might have already lost heat during the previous cycles of oil production. Monitoring data from CO₂-EOR projects shows that temperature decline over the years of oil production is negligible.

The parallel configuration implies that after CO₂-EOR has initiated, and the demand for CO₂ declines, a different non-hydrocarbon holding formation in the vicinity or below the reservoir is used for CO₂-EGS. This way, the systems still share critical infrastructures like capture facilities, transport pipelines, compressors and monitoring equipment. An additional advantage is that it is possible to use a deeper and hotter reservoir for CO₂-EGS while using a colder reservoir for EOR, reducing the minimum miscibility pressure (MMP). As the temperature potential here is higher, it might be possible to use produced heat for preheating the CO₂-hydrocarbon mixture for separation.

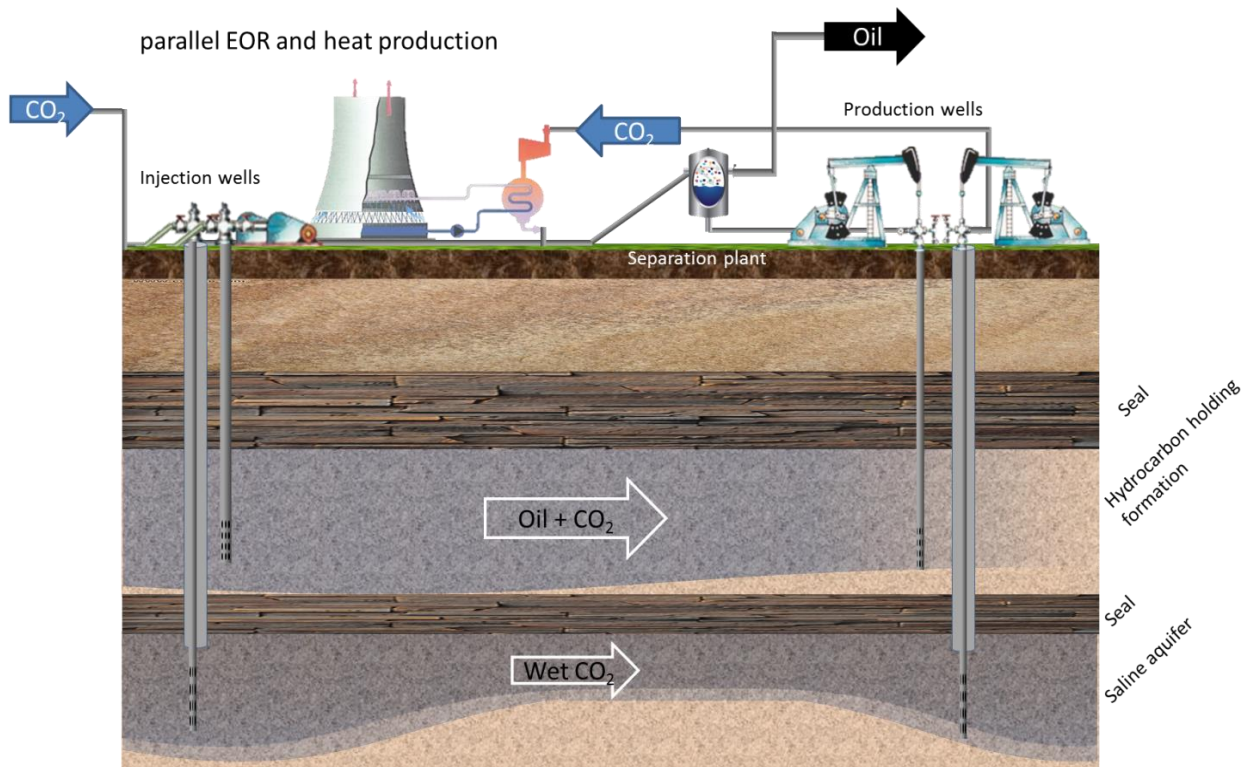


Figure 3.11: The parallel configuration for CO₂-EOR and CPG. The CO₂ injection will first take place in the oil, holding formation. If CO₂-EOR is finished, CPG will take place in a different formation while using much of the same infrastructure.

The advantage of the parallel configuration is that a deeper unaffected reservoir can be used that can be hotter and at higher pressure and specifically chosen for its geothermal properties. Although this research focusses on CPG, the geothermal formation might, in this case also be an

engineered (fracked) formation, as it is not bound to the criteria for EOR. This would reduce the startup time and thus simplify the system.

Barriers for this configuration are that since the formation has not been used before, only a small portion of the infrastructure can be reused. Wells will still have to be drilled, and a higher reservoir pressure will mean higher compressor capacity is required.

As the CPG-formation has not been previously injected with CO₂, it will take more time before the CO₂ stream is pure enough to meet turbine criteria. During this startup phase, Operating costs are high as the CO₂ will have to be separated and re-injected, and much CO₂ will remain trapped in the reservoir.

The combined configuration is the most technically challenging option as, in this case, the CO₂ will have high levels of impurities and compositional inconsistency. The produced stream of CO₂, brine and oil brings up heat from the reservoir. By utilizing not only the produced oil but also the heat recovered from the reservoir it might be possible to keep EOR operations profitable for a longer time. To utilize the heat for electricity generation, a binary system is required using a purer working fluid. This methodology for combining CPG with EOR was first suggested by Randolph and Saar (2011) (figure 2.12) [19].

If it is possible to utilize heat from the CO₂ and water that is already being produced alongside the oil, this would mean a bolt on system onto a conventional CO₂-EOR configuration. Because of the composition of the produced fluid, a binary system is required for the energy extraction.

Although this is the configuration that is proposed by Randolph and Saar (2011) [19] it does not appear very lucrative from a thermodynamic perspective. Because of the high Joules Thompson cooling associated with the depressurization of CO₂ in the production well, temperatures at the surface will not be very high. Due to the efficiency losses associated with a binary system, higher production temperatures ($\pm >100$ °C) are needed to make indirect electricity production lucrative. Looking at the temperature range in current CO₂-EOR projects, to the knowledge of the author, none of the current fields meets this criterion.

Further complications arise with processing the produced stream into oil, gas, pollutants and recycled CO₂. Many of these separation processes require the addition of additional energy that makes initial energy extraction an illogical choice. Heavy hydrocarbons are significantly more mobile at high temperature. Cooling them after production increases their viscosity making them much harder to handle.

Additional pitfall for all the technologies might be the deposition of solids in the system causing clogging. More research is needed into the reactivity of dry CO₂ with reservoir minerals at elevated pressures and temperatures. However, as long as there is still brine in the system, the CO₂ saturated brine will transport some mineral species. If deposition of these species takes place in the system due to temperature and pressure drops, this might lead to clogging.

For the modelling work in this thesis, the **consecutive configuration** was selected for the following reasons:

- Reservoir criteria for CO₂-EOR and CPG overlap, thus the same reservoir may be used.
- No insurmountable barriers for the deployment were identified.

4. Modeling in Matlab

The modelling study was performed using Matlab and consisted of three separate steps. The first step focused on the CO₂-EOR phase of the project and lasted to a point where injection would normally be stopped. The second phase focused on the drying period (flushing) of the reservoir to the point where the CO₂ percentage in the production stream was high enough to allow direct turbine operation. The final phase of the modelling describes the CPG part. The Matlab scripts used to calculate the different phases are included in Appendix I to XVI.

4.1 Site selection

A fictional reservoir will be assessed based on the parameters that were identified in the literature study. In the case of the combined configuration and the consecutive configuration, reservoir parameters were chosen that matched both the criteria for CO₂-EOR and CPG. Table 4.1 lists the input parameters that were chosen for the reference case.

Table 4.1: Input parameters for the reference case modelling study in Matlab.

Input parameters for the calculation			
	Parameter	base quantity	Unit
Reservoir	Massflowrate production well	120	Kg s ⁻¹
	Reservoir pressure	50	Mpa
	Reservoir temperature	225	°C
	Distance between wells	707.1	m
	Ambient temperature	15	°C
	Geothermal gradient	45	°C km ⁻¹
	Reservoir permeability	1.4E-14	m ²
	Reservoir depth	5000	m
	Porosity	10%	
	Height of the reservoir	300	m
Wells	CO2 storage factor	0,5%	
	Injection well diameter	0,23125	m
	Production well diameter	0,23125	m
	Number of injection wells	1	#
Hydrocarbons	Number of production wells	4	#
	Specific gravity of the oil	32	°API
	Oil pore volume fraction	60,00%	
	OOIP	113216590	bbbl
	Oil to CO2 ratio	2.5	Bbl t _{CO2} ⁻¹
	Recovery factor	15.00%	
Thermal	Rock specific heat	920	J kg ⁻¹ K ⁻¹
	Thermal conductivity	2.1	W m ⁻¹ k ⁻¹
	Rock grain density	2650	Kg m ⁻³
	volume of the reservoir	250000	m ³

The properties chosen for the reservoir correspond to a sandstone reservoir in a region with a geothermal gradient of 45 °C/km and an ambient temperature 15°C. At the reservoir depth and pressure, the ratio (P/MMP) ranges from 1 to 1.2 depending on the exact oil gravity. The oil type and oil saturation both fit well within the range of current CO₂-EOR projects (27 - 44 °API, 15-70 %PV) [24] [20]. For the reference case, the reservoir permeability is set to 1,7E-12 m² (17mD). The effect of lower permeabilities was also assessed. A five-spot well pattern was used, covering a total area of 1 km² based on earlier modelling studies performed by Randolph, 2011 [37].

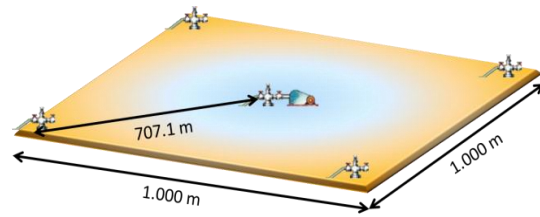


Figure 4.1: five-spot well configuration as used in the modelling .

4.2 Modelling assumptions

The analysis described in this paper is based on steady-state conditions and a number of assumptions:

- 1) **The reservoir has been assumed to be homogeneous**, which is unlikely to be the case in reality. However, since there is no data on the amount of heterogeneity in the reservoir, this is a common assumption.
- 2) **The reservoir formation is non-reactive**. This assumption is believed to be reasonable for the untouched formation brine and the supercritical CO₂ in a sandstone formation. The brine has had ample of time to equilibrate with the formation mineralogy, and dry supercritical CO₂ is a poor solvent for rock minerals. The CO₂ saturated brine, however, will be reactive with some reservoir as well as caprock minerals. However, these reactions will occur so slow and mainly localized at the edges of the flow system, that they will be of limited influence on the flow dynamics.
- 3) **Heat transfer from the wells to the surrounding rock is neglected**. For the injection well, this is reasonable due to the limited temperature difference between the borehole and the surrounding rock over most of the length of the well, and the poor conductivity of the rock. Heat transfer to the surroundings is expected to be higher in the production well than the injection well due to the larger temperature difference between the production well and the surrounding rock. However for the same reasons as discussed above, it is still expected to be low. Any heat losses in the production well will also be smaller for the CO₂ thermosiphon than for the water-based EGS, due to the lower temperatures of the CO₂ flow, leading to smaller driving forces for heat transfer.
- 4) **The reservoir fluid is assumed to follow a linear temperature increase with distance** from the injection well in order to simplify the calculation. In reality, the temperature profile in the reservoir changes throughout the life of the EGS project. However, a general model of low temperatures near the injection well, and high temperatures near the production well is likely to be valid throughout the commercial operation period. As most of the reservoir pressure drop occurs in regions near the injection and production wells, changes in the temperature profile in other areas of the reservoir have only second-order effects.
- 5) **Uniform reservoir heat depletion over the entire swept area**. Although in a realistic scenario for reservoir depletion, the region closest to the injection well will deplete first creating a cold front that migrates towards the production well. However, the previous

assumption implies that if this were modelled accordingly, production temperatures would decline too soon. Furthermore, the effect of flow path will have to be implemented. The assumption of uniform reservoir depletion will limit the predictability with time, however over the total lifetime it is a reasonable assumption.

- 6) **The CO₂-injection rate stays the same during the CO₂-EOR phase.** The oil/injected CO₂ ratio and thus the oil production follow a lognormal curve. In a normal EOR project, operators might choose to alter the CO₂ injection rate in order to keep production up.
- 7) **Reservoir pressure increases hydrostatically with depth.** This assumptions is conservative as under an impermeable layer; reservoir pressures tend to be in between hydrostatic and lithostatic. Furthermore, the initial pressure strongly depends on the previous phases of primary (pressure drop) and secondary (pressure increase) oil production.

4.3 The CO₂-EOR phase

The first step is modelling the enhanced oil recovery phase. This step will cover the process from the point where CO₂ injection starts, up to the point where CO₂-EOR becomes no longer economically viable and in a typical CO₂-EOR project, the injection of CO₂ would be terminated.

The first step is to determine whether displacement takes place according to miscible or immiscible principles. Equation 4.1 estimates the MMP for pure CO₂ based on the temperature (T_R), C₅₊ oil fraction (MWC_{5+}) and the ratio of the volatile oil fraction (X_{vol}) consisting of CH₄ and N₂ to the intermediate oil fraction (X_{int}) consisting of C₂H₆, C₃H₈, C₄H₁₀, CO₂ and H₂S [107].

$$\text{(Eq. 4.1)} \quad MMP_{pure\ CO_2} = 6.05 \times 10^{-6} (1.8T_R + 32)^{1.06} \times (MWC_{5+})^{1.78} \times \left(\frac{X_{vol}}{X_{int}}\right)^{0.136}$$

Hence, the presence of intermediate hydrocarbons including CO₂ and H₂S lowers the MMP while the presence of volatile species increases the MMP. Using formula 4.2, it is possible to calculate the molar weight of the C₅₊ fraction of the oil from the °API [108].

$$\text{(Eq. 4.2)} \quad MW\ C_{5+} = \left(\frac{7864.9}{^\circ API}\right)^{\frac{1}{1.0386}}$$

For the calculations, the composition of the reservoir oil was based on the composition of the Weyburn field hydrocarbons. In this field the $MW\ C_{5+}$ was 205 g/g mole [107], which corresponds to a gravity of ±32 °API.

Table 4.2: Composition of crude oil and CO₂.

	Formation oil [107]	injected CO ₂ [20]
N₂	0.96 %	0.6 %
CO₂	0.58 %	97 %
H₂S	0,3 %	
CH₄	4.49 %	2.4 %
C₂H₆	2.99 %	
C₃H₈	4.75 %	
C₄H₁₀	2.73 %	
C₅H₁₂	3.46 %	
C₅₊	79.74 %	

The composition of the injected CO₂ was based on the composition of CO₂ from the sheep mountain dome. These compositions were chosen because of their use in previous EOR-projects. Table 4.2 shows the composition of the reservoir oil and the composition of the injected CO₂ used in the calculations. To account for the effect of impurities in the injected CO₂ stream on the miscibility with crude oil, an impurity factor (F_{imp}) has to be added. This factor was calculated based on equation 4.3 [109].

$$\begin{aligned}
 \text{(Eq. 4.3)} \quad F_{imp} &= 1 - 0.0213 (P_c - 304.2) \\
 &\quad + 2.51 \times 10^{-4} (P_c - 304.2)^2 \\
 &\quad - 2.35 \times 10^{-7} (P_c - 304.2)^3
 \end{aligned}$$

Where P_c is the pseudo critical temperature of the mixture based on the mole fractions of the species in the mixture (f_i) and their respective critical temperatures (T_{ci}).

$$\text{(Eq. 4.4)} \quad P_c = \sum f_i T_{ci}$$

The impure MMP is then calculated by multiplying the pure MMP by the impurity factor. Based on the input parameters, Matlab determines whether displacement takes place according to miscible ($P > \text{MMP}$) or immiscible ($P < \text{MMP}$) principles.

If the reservoir conditions are favorable for miscible displacement, the oil produced using a simple box model. Figure 4.2 presents a schematic overview of the model used to estimate the CO₂-EOR phase. The main goal of this model is to provide the input CO₂-pore fraction for the drying and the CPG phase. Therefore, apart from the ones needed to estimate the lifetime, no revenue estimations will be made based on this phase.

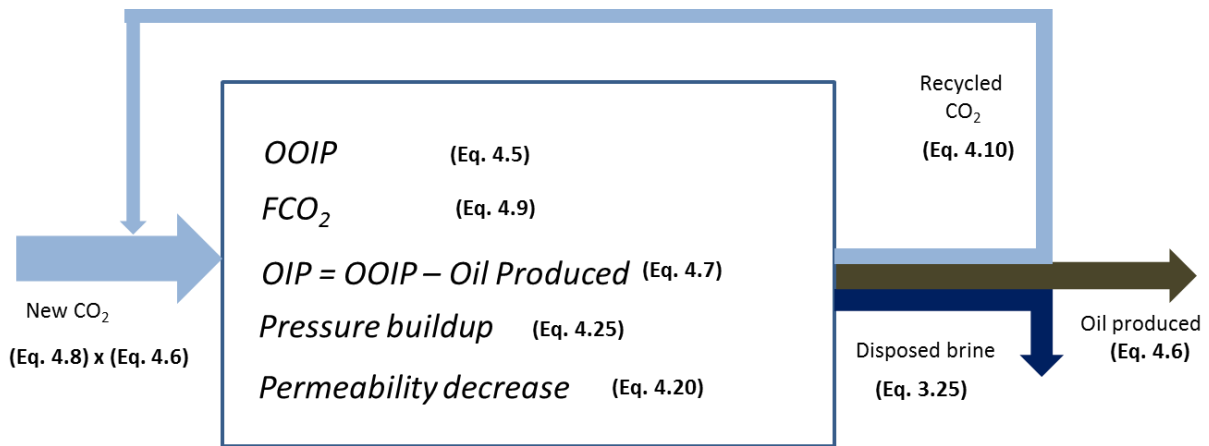


Figure 4.2: Schematic presentation of the box model used for the EOR part of the model.

An estimate for the OOIP was based on the reservoir dimensions, the original pore volume occupied by oil and the amount of barrels per cubic meter.

$$\text{(Eq. 4.5)} \quad OOIP = L \times W \times H \times \phi \times F_{oil} \times Vol_{oil}$$

In equation 4.5, the original pore fraction occupied by oil was taken to be 45%, and the amount of barrels per cubic meter pore volume was taken to be 6.2898 Bbl/m³ [24]. CO₂ injection over time is estimated using a lognormal distribution curve based on the methodology used in Element Energy (2012) [110]. Equations 4.6 and 4.7 describe the oil production and the cumulative CO₂-EOR oil production respectively from the time of injection (t=0).

$$\text{(Eq. 4.6)} \quad \Delta Oil = \frac{1}{t\sigma\sqrt{2\pi}} e^{-\frac{(\ln(t)-\mu)^2}{2\sigma^2}} \times SF \quad \text{(Eq. 4.7)} \quad Cum Oil = \frac{1}{\sigma\sqrt{2\pi}} \int_0^t \frac{e^{-\frac{(\ln(t)-\mu)^2}{2\sigma^2}}}{t} \delta t \times SF$$

Where $\mu = \text{mean}$ and $\sigma = \text{standard deviation}$
 $SF = \text{ScaleFactor} = OOIP \times \text{Recovery Factor}$

A delay factor of 2 years was built in, to account for the fact that the effects of CO₂ injection on oil production do not occur immediately after injection started. The standard deviation of the lognormal curve was taken to be 0.74 year, and the mean was taken to be two years after the delay period [111].

The recovery factor represents the total amount of additional oil production that can be extracted using CO₂-EOR as a percentage of the OOIP⁹. Recovery rate estimates show large variation, ranging from 4-9% from the European Committee to 10-20% from the US department of energy [111]. For the reference case, a recovery rate of 10% was used. The volume decrease in oil due to evaporation of volatiles and pressure losses were assumed to have been included in the recovery factor (this was not clear from sources).

The Oil/CO₂ ratio represents the ratio of oil produced in bbl for each tonne of CO₂ injected and is given by equation 4.8. The amount of CO₂ that is needed to be injected in order to produce a certain amount of oil is not constant over time but follows a lognormal pattern. This ratio also shows considerable variability and strongly depends on the reservoir. In this research, the amount of CO₂ injected for the oil production is calculated using an average ratio (*ARF*) of 2.5 bbl of oil/ t CO₂ [8]. The mean, delay and standard deviation were chosen to be the same as for Eq. 4.6 to create a constant injection rate.

$$\text{(Eq. 4.8)} \quad CO_2 Ratio = \frac{1}{t\sigma\sqrt{2\pi}} e^{-\frac{(\ln(t)-\mu)^2}{2\sigma^2}} \times ARF$$

Using this ratio, the amount of CO₂ injected was calculated by dividing the oil production curves and cumulative oil production curves by the curve for the oil/tCO₂ ratio. The volume fraction of CO₂ in the reservoir pores (Eq. 4.9), initially starts off at zero. From the start of injection, it increases based on the injection rate of CO₂, the mixing rate of CO₂ in the reservoir and the loss fraction over the system [63].

$$\text{(Eq. 4.9)} \quad fCO_2(t) = fCO_2(t-1) + \frac{VIR_{CO_2} - fCO_2(t-1)(Vm+Vp+Vl)}{Volume_{reservoir}}$$

Where, $fCO_2(t)$ is the pore fraction of CO₂ at time t, VIR_{CO_2} is the volumetric injection rate of CO₂ at reservoir density, Vm is the rate of mixing, Vp = the production rate and Vl is the loss rate in the system. The recycling rate was calculated using equation 4.10 where the efficiency of the recycling facility (η_{recfac}) was put to be 90%. Based on the recycling rate, the maximum throughput of the recycling facility was calculated.

⁹ OOIP = the original oil in place prior to any form of extraction from the reservoir

$$\text{(Eq. 4.10)} \quad CO_2 \text{ recycled } (t) = \frac{V_p \times f_{CO_2}(t)}{\rho_{CO_2, \text{wellhead}}} \times \eta_{recfac}$$

The time when the project would generally be terminated or paused is when the marginal costs are equal to the marginal revenues (including 17.5% royalties of the barrels produced are from federal and state lands and 5% Production and ad valorem taxes [112]). The additional costs to let the CO₂-EOR project run are based on the operational costs and the costs of the injected CO₂. The revenues of continued operation are the oil production revenues and the costs difference between the bought and the recycled CO₂. The additional oil production in during the drying phase will be further discussed in the next section.

4.4 Drying time to start CPG operation

The second part of the modelling study cover the transition period that is necessary to generate a CO₂ stream that is pure enough to allow for direct utilization in a turbine. The purity thresholds for the fraction of H₂O that can be present in the CO₂ while remaining undersaturated over the most crucial phases of the cycle can be calculated using the pressure-temperature saturation relations for H₂O in CO₂. [113]. At threshold values, the full pore volume along the main CO₂ pathway is assumed to be occupied by CO₂. This is not an unreasonable assumption due to the high solubility of H₂O in supercritical CO₂ and the high homogeneity of sandstone reservoirs.

Due to the corrosive properties of CO₂ saturated H₂O, it is important that a minimal amount of H₂O precipitates from the supercritical CO₂ stream within the system. Hence, the CO₂ has to remain undersaturated with respect to H₂O during the most critical parts of the CPG system. For the reference case, the threshold was put at 0.05 mole % H₂O. At this threshold, no H₂O precipitates at the production wellhead or the turbine. This threshold is based on an intermediate result and will be further discussed in section 5, figure 5.10. For the cooling system and the compressor, either a dehydration phase needs to be added or corrosion resistive materials have to be used.

$f_{CO_2, \text{threshold}}$ is the required volume fraction of CO₂ in the reservoir and can be calculated from the equipment threshold using equation 4.11 [63].

$$\text{(Eq. 4.11)} \quad f_{CO_2, \text{threshold}} = \frac{X_{CO_2} \frac{M_{CO_2}}{\rho_{CO_2}}}{(1-X_{CO_2}) \frac{M_{CO_2}}{\rho_{CO_2}} + X_{CO_2} \frac{M_{H_2O}}{\rho_{H_2O}}}$$

In equation 3.11, X_{CO_2} is the threshold for the molar fraction of H₂O that can be contained by the CO₂ stream. This threshold value is based on the solubility of water at the various stages of the system. The time required to dry out the reservoir enough to be used or direct cycle geothermal heat extraction is dependent on initial conditions from the EOR phase, the volume of the reservoir and the mixing rate. The drying time can be calculated using equation 4.12 [63]:

$$\text{(Eq. 4.12)} \quad T_{drying} = \frac{V_R}{V_{cl}} \ln \left[1 - f_{CO_2, \text{threshold}} \frac{V_M + V_{cl}}{V_{cl}} \right]$$

In this equation, V_R is the constant volume of free space, V_{cl} is the volume of the injected CO₂ ($\dot{m}_{CO_2}/\rho_{CO_2}$). V_m is the mixing rate at which CO₂ mixes in with the formation by dissolution trapping and convective flow and is replaced with pure H₂O.

During the phases where there are still more hydrocarbons and water present in the production stream than the threshold, it might be possible to utilize the heat via a binary system. If the binary system uses a transcritical cycle with CO₂ as a working fluid, the same facility, apart from the heat exchanger, may later be used for direct CO₂ power production when threshold values are met.

Pressure buildup

As explained in section 2.4, pressure buildup in the reservoir can be dangerous as it may lead to induced seismicity and leakage of CO₂ from the reservoir. During the dry out phase, in particular, the pressure in the reservoir may build up due to two factors:

- The presence of brine, CO₂ and hydrocarbons causes flow to take place, according to multiphase flow, this means that pathways may be blocked by other immiscible phases, causing local rises in pore pressures
- During the drying phase, the reservoir is displaced by supercritical CO₂ at a high rate. This means that the disconnected pockets of brine will remain trapped within the CO₂ flow path. As long as the CO₂ phase contacts the brine, H₂O dissolves into the CO₂(sc). Thus, the brine becomes more concentrated. As the brine becomes saturated with respect to salts, salt minerals precipitate in the reservoir pores. This effect can have a significant effect on the reservoir permeability and local pressure differences [74].

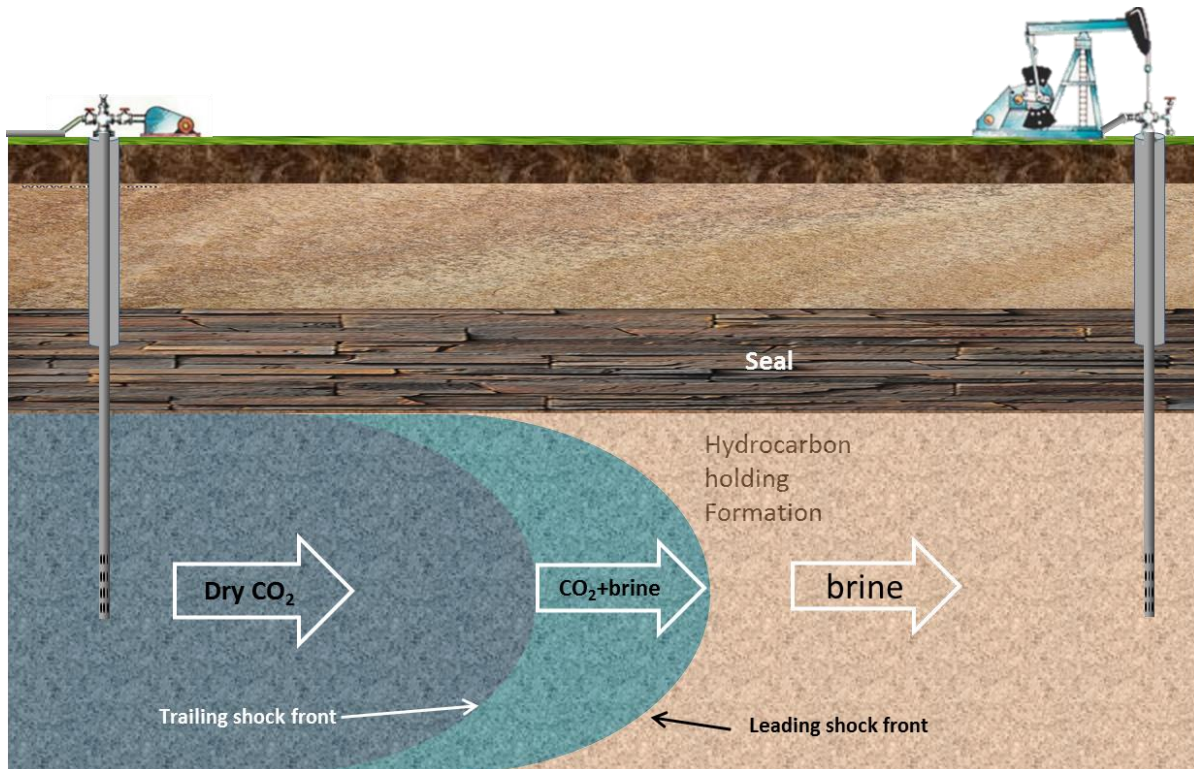


Figure 4.3: Different phases in the reservoir during the drying with the leading shock front between the brine and the mixed phase and the trailing shock front between the dry CO₂ and the mixed phase.

The pressure drop in the reservoir is modelled as this factor might affect the possible injection rates and therefore drying time. Figure 4.3 shows the different phases present in the reservoir during the drying with the leading and trailing shock fronts. Because of mutual solubility, the situation differs from classical two-phase immiscible flow, which has a single front separating

two regions [76]. The mixed region is in equilibrium meaning no salt will precipitate here, salt deposition will only occur in the dry region. The limit for the pressure gradient that is considered acceptable are reservoir specific and depend on permeability, lithology of the caprock and the overburden, the degree of fracturing and the presence of faults.

Multi-phase flow

Since the reservoir at the point of drying still contains considerable amounts of brine and hydrocarbons, multi-phase flow principles have to be taken into account. The fractional flow formulation for radial flow of the injected CO₂:

$$\text{(Eq. 4.13)} \quad \frac{\delta S_g}{\delta t} = \frac{q(t)}{\phi} \frac{\delta f_g}{\delta S_g} \frac{\delta S_g}{\delta r^2} = 0$$

Where S_g is the gas saturation, $q(t)$ is the total flow rate, ϕ is porosity and f_g is the fractional gas flow defined in equation 4.14.

$$\text{(Eq. 4.14)} \quad f_g = \left(\frac{\lambda_g}{\lambda_g + \lambda_l} \right) \left[1 + \frac{\lambda_l}{q(t)} \frac{\delta P_c}{\delta x} - \frac{\lambda_l g \Delta \rho_{gl}}{q(t)} \frac{\delta z}{\delta x} \right]$$

As we assume that the CO₂ is miscible with oil, the capillary pressure P_c of the oil and CO₂ mixture interface reduces to 0. Therefore hydrocarbons are left out of the equation. in equation 4.14, λ_g and λ_l are the mobility's of the gaseous and liquid phases respectively. The expansion of the injected plume radius r can be calculated using equation 4.15.

$$\text{(Eq. 4.15)} \quad \frac{r^2 - r_w^2}{t} = \frac{q(t)}{\phi \pi h} \frac{\delta f_g}{\delta S_g}$$

In this equation, r_w is the radius of the wellbore and $\frac{r^2 - r_w^2}{t}$ is the speed with which the dried out regions spreads over the reservoir. The pressure drop in the dry-out region can be calculated using equation 4.16 [76]:

$$\text{(Eq. 4.16)} \quad \Delta P_{dry} = \frac{q \mu_g}{2\pi h \kappa \kappa_{s,g}} \ln \left(\frac{r_{dry}}{r_w} \right)$$

Where $\kappa_{s,g}$ is the relative permeability for CO₂.

Salt precipitation

The permeability and porosity can be reduced in this dry out zone due to salt precipitation. Porosity reduction is given by equation 4.17 [76]:

$$\text{(Eq. 4.17)} \quad \phi = \phi_0 - \phi_0 (1 - S_{g,dry}) V f_{fsalt}$$

In equations 4.17 and 4.18, ϕ_0 is the initial porosity, $S_{g,dry}$ the gas saturation just downstream of the dry out and $V f_{fsalt}$ is the volume fraction of the salt, which is given by equation 4.19 [76]:

$$\text{(Eq. 4.18)} \quad V f_{fsalt} = \frac{S \rho_{salt}}{10^6 \rho_{salt}}$$

S is the salinity of the brine, ρ_{sol} is the density of the solution and ρ_{salt} is the density of the salt. The Kozeny-Carman grain model (equation 4.19) based on grain spheres [114] was used to calculate permeability based on porosity.

$$(Eq. 4.19) \quad k = \frac{R_0^2}{45} \left(\frac{\phi^3}{1-\phi^2} \right)$$

k_0 is the initial permeability, k the absolute permeability and R_0 is the grain radius. Since R_0 does not change, the permeability reduction can be calculated based on the porosity decrease using equation 4.20.

$$(Eq. 4.20) \quad \frac{\kappa}{\kappa_0} = \left(\frac{\phi}{\phi_0} \right)^3 \left(\frac{1-\phi_0}{1-\phi} \right)^2$$

The permeability reduction caused by the deposition of precipitation of solid salt is then given by equation 4.21 [74]:

$$(Eq. 4.21) \quad \frac{\kappa}{\kappa_0} = \frac{(1-S_s)^3}{\left(1 + \frac{\phi_0}{1-\phi_0} S_s\right)^2}$$

Where S_s is the solid phase saturation of the salt and change in porosity can also be calculated from the S_s : $\phi = \phi_0(1 - S_s)$. S_s is given by the density of the salt ρ_s (eq. 4.23), the density of the injected gas ρ_{inj} the salinity s and the global concentration of the brine downstream of the trailing shock G_{brine}^c (eq 4.22) [74]:

$$(Eq. 4.22) \quad G_{brine}^c = \omega_{water} S_g^c \rho_g + \omega_{brine,a} (1 - S_g^c) \rho_a$$

$$(Eq. 4.23) \quad S_s = \frac{S \rho_{inj} G_{brine}^c}{\rho_s}$$

Where ω is the mole fraction and S_g^c is the trailing shock gas saturation. The formation damage due to salt precipitation can also be expressed with a skin factor. The skin factor is a phenomenon near the wellbore that causes an additional pressure drop due to the damaged rock. A positive skin factor has a negative influence on the injectivity. Vice-versa, a negative skin factor has a positive influence on the injectivity. A formulation for the skin factor is given by equation 4.24 [74].

$$(Eq. 4.24) \quad Skinfactor = \left(\frac{\left(1 + \frac{\phi_0}{1-\phi_0} S_s\right)^2}{(1-S_s)^3} - 1 \right) \ln \left(\frac{r_{dry}(t)}{r_w} \right)$$

The total pressure drop increase in the dry out region can then be calculated using equation 4.25. [74].

$$(Eq. 4.25) \quad \Delta P_{dry} = \frac{q \mu_g}{2\pi h \kappa \kappa_{s,g}} \left(\ln \left(\frac{r_{dry}}{r_w} \right) + SF \right)$$

Brine disposal

During both the EOR and the drying phase of the reservoir, mineral rich, thermal brine is produced that needs to be disposed of. Various methodologies exist for the environmentally safe disposal of this brine, like desalination using membranes or reinjection into aquifers. The amount of brine that was produced in these phases was calculated using equation 4.26:

$$(Eq. 4.26) \quad Brine_{surface} = \sum_0^T (1 - F_{CO_2}(t)) \times (1 - F_{oil}(t)) \times V_p(t) \times \rho_{H_2O}$$

Where $F_{CO_2}(t)$ is the volumetric pore fraction of CO₂ at time t , $F_{oil}(t)$ is the volumetric pore fraction of oil at time t and $V_p(t)$ is the production volume at time t . For simplicity it was assumed that the different phases were produced at rates corresponding to their volume percentage of the total pore volume, hence assuming perfect mixing. This will not provide a realistic production profile over time as the CO₂ is more likely to displace more water in the beginning according to the mechanism described in figure 3.3. However, the total brine disposal will be similar as the H₂O threshold remains the same.

4.5 CO₂-plume geothermal energy recovery

The final part covers the geothermal energy production phase of the system. Since the reservoir stream is assumed to be close to pure supercritical CO₂ at this stage (single phase flow), Darcy's law can be used to estimate the flow in the reservoir. A 1-D model was used to calculate the flow of CO₂ through the wells and the reservoir. The studied system includes the CO₂-thermodynamics within the reservoir and the surface processing facility. Figure 4.4 presents a schematic view of the system, the numbers represent the different phases of the system and will remain constant for the rest of the report. Power generated by the thermosiphon effect is produced using a direct CO₂ turbine. The excess heat is either used for additional electricity production or can be utilized for district heating.

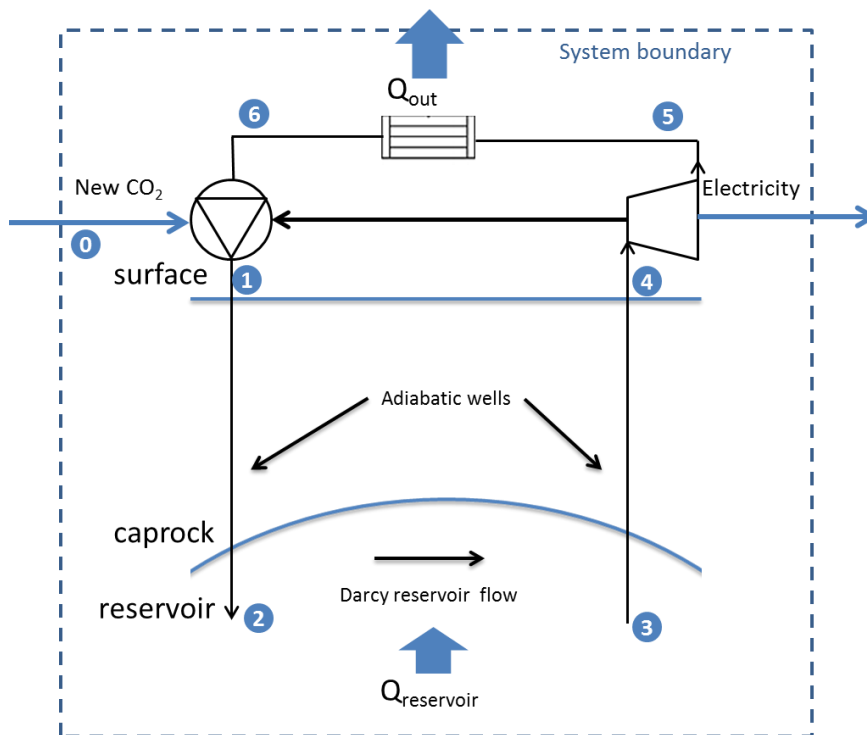


Figure 4.4: Schematic representation of the CPG system, the numbers represent the different stages of the system.

Well profiles

Randolph et al. (2012) performed pressure and heat loss calculations for the production well in a CPG system [115]. They found that for a wellbore temperature of 100°C, an ambient temperature of 12°C, and reservoir depth of 2500 meter, pressure and temperature losses to the well were negligible. After the first five days of production, heat losses were less than 2°C compared to the adiabatic case. It should, however, be noted that they assume heat loss through the well will diminish over time due to heating of the rock in the vicinity of the well considering

minimal advection around the well casing. However, monitoring of well temperature losses in conventional and enhanced oil production does not confirm this finding (personal correspondence with Raul Valdez, principal reservoir engineer of the greater Birba Cluster at Petroleum Development Oman). In the calculations, the flow through the production and injection wells was calculated without heat loss to the surrounding formations.

During the injection and production of CO₂ in the wells, pressure, density and temperature all vary with depth and are all interlinked. Newtonian iteration was used to establish the pressure, temperature and density profiles over the wells. The iterations were performed in Matlab version R2014b. Since CO₂ is close to its supercritical pressure and temperature conditions, it would not suffice to model it as an ideal gas and real gas modelling is required. Real gases differ from ideal gases in two ways. First, they have finite size. Secondly, there are forces acting between the particles or molecules in a real gas. These microscopic forces should be taken into account as they affect the macroscopic equation of state. In the calculations, the properties of CO₂ were determined using the Helmholtz free energy equations of state [116]. The equation of state transformed into MATLAB code is presented in Appendix XII.

The wells were modelled to be adiabatic, meaning pressure differences over the wellbore where only resulting from static pressure differences and friction losses to the wellbore. The frictional heat and pressure losses in the well can be calculated using formula 4.27 [106]:

$$\text{(Eq. 4.27)} \quad \Delta P_{fr,well} = f \frac{\Delta z}{D} \rho \frac{V^2}{2} = f \frac{8\pi^2 \Delta z \dot{m}^2}{\rho D^5}$$

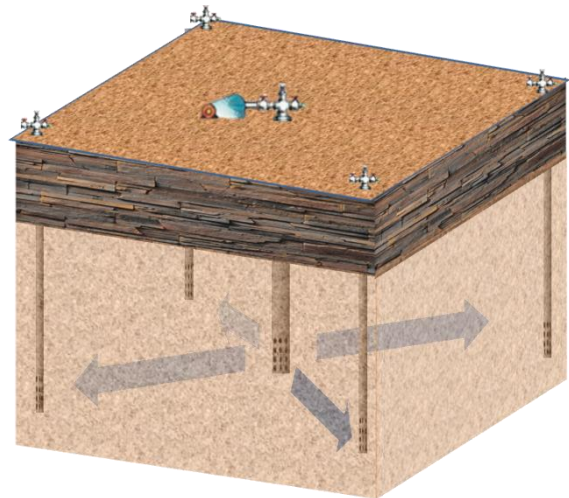
Where:

$$\text{(Eq. 4.28)} \quad f = \left[-1.8 \log \left[\frac{6.9}{Re} + \left(\frac{\varepsilon}{3.7D} \right)^{1.11} \right] \right]^{-2}$$

In this equation f is the friction factor, Re is the Reynolds number, V is the velocity of the CO₂, \dot{m} is the mass flow rate and Δz is the reservoir depth.

Reservoir flow

Over the reservoir, the flow is modelled as Darcy flow since it would not be realistic to take heterogeneity into account in a 1-D model. The reservoir was divided into N segments for which the properties of CO₂ were calculated from the equation of state, flow, and the temperature. The flow was modelled through a cross-sectional flow geometry that starts from the area of the injection well. Over the reservoir, then gradually increases until it takes up the height of the reservoir and from there decreases again to the area of the production well. The temperature increase over the reservoir was modelled to be linear. Variations in temperature increase profile to a concave or convex function of length did not van significant effect on the flow behavior.



After injection, the CO₂ from the centralized injection well spreads over the reservoir to the four production wells. Hence, the flow rate of CO₂ through the reservoir section towards each

injection well will be one fourth of the injection rate. A wider field consists of many of these contiguous 5-spot patterns and a production well receives CO₂ from four injectors. Hence, if all injectors inject at the same rate and a close system is considered, the flow rate of the production well equals that of the injection well.

To model the thermal depletion over time (t), the heat extraction was calculated for each of the N segments for t = 1: T₃. Where T₃ represents the lifetime of the CPG system, in this study taken to be 25 years. The depletion of the reservoirs was considered to be the total heat capacity of the swept volume of the formation.

$$(Eq. 4.29) \quad C_{p_{reservoir(i)}} = A(i) \times \frac{L}{N} \times (1 - \emptyset) \rho_{rock} \times T_c rock$$

Where $C_{p_{reservoir(i)}}$ is the heat capacity of the formation at section (i), $A(i)$ is the cross sectional flow area at section (i), $\frac{L}{N}$ is the length of each reservoir section, $(1 - \emptyset) \rho_{rock}$ is the rock grain density of the formation and $T_c rock$ is the thermal capacity of the rock. The heat flux from the reservoir at section (i) is calculated using equation 4.30.

$$(Eq. 4.30) \quad Q(i) = \dot{m} \frac{2(T_3 - T_2)}{T_{c_2} + T_{c_3}}$$

The thermal depletion over time can then be calculated using equation 4.31 [117]. The thermal replenishment rate, $Q_{restore}$, was set to 80 mW/m², which is little over average for a field in the western United States (figure 2.11).

$$(Eq. 4.31) \quad T_{res}(t) = T_{res}(t - 1) - (Q(t - 1) + Q_{restore}) / C_{p_{reservoir}}$$

The effective viscosity was calculated separately based on the reduced effective cross section of the stream. The effective viscosity was calculated based on the methodology described by Fenghour, Wakeham and Vesovic, 1998 [118]. For which the Matlab model is included in Appendix X. The pressure drop over the length of the reservoir sections can then be modelled according to equation 4.32:

$$(Eq. 4.32) \quad \Delta P_{f,res} = \frac{\dot{m} \mu \Delta L}{\rho \kappa A}$$

From these, combined equations, the relationship between injection pressure and mass flow through the injection system can be derived:

$$(Eq. 4.33) \quad P_{inj} = P_{res} + \Delta P_{f,well} + \Delta P_{f,res} - \rho g \Delta z$$

While, in their studies, Pruess and Randolph decided to fix the downhole pressure at the bottom of the injection well [37] [66]. In this study, it was chosen to make this variable depending on the mass flow rate based on Atrens' previous work [102]. Meaning that the injection pressure of the CO₂ is calculated based on the reservoir pressure and the pressure losses over the reservoir and injection well. The minimum injection pressure required to achieve efficient flow was found using the 'fminsearch' function in Matlab. Since a phase change towards a gas in the system would mean that a compressor has to be used instead of a pump, the minimum injection pressure was set at 7.38 Mpa, the critical pressure for CO₂. Compression of a gas takes significantly more energy, and compressors are more expensive than pumps. Using the formulas for well flow and reservoir flow, some thermodynamic properties of CO₂ were calculated for

each point in the system (figure 4.2). The remainder of the properties was calculated by plugging in these properties in the equations of state for CO₂,

Electricity generation

After production, the expansion of the CO₂ through a turbine was modelled to take place isentropically (Eq. 4.34). The subscripts in the equations used in this section represent the stage of the system at which the property is taken. The pressure after expansion through the turbine is put equal to the injection pressure meaning that no additional compression is needed in the system. From the Helmholtz free energy equations of state, the other parameters can then be calculated based on the pressure and entropy. After expansion through the turbine, the CO₂ is then cooled isobaric to the right temperature for injection.

$$\text{(Eq. 4.34)} \quad W_{turbine} = \dot{m} \eta_{isen} (h_4 - h_5)$$

In the case of a thermosiphon, the exit pressure is set to match the injection pressure to ensure maximum efficiency. Therefore, the work provided by the compressor $W_{compressor}$ is 0. For the CO₂ that arrives from the natural field or capture plant, additional compression may be required. In this case, the compression can be calculated using equation 4.35.

$$\text{(Eq. 4.35)} \quad W_{compressor} = \dot{m} \eta_{isen} (h_1 - h_6)$$

In the case of a fan-forced dry cooling heat exchanger, an additional parasitic load of 18.9 kWe per 1 MWh has to be taken into account $W_{Heatex} = 0.0189Q_{Heatex}$ [100]. The total efficiency of the system can then be calculated using equation 4.36:

$$\text{(Eq. 4.36)} \quad \eta_{CPG} = \frac{(W_{turbine} - W_{compressor} - W_{Heatex})}{\dot{m} (h_3 - h_2)}$$

Where $\dot{m} (h_3 - h_2)$ is the heat extracted from the reservoir (Q).

Cost and benefits of the heat

The heat that is left after the direct turbine can either be used to expand a secondary working fluid through a turbine via a binary system or be used for district heating or preheating of industrial processes. The benefits that can be obtained from the additional heat are difficult to quantify as they strongly depend on the quality of the heat produced and the demand in the vicinity of the plant. Transport losses are high if the heat has to be transported over long distances, and CO₂ injection is unlikely to take place in a residential area. Furthermore it is difficult to put a price on the benefits of rest heat as this strongly depends on the requirements. Therefore, it was assumed that the heat was either used in a binary ORC or cooled using air cooling.

If the heat would be utilized for additional electricity generation using an Organic Rankine Cycle (ORC), the power can be calculated using equation 4.37.

$$\text{(Eq. 4.37)} \quad W_{Bin,turbine} = \dot{m} * (h_5 - h_6) * \eta_{Carnot} * \eta_{bin}$$

Where $(h_5 - h_6)$ is the enthalpy difference over the heat exchanger, η_{Carnot} is the Carnot efficiency calculated using equation 2.4. η_{bin} is the efficiency of the binary system, taken to be 50% [18].

4.6 Economic analysis of the CPG-EOR system

Introducing cost equations into Matlab, a model was made to allow for economic optimization of the system. In this section, conversion costs indexes will be used to convert the costs from the original publication date the methodology to the costs in the final quarter of the year 2014. The costs conversion indexes for North America were obtained from the IHS website [119]. For the costs concerning the wells, recycling facility and pump, the Upstream Capital Costs Index (UCCI) was used. For the costs concerning the turbine and the heat exchanger, the Power Capital Costs Index (PCCI) without nuclear energy were used. Usually, O&M costs should be corrected with the inflation index rather than with the UCCI. However, the maintenance costs in the model were given as a percentage of the capital costs.

The most important cost factors for a CPG system are the costs for the drilling or refurbishment of wells (if required), the costs of the turbine, the costs for the heat exchanger and the costs for CO₂. To calculate the costs of CO₂, three scenarios were assumed. The capture and transport costs at the plant gate are taken to be \$45/tCO₂ for the base case, ranging from \$30 (low scenario) to \$60 (high scenario) delivered at plant gate [8]. The costs for recycling CO₂ are taken to be \$13.45/tCO₂ [7]. Since the CO₂ is stored in the subsurface during the project, additional income can be generated depending on the Emission Trading Scheme price (ETS). Although the U.S. is no member of the Emission Trading System, in this thesis the term ETS is used for the costs for the right to emit CO₂ (\$/tonne).

For the evolution of the carbon tax in the US, three scenarios were taken into account based in predictions in the CO₂ Price Report, Spring 2014 published by Synaps Energy [120]. An even higher uncertainty range is assumed in IPCC (2014), where the ETS¹⁰ (for the European Union) price varies from €6-50 in 2020 to €34-250 in 2050 [121]. The scenario's from Synaps Energy were used as they were specifically about the U.S.

Low ETS scenario:

The ETS price starts at around \$11/tonne in 2020 and increases to \$44/tonne in 2040 (a linear rise of \$1.65/tonne/year and a Levelized costs of \$24/tonne over the period). This price projection represents a scenario in which federal policy, either regulatory or legislative, exist but are not very stringent [120].

Base ETS scenario:

The scenario that is used for the base case calculations in the model starts at a price of \$16.5/tonne in 2020 and increases to \$66/tonne in 2040. This corresponds to a linear rise of \$2.48/tonne/year and a Levelized costs of \$37.5/tonne over the period. This forecast represents a scenario in which federal policies are implemented with significant but reasonably achievable goals [120].

High ETS scenario:

The upper bound is given by a scenario in which is consistent with the occurrence of one or more factors that have the effect of raising carbon prices. These factors include somewhat more aggressive emissions reduction targets such as greater restrictions on the use of offsets, restricted availability or high cost of technological alternatives such as nuclear, biomass, and

¹⁰ The National Emission trading System includes the European Union, Switzerland, New Zealand, Australia, South Korea and Kazakhstan. The European Union ETS with all 15 member states is the oldest system.

carbon capture and sequestration and more aggressive international actions. CO₂ market prices in this scenario are projected to rise from \$27.5/tonne in 2020 to ± \$100/tonne in 2040. This corresponds to a linear rise of \$3.60/tonne/year and a Levelized costs of \$57/tonne over the period [120].

The price for CO₂ at plant gate was then calculated by subtracting the ETS from the costs at the plant gate. If the ETS was higher than the costs of capture and transport (PCO₂ < 0), the profits of storage were assumed to be split 66.6/33.3% between the capture facility and the CPG-EOR project.

4.6.1 CO₂-EOR

For the costs for EOR, the costs were calculated based on two different scenarios. The first scenario is based on the methodology used in PSS and assumes drilling new wells. The second method uses the costs of historic leases that were adjusted for the reservoir size and the year.

New wells

The primary capital expenses for subsurface systems exist of the wells. Depending on whether the Equation 4.38 [122] was used to calculate the costs for a new CO₂-well. Wells are the most expensive capital investments of a CO₂-plume geothermal system. The costs depend strongly on the material, diameter, formation type and depth. Practice teaches that uncertainties in the costs of wells are very high [122].

$$\text{(Eq. 4.38)} \quad C_{well} = \left(\frac{229}{218}\right) UCCI * K e^{bz}(1 - \zeta) + \left(\frac{D}{D_0}\right)^2 \zeta K e^{bz}$$

In this formula, K and b are constants that describe the relationship between costs and depth and are derived from an exponential fit of well cost and depth for geothermal wells [123]. ζ is the fraction of total time spent drilling and z = the depth. The values used in this study are: K=0.554 \$, b=6.13E⁻⁴ m⁻¹, ζ = 0.25, based on the estimates for geothermal wells [124]. $\left(\frac{D}{D_0}\right)$ is a scaling factor, to account for the costs for larger wellbores. In this factor, D is the chosen diameter and D₀ is a standard diameter used as a baseline (0.2313m) [106].

For the recycling plant, the costs are calculated based on the maximum throughput of the facility $MaxRec(MCcf)$ ¹¹ calculated using Matlab. No attempt was made here to itemize separately the individual components (Approximately half of the total costs for the recycle plant correspond to the costs of compression). If the peak rate is less than 30 million cubic feet per day (MMcfd) or 0.579 million tonnes per year, then Capital cost are calculated by equation 4.39a, for higher peak rates the costs are calculated based on equation 4.39b [125].

$$\text{(Eq. 4.39a)} \quad C_{Recfac} = 12 (M\$) \times MaxRec$$

$$\text{(Eq. 4.39b)} \quad C_{Recfac} = 36 (M\$) + 0.75 * (MaxRec - 30)$$

During the EOR and drying phases of the system, the CO₂ may need to be compressed to the injection speed (in the CPG phase this is not necessary due to the thermosiphon effect). The

¹¹ The maximum trueput is converted to MMcfd is using a conversion factor of 1 tonne/year : 51.813 MMcfd [125].

work requirements for the pump (W_p) assuming a minimal injection pressure is $P_c = 7.38$ Mpa, are calculated using equation 4.40 [126].

$$\text{(Eq. 4.40)} \quad W_p = \left(\frac{1000 \cdot 10}{365 \cdot 24 \cdot 36} \right) \left(\frac{\dot{m}(P_{inject} - P_{in})}{\eta_{is} \cdot \rho} \right)$$

And the costs for the CO₂ pump are calculated using equation 4.41 [126].

$$\text{(Eq. 4.41)} \quad C_{pump} = \left(\frac{229}{126} \right) UCCI * 1.11 \times 10^6 (\$) \times \frac{W_p}{1000} + 0.07 \times 10^6 (\$)$$

During the EOR and drying phases of the system, brine will be produced from the reservoir. Because this brine contains heavy metals, dissolved and precipitated petroleum compounds, and dissolved salts, it cannot be directly disposed of without causing damage to the environment. Various methods like desalination via reversed osmosis, transportation to the ocean and reinjection into aquifers exist to abate environmental impacts of produced brine [127]. In the case of reinjection of the brine, an additional well needs to be drilled into an over or underlying aquifer. The inside diameter of the well is calculated based on the maximum annual flow rate (W) and the density of brine (ρ_{brine}) using equation 4.42 [128].

$$\text{(Eq. 4.42)} \quad D_{disp} = 2.54 \times 10^{-2} \times \frac{2.2W^{0.45}}{\rho_{brine}^{0.31}}$$

To minimize the risk of brine injection affecting potable aquifers the depth of the well was taken to be 1500m. The costs for the disposal well were then calculated using equation 4.38. The operational costs for brine disposal $\left(\frac{199}{132} \right) UOCI * \$1 = \$1.503$ per 1,000 gallons (8,345 Liters) of brine injected [127]. To calculate the time.

Refurbished wells

For the purpose of the CO₂-EOR phase, the assumptions are made that the field has undergone primary and secondary flooding. A field that has been subject to secondary flooding, i.e., water flooding, has both production and injection wells. For WAG injection, it is adequate to assume that no additional injection wells are required [90]. The EIA 'Costs and Indices for Domestic Oil and Gas Field Equipment and Production Operations' report [129] includes a scenario for secondary oil recovery using water flooding. Costs and indices for additional secondary oil recovery equipment and its operation are provided for a representative lease, located in West Texas. This lease, or a module, comprises ten production wells, 11 water injection wells and one disposal well, and the wells are nominally 1,219 m, deep [90]. This scenario was modified for CO₂ flooding and used as the basis for field equipment and production operations costs. Table 4.2 lists the costs of the EOR phase of the project, corrected for 2014 using deflation indexes (1.08 with respect to 2010) [130] for labor expenses and UPCC for equipment.

Table 4.2: Costs for CO₂-EOR system, based on a representative case in Texas [90].

Cost allocation		
Capital costs		
<i>injection Equipment</i>		
Recycle & Vapor compressors	\$194.266,51	\$/well pair
Injection plant	\$12.447,08	\$/well pair
distribution lines	\$8.458,76	\$/well pair
Header	\$6.694,69	\$/well pair
Electrical Service	\$10.672,06	\$/well pair
<i>Production equipment</i>		
Tubing Replacement	\$9.948,90	\$/well pair
Rods & pumps	\$4.492,34	\$/well pair
Equipment	\$44.375,60	\$/well pair
Refurbishment of existing wells	\$54,38	\$/m/well pair
O&M costs		
<i>daily expenses</i>		
Supervision & Overhead	\$5.734,80	\$/day
Labor	\$6.760,80	\$/day
Consumables	\$810,00	\$/day
Operative supplies	\$831,60	\$/day
Electricity	\$8.750.916,00	\$/year

The costs for CO₂ were calculated using equation 4.43.

$$\text{(Eq. 4.43)} \quad C_{CO_2}(t) = (CO_2(\text{new}) \times PCO_2) + CO_2(\text{recycled}) \times PCO_2(\text{recycled})$$

Where PCO_2 is the price of new CO₂ (\$/tonne) and $PCO_2(\text{recycled})$ are the costs for recycling the produced CO₂ (\$/tonne).

CO₂-EOR remains profitable, an estimation was made for the operational expenses during the EOR phase. The operational expenses for a well pair in the EOR phase of the model were estimated based on the costs allocations in Table 4.1 [90]. $OPEX_{EOR}(t) = \$13.930.185$. The annual maintenance costs are estimated to be 5% of the capital expenses for the EOR system (assuming new wells), and are calculated using equation 4.44.

$$\text{(Eq. 4.44)} \quad CAPEX_{EOR} = \sum_i^{pr,well} C_{well}(D_p) + \sum_i^{inj,well} C_{well}(D_i) + C_{pump} + C_{Recfac} + C_{disposal\ well}$$

The marginal costs for CO₂-EOR can then be calculated using equation 4.45.

$$\text{(Eq. 4.45)} \quad C_{EOR}(t) = OPEX_{EOR}(t) + 0.05 * CAPEX_{EOR} + C_{CO_2}(t) + C_{brine\ disposal}(t)$$

$C_{brine\ disposal}(t)$ is calculated from the production stream $((1 - F_{CO_2}) * \frac{F_{brine}}{F_{oil}})$ times the disposal costs, the costs for CO₂ are calculated based on Equation 4.43.

Drying and the CO₂-plume geothermal system

Before the reservoir can be used for geothermal energy extraction using a direct CO₂-turbine, the reservoir needs to reach the purity threshold. Since the drying occurs at the start of the CPG project, the costs are added to the capital investments at the start. The total costs of drying of the reservoir are calculated using Eq. 4.46.

$$\text{(Eq. 4.46)} \quad C_{drying} = \sum_t^{T^2} C_{brine\ disposal}(t) + C_{CO_2}(t) + OPEX(t) + 0.05 * CAPEX_{EOR}$$

The operational expenses at year 't' ($OPEX(t)$), are calculated using the same methodology as in the EOR phase. It is assumed that although the injection rate of CO₂ is increased during the drying phase, no additional equipment would be needed. Since either means the equipment had an overcapacity or less 5-spot cells are operated at the same time then was the case during the EOR-Phase.

For the turbines, the main parameters that affect the price are the flow rate and the thermodynamic properties within the turbine. Under normal geothermal turbine conditions, the density of CO₂ under turbine conditions is lower than steam limiting the size and material costs. The total costs of CO₂ turbines can be estimated using equation 4.47 [100].

$$\text{(Eq. 3.47)} \quad C_{turbine} = \left(\frac{187}{176}\right)_{PCCI} * \alpha W_t F_s = \left(\frac{187}{176}\right)_{PCCI} * \alpha W_t^\beta \rho_{out}^\gamma$$

In this formula, W_t is the work of the turbine, and F_s is the size factor depending on the density of the outlet CO₂. α , β and γ are constants derived from empirical fit on CO₂ turbine cost data; $\alpha = 1.066 \$ kW^{-.5439} kg^{0.1472}$, $\beta = 0.5439$ and $\gamma = -0.1472$ [100].

After expansion through the turbine, the CO₂ needs to be cooled back to its injection state. The costs for the heat exchanger strongly depend on the type of heat exchanger used. This study uses an air-cooled heat exchanger to cool down the CO₂. Using a water cooling heat exchanger would strongly reduce costs, however, for consistency reasons it was chosen to use costs equations from a single source, limiting the uncertainty. The cost for the heat exchanger was calculated using Equation 4.48 [122]:

$$\text{(Eq. 4.48)} \quad C_{Heatex} = \left(\frac{187}{176}\right)_{PCCI} * (B_1 + B_2 F_m F_p) C_p$$

B_1 and B_2 are constants based on the equipment type, $B_1=0.96$, $B_2=1.21$. F_m is the material factor which in this case (based on stainless steel) is 2.9. C_p is the original costs of the heat exchanger based in a heat exchanger made from carbon steel and depends on heat exchanger area (A). Since CO₂-saturated water is highly corrosive and condensation of H₂O from the CO₂ might take place in the heat exchanger, it would be good to use more acid resistant stainless steel [100].

$$\text{(Eq. 4.49)} \quad C_p = 10^{4.0336+0.2341 \log A+0.0497 \log[A]^2}$$

The pressure factor F_p can be calculated using formula 4.50 [122]:

$$\text{(Eq. 4.50)} \quad F_p = 10^{-0.1250+0.15361 \log P+0.02861 \log[P]^2}$$

The total capital costs of the CPG system are then summed by equation 4.51:

$$\text{(Eq. 4.51)} \quad CAPEX_{CPG} = 0.9 * (C_{drying} + C_{Heatex} + \lambda C_{turbine})$$

Where λ is a constant to scale up for additional piping, control, freight, labor, etc. ($\lambda=2.4$) [122]. In this equation, the 0.9 is based on the permanent 10% investment tax credit for geothermal and solar technologies [131]. Two different methodologies were used to calculate the operational expenses during the CPG phase. The base case methodology calculated the operational expenses to be \$0,01/kWh, with an operating cost escalation rate of 1% (eq. 4.52a) based on Athrens et al. [100] for comparison, a second methodology calculated the annual operational expenses as 5% of the capital expenses (eq. 4.52b) as is used by Holt et al [132] for calculation the operational costs of a North Sea EOR/CCS project.

$$\text{(Eq. 4.52a)} \quad OPEX_{CPG}(t) = (0.01 * W_{turbine} * 8766) * 1.01^t + C_{CO_2}(t) - E * 21.5 \left(\frac{\$}{MWh}\right)$$

$$\text{(Eq. 4.52b)} \quad OPEX_{CPG}(t) = 0.05 * (CAPEX_{CPG} + \sum_i^{pr,well} C_{well}(D_p) + \sum_i^{inj,well} C_{well}(D_i)) \\ + C_{CO_2}(t) - E * 21.5 \left(\frac{\$}{MWh}\right)$$

In these equations, E is the annual electricity generation in MWh, and 21.5 is based on the production tax credit for geothermal power generation [131]. The Levelized costs for electricity are calculated using equation 4.53.

$$\text{(Eq. 4.53)} \quad LCE = \frac{\sum_{t=1}^n \frac{I_t + M_t + F_t}{(1+r)^t}}{\sum_{t=1}^n \frac{E_t}{(1+r)^t}}$$

In this formula n is the lifetime of the system, I_t are the investment costs in year t , M_t are the operational costs in year t , F_t are the expenses on fuel in year t , E_t are the revenues from energy in year t , assuming a 90% capacity factor¹² [100] and r is the discount rate, assumed to be 5%. The levelized costs for oil production were also calculated based using equation 4.53. For the oil production, a royalty rate of 15% was assumed (average for the U.S.).

¹² The capacity factor of a power plant is the ratio of its actual output over a period of time, to its potential output if it were possible for it to operate at full capacity continuously over the same period of time.

5. Modelling results

In this section, the results of the modelling will be represented. For the most relevant parameters, a sensitivity analysis is performed over a range of possible values. First the results for the EOR part are discussed, followed by the time necessary to dry the reservoir and the CPG system.

5.1 CO₂-EOR

Due to time limitations, the CO₂-EOR modelling was performed by estimating an average performance based on data from existing fields. The main goal of the CO₂-EOR modelling in this thesis is, therefore, to provide an estimation of the time CO₂ will be injected, the injection rate and the fraction of CO₂ that is present in the formation after the EOR phase.

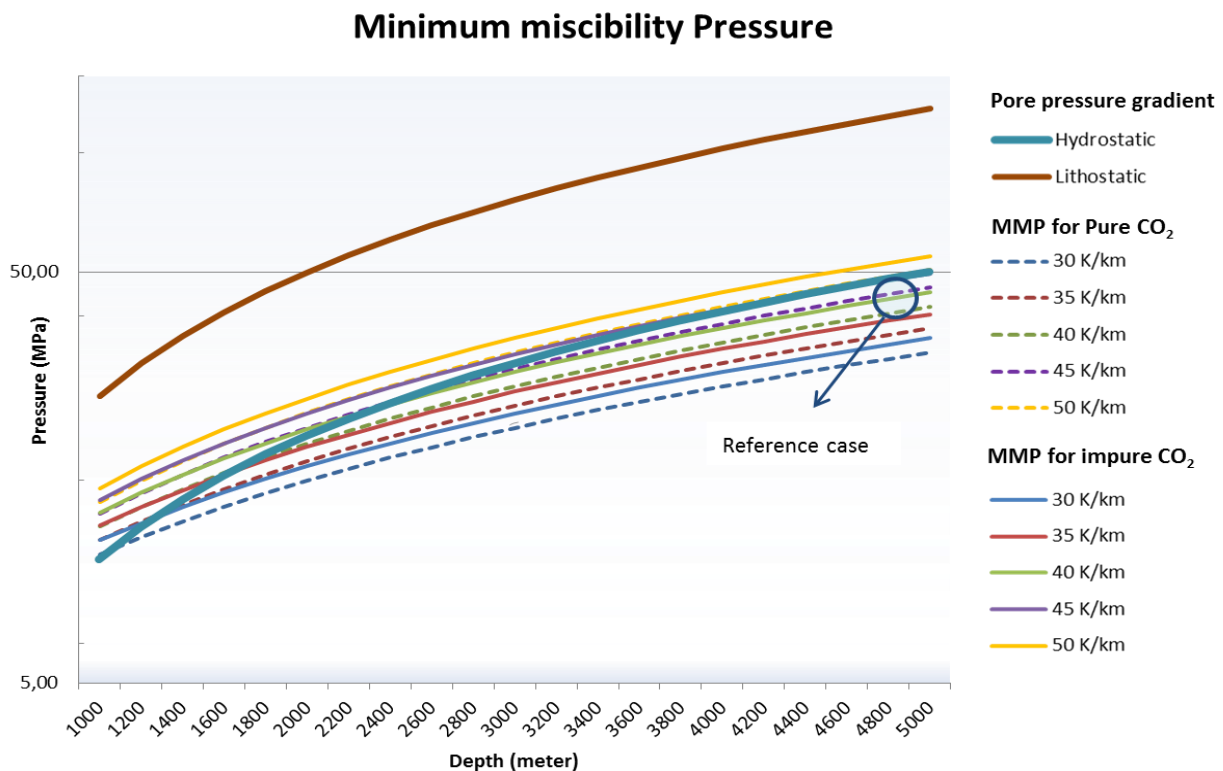


Figure 5.1: Minimum miscibility pressure vs depth for different geothermal gradients, the MMP for pure CO₂ (Dotted lines), the MMP for impure CO₂ (solid lines), the hydrostatic (blue) and the lithostatic (brown) pressure gradients.

For the reference case, the pure MMP of CO₂ with H₂O was calculated to be 36.53 Mpa in the case of pure CO₂. However, the CO₂ will not be pure. Therefore, the composition of the bought CO₂ was based on the composition of natural CO₂ from the sheep mountain dome. The MMP is taking into account the effect of impurities was calculated to be 39.57MPa.

Figure 4.8 represents the minimum miscibility pressure for pure and impure CO₂ versus depth at various geothermal gradients. The composition of the oil was based on oil from the Weyburn Field and the composition of the CO₂ were based on the CO₂ from sheep mountain. The blue and brown lines represent the hydrostatic and lithostatic pressure gradients respectively. In general, it can be said that reservoirs that fall above the blue line, are unsuitable for miscible production enhancement. However, over pressurized reservoirs might be an exemption on this. It was

argued that a pressure/MMP ratio of 1.1 would be advisable to account for pressure fluctuations over the lifetime of the project and spatial pressure fluctuations [58]. Therefore, deeper reservoirs with smaller geothermal gradients would be advisable. Assuming hydrostatic pressure increase in the reservoir, this ratio for the reference case will be 1.26.

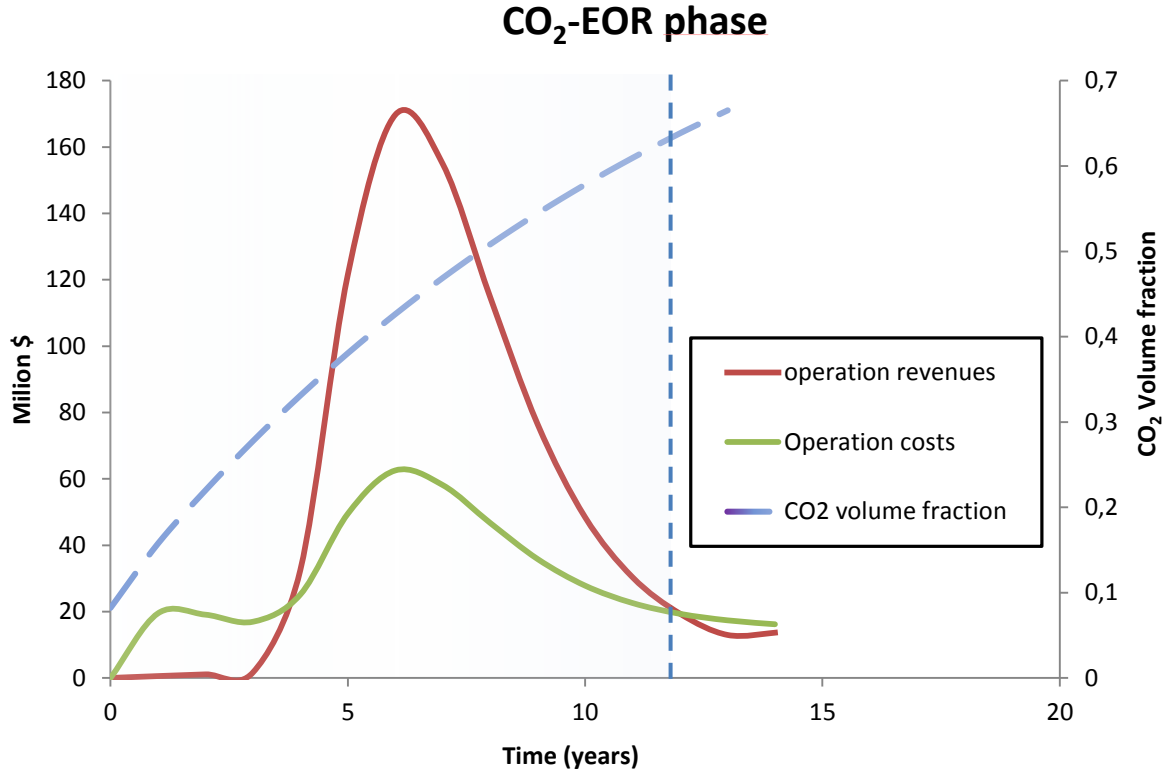


Figure 5.2: Costs and revenue profiles for the CO₂-EOR phase vs. time since injection started and the average volume fraction of CO₂ in the reservoir pores. The vertical line represents the time where CO₂-EOR is terminated.

Figure 5.2 represents the oil revenue curve for an oil price of \$60/bbl, the operational costs of the oil production, listed in Table 4.2, and the average CO₂ volume fraction in the reservoir pores. The operational costs depend on the amount of oil produced via the processing costs and are based on a CO₂ at plant gate price of \$45/tonne. In the reference case, the time at which CO₂-EOR would be terminated at this reservoir section was calculated to be 12 years.

5.1.1 CO₂-EOR sensitivity analysis

The viability of the EOR strongly depends on the strongly depend on the oil price, the costs for CO₂, the CO₂-EOR ratio and the recovery factor. Table 5.1 to 5.4 present their effect on the lifetime of the project, Levelized oil production costs, CO₂ pore fraction after the EOR phase, total production and CO₂-storage volume during this phase.

Static CO₂ price

The price of CO₂ strongly depends on the capture costs. If additional income can be generated from carbon credits, prices for CO₂ may drop to zero. If the costs for pollution are deducted from the price that CO₂-EOR projects would otherwise have to pay, this leads to a much more optimistic cost price for CO₂-EOR. Table 5.1 lists the performance of CO₂-EOR assuming static CO₂ prices over a range of -10 to 40 (\$/tonne).

Table 5.1: The effect of static CO₂ price on the performance of the CO₂-EOR phase.

CO ₂ price (\$/tonne)	Levelized costs (\$/Bbl) ¹³	Levelized costs (\$/Bbl) ¹⁴	Total oil (million BBL)	CO ₂ stored (Mtonne)	CO ₂ fraction (% pore)
-\$20,00	10,69	3,18	25,06	6,86	85%
-\$10,00	14,56	5,99	25,06	6,86	85%
\$0,00	18,43	8,80	25,06	6,86	85%
\$10,00	22,29	11,61	25,06	6,86	85%
\$20,00	26,16	14,42	25,06	6,86	85%
\$30,00	30,03	17,23	25,06	6,86	85%

The table clearly shows that the Levelized costs for oil production are strongly dependent on the CO₂ price. If additional income can be generated by CO₂ storage, the oil prices for production via CO₂-EOR were calculated to be extremely low.

Dynamic ETS

The CO₂ price evolution is assessed according to three dynamic scenarios for the ETS. Table 5.2 lists the effects of changing the price of CO₂ during the EOR phase. Estimations for the development of the ETS price¹⁵ in the coming decades show high uncertainty though all predictions agree that the market price is most likely to increase depending on the urgency of mitigation [111].

Figure 5.3 presents the evolution of the CO₂ price for the project for the three scenarios. If the ETS price is

higher than the CO₂ capture and transport costs, the gradient

becomes less steep as the majority of the profits were assumed to be for the capture plant.

Recovery factor

The recovery factor for EOR strongly depends on the reservoir and fluctuates with the reservoir previous oil recovery phases, oil type, etc. Estimations for the recovery factor of miscible CO₂-EOR vary between 10-15% [133], 5-15% [25] and 10-20% [8]. Table 5.2 list the dependency of performance indicators for the EOR phase on the recovery factor.

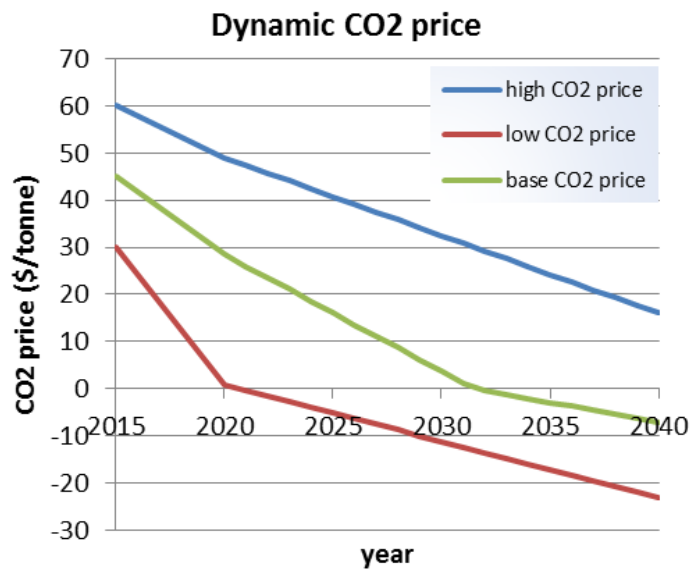


Figure 5.3: CO₂-price for the CO₂ project over the years for the period from 2020 to 2040.

¹³ Calculated based in the new wells methodology

¹⁴ Calculated based on data from representative fields in the U.S. [90]

¹⁵ The ETS price are the costs a company pays for the right to emit a tonne of CO₂.

Table 5.2: The effect of the recovery factor on the performance of the CO₂-EOR phase.

Recovery factor	Levelized costs (\$/Bbl) ¹³	Levelized costs (\$/Bbl) ¹⁴	Total oil (million BBL)	CO ₂ stored (Mtonne)	CO ₂ fraction (% pore)
0,05	787,43	365,45	0,34	1,31	24%
0,1	43,63	25,52	16,51	4,83	70%
0,15	35,84	21,45	25,06	6,86	85%
0,2	30,60	18,67	33,41	8,40	92%

Average CO₂-oil ratio

The EOR ratio represents the number of barrels of crude oil that are produced for each tonne of injected CO₂. In this model, these values represent an average EOR ratio as the actual ratio is projected to follow a lognormal curve. At first no oil is produced per tonne CO₂ injected, this then rapidly increases to a maximum value, from where it declines and asymptotically approaches zero. The U.S. Department Of Energy (USDOE) uses a standard range from 3.1-3.8 Bbl/tonne CO₂ for miscible CO₂ projects [8]. The IEA assumes a slightly wider range, varying from 2.8 to 4.2 bbl/tonne CO₂. The previous CO₂ solvent flooding results from projects in the US find an average EOR ratio of 1.9 bbl/tonne CO₂ [134]. The Average oil to CO₂ ratio was calculated for a range from 1-4. Table 5.3 list the dependency of performance indicators for the EOR phase on the Oil/CO₂ ratio.

Table 5.3: The effect of the average oil/CO₂ ratio on the performance of the CO₂-EOR phase.

Avg. oil/CO ₂ ratio	Levelized costs (\$/Bbl) ¹³	Levelized costs (\$/Bbl) ¹⁴	Total oil (million BBL)	CO ₂ stored (Mtonne)	CO ₂ fraction (% pore)
1	444,02	275,08	1,04	4,28	76%
1,5	49,02	31,15	24,76	10,96	98%
2	42,08	26,24	24,76	8,90	94%
2,5	37,80	23,21	24,76	7,60	89%
3	36,85	22,15	25,06	7,18	87%
3,5	34,53	20,54	25,06	6,45	83%

Table 5.1 to 5.4 show that under favorable conditions, oil production using CO₂-EOR is economically viable even at relatively low oil prices using anthropogenic CO₂ (\$45/tonne). A profitable EOR phase furthermore leads to a higher reservoir pore fraction and, therefore, fewer startup costs for the CPG phase.

5.2 Drying the reservoir

In this section the CO₂ threshold only takes into account H₂O, as an impurity. Other impurities that may be present in the stream, like N₂ and CH₄, are not taken into account as these will not precipitate in the system. Figure 5.4 represents the dew lines at which CO₂ concentration H₂O rich liquid will precipitate. The blue line with numbers represents the various phases of the CPG system as introduced in figure 4.4. From the figure, the threshold values can be derived for the equipment. For any overall fluid composition, the dew line divides the pressure-temperature plane into a region where the compounds are fully miscible, and a region where two phases are present. On the right side of the dew line, a single phase exists. To the left of the dew line, two phases coexist.

For the reference case, the threshold value for CO₂ purity at the production wellhead is around 91%. For the turbine, this percentage is even 95,5%. The corrosion potential of a condensed water phase is more significant than the solution pH would suggest, due to the buffering provided by dissolved CO₂ and CO₂-related species. Figure 5.5 represents the bubble lines for CO₂ dissolved in H₂O for the different conditions in the system. From this figure, it becomes clear that, even for a H₂O percentage of 1%, some liquid water might precipitate in the turbine. However, the concentration of CO₂-related species in the precipitate will be rather low. For the cooling equipment and the pump, the equipment materials should be able to withstand small amounts of CO₂ saturated water.

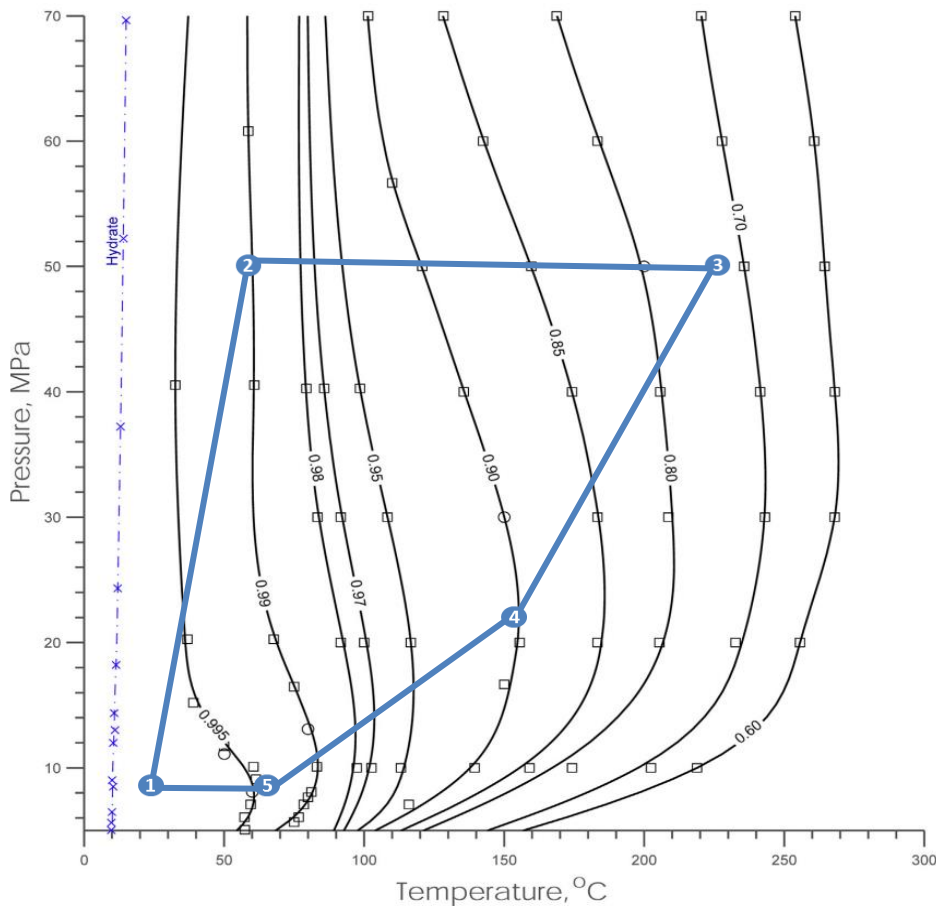


Figure 5.4: Dew lines for a CO₂-H₂O mixture at the conditions in the various phases of the system. Each line defines the CO₂ mole fraction conditions for dew formation. (methodology based on Atrens, (2014) [113]).

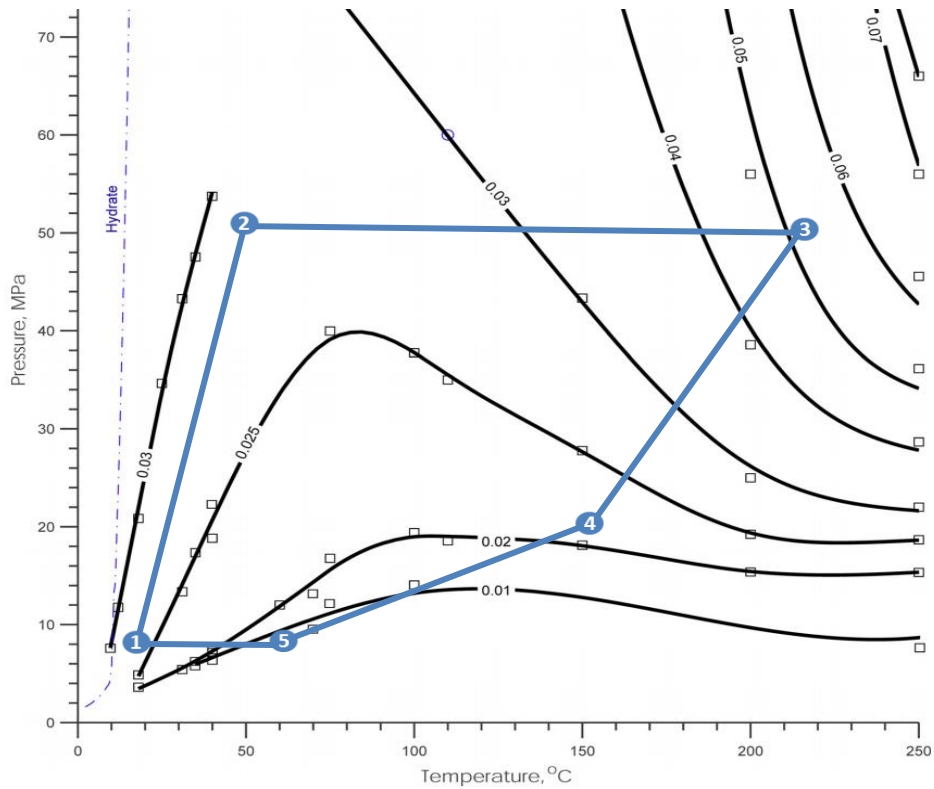


Figure 5.5: Bubble point lines for a CO₂-H₂O mixture at the conditions in the various phases of the system. Each line defines the CO₂ mole fraction conditions for bubble formation. Squares indicate interpolated or extrapolated data points. (methodology based on Atrens, (2014) [80].

For the CO₂-EOR phase, it was assumed that the CO₂ injection rate was kept constant while the amount of oil produced per metric ton of injected CO₂ and thus the oil production rate declined in a lognormal pattern. During the drying phase, the injection rate is then increased to speed up the drying of the reservoir. The ideal injection rate depends on the availability of CO₂ (for anthropogenic CO₂ this depends on the capture rate at the plant), the reservoir limitations

discussed in section 2.4, and the limitations of the equipment. Figure 5.5 shows the volumetric CO₂ fraction in the reservoir pores over time for various injection rates. Due to the compressible nature of CO₂, its density and therefore volume strongly depends on the depth of the reservoir, increases in reservoir depth will, therefore, increase reservoir drying time. Figure 5.5 is based on the reference case with a depth of 5 km.

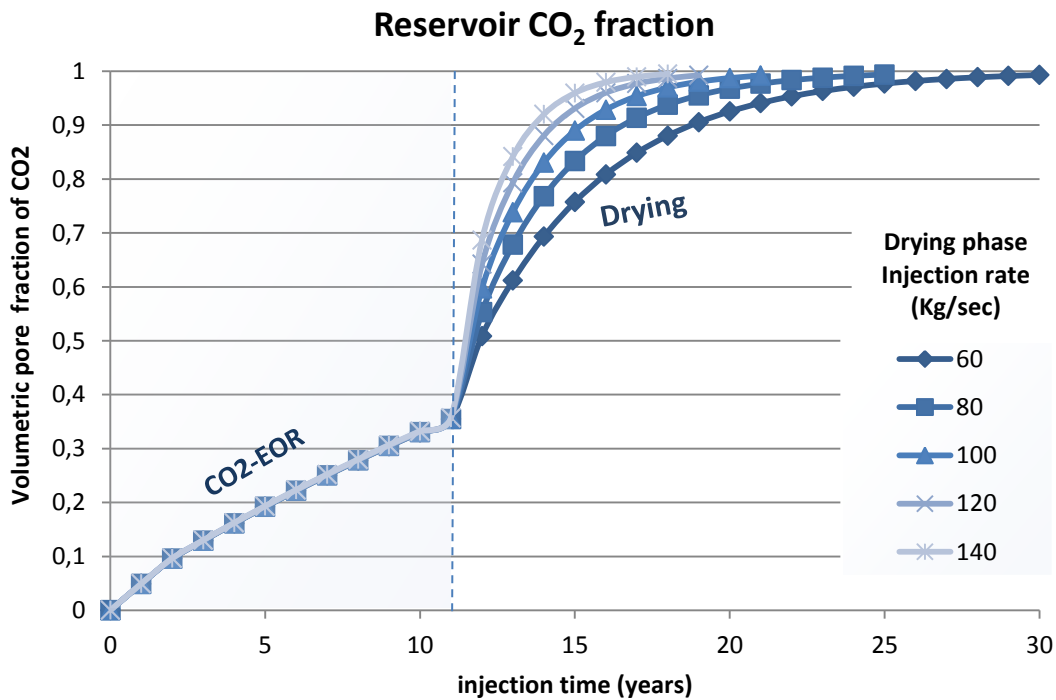


Figure 5.6: Volumetric pore fraction of CO₂ during the CO₂-EOR phase and the drying phase for the reference case at different injection rates for the Drying phase.

Figure 5.6 shows that the drying time of the reservoir increases exponentially with an increase of the CO₂ purity threshold. Furthermore, it also shows that the drying time, to reach the CO₂ purity threshold strongly depends on the injection rate at which CO₂ can be injected. In order to minimize the risk of induced seismicity, it is important that pressure gradients are kept low during the drying phase.

As was mentioned in section 3.3.2, the salting out effect leads to a reduction in permeability of the dried out region that is proportionate to the salinity of the formation brine and the porosity of the formation. Since the solid salt saturation in the dry-out zone is constant, the permeability reduction in the dry-out zone is independent of the radius. However, with the expansion of the dry-out zone with time, the permeability reduction affects an increasingly larger area of the aquifer. Figure

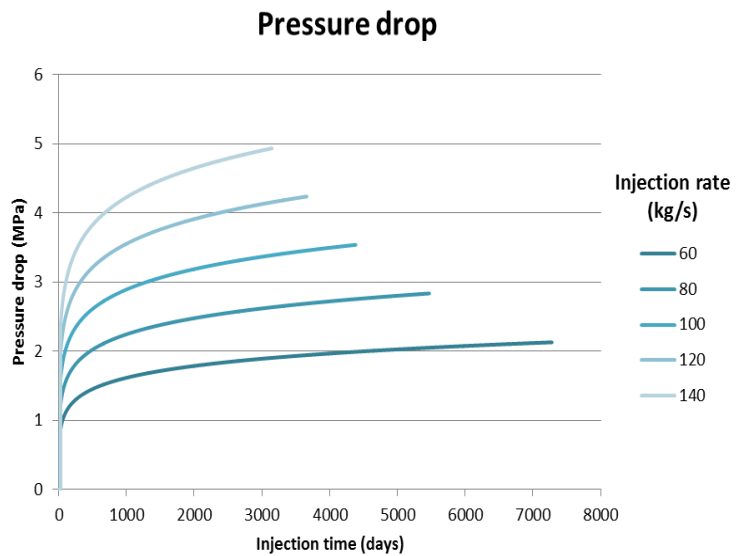


Figure 5.7: Pressure drop over the drying front during the drying phase for various injection rates

5.7 presents the total pressure drops over the two fronts and drying times for different injection rates in the drying phase. The figure shows that the pressure drop is significantly lower at lower injection rates. Especially at low depths, the pressure increases

NOTE:

The clear question that arises from this graph is: ‘if the reservoir can sustain these high pressure gradients, why was the injection rate not increased in the EOR phase?’ It should be noted that during the EOR phase, much more oil and brine are present in the reservoir. As both these substances have viscosities much higher than that of supercritical CO₂. Therefore, with a shift in the reservoir toward more CO₂ rich, the effective permeability of the combined reservoir fluids increases. Before CO₂ breakthrough in the production well, no preferential pathways have formed yet connecting the wells. These will have established in the drying phase.

5.3 CO₂-plume geothermal

The calculated phases at the various stages in the system are presented in figure 5.8. This shows that the injection takes place in the dense phase meaning that a pump can be used, rather than a compressor. Pumps are generally far cheaper, more compact and require less energy.

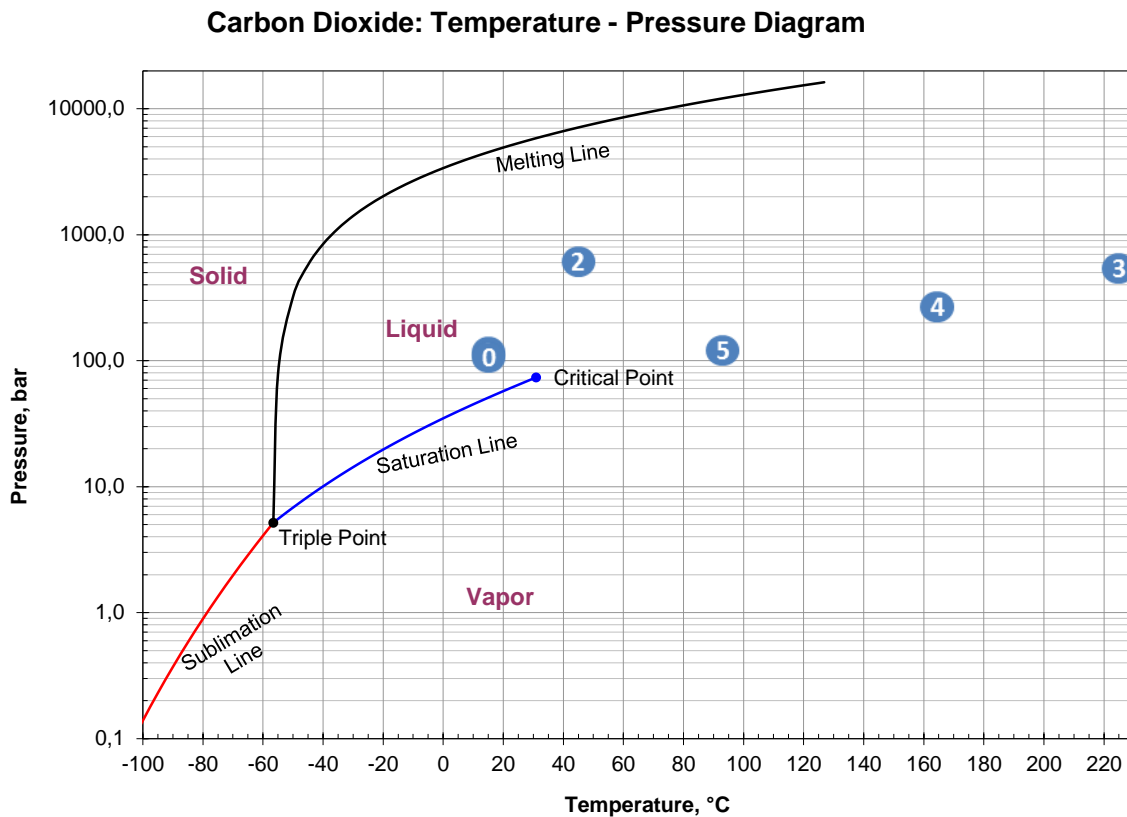


Figure 5.8: Phase diagram for the CO₂ in different phases in the CPG system. The numbers represent the different stages of the system as depicted in figure 4.4.

The thermodynamic property data for CO₂ was obtained from the Chemicalogic website [135]. The phase diagram again shows the importance of the rejection temperature. Cooler environments, allow a higher density of the CO₂, meaning that less volume has to be pumped. Figure 5.9 presents the pressure profiles for the injection- and production well for the reference case at different reservoir depths. At small depths, if the pressure would be maintained at

reservoir pressure, pressures in the injection well will become too low to maintain CO₂ in supercritical or dense state. If the CO₂ is injected in the gaseous phase, compressors have to be used, meaning significantly higher parasitic losses.

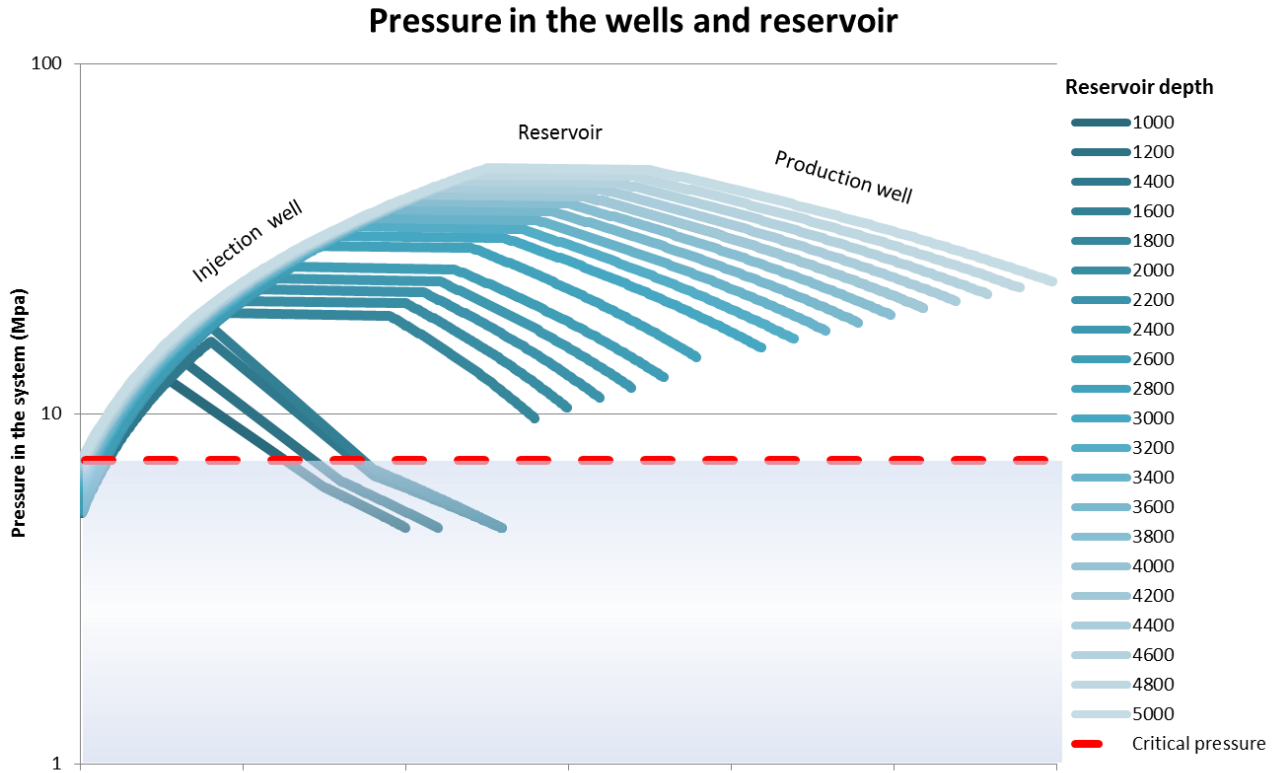


Figure 5.9: Pressure profile for the CO₂ as it moves through the subsurface. The initial increase in the injection well, the pressure slowly declines over the reservoir followed a faster decline over the production well. The blue area represents an area where the pressure is not enough to be produced by the thermosiphon.

To remedy this, it may be chosen to increase the pressure in the system to >7.38MPa. This overpressurization of the reservoir increases the risk of induced seismicity. Especially in the case of shallow reservoirs, induced seismicity can be risky as it may lead to leakage into potable aquifers and surface waters. If the temperature of the CO₂ falls below the critical temperature, the CO₂ will become a saturated mixture of gaseous and liquid CO₂. Figure 5.10 presents the Mollier's chart with the thermodynamic properties of CO₂ at the various processes in the system.

Newly bought CO₂ enters the plant at the condition represented by point '0' and is then pressurized to the injection pressure '1'. The section 1→2 represents the adiabatic pressure and temperature increase over the injection well. Within the reservoir, the temperature is heated to the reservoir temperature at that time (2→3). Section 3→4 represents the adiabatic rise through the production well, where the pressure drops due to static pressure losses and frictional losses leading to a temperature reduction caused by Joules-Thompson cooling. The isentropic expansion through the direct CO₂ turbine is represented by the section between 4 and 5. Finally, the CO₂ is cooled back to the injection temperature (5→1). Depending on the heat requirements, this heat can be used for district heating or an Organic Rankine Cycle.

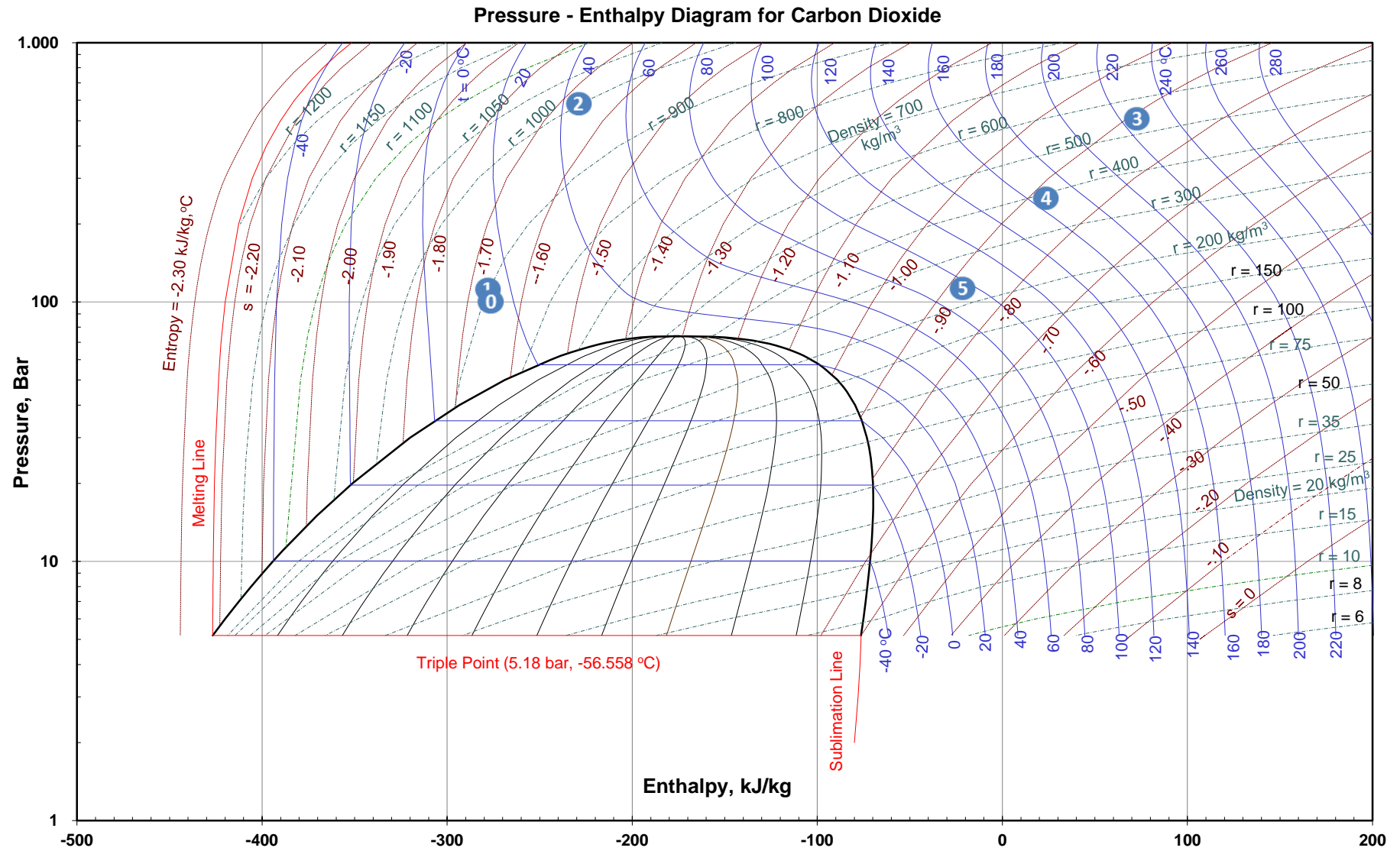


Figure 5.10: Moliers chart for CO₂ at the various phases of the system. The numbers represent the different stages of the system as depicted in figure 4.4.

A binary system can be used in addition to the direct turbine, to utilize the extra heat for electricity generation using an organic Rankine cycle. In this case, the electricity production is calculated as the output of the direct power system plus the ORC turbine minus the parasitic load of the compressor and heat exchanger fan. Figure presents the relation between the electricity production by the thermosiphon that is generated using the direct CO₂ turbine and the reservoir depth over a range of geothermal gradients. The pressure is assumed to increase hydrostatically. Although, this does not necessarily has to be the case, porosity and permeability tend to decrease with reservoir depth due to the compaction caused by the increase in lithostatic pressure (figure 3.4). To account for compaction, a porosity gradient of 3% km⁻¹ was applied starting from 25% based on sandstone reservoirs [88]. Based on the porosity reduction, the permeability was calculated from Eq. 4.20. For the salinity, a gradient 40ppm m⁻¹ was applied starting from 50.000 ppm.

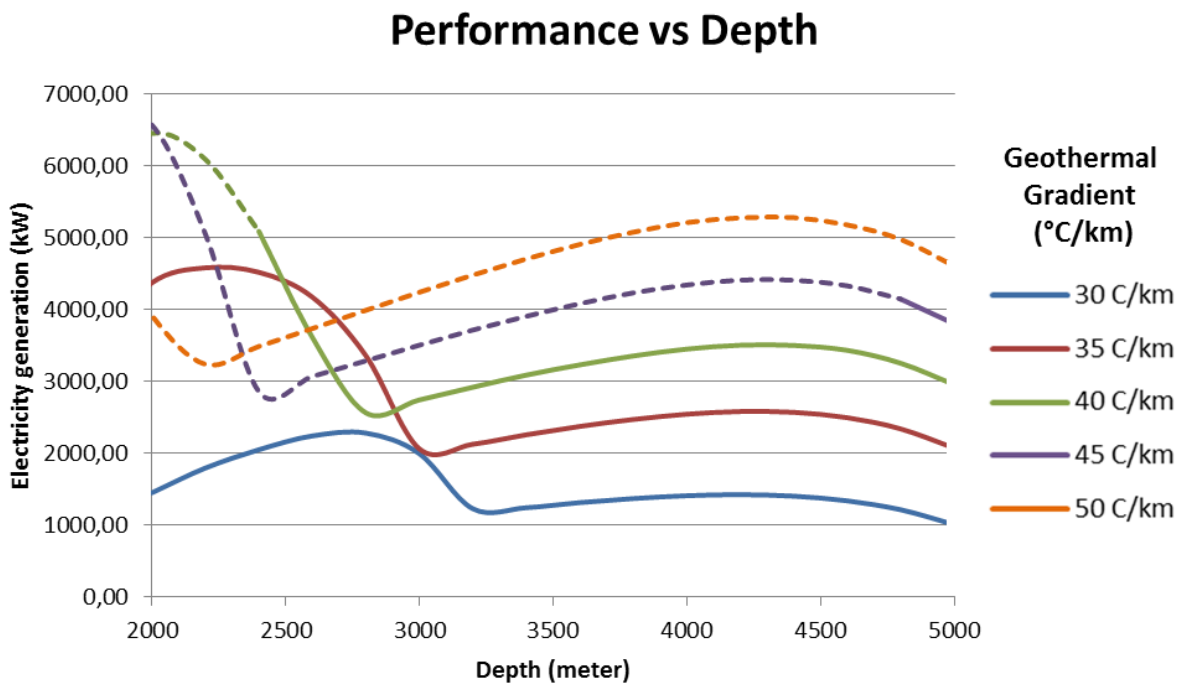


Figure 5.11: performance of the CPG-phase of the project for different depths and at various geothermal gradients. The dotted lines represent the performance of the CPG system in reservoirs where CO₂ is not miscible with oil using the CO₂ and oil compositions in Table 4.2.

It should be noted that the efficiency drop in deeper reservoirs may be partially contributed to the permeability increase that is assumed. Higher permeability reservoirs require a higher production pressure and therefore less pressure difference over the production and injection wellheads. if higher permeability reservoirs can be found at this depth, the efficiency of deeper reservoirs will go up.

With an increase in depth, the temperature of the CO₂ that exits the direct turbine increases. Apart from geothermal hotspots, utilization of this heat does not appear viable from shallow reservoirs. However, in deeper and hotter reservoirs, additional binary power production from the heat might even overtake the role of main power producer from the direct system. Figure 5.11 shows the relation between the heat produced from the reservoir after the direct turbine

and the depth. As the temperature increases, the Carnot efficiency (eq. 2.4) increases, explaining the non-linear increase with depth.

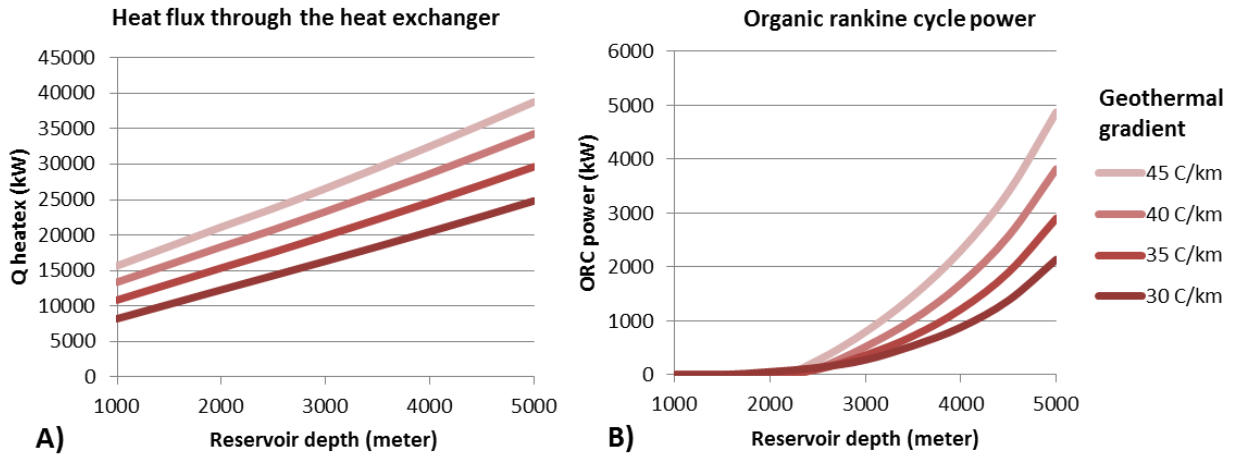


Figure 5.11 : Heat recovery from the reservoir. A) heat flow through the heat exchanger B) additional power that can be generated using a binary ORC turbine.

Besides reservoir conditions, the productivity of the CPG system strongly depends on the flow rate. At higher flow rates, the frictional pressure drops over the reservoir and wells become much higher leading to lower overall production pressures. Since the direct turbine utilizes the pressure difference generated by the expansion of the heated CO₂ over the production and injection well, the performance will decrease (figure 5.12 In red). As the heat extraction from the reservoir will still increase with an increase in flow rate (figure 5.13), this further reduces the efficiency of the system. The amount of heat that flows through the heat exchanger and therefore can be used for district heating or ORC power production increases. The blue line in figure presents the power that can be generated from the heat using a binary efficiency of 50%.

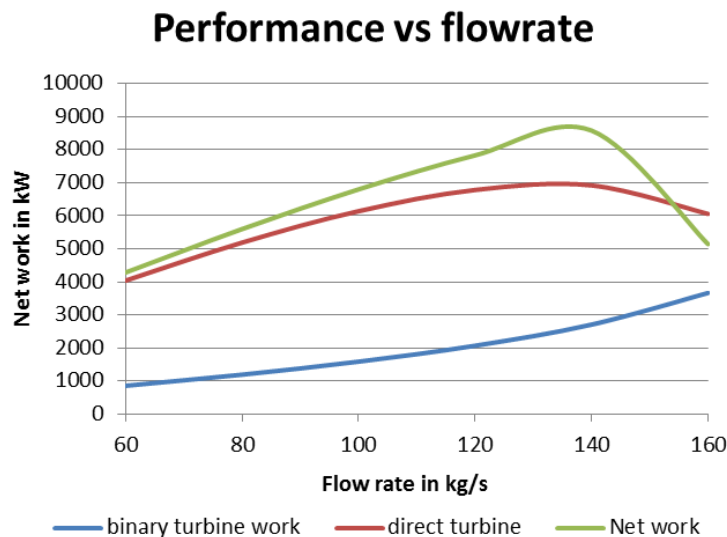


Figure 5.13: The output of the direct turbine, potential secondary binary ORC turbine and Net Work (adjusted for parasitic load of the pump and the cooling fan vs injection rate).

The green line presents the Net electricity production of the turbines minus the parasitic load of

the pump and the cooling systems. Since both these loads increase with an increase in flow rate, they further suppress the performance of the total combined system at higher flow rates.

Over time, the extraction of heat from the reservoir will mean that the temperature in the reservoir drops and thus the energy extraction rate drops. The rate at which the temperature drops strongly depends on the CO₂ injection rate. Figure 5.14 presents the average temperature depletion of the reservoir over time for different injection rates. The temperature regeneration rate in this calculation is kept constant. However, as the temperature gradient increases it is more likely that the thermal recovery rate increases with a reduction in reservoir temperature.

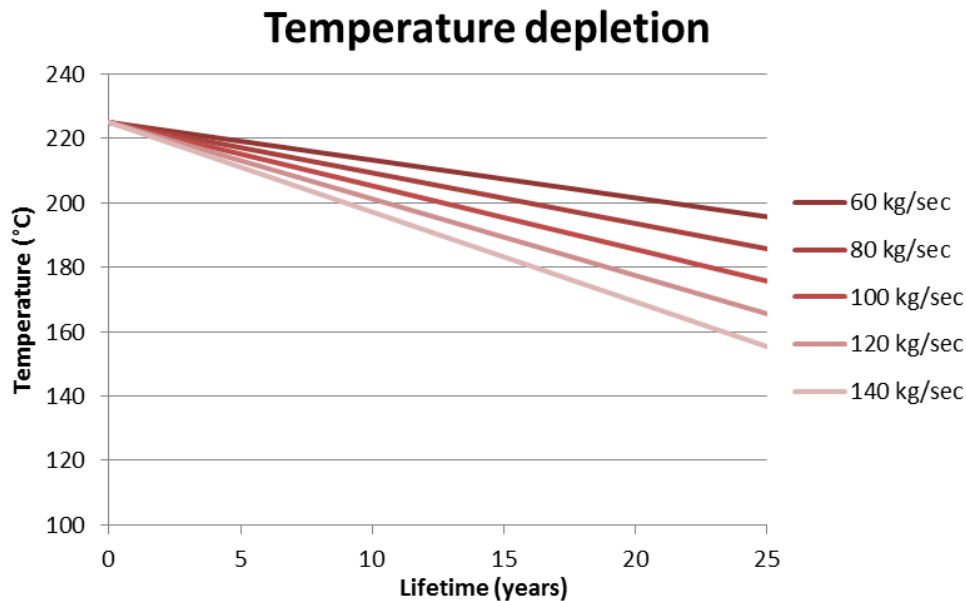


Figure 5.14: Reservoir temperature depletion over the lifetime of the CPG system vs the flowrate for the reference case 50Mpa and 225°C.

With the temperature, the electricity generation over the years declines. Since the temperature is modelled to decline linearly instead of a propagating cold front, the effect of temperature decline will most likely be overestimated using this methodology.

5.4 Costs analysis

The economics the technology strongly depends on the configuration and the needs in the vicinity of the project. Multiple cash flows can be generated in the form of additional hydrocarbon sales, electricity production and district heating. Furthermore, depending on local policy, carbon sequestration and energy market buffering have the potential to generate additional cash flows. Their environmental benefits have to be taken into account when assessing the full potential of the project.

Figure 5.15 and 5.16 present the capital costs for the CO₂-EOR phase of the project and the CPG phase of the project respectively for the reference case. The capital investments for wells and brine desalination/reinjection systems were allocated to the CO₂-EOR phase of the project. The capital costs of the EOR operation increase with depth due to the exponential cost dependence of the drilling costs with depth. Furthermore, from a certain depth, additional pumping is required. The capacity of the recycling facility is adjusted to the requirements during the drying phase.

Higher CO₂ injection rates during the drying phase lead to higher maximum load for the recycling facility and therefore higher capital costs. These effects have only been accounted for in the new wells methodology.

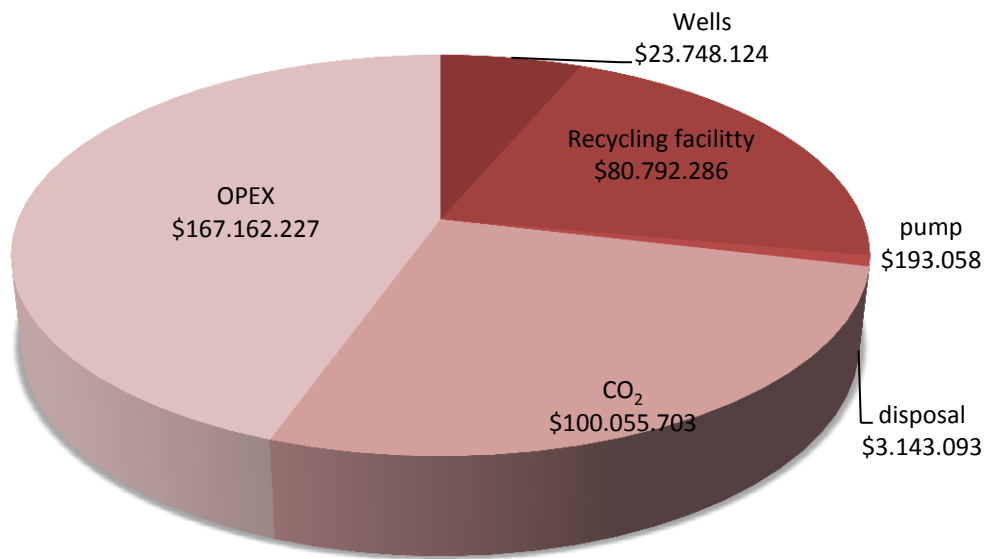


Figure 5.15: Cost buildup of the EOR phase using the new well methodology. The total capital costs of were calculated to be 107.7 Million USD.

The costs were based on the reference case with a CO₂ at plant gate cost of \$45/tonne, the low ETS scenario and recycling costs of \$13.45/tonne. Figure shows that the majority of the costs are for CO₂ and the operational costs. The reason for this is that the recycling and recompression of the CO₂ requires a large amount of power (Table 4.2), this makes up more than half of the operational expenses in CO₂-EOR. The scenario depicted above includes the drilling of new wells.

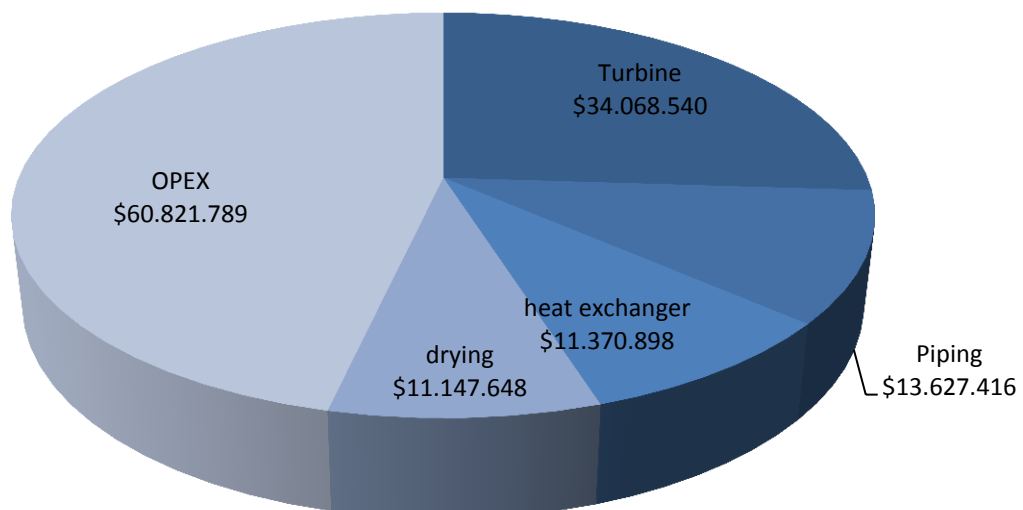


Figure 5.16: Cost buildup of the CPG phase. The total capital costs of were calculated to be 70.2 Million USD.

In this figure, the cost allocation ‘piping’ includes additional costs made for piping, control, freight, labor, etc calculated from the factor (λ) in equation 4.45. The total capital expenses for the CPG system increase with depth and flow rate. During the geothermal phase, the operational costs are the majority that is to be expected since most of the infrastructure is reused. However, for comparison, the operational expenses were calculated according to two methodologies (Eq 4.52a & 4.52b). These methodologies lead to very different operational expenses ranging from \$5.704.021 (4.52a) to \$60.821.789 (4.52b), over the lifetime of the CPG system. The effect of the OPEX calculation method leads to a difference of 0.18 – 0.29 \$kWh⁻¹ for the Levelized costs of electricity.

To calculate to costs for the drying phase, the oil that is produced alongside the CO₂ and can be sold should be taken into account. Figure represents the oil production during the oil production

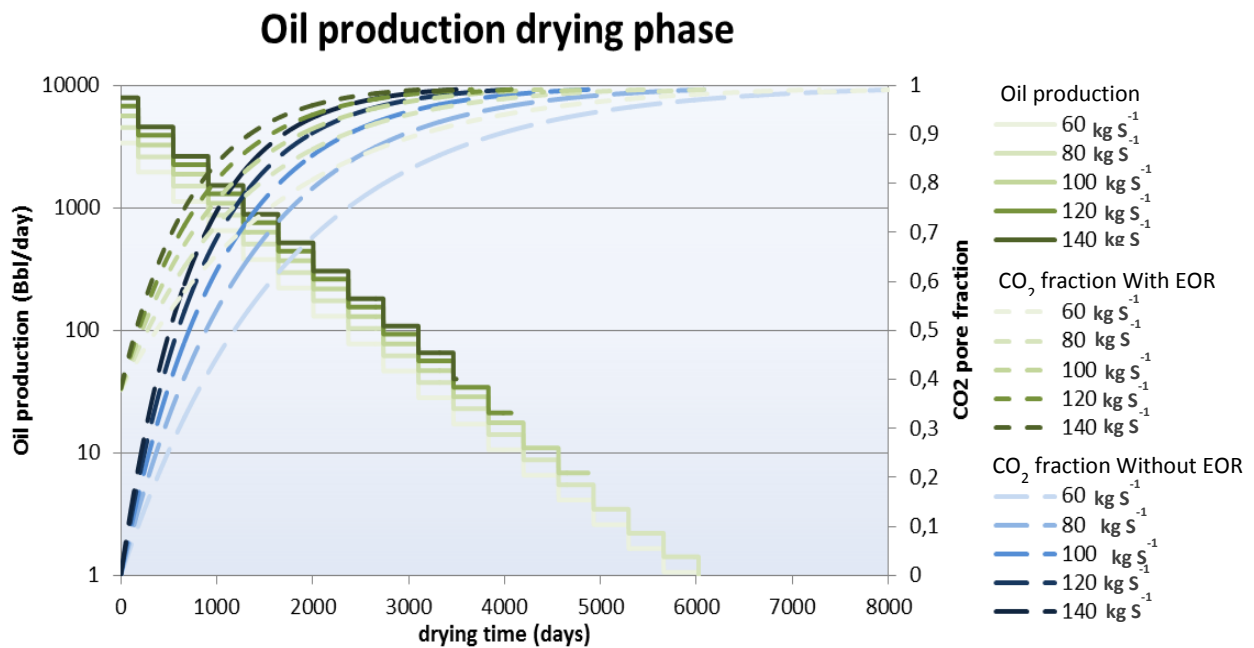


Figure 5.17: Oil production (stepped solid green) and CO₂ pore fraction for the CPG-EOR (dotted green) and normal CPG case (dotted blue) during the drying phase.

per day (stepped line). The green lines represent the reservoir fraction with previous CO₂-EOR, the blue lines without previous CO₂ injection.

Costs or benefits of the stored CO₂

The costs for CO₂ are based on the costs of the pressurized CO₂ at plant gate minus the ETS price for CO₂ emission. To account for the uncertainty in these costs, Table 5.5 lists the Levelized costs of electricity and the total costs of the drying for the reference case with different CO₂ prices. Negative drying costs mean that the income for storing CO₂ plus the additional oil recovery during this phase can generate additional revenues. The effects of dynamic CO₂ prices is presented in figure 5.18. In the case of the high ETS scenario, the costs for drying can be completely compensated for by the benefits from CO₂ storage and the additional oil recovery. For the base case, the costs are significantly reduced.

Table 5.5: Costs/Benefits of CO₂ storage.

Price CO ₂ (\$/tonne)	LCE (\$/kWh)	Drying costs
-15	\$0,14	-\$31.214.068
-10	\$0,16	-\$22.540.713
-5	\$0,18	-\$13.867.358
0	\$0,20	-\$5.194.003
5	\$0,22	\$3.479.351
45	\$0,26	\$18.202.051

Especially in the drying phase, a significant amount of CO₂ is stored in the formation. The CO₂ stored during the CPG phase is highly dependent on the mixing rate of the reservoir. The total amount of CO₂ that can be stored in the reservoir depends on the porosity of the reservoir and the reservoir pressure via its effect on the density of CO₂. The amount of CO₂ stored in the reservoir varied from 191.4 Mtonne of CO₂ in a 1000m

deep reservoir to 68.5Mtonne in a 5000m deep reservoir. This variation can be contributed to the porosity reduction, therefore, more porous reservoirs at these depths can store higher amounts of CO₂.

Cost of electricity

To calculate the costs of oil production for reservoirs at different depths, the same parameter gradients were used as in the performance calculations. The geothermal gradient, in the reference case, is 45 °C km⁻¹. In figure 5.18, the solid blue line represents the costs of oil production per barrel, the dotted blue lines above and present the Lifting costs for a barrel of crude oil with EOR for the 'low ETS' and 'high ETS' scenarios respectively.

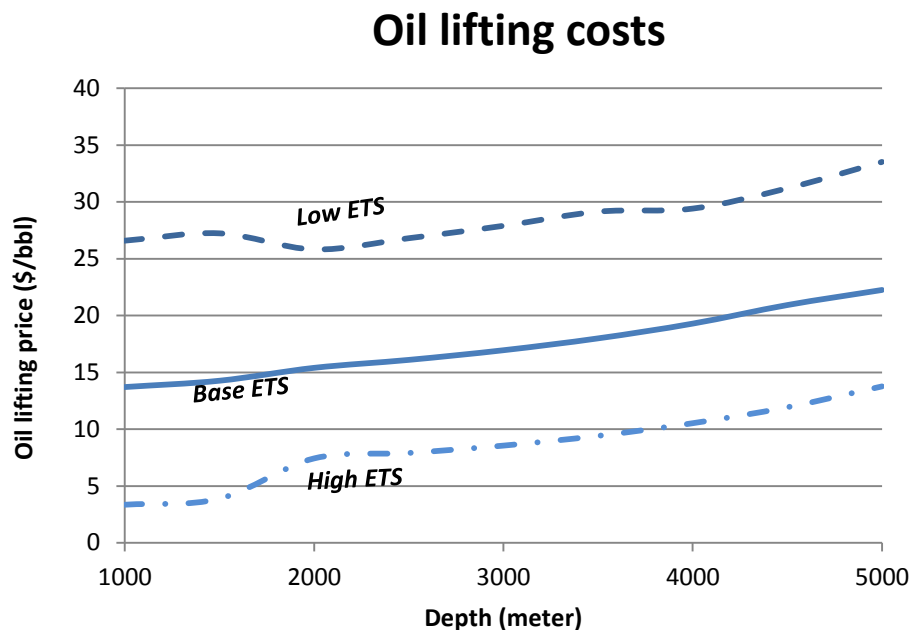


Figure 5.18: Relation between the Levelised costs oil production with depth. The costs for oil were calculated using the refurbished wells methodology and based on the different CO₂-price scenarios.

The same methodology was used to calculate the levelized cost of Electricity production. In figure 5.19, the solid green line represents the Levelized costs of electricity, the dotted green lines above and present the levelized costs of electricity for the 'low ETS' and 'high ETS' scenarios respectively. To the regret of the author, there was not enough time left to include a

full economic assessment of the system including a secondary binary ORC cycle. Since there was no cost calculation included in the model, the additional electricity productions of the binary system were not taken into account in the calculations of the Levelized costs for electricity.

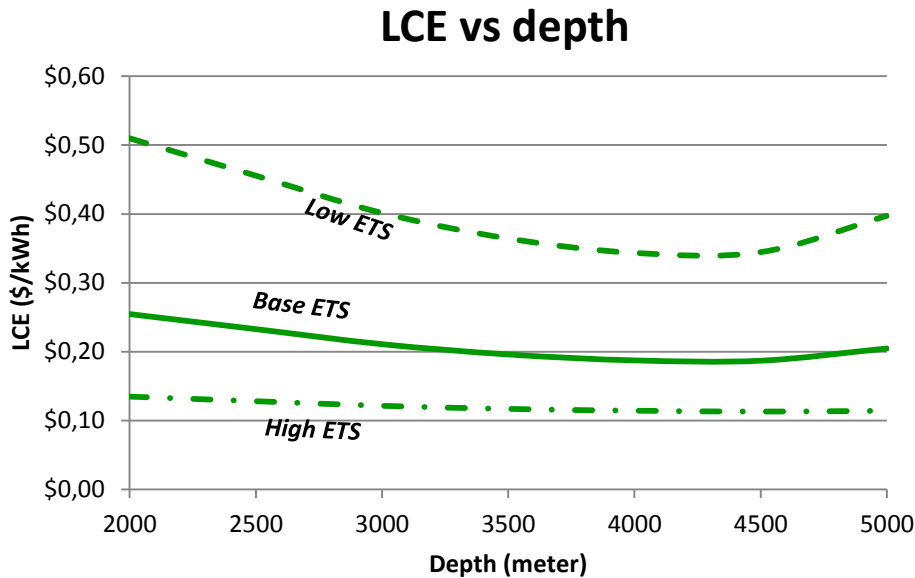


Figure 5.19: Relation between the Levelized costs of electricity with depth. The costs for electricity were calculated based on the different CO₂-price scenarios.

The LCOE values shown for each utility-scale generation technology in figure are obtained from the U.S. annual energy outlook 2015 [131] and are calculated based on a 30-year cost recovery period compared to other forms of electricity production in the U.S. the costs of electricity production using CPG would be high. It should be noted that these costs are based on the average costs of large scale facilities.

Furthermore, the benefits that may be obtained from the additional heat are not yet taken into account. In remote areas like many oil fields, energy prices may be much higher and if the heat can be utilized for industrial processes or compound heating, the technology might still prove lucrative. To put this into perspective, for a standalone coupled PV/diesel generator system with similar capacity (1-4MW), the costs of electricity are \$0.38/kWh at a the current average U.S. diesel price of \$0.80/L¹⁶. For a standalone diesel generator, this will even be \$0.40/kWh [136]. the largest component of CO₂ recycling O&M costs is associated with the energy for compression of the CO₂ for reinjection, and this energy is often produced on-site [125].

¹⁶ Obtained from http://ycharts.com/indicators/us_diesel_price on the 12th of Jan 2015.

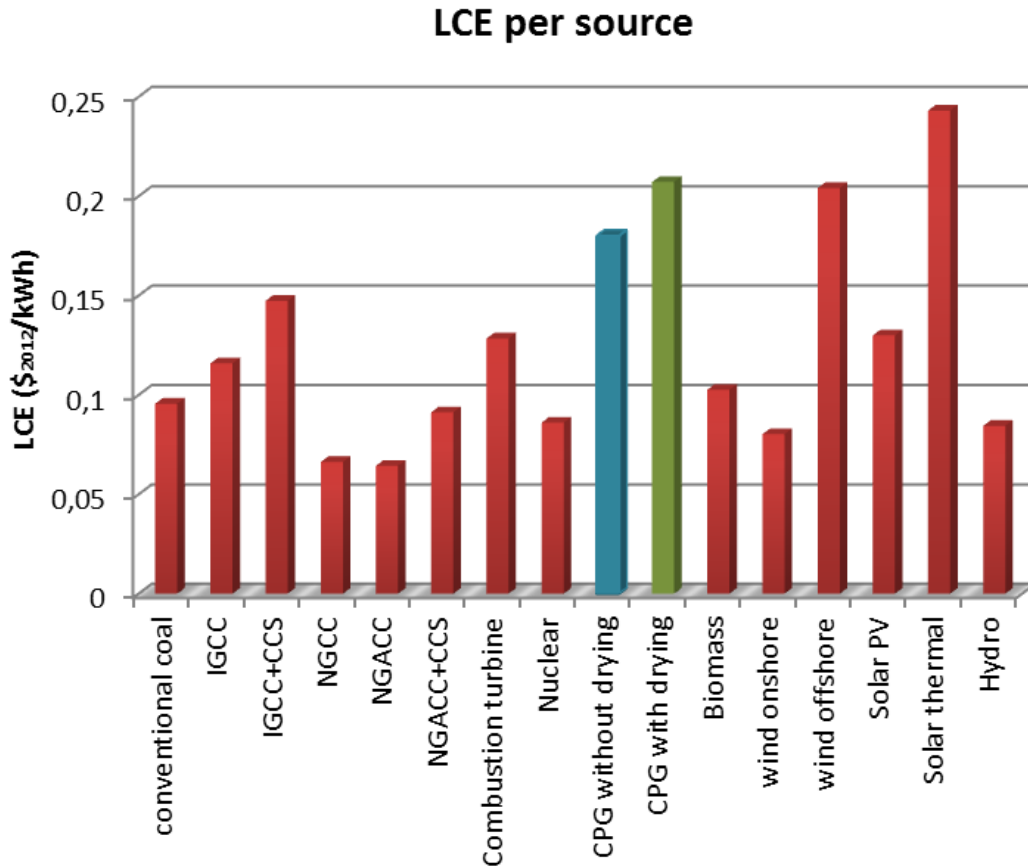


Figure 5.20: U.S. average levelized costs (2012 \$/MWh) for plants entering service in 2019 [131].

Due to time limitations, no additional costs scenario was calculated for a system that is equipped with a secondary, ORC turbine. Therefore, the additional electricity that would be generated in such a system is not taken into account in the Levelized costs of electricity presented above. Combining the performance of such a system (figure 5.12) with the graph above (figure 5.20) it appears that, at larger depths, the two turbines in series, may generate electricity at a competitive rate, especially if ETS prices increase.

5.5 Technical sensitivity analysis

In this section the uncertainties for important input parameters will be discussed. The effects of reservoir depth, pressure, temperature and flow rate on the performance indicators and costs have already been addressed in the sections above. The effect of three technical parameters: permeability, well density or well distance and well diameter on the system performance were assessed.

Reservoir permeability

The effect of permeability has been indirectly assessed via the depth. However, it should be noted that porosity and permeability of reservoirs depend on mineralogical composition and diagenesis that has taken place over the history of the formation rather than directly on depth. Therefore high porosity reservoirs might still be present at relatively high depths. To isolate the effect of permeability on the performance and safety of CPG operation, the input permeability of the base case was varied between 10^{-10} and 10^{-15} m² through precipitation of salts, this

permeability is further reduced by about 14%. Up to permeability's of around 10^{-14} , the effect of permeability is relatively insignificant. Lower permeability however strongly affects the electricity potential from the thermosiphon. For a permeability of 10^{-14} ($8.48E-15$ after drying). The production pressure is 21.3 Mpa while the injection temperature is 23.3 Mpa. Hence, no power generation is possible using a direct turbine.

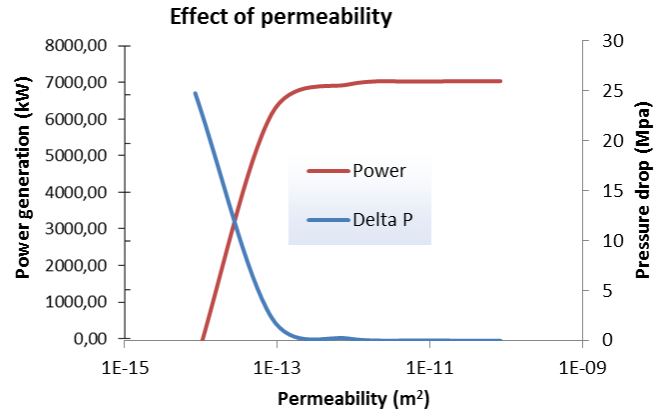


Figure 5.21: thermosiphon performance vs. permeability.

Well distance

The well distance, chosen in a CO₂-EOR projects, strongly depends on the formation, geometry of the reservoir and the fluids in the formation. Table 3.3 lists the well densities for the six largest CO₂ projects in varying from 1.9 to 18.3 wells km⁻². To assess the costs for reservoirs that require higher well density the distance between the production and the injection wells was varied from 500-1000 meters. Increasing the number of wells mainly affected the pressure drop over the wells due to the reduced flow rate. Since the pressure drop over the reservoir is not very high at (permeability's higher than 10^{-14}), the well distance did not strongly affect the injection pressure. Due to the models limitations with respect to reservoir heat flow, it was not possible to take into account the effect of shorter heat absorption in the reservoir. Therefore, the power increases due to increased well density were similar to those of increased well diameter (67% for double the amount of wells). The increase of well diameter however is much cheaper (25% vs. 100% of the well costs).

Well diameter

As can be shown from figure (flowrate), the flow rate through the wells greatly affects the friction losses and therefore the performance of the CPG system. Athrens therefore argues that increasing the diameter of particularly the production wells, will increase the productivity of the CPG system [106]. To calculate the effect of larger wellbores the well diameters of the production and injection wells were varied over a range of 100%-400% of the base case of 0,23125m. Figure shows the result of varying well diameter.

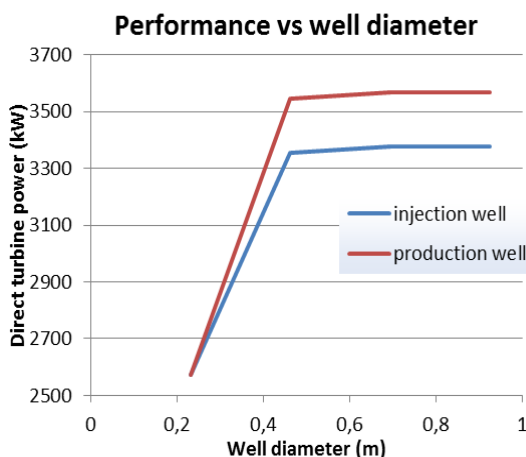


Figure 5.22: Effect of increasing wellbore diameter on performance of the CPG system.

For the first doubling of the well diameter, there is a very high increase in performance of the system. Beyond the first doubling, additional increases in well size do not seem to be of significant contribution to the performance of the system at the reference flow rate of 120 kg s^{-1} . It should be noted that for higher flow rates this may still be the case. If both the diameter of the production and the injection well would be doubled, the performance of the direct turbine were calculated to increase by 67% for a well costs increase of only 25%. If another 0,23125m would be added to both well diameters, this would mean an additional performance increase

of only a meagre 1% while the costs for the wells would increase 20%.

5.6 Sensitivity analysis for the costs

The main costs parameters that determine the economic viability of CPG-EOR show high uncertainties. Market price predictions for CO₂ range from

Furthermore, the effect of three cost parameters, CO₂ price, costs of wells and CO₂ purity threshold on the Levelized costs of electricity were examined.

Mixing rate in the reservoir and CO₂ price drying phase

The economic performance strongly depends on the price of CO₂ and the mixing rate in the reservoir. For the base case, the mixing rate for supercritical CO₂ with brine in the reservoir was in the base case assumed to be almost negligible as would be the case for a closed system. However, if the system is subjected to subsurface convective flow, mixing rates might seriously affect the time it takes for a dry CO₂ stream to establish.

New wells vs Refurbishing wells

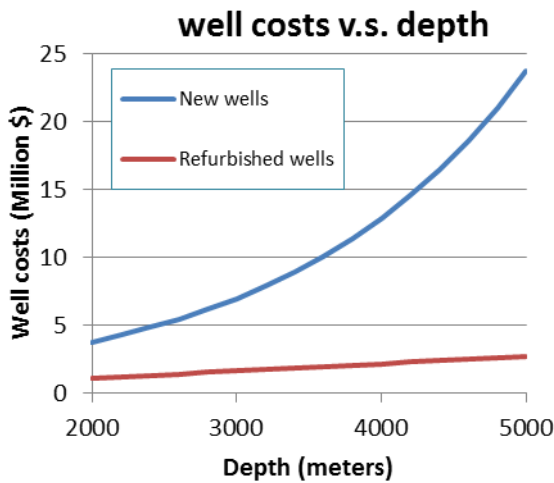


Figure 5.23: difference in well costs calculations for the new wells and refurbished well scenarios.

exponentially increase with depth. It was assumed that no additional drilling was required for the refurbishment and therefore the costs were mainly based on material and labor. Unlike drilling, these costs do not increase exponentially with depth.

Two different methodologies were used to calculate the costs for the CO₂-EOR phase. The first one was based on the assumption of new wells. Both the capital costs and the costs for oil production were reduced by refurbishing existing wells. More research is required into the compatibility of CO₂-EOR equipment and the equipment needed for a CPG system. However, the results of this model suggest that the costs for a CPG system can be dramatically reduced by using existing wells from an EOR operation.

The costs for refurbishing wells were in this case corrected for depth using a linear correlation where the costs for new wells

H₂O Threshold

The time it takes to dry the reservoir increases exponentially if the threshold becomes higher. For thresholds higher than 99%, additional costs for drying the reservoir may outweigh the costs for making important components in acid resistant materials.

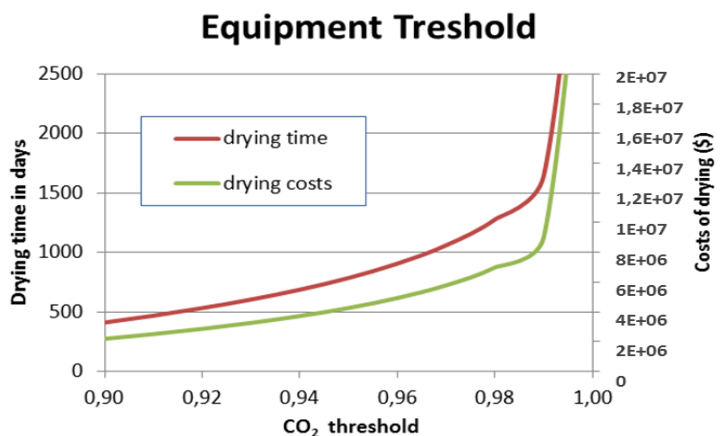


Figure 5.24: Cost of the drying phase and drying time vs. CO₂ – purity threshold.

6. Discussion

This section will discuss how these results, relate to the existing literature, where the knowledge gaps are in the technology and suggestions will be done for future research.

6.1 limitations of the model

The most important assumptions used for the modelling are summarized in section 4. Some other uncertainties are not accounted for in the model since they are either, too uncertain or too complex. Therefore, adding them would probably add more uncertainty than it takes away. Limitations of the model and their expected effects are shortly discussed in this section.

Continuous CO₂ rather than WAG injection

For simplicity it was assumed that CO₂ was injected continuously during the CO₂-EOR phase of the system. This choice was made since the EOR model is a box model and would not account for the complex CO₂-brine-oil distribution over the reservoir. WAG injection during the CO₂ flood will lead to increased presence of brine in the reservoir and therefore an increased drying time and therefore drying costs. Although continuous CO₂ injection has been the injection strategy for many EOR projects, the more recent projects tend to shift more towards WAG injection [90]. For the predictions made for the oil recovery factor, to the knowledge of the author, it is unknown if they are based in WAG- or continuous injection. It should therefore be noted that recovery factors may be lower using just CO₂.

Infrastructure compatibility assumption

In the modelling it was assumed that, the infrastructure used in the different phases would be compatible and could be reused without extra modifications for the follow-up phase. This is a very optimistic assumption as the infrastructure would most likely be optimized for the enhanced oil production. As the injection rate increases during the drying phase, additional capacity might be needed adding to the costs of the CPG system. Since the pipeline transportation to the field is not included within the framework of this thesis, these costs were not taken into account. Furthermore, it should be noted that the well distance is only partially taken into account. An increase in well distance increases the complexity of the system (especially in a heterogenic reservoir).

Heavy carbon fraction

Although the model does take into account the increase of the MMP due to the presence of heavy carbon molecules and its effect on the recovery factor, it assumes that all the oil and brine in the flow path can be produced. In reality, the heavier carbon fractions will still remain trapped due to their high viscosity and might be slowly co-produced over the years. This might reduce the lifetime of the turbines and affect flow paths to the reservoir.

(Almost) Closed system

For the reference case, once the dry stream is established, the mixing rate of super critical CO₂ and brine at the edge of the plume was chosen to be almost negligible (0,5%). This might be the case for a fully closed structural trap like some oil reservoirs. However, higher mixing rates may strongly affect the feasibility of the drying the reservoir to a level that's pure enough for direct utilization in a direct turbine. Furthermore, the positive effect of the reservoir mixing on temperature regeneration is also not taken into account.

High oil productivity during the drying phase

During the drying phase it was assumed that the injection rate for the CO₂ was increased to reduce the drying time. This is where the transition from a techno-economical model to a more technical model fails. Since the EOR ratio is based on a time curve derived from historical field data and does not directly depend on injection rate, an increase in injection rate increases the oil production according to the normal time profile. Hence, the model is likely to overestimate the oil production during the drying phase.

6.2 Comparison with literature

The oil production priced found in this research appear to be very low. If these production prices are assumed, CO₂-EOR would be extremely profitable at even the relatively low oil prices we have today. However, these costs do match the range of the oil production prices found by heddle et al. (2003) which is 12-20 \$/bbl. Figure 6.1 presents the average lifting costs (2008) for various oil producing regions as presented by the US DOE (2010) [137]. If these prices are compared to the costs for oil production in this thesis, the costs appear to be quite high even in the case of the refurbished well scenario.

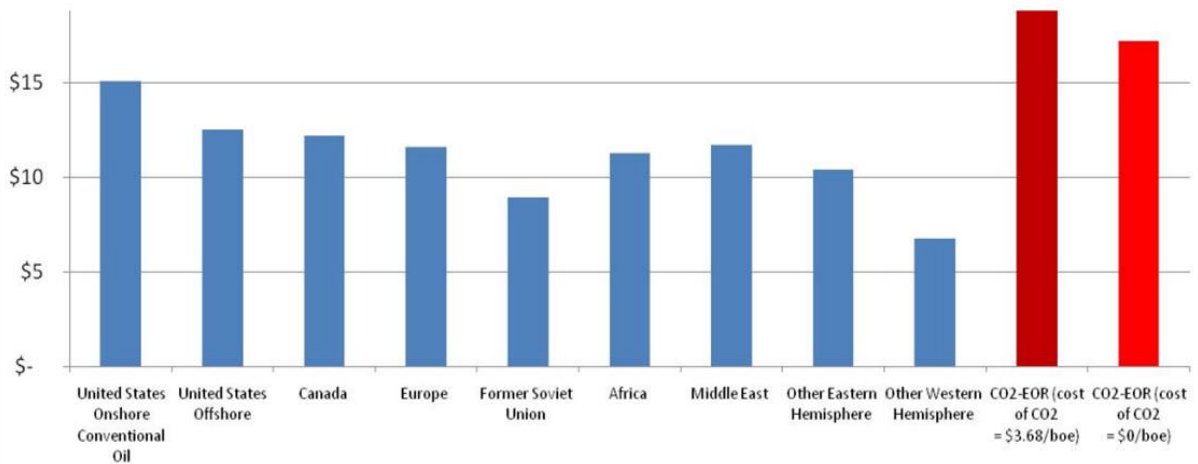


Figure 6.1: lifting costs (2008) for various oil producing regions [137].

Although quite some articles have been published on the use of CO₂ as a working fluid for geothermal heat extraction, most of them are based on a small set of models. These models have been extended many times but have remained the same in their basic assumptions and for the majority of the input parameters. Table 6.1 lists the input parameters for the base case of this research compared to the (base case) input parameters of the models that are used by Randolph and Saar from university of Minnesota, US, and Athrens et al. from Queensland University, Australia.

The idea of CO₂-plume geothermal heat recovery was first proposed by Randolph and Saar in their paper in 2010 [17]. Since their sole focus lies in geothermal energy extraction the reservoir they use is an aquifer. This means that it will most likely have higher permeability than would be the case for a depleted hydrocarbon field. In their modelling studies, they therefore assume high flow rates, which may not be achievable for the hydrocarbon reservoirs, particularly during the drying phase. Furthermore, the reservoir characteristics that are used in their research would not be suitable for CO₂-enhanced oil recovery since the Pressure/MMP ratio is rather low. In their calculations, they calculate the pressure drop over the wells using Newtonian iteration of

the static pressure profile. Hence, not taking into account friction losses to the wellbore. If we take into account these friction losses, at the reservoir temperature and depth they propose, the thermosiphon effect would not be strong enough to produce the CO₂ on its own power.

Table 6.2: Comparison of the input parameters from different modeling studies on CPG.

Input reservoir parameters					
	Parameter	Base case	Atrens et al.	Randolph et al.	Unit
Reservoir	Mass flowrate	120	120	300	kg/s
	Reservoir pressure	50	49.05	25	Mpa
	Reservoir temperature	225	225	100	°C
	Distance between wells	707.1	1000	707.1	m
	Ambient temperature	15	25	15	°C
	Geothermal gradient	45	35	34	°C/km
	Reservoir permeability	1.4E-14	8.6E-11	5.0E-14	m ²
	Reservoir depth	5000	5000	2500	m
	Porosity	10%	20%	20%	%
	Height of the reservoir	300	500	305	m
Wells	CO ₂ storage factor	0.5%	10%	0%	%
	Injection well diameter	0.23125	0.23125	0.41	m
	Production well diameter	0.23125	0.23125	0.27	m
	Number of injection wells	1	1	1	#
Thermal	Number of production wells	4	4	4	#
	Rock specific heat	920	-	1000	°API
	Thermal conductivity	2.1	-	2.1	W/mk
	Rock grain density	2650	-	2650	Kg/m ³
	brine salinity	250000	-	200000	ppm

These effects however will be more prudent when electricity generation is taken into account. For electricity generation they use a binary system with an ORC turbine. In the main dissertation, they primarily report the heat extraction rate from the reservoir. For a geothermal reservoir of the same size, 100°C and 2.5 km depth (table 6.1), they report an average 25 year heat extraction rate of 47MW. Using a binary cycle, they calculate a power output of 5.7MW. At these conditions, the heat extraction rate from the reservoir was calculated using the model made for this thesis. The heat extraction rate was calculated to be 45.2MW. However, due to the high joules Thompson cooling and low Carnot efficiency at this temperature power generation using a binary cycle was found to be only 174 kW while the thermosiphon produced 4.17MW.

Adams et al (2015) [138] performed a study comparing different power generation systems for CPG systems. They modelled the performance for the CO₂ flow through the reservoir using TOUGH2 modeling software. Figure 6.1a and 6.1b show the performance of the power generation methods versus the mass flowrate (a) and depth (b). Comparing their findings with figure 5.10 and figure 5.11 of this report, we see that they also find a maximum turbine efficiency at a mass flow rate of $\pm 140 \text{ kg s}^{-1}$. For the depth relation they find a performance range that is similar to the range found in this study, ranging from ± 1 to 5 MWe over the range of 2 to 5 km.

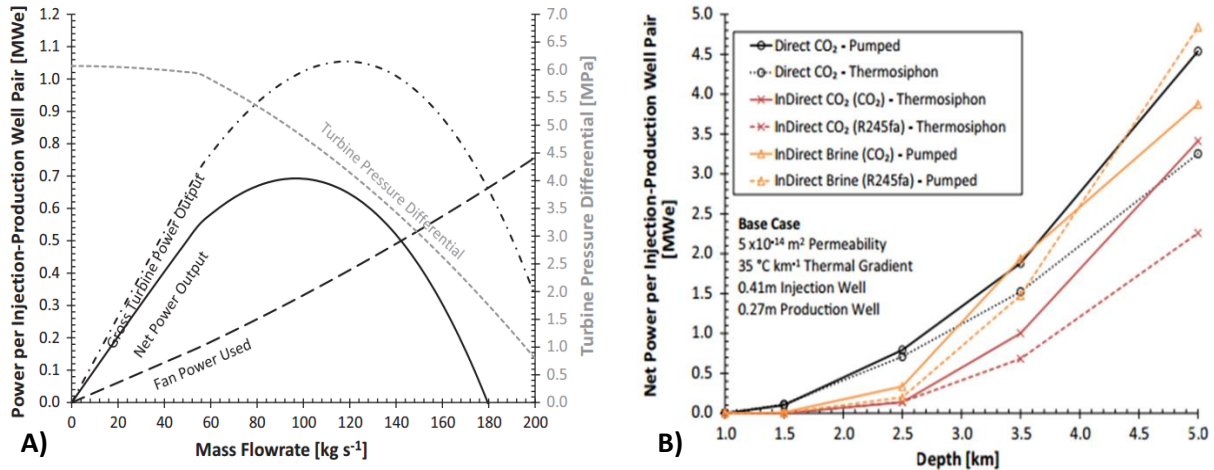


Figure 6.2 Performance of the CPG system for various injection rates (A) and performance of different electricity generation methods vs. depth (B) [138].

However, they report an exponential increase in performance with an increase in depth. A possible explanation for this is that they only take into account the effect of depth on well length and temperature (geothermal gradient of 35 °C km⁻¹) whereas in this study, the depth also affects porosity, permeability, salinity and pressure. At higher reservoir pressures the enthalpy difference for the temperature increase over the reservoir is lower. If the power is considered that can be generated using the (secondary) binary ORC turbine, the generation with depth looks similar to figure 6.1b.

Athrens [100] calculated the costs for a CPG system assuming new wells and taking into account the time needed for drying the reservoir. He also found a strong correlation for the CO₂ costs and the Levelized costs of electricity as would be expected. In his article on removal of H₂O from the reservoir [63], he finds a drying time of 6 years to achieve a 94% CO₂ threshold. These calculations are based on an injection rate of 133 kg s⁻¹, no mixing and no previous CO₂ injection. He also finds that the mixing rate is a strong effect on the drying time and feasibility of the system, high mixing rates lead to extended periods of drying and might even prevent the threshold from being achieved at all. It should be noted that he uses a saline aquifer rather than an oil reservoir. Hydrocarbon reservoirs are (partially) closed traps and therefore high mixing rates would not be expected.

Athrens, Gurgenci and Rudolph (2010), report that CO₂ thermosiphon electricity generation using a direct turbine performs particularly well compared to brine based system in shallow reservoirs. Since they only take into account the power, that is produced using a direct system and consider the additional heat to be disposed of, this matches the findings in this study. However, at higher production temperatures, this heat may actually become the main source of energy production as was seen in figure 5.12.

6.3 Knowledge gaps

The major knowledge gaps that need to be researched to assess whether the transition from a CO₂-EOR operation to a CPG operation is possible are:

- 1) **the relationship between miscibility of CO₂ and oil at higher temperatures.** Since most of the current CO₂-EOR projects are situated in low thermal regions, no experimental data for higher temperature regions. As higher geothermal gradient regions would be more interesting for CPG, empirical data is needed to establish where the limits are for miscible displacement.
- 2) **The loss rate of injected CO₂ with the formation brine should be better examined.** In this thesis, an annual loss rate of 5% of the CO₂ in the reservoir is used meaning that this amount of CO₂ is sequestered and has to be replaced by newly bought CO₂ to keep water from mixing in with the system.
- 3) **The dry rate in presence of hydrocarbons should be modelled.** In order to make better predictions on the oil fraction dissolved in the produced CO₂ stream. In the case of miscible displacement, the lighter oil fractions will be out rather rapidly. The heavier oil fractions might be co-produced long after. No literature was found on the effect of hydrocarbon precipitation in turbines. Although it might lubricate the system it is more likely to cause damage to the fans.
- 4) **The effects of previous stages of oil extraction on the reservoir temperature are not well known.** In this research, these effects were assumed to be negligible corresponding to measurements of production well temperatures during CO₂-EOR projects. However, these losses may be significant in the case of high flowrates and production times during these phases.

7. Conclusion

This section answers the research question: '*Could CO₂-enhanced oil recovery and CO₂-plume geothermal heat extraction be used in a complementary way to allow a more efficient use of reservoirs, infrastructure and monitoring equipment?*', based on the sub-questions:

What reservoir parameters affect the feasibility of CO₂-EOR and CPG?

In this study, the economics and related thermodynamics of CO₂-EOR and CO₂-plume geothermal heat extraction have been examined. Optimization of some system parameters and site considerations has been addressed for both technologies. A number of conclusions can be drawn from the results:

The main reservoir parameters that affect the feasibility of CO₂-EOR in a reservoir are the miscibility conditions, the heterogeneity of the reservoir and the wettability. The heterogeneity and wettability of the reservoir determine the sweep efficiency. Sandstone reservoirs appear to be best suited due to their high homogeneity and low reactivity.

Miscibility is mainly affected by the oil type, the pressure and the temperature. Light oils are miscible under relatively low pressures where heavier oils require much higher pressures to become miscible with CO₂. The temperature has a negative influence on the miscibility, therefore regions with high geothermal gradients of 45-50 °C/km are generally unsuitable for miscible displacement. For high temperature reservoirs, the reservoir either needs to be over pressurized or deep enough for the hydrostatic pressure (depth) to allow miscibility. Deeper reservoirs however, have the disadvantage of higher drilling costs and generally lower porosity and permeability and therefore, lower oil production.

For CO₂-plume geothermal energy generation, the most important parameters that affect the reservoir suitability are the temperature and depth of the reservoir, the mixing rate and the presence and purity of previously injected CO₂. It is important that the temperature and pressure of the CO₂ are high enough over the various stages of the system to keep the CO₂ in supercritical or dense phase. The power that can be generated using a CPG system depends on the pressure difference and the temperature of the produced fluids.

Furthermore the CO₂ needs to be pure enough to meet the high purity thresholds of the system so that no H₂O precipitates in vital components of the system. High reservoir permeability is desirable, although the high mobility of dry supercritical CO₂ also allows high flowrates in low permeability reservoirs. The salinity of the reservoir is important, especially in low porosity reservoirs as salt precipitation during the drying of the reservoir may cause permeability reduction in the reservoir.

Due to the criteria for miscibility and the pressure and temperature drops in the wellbore, the technology is not feasible for all reservoir depths. There is a region in which the reservoir criteria for miscible CO₂-EOR and CPG overlap and both technologies will be feasible. This is mainly the case in relatively deep reservoirs with geothermal gradients of up to 45 °C km⁻¹. Reservoir parameters were determined for a fictional reference reservoir in which both CO₂-EOR and CPG would be technically feasible.

What configuration would be best for CPG-EOR and what are the most important pitfalls and benefits ?

Due to the novelty of the concept, the first step was to establish the most feasible configuration to combine the two technologies in a single reservoir. The feasibility was assessed based on the economics and thermodynamics for three different configurations; using a parallel reservoir, combining the two at once, or performing CPG as consecutive phase of CO₂-EOR. The parallel configuration would lack most of the benefits of combining the technologies, while the combined configuration would most likely lead to difficulties in the later processing of oil and separation of CO₂. If heat is extracted from the production stream prior to this separation, the heavier oil fractions will become more viscous and harder to handle. While in later stages of separation, this heat might have to be added again. Surface equipment is optimized for the conditions of the reservoir. For these reasons, the consecutive configuration was chosen to have the best potential.

The configuration modelled in this research assumes that CO₂-EOR takes place after primary and secondary oil recovery where water injection was used. This means that both production as well as injection wells are present. It also means that a combination of brine and hydrocarbons is present in the reservoir. The CO₂-EOR injection method for EOR is continuous injection. CO₂ is injected until the level of H₂O that is coproduced falls below a threshold of 1%. When the CO₂ production stream is pure enough, the produced CO₂ is then expanded through a direct CO₂ turbine to utilize the pressure difference between the production and injection wellheads directly. The heat that leaves the direct turbine can be used in a binary system; either by using an ORC turbine to generate additional electricity or for district heating.

The main benefits of this configuration are that both the pressure difference generated by the thermosiphon effect and the heat can be used. Furthermore, the availability of CO₂ injection and production infrastructure would significantly reduce the capital investments and the previous injection of CO₂ limits the requirement for additional CO₂ to start up the electricity generation. Additional oil production during the drying of the reservoir could partially offset the costs. Additional performance enhancement may be possible if the CO₂ injection is initiated after the primary oil recovery phase instead of after secondary recovery as this would greatly reduce the requirements for reservoir drying.

Pitfalls of the configuration are that the effect of the presence of hydrocarbons on geothermal systems and the deposition of reservoir minerals in the machinery are largely unknown. Furthermore, the demand for CO₂ will not be very stable as the EOR and CPG phases require different injection rates and CO₂ is increasingly more recycled. Furthermore, the effect of WAG injection and the use of viscosity enhancers like foams or polymers might negatively affect the CPG operation. More research is needed into the effect of oil production on reservoir temperatures to better assess the potential for consecutive geothermal heat extraction.

What is the rough potential for CO₂ storage and electricity and oil production in the case reservoir?

A model was created to estimate the performance, costs and revenues of using consecutive deployment of CO₂-EOR and CPG from reservoirs at various depths. The storage potential varied from 68 to 191 Mtonne CO₂ depending mainly on the porosity and dimensions of the reservoir.

Two different methodologies were used to calculate the Levelized costs of oil production. Although both methodologies resulted in very different prices, both methodologies calculated oil production from CO₂-EOR to be economically viable using the current oil price (± 60 \$/bbl). The oil production was calculated based on the results from previous EOR projects. Therefore, the oil production is only partially dependent on the technical parameters of the reservoir. Sensitivity tables provided for the most important input parameters show that the price of oil varies strongly over the range of input parameters. After the EOR phase, the CO₂ fraction in the reservoir pore space varies from ± 70 -92%. This means that the start-up time and costs for CPG were significantly reduced.

The electricity generation that can be generated using the direct CO₂ turbine is the main source of power in relatively shallow reservoirs. Although the temperature difference and therefore the thermosiphon effect increases, this additional pressure is compensated for by the additional friction losses in deeper wells and the higher injection pressures required. Increasing the diameter of the production wells reduces the friction in the wellbore and therefore favors the performance of especially deeper reservoirs.

To the regret of the author, there was not enough time left to include a full economic assessment of the system including a secondary binary ORC cycle. Since there was no cost calculation included in the model, the additional electricity productions of the binary system were not taken into account in the calculations of the Levelized costs for electricity. Especially for deep reservoirs, utilizing this potential for either district or industrial (pre)heating or additional electricity generation may generate significant additional income, improving the economics of the system. If the Levelized costs of electricity are compared to Utility scale energy generation methods for the U.S, the technology is not yet competitive. However, if the technology is compared to on-site energy production method like diesel generators, the costs may be favorable, especially if the heat can be put to use.

Only CPG vs CPG-EOR

In the case of only CO₂ plume geothermal heat recovery, the high costs for wells and drying of the reservoir do not allow for competitive electricity production. The previous oil exploration and therefore availability of wells and infrastructure have a significant effect on the capital costs. Furthermore, the drying time may be reduced significantly by using a reservoir that has already been injected with CO₂. Since the drying costs (mainly storage costs) strongly depend on the price of CO₂, a decrease in drying time (or storage potential) may either positively or negatively affect the economics of the project.

Could CO₂-enhanced oil recovery and CO₂-plume geothermal heat extraction be used in a complementary way to allow a more efficient use of reservoirs, infrastructure and monitoring equipment?

Now, to answer the main research question. This report provides an exploratory overview to assess the potential of the proposed technology. Mainly for the costs calculation, high uncertainties exist in the input parameters.

For some cases, the same reservoirs that can be used for CO₂-enhanced oil recovery could be used for CO₂-plume geothermal. For deeper and hotter reservoirs, enough pressure difference is generated to successfully operate a direct supercritical CO₂ turbine. Based on the model, assuming a closed system with minimal mixing in the reservoir, a dry stream of supercritical

CO₂ can be achieved in a relatively short period of time. Additional research is required on the effect of the presence of heavy oil fractions on CPG- deployment in a reservoir. The power generated by a CPG system was found to maximize at low depths or depths of 4 – 4.5 km. For the reference case, an injection rate of 140 kg s⁻¹ was found to have the best performance. At higher flow rates, the additional friction in the wellbore will reduce the efficiency of the system. Due to the high mobility of supercritical CO₂ these injection rates would not lead to high pressure drops (<10MPa), as long as there is single phase flow, even at very low permeability (10⁻¹⁵m²). However, if multi-phase flow is taken into account, injection rates, may have to be reduced.

If the CPG is regarded as a standalone, optional part of the system, the costs of electricity are not yet competitive with other large scale energy generation methods. The levelized cost of electricity greatly depend on the price of CO₂. In the future, if policies with respect to CO₂ become more rigorous the storage of CO₂ could generate enough additional income to become competitive, even compared to utility size generation technologies. In the case of high ETS prices, power generation and additional oil recovery may completely offset the costs of storage.

Especially in remote areas electricity like many oil fields, electricity prices are a lot higher as electricity is often generated on site. if the heat can be put to use. Power costs for compression are one of the major costs for a CO₂-EOR operation, this electricity is often produced on site. CPG power generation from some sections of the reservoirs may therefore be used to replace expensive diesel generators in for other sections.

To conclude, the transition from miscible CO₂-EOR to CPG appears to be feasible for a range of reservoir parameters. Although without the use of the heat the electricity price is not competitive with large scale electricity generation methods, additional power produced from the heat and income generated from storing CO₂, may make the technology economically viable. In the future, if taxation on CO₂ emissions go up, this technology provides a cost effective way of storing CO₂.

8. Future research

The aim of this research was to perform an explorative study on the feasibility, opportunities and pitfalls of the combination of two technologies. Thereby, the study provides a basis for further research into the specifics of operation. Since the idea for the utilization of supercritical CO₂ as a working fluid for geothermal heat extraction is a fairly novel one, there are still many uncertainties about the application and subsurface behavior at higher temperatures.

8.1 3D-Modelling for the drying and EOR

Due to the limited time and means available for this master thesis, a simplistic model was chosen for the model. Box models were chosen to model the CO₂-EOR and drying phases. These models do not take into account spatial distribution of the injected CO₂ over the reservoir but treats the reservoir as a confined open over which the contents are homogeneously spread. More advanced modelling tools that take into account spatial distribution of the reservoir fluids over the reservoir would provide additional insights on the feasibility of the system.

8.2 CPG-EGR

Besides CO₂-EOR, another promising new technology is Carbon Sequestration with Enhanced Gas Recovery (CSEGR). This can be done in two ways, the first one being enhanced coalbed methane recovery (ECBM) in which you use the fact that CO₂ has an affinity to coal that is higher than that of nitrogen and methane, but smaller than that of hydrogen-sulfide (H₂S) and sulphur-dioxide (SO₂). As CO₂ is injected into a coal seam, it takes the place of the adsorbed CH₄, which can subsequently be produced [139]. Another method, is to use CO₂ for re-pressurizing a mature gas field, forcing out more methane. CO₂ has a significantly higher viscosity than methane leading to efficient sweep of the reservoir. After a certain time, a mixture will be produced of CH₄ with an increasing percentage of CO₂. Although it strongly depends on the price of CO₂ and the breakthrough time of CO₂, research has shown that the technology is economically viable [140]. CSEGR might be suitable for combination with CPG systems similar to those with EOR. While the CO₂-EOR technology has been developed and applied successfully over 40 years, CO₂-EGR is still very new and far from being implemented on a large scale. At this point there are only a few small CO₂-EGR demonstration projects in practice. Therefore, this thesis focusses on EOR.

8.3 The effect of viscosity enhancers and WAG-Operation on CPG

As is mentioned in section two, viscosity enhancers like foam are often added to CO₂ in order to reduce the viscosity of the CO₂(sc) and improve the sweep efficiency during EOR. The presence of these enhancers in the reservoir might affect the reservoir suitability for CO₂-plume geothermal energy extraction as it affects the flow rate or blocks of certain parts of the reservoir for heat extraction. Experimental studies using a flow-through reactor could determine the effect of these substances on subsequent CPG operation.

Another approach that is often used in CO₂-EOR is alternating the injection of CO₂ with water to mechanically push out the mixture of oil and CO₂. This was not taken into account in this model as it makes the spatial positioning of the phases very complex. It may however be a very important factor in determining the duration, CO₂ storage potential and pressure drops during the drying phase.

8.4 The effect of economic and policy parameters

Besides the reservoir criteria another factor that is highly important for the viability is the location of field. Location factors that affect the suitability of a reservoir are the proximity of natural or anthropogenic sources of CO₂ and local demand for heat and electricity, terrain factors and local legislation. Offshore fields have higher operating costs and higher uncertainties which make them less favorable for CPG-EOR. Furthermore, the distance between injection and production wells is often much larger than for onshore fields reducing the sweep efficiency.

8.5 Reactive transport modelling

The present model does not take into account the dissolution and precipitation of reservoir minerals apart from salts during the drying. Dissolution of reservoir minerals in and around preferential flow paths could enhance the permeability of the reservoir allowing higher flow rates. On the other hand, deposition of minerals close to and in the production wells might decrease the permeability and lead to clogging. Deposition in the turbines and heat exchanger may lead to breakdown of equipment and pressure buildup. It would be very interesting to model the process using reactive transport models for different reservoir compositions to determine if this is a problem for the system.

8.6 The option of skipping secondary oil recovery

After the initial depressurization of the reservoir (primary oil recovery) the pressure is increased by injecting water into the reservoir (secondary oil recovery). If no water is injected during the first steps of oil production, and after primary oil production, the reservoir is pressurized with supercritical CO₂, a minimal amount of brine will be present in the system.

The choice to inject water is based on the fact that it's much cheaper than CO₂ and the high viscosity allows for efficient sweep of the reservoir. These problems might be overcome in the future using viscosity enhancers and additional cash flows can be generated by storing the CO₂. To research this, the solubility for a specific oil composition in supercritical CO₂ should be determined, under influence of pressure and temperature. The threshold for dissolved hydrocarbons in the supercritical CO₂ stream can be determined using the same methodology as was applied for H₂O in this thesis. Based on this threshold, the time it takes to flush CO₂ through the system before a direct turbine can be used, can then be calculated. Before this, a binary system may be used.

Separation of non-volatile hydrocarbons from the production stream can be done using flashing, a technique that does not require heat, hence, a binary system may be used to generate electricity. Since the volatile fraction left at this stage is most likely very small due to its high mobility, and furthermore is unlikely to have a great impact on the turbine operation, this may be left in (CH₄ is often re-injected in oil operations to increase recovery).

Nomenclature

CPG = CO₂ plume geothermal

EOR = enhanced oil recovery

T_c = Critical temperature in K

P_c = Critical pressure in Mpa

σ_{nw,w} = interfacial tension between the oil and the brine

θ = contact angle between the wetting and non-wetting phase

P_c = the capillary pressure in Mpa

OOIP = original oil in place in bbl

g = gravitaional constant 9.81 ms⁻²

P = pressure in Mpa

Z = well depth in m

T = temperature in K

K = permeability in m²

K_r = relative permeability in m²

T_s = surface tension

ρ = density in kg m⁻³

η_{Carnot} = Carnot efficiency

MW₅₊ = molar weight of the carbon chains longer than 5 C atoms.

Oil gravity = relative density of the oil compared to H₂O in °API

V = volume in m³

R_f = recovery factor of the OOIP (%)

CO₂ ratio = bbl produced/ tonne CO₂ injected

f_{CO₂,threshold} = threshold needed for the direct system in %

S_g = gas saturation in %

λ = mobility of liquid or gas

F_g = fractional flow of the gas phase

D = well diameter in m

Vol., % = pore volume fraction occupied by oil

MMP = minimum miscibility pressure in Mpa

Φ = porosity of the resevoir (%)

PR = reservoir pressure Mpa

h = height of the reservoir in m

q = the total flow rate kg s⁻¹

V_{f_{salt}} = the volume fraction of salt (%)

f = friction factor, dimensionless

C_p = heat capacity in J kg⁻¹ K⁻¹

W = electricity generated or used

η = efficiency

ṁ = mass flow rate kg s⁻¹

MaxRec = maximum troughput of the recycling facility tonne CO₂ year⁻¹

PCCI = Power Capital Costs Index

UCCI = Upstream Capital Costs Index

UOCI = Upstream Operating Costs Index

OPEX = operational expenses in \$ year⁻¹

CAPEX = Capital expenses in USD

Bibliography

- [1] Mauna Loa Observatory, "<http://co2now.org/images/stories/data/co2-atmospheric-mlo-monthly-scripps.pdf>," University of California, San Diego, 2014.
- [2] C. White, B. Strazisar, E. Granite, J. Hoffman and H. Pennline, "Separation and capture of CO₂ from large stationary sources and sequestration in geological formations - coalbeds and deep saline aquifers," *Journal of the air and Waste management association*, pp. 645-715, 2003.
- [3] B. Metz, O. Davidson, H. de Coninck, M. Loos and M. Meyer, "IPCC special report on Carbon Dioxide capture and storage," Cambridge University Press, 2005.
- [4] R. Allis, T. Chidsey, W. Gwynn, C. Morgan, S. White, M. Adams and J. Moore, "Natural CO₂ Reservoirs on the Colorado Plateau and Southern Rocky Mountains: Candidates for CO₂ Sequestration.," government, [Online]. Available: <http://geology.utah.gov/emp/co2sequest/pdf/reservoirs.pdf>.
- [5] J. M. Ketzer, R. Iglesias, S. Einloft, J. Dullius, R. Ligabue and V. De Lima, "Water-rock-co₂ interactions in saline aquifers aimed for carbon dioxide storage: experimental and numerical modeling studies of the Rio Bonito formation (Permian), Southern Brazil," no. 24, 2009.
- [6] Global CCS Institute, "CO₂-EOR Dominates Geologic Storage," Global CCS Institute, Melbourne, 2013.
- [7] F. Gozalpour, S. R. Ren and B. Tohidi, "CO₂ Eor and Storage in Oil Reservoirs," *Oil & Gas Science and Technology*, vol. 60, no. 3, pp. 537-546, 2005.
- [8] R. C. Ferguson, C. Nichols, T. Van Leeuwen and V. A. Kuuskraa, "Storing CO₂ with Enhanced Oil Recovery," *Energy Procedia*, vol. 1, pp. 1989-1996, 2008.
- [9] B. ZareNezhad and N. Hosseinpour, "Sharp Separation of CO₂ from Recovered Hydrocarbon Mixtures in EOR Fields for Recycling in Petroleum Reservoirs," [Online]. Available: <http://www.aidic.it/icheap9/webpapers/59Zarenezhad.pdf>. [Accessed 4 November 2014].
- [10] V. Stefansson, "World geothermal assessment," in *Proceedings World Geothermal Congress*, Antalya, 2005.
- [11] S. Frick, M. Kaltschmitt and G. Schröder, "Life cycle assessment of geothermal binary power plants using enhanced low-temperature reservoirs," *energy*, pp. 2281-2294, 2010.
- [12] K. pruess and M. Azaroual, "on the feasibility of using supercritical CO₂ as heat transmission fluid in an engineered hot dry rock geothermal system," in *Thirty-First Workshop on Geothermal Reservoir Engineering*, stanford, 2006.

- [13] D. W. Brown, "A hot dry rock geothermal energy concept utilizing supercritical CO₂ instead of water," in *Twenty-Fifth Workshop on Geothermal Reservoir Engineering*, Stanford, 2000.
- [14] G. Tao, W. HuaiXin and Z. ShengJun, "Comparative analysis of CO₂-based transcritical Rankine cycle and HFC245fa-based subcritical organic Rankine cycle using low-temperature geothermal source.," *Science China*, vol. 53, no. 6, p. 1638–1646, 2010.
- [15] US department of energy, "Geothermal Technologies Program 2010 Peer Review," 8 May 2010. [Online]. Available: http://energy.gov/sites/prod/files/2014/02/f7/reservoir_pruess_co2_transmission.pdf. [Accessed 27 November 2014].
- [16] J. H. Biagi, "Numerical Simulation and Optimization of Carbon Dioxide Utilization and Storage in Enhanced Gas Recovery and Enhanced Geothermal Systems," Washington University , St. Louis, 2014.
- [17] J. B. Randolph and M. O. Saar, "Coupling Geothermal Energy Capture with Carbon Dioxide Sequestration in Naturally Permeable, Porous Geologic Formations: A Comparison with Enhanced Geothermal Systems," *GRC Transactions*, vol. 34, pp. 433-437, 2010.
- [18] B. M. Adams, T. H. Kuehn, J. M. Bielick, J. B. Randolph and M. O. Saar, "On the importance of the thermosiphon effect in CPG (CO₂ plume geothermal) power systems," *Energy*, vol. 69, pp. 409 - 418, 2014.
- [19] J. B. Randolph and M. O. Saar, "Coupling carbon dioxide sequestration with geothermal energy capture in naturally permeable, porous geologic formations: Implications for CO₂ sequestration," *energy procedia*, vol. 4, pp. 2206-2213, 2011.
- [20] J. P. Meyer, "Summary of Carbon Dioxide Enhanced Oil Recovery (CO₂-EOR) Injection Well Technology," [Online]. Available: <http://www.api.org/~media/Files/EHS/climate-change/Summary-carbon-dioxide-enhanced-oil-recovery-well-tech.pdf>. [Accessed 4 Februari 2015].
- [21] S. Bachu, "Screening and ranking of sedimentary basins for sequestration of CO₂ in geological media in response to climate change," *environmental geology*, no. 44, pp. 277-289, 2003.
- [22] F. Blunt, J. Fayers and M. Franklin, "Carbon dioxide in enhanced oil recovery," *energy conversion management*, vol. 43, no. 9-11, pp. 1197-1204, 1993.
- [23] S. Thomas, "Enhanced Oil Recovery – An Overview," *Oil & Gas Science and Technology* , vol. 63, pp. 9-19, 2008.
- [24] J. J. Taber, F. D. Martin and R. S. Seright, "EOR screening criteria revisited - part 2: Applications and impact of oil prices," *SPE reservoir engineering*, pp. 199-205, 1997.
- [25] IEA, "CO₂ storage in depleted oil fields: global application criteria for carbon dioxide enhanced

- oil recovery," IEA greenhouse gas R&D programme, 2009.
- [26] F. F. Craig, "Reservoir Engineering Aspects of waterflooding," *Society of Petroleum Engineers Inc*, p. 3, 1971.
- [27] R. Farajzadeh, enhanced transport phenomena in CO₂ sequestration and CO₂ EOR, 2009.
- [28] D. Yang and Y. Gu, "Interfacial Interactions Between Crude Oil and CO₂ Under Reservoir Conditions," *Petroleum Science and Technology*, p. 1099–1112, 2005.
- [29] A. B. U. Zolotukhin, introduction to petroleum reservoir engineering, 2000.
- [30] W. F. Yellig and R. S. Metcalfe, "Determination and Prediction of CO₂ Minimum Miscibility Pressures," *Journal of petroleum technology*, p. 160–168, 1980.
- [31] IEA, "Technology Roadmap: Carbon Capture and Storage 2013," IEA, Paris, 2013.
- [32] Prosternat, "Solid bed desiccant," prosternat, 16 Januari 2015. [Online]. Available: <http://www.prosternat.com/en/solutions/upstream/gas-dehydration/solid-bed-desiccant.html>.
- [33] Z. Li and Y. Gu, "Optimum Timing for Miscible CO₂-EOR after Waterflooding in a Tight Sandstone Formation," *Energy and fuels*, pp. 488-499, 2013.
- [34] E. Manrique, C. Thomas, R. Ravikiran, M. Izadi, M. Lantz and J. Romero, "EOR: Current Status and Opportunities," in *Improved Oil Recovery Symposium*, Tulsa, 2010.
- [35] D. Espinoza, S. Kim and J. Samtamarina, "CO₂ Geological storage - geotechnical implications," *journal of civil engineering*, vol. 15, no. 4, pp. 707-719, 2011.
- [36] J. J. Taber and R. S. Seright, "Horizontal injection and production wells for EOR or waterflooding," in *SPE/DOE symposium on enhanced oil recovery*, 1992.
- [37] J. B. Randolph, "Coupling geothermal energy capture with carbon dioxide sequestration in naturally permeable, porous geologic formations – a novel approach for expanding geothermal energy utilization.," 2011.
- [38] F. Pan, B. McPherson, P. Lichtner, J. Kaszuba, C. Lo Ré, S. L. C. Karra and T. Xu, "numerical evaluation of energy extraction, CO₂-rock interactions, and carbon sequestration in enhanced geothermal systems (EGS) with supercritical CO₂ as a working fluid," in *Thirty-Eighth Workshop on Geothermal Reservoir Engineering*, Stanford, 2013.
- [39] C. Oldenburg, "Joule-Thomson cooling due to CO₂ injection into natural gas reservoirs," *Energy Conversion and Management*, no. 48, p. 1808–1815, 2007.
- [40] K. Pennel, G. Pope and L. Abriola, "influence of viscous and buoyancy forces on the mobilization of residual tetrachloroethylene during surfactant flushing," *environmental science*

and technology, vol. 30, no. 4, pp. 1328-1335, 1996.

- [41] S. Yousefi, A. D. Atrens, E. Sauret, M. Dahari and K. Hooman, "CFD Convective Flow Simulation of the Varying Properties of CO₂-H₂O Mixtures in Geothermal Systems," *the Scientific World Journal*, 2014.
- [42] K. Pruess and S. Spycher, "Enhanced Geothermal Systems (EGS) with CO₂ as Heat Transmission Fluid - A Scheme for Combining Recovery of Renewable Energy with Geologic Storage of CO₂," in *World Geothermal Congress*, 2010.
- [43] D. D. Blackwell, M. C. Richards, Z. S. Frone, J. F. Batir, A. A. Ruzo and R. K. Dingwal, "Geothermal map," 2011. [Online]. Available: http://www.smu.edu/~media/Site/Dedman/Academics/Programs/Geothermal%20Lab/Graphics/SMUHeatFlowMap2011_CopyrightVA0001377160_jpg.ashx?la=en. [Accessed 5 3 2015].
- [44] A. D. Atrens, H. Gurgenci and V. Rudolph, "CO₂ Thermosiphon for Competitive Geothermal Power Generation," *Energy & Fuels*, vol. 23, p. 553–557, 2009.
- [45] Y. Wan, T. Xu and K. Pruess, "impact of fluid-rock ionteractions on enhanced geothermal systems with CO₂ as transmission fluid," in *Thirty-Sixth Workshop on Geothermal Reservoir Engineering*, Stanford, 2011.
- [46] K. Pruess, "The TOUGH codes — A family of simulation tools for multiphase flow and transport processes in permeable media.," *Vadose zone journal*, vol. 3, p. 738–746, 2004.
- [47] J. Glanz, "Quake threat leads Swiss to close geothermal project.," *New york times*, 2009.
- [48] B. Freifeld, S. Zakim, B. Cutright, M. Sheu, C. Doughty and T. Held, "Geothermal energy production coupled with CCS: a field demonstration at the SECARB Cranfield Site, Cranfield, Mississippi, USA," *Energy Procedia*, vol. 37, p. 6595 – 6603, 2013.
- [49] A. Borsukiewicz-Gozdur and W. Nowak, "Maximising the working fluid flow as a way of increasing power output of geothermal power plant.," *applied thermal engineering*, vol. 27, p. 2074–2078, 2007.
- [50] N. Garapati, J. B. Randolph and M. O. Saar, "Total Heat Energy Output From, Thermal Energy Contributions To, and Reservoir Development of CO₂ Plume Geothermal (CPG) Systems.," in *Thirty-Ninth Workshop on Geothermal Reservoir Engineering*, stanford, 2014.
- [51] P. Welch and P. Boyle, "New Turbines to Enable Efficient Geothermal Power Plants," *GRC Transactions*, vol. 33, pp. 765-772, 2009.
- [52] Y. A. Cengel and M. A. Boles, *Thermodynamics: an engineering approach*, 2010.
- [53] J. B. Randolph and M. O. Saar, "57th Annual Midwest Ground Water Conference," 02 Oktober 2012. [Online]. Available: http://www.mgwa.org/meetings/2012_fall/geothermal/randolph.pdf. [Accessed 02 December

- 2014].
- [54] B. Metz, O. Davidson, d. C. H.C., M. Loos and L. Meyer, "IPCC special report on carbon dioxide capture and storage," cambridge university press, Cambridge, 2005.
- [55] IEA, "Technology Roadmap: Carbon Capture and Storage.," OECD / International Energy Agency, Paris, 2013.
- [56] S. Bachu, "CO₂ storage in geological media: Role, means, status and barriers to deployment," *Progress in energy and combustion science*, no. 34, pp. 254-273, 2008.
- [57] M. Sahimi, *Flow and Transport in Porous Media and Fractured Rock*, vol. 2, Weinheim: Wiley-VCH, 2011.
- [58] W. Gunther, S. Bachu and S. Benson, "The role of hydrogeological and geochemical trapping in sedimentary basins for secure geological storage of carbon dioxide," *Geological Society, London, Special Publications 2004*, pp. 129-145, 2004.
- [59] R. Garrels and C. Christ, "Solutions, Minerals, and Equilibria: Freeman-Cooper," 1965.
- [60] L. Andre, P. Audigane, M. Azaroual and A. Menjoz, "Numerical modeling of fluid–rock chemical interactions at the supercritical CO₂–liquid interface during CO₂ injection into a carbonate reservoir, the Dogger aquifer (Paris Basin, France)," *Energy conversion and management*, no. 48, p. 1782–1797, 2007.
- [61] J. W. Johnson, J. J. Nitao and K. G. Knauss, "Reactive Transport Modelling of CO₂ Storage in Saline Aquifers to Elucidate Fundamental Processes, Trapping Mechanisms, and Sequestration Partitioning," *Geological Society of London Special Publication on Carbon*, Vols. UCRL-JRNL-205627, 2004.
- [62] W. O. Gunther, E. H. Perkins and T. J. McCann, "Aquifer disposal of CO₂-rich gases: reaction design for added capacity.," *energy conversion management*, vol. 34, pp. 941-948, 1993.
- [63] A. Atrens, H. Curgency and V. Rudolph, "Removal of water from a carbon dioxide based EGS system," in *Thirty-Sixth Workshop on Geothermal Reservoir Engineering Stanford University*, Stanford, 2011.
- [64] T. Xu, K. Pruess and J. Apps, "Numerical studies of fluid-rock interactions in enhanced geothermal systems (EGS) with CO₂ as a working fluid," in *PROCEEDINGS, Thirty-Third Workshop on Geothermal Reservoir Engineering*, Stanford, 2008.
- [65] H. Lin, T. Fujii and R. Takisawa, "Experimental evaluation of interactions in supercritical CO₂/water/rock minerals system under geologic CO₂ sequestration conditions," *Journal of material science*, vol. 43, p. 2307–2315, 2008.
- [66] K. Pruess, "Enhanced geothermal systems (EGS) using CO₂ as working fluid—A novel approach for generating renewable energy with simultaneous sequestration of carbon," *Geothermics*,

vol. 35, p. 351–367, 2006.

- [67] C. Doughty, K. Pruess, S. M. H. S. Benson, R. Knox and C. Green, "Capacity investigation of brine bearing sands on the Frio Formation for geologic sequestration of CO₂," in *First National Conference on Carbon Sequestration*, Washington DC, 2001.
- [68] J. Moore, M. Adams, R. Allis, S. Lutz and S. Rauzi, "mineralogical and geochemical consequences of the long-term presence of CO₂ in natural reservoirs: an example from the Springerville-St. Johns Field, Arizona, and New Mexico, U.S.A.," *chemical geology*, no. 217, pp. 365-385, 2005.
- [69] I. Gaus, "Role and impact of CO₂-rock interactions during CO₂ storage in sedimentary rocks," *international journal of greenhouse gas control*, vol. 4, p. 73 - 89, 2010.
- [70] J. Verdon and A. Woods, "gravity-driven reacting flows in a confined porous aquifer," *journal of fluid mechanics*, vol. 588, p. 29-41, 2007.
- [71] I. Gaus, M. Azaroual and I. Czernichowski-Lauriol, "Reactive transport modelling of the impact of CO₂ injection on the clayey cap rock at Sleipner (North Sea)," vol. 217, p. 319–337, 2005.
- [72] R. Vernooij, "Mineral alterations caused by the injection of CO₂ in crushed, and sheared caprock material," Utrecht, 2014.
- [73] J. W. Johnson, J. J. Nitao and K. G. Knauss, "Reactive Transport Modelling of CO₂ Storage in Saline Aquifers to Elucidate Fundamental Processes, Trapping Mechanisms, and Sequestration Partitioning," *Geological Society of London Special Publication on Carbon*, 2004b.
- [74] M. Zeidouni, M. Pooladi-Darvish and D. Keith, "Analytical Solution to Evaluate Salt Precipitation during CO₂ Injection in Saline Aquifers," Department of Chemical and Petroleum Engineering, University of Calgary, Canada, 2009.
- [75] J. Rutqvist, "The Geomechanics of CO₂ Storage in Deep Sedimentary Formations," *geotechnical geology and engineering*, vol. 30, p. 525–551, 2005.
- [76] M. Burton, N. Kumar and S. Bryant, "Time-Dependent Injectivity During CO₂ Storage in Aquifers," The University of Texas, Austin, 2008.
- [77] I. Gaus, "Role and impact of CO₂-rock interactions during CO₂ storage in sedimentary rocks," *international journal of greenhouse gas control*, vol. 4, pp. 73 - 89, 2010.
- [78] J. Kaszuba, D. Janecky and M. Snow, "Carbon dioxide reaction processes in a model brine aquifer at 200C and 200 bars: implications for geological sequestration of carbon," *Applied geochemistry*, vol. 18, pp. 1065-1080, 2003.
- [79] L. Pan, B. Freifeld, C. Doughty, S. Zakem, M. Sheu, B. Cutright and T. Terrall, "Fully coupled wellbore-reservoir modeling of geothermal heat extraction using CO₂ as the working fluid,"

Geothermics, vol. 52, p. 100–113, 2014.

- [80] A. W. Lyoho, "selecting enhanced oil recovery processes," *world oil*, vol. 187, pp. 61-64, 1978.
- [81] M. Eissa and E.-M. Shokir, "CO₂–oil minimum miscibility pressure model for impure and pure CO₂ streams," *Journal of Petroleum Science and Engineering*, vol. 58, p. 173–185, 2007.
- [82] O. Alomair and M. Iqbal, "CO₂ Minimum miscibility pressure (MMP) estimation using multiple regression (MLR) technique," in *Annual technical symposium and exhibition*, al khobar, 2014.
- [83] W. F. Yelling and R. S. Metcalfe, "Determination and Prediction of CO₂ Minimum Miscibility Pressures," *journal for petroleum engineering*, vol. 32, pp. 161-169, 1980.
- [84] J. Shaw and S. Bachu, "Screening, evaluation and ranking of oil reservoirs suitable for CO₂-flood EOR and carbon dioxide sequestration," *Journal of Canadian Petroleum Technology*, pp. 51-61, 2002.
- [85] N. Mungan, "Carbon Dioxide Flooding-fundamentals," *Journal of Canadian Petroleum Technology*, vol. 20, no. 1, 1981.
- [86] L. Lake, *Enhanced Oil Recovery*, Prentice-Hall, 1989, p. 262.
- [87] US department of Energy, "Identification and Selection of Major Carbon Dioxide Stream Compositions," Pacific Northwest national laboratory, 2011.
- [88] S. N. Ehrenberg and P. H. Nadeau, "Sandstone vs. carbonate petroleum reservoirs: A global perspective on porosity-depth and porosity-permeability relationships," *Geologic note*, vol. 4, no. 89, p. 435–445, 2005.
- [89] A. R. Kavscek, "screening criteria for CO₂ storage in oil reservoirs," *Petroleum science and technology*, vol. 20, p. 841–866, 2002.
- [90] G. Heddle, H. Herzog and M. Klett, "The Economics of CO₂ storage," Massachusetts Institute of Technology, Cambridge, 2003.
- [91] M. Sadfar, N. Al alawi, H. al sahn, T. Obeida, J. W. M. Khoury and M. Biterge, "WAG-CO₂ EOR horizontal wells pilot surveillance at a giant Abu Dhabi Oilfield," in *Adipec 2013 technical conference manuscript*, 2013.
- [92] Geffen, "improved Oil recovery could ease energy shortage," *world oil*, vol. 177, no. 5, pp. 84-88, 1977.
- [93] US FEA, "the potential and economics of enhanced oil recovery," 1976.
- [94] national petroleum council, "enhanced oil recovery - an analysis of the potential for enhanced oil recovery from known fields in the united states," washington, 1976.

- [95] B. C. MCree, "CO₂: How it works, where it works," *petroleum engineering*, pp. 52-63, 1977.
- [96] office of technology assessment, "enhanced oil recovery potential in the united states," US government printing office, washington, 1978.
- [97] S. o. P. e. o. AIME, "Third joint spe/DOE symposium on enhanced oil recovery," in *enhanced oil recovery in Romania*, Dallas, 1982.
- [98] J. J. Taber and F. D. Martin, "Technical screening guides for the Enhanced recovery of oil," in *Society of petroleum engineers annual technical conference and Exhibition*, San Francisco.
- [99] US department of energy, "Carbon Dioxide enhanced oil recovery," US department of energy, Albany, 2010.
- [100] A. D. Atrens, H. Gurgenci and V. Rudolph, "Economic Optimization of a CO₂-Based EGS Power Plant," *Energy and fuels*, vol. 25, p. 3765–3775, 2011b.
- [101] P. A. Dickey, "Increasing concentration of subsurface brines with depth," *Chemical Geology*, vol. 4, pp. 361-370, 1969.
- [102] A. D. Atrens, H. Gurgenci and V. Rudolph, "Electricity generation using a carbon-dioxide thermosiphon," *Geothermics*, vol. 31, p. 161–169, 2010.
- [103] E. C. Robertson, "Thermal properties of rocks," USGS, 1988.
- [104] Engineeringtoolbox, "Specific heat solids," [Online]. Available: http://www.engineeringtoolbox.com/specific-heat-solids-d_154.html. [Accessed 19 December 2014].
- [105] J. B. Randolph and M. O. Saar, "Impact of reservoir permeability on the choice of subsurface geothermal heat exchange fluid: CO₂ versus water and native brine.," *GRC Transactions*, 2011.
- [106] A. Athrens, H. Curgency and V. Rudolph, "Exergy analysis of a CO₂ thermosiphon," in *Thirty-Fourth Workshop on Geothermal Reservoir Engineering stanford university*, Stanford, 2009.
- [107] M. Dong, S. Huang, S. B. Dyer and F. M. Mourits, "A comparison of CO minimum miscibility pressure determinations for Weyburn crude oil," *Journal of Petroleum Science and Engineering*, vol. 31, pp. 13-22, 2001.
- [108] J. A. Lasather, "Bubble point pressure correlation," *Transript AIME*, p. 379, 1958.
- [109] H. M. Sebastian, R. S. Wenger and T. A. Renner, "Correlation of minimum miscibility pressure for impure CO streams," in *SPErDOE Enhanced Oil Recovery Symp*, Tulsa, 1984.
- [110] Element Energy, "Economic impacts of CO₂-enhanced oil recovery for Scotland," Scottish Enterprise, London, 2012.

- [111] J. W. Rupert, "Impact of geological uncertainty on project valuations for offshore CO₂-enhanced oil recovery," unpublished, Utrecht, 2014.
- [112] IEA, "From CO₂-EOR to CCS: "Prospects and Challenges of Combining CO₂-EOR with storage"," in *IEA – OPEC CO₂-EOR Kuwait Workshop*, Kuwait City, 2012.
- [113] A. Athrens, H. Gurgenci and V. Rudolph, "Water condensation in carbon-dioxide-based engineered geothermal power generation," *Geothermics*, vol. 51, pp. 397-405, 2014.
- [114] E. Bolton, A. Lasaga and D. Rye, "Long-term flow/chemistry feedback in a porous medium with heterogeneous permeability: kinetic control of dissolution and precipitation," *american journal of science*, vol. 299, p. 1–68, 1999.
- [115] J. Randolph, B. Adams, T. Kuehn and M. Saar, "Wellbore heat transfer in CO₂-based geothermal systems," in *Geothermal Resources Council Annual Meeting*, 2012.
- [116] R. Span and W. Wagner, "A new equation of state for carbon dioxide covering the fluid region from the Triple-point Temperature to 1100 K at pressures up to 800 Mpa," *Journal of physical and chemical reference data*, vol. 25, no. 6, pp. 1509-1590, 1996.
- [117] T. H. Sandve, I. Berre, E. Keilegavlen and J. M. Nordbotten, "Multiscale simulation of flow and heat transport in fractured geothermal reservoirs: inexact solvers and improved transport upscaling," in *Thirty-Eighth Workshop on Geothermal Reservoir Engineering*, Stanford, 2013.
- [118] A. Fenghour, A. Wakeham and V. Vesovic, "The viscosity of carbon dioxide," *Journal of physical and chemical reference data*, vol. 27, no. 1, pp. 31-44, 1998.
- [119] IHS, "Costs & Strategic Sourcing," IHS inc., 23 April 2015. [Online]. Available: <https://www.ihs.com/info/cera/ihsindexes/Index.html>. [Accessed 23 April 2015].
- [120] Synaps energy economics inc. , "CO₂ Price Report," Synaps energy inc. , Massachusetts, 2014.
- [121] IPCC, "Working Group III Contribution to the Fifth Assessment Report of the Intergovernmental Panel on Climate Change," International panel on climate change, new york, 2014b.
- [122] A. D. Atrens, H. Curgenci and V. Rudolph, "Economic analysis of a CO₂ thermosiphon," in *World Geothermal Congress* , Bali, 2010b.
- [123] C. Augustine, J. W. Tester and B. Anderson, "A comparison of geothermal with oil and gas well drilling costs," in *Thirty-First Workshop on Geothermal Reservoir Engineering* , Stanford , 2006.
- [124] Y. A. J. M. e. a. Polsky, "Enhanced geothermal systems (EGS) well construction technology evaluation synopsis.," in *Thirty-Fourth Workshop on Geothermal Reservoir Engineering* . , Stanford, 2009.

- [125] U.S. department of energy, "Acquisition and Development of Selected Cost Data for Saline Storage and Enhanced Oil Recovery (EOR) Operations," National Energy technology laboratory, 2014.
- [126] D. L. McCollem and J. M. Ogden, "Techno-Economic Models for Carbon Dioxide Compression, Transport, and Storage," University of California, Davis , California, 2006.
- [127] D. Burnett, "Desalinating Brine From Oil and Gas Operations in Texas," Global Petroleum Research Institute, Texas, 2005.
- [128] U.S. environmental protection agency, Brine disposal treatment practices relatign to the oil production industry, Washington D.C., 1974.
- [129] IEA, "Oil and Gas Lease Equipment and Operating Costs 1986 Through 2002," 2002. [Online]. Available: http://www.eia.gov/oil_gas/natural_gas/data_publications/cost_indices/c_i.html. [Accessed 23 April 2015].
- [130] Bureau of labor statistics, "US inflation calculator," 2015. [Online]. Available: <http://www.usinflationcalculator.com/about/>. [Accessed 24 April 2015].
- [131] U.S. Energy Information Administration (EIA), " Annual Energy Outlook 2015," US Department of energy, Washington DC, 2015.
- [132] T. Holt, E. Lindeberg and D. Wessel-Berg, "EOR and CO₂ disposal — Economic and capacity potential in the North Sea.," *Energy procedia*, vol. 1, no. 1, p. 4159–4166, 2009.
- [133] Y. Huang, S. Rezvani, D. Mclveen-Wright, A. Minchener and N. Hewitt, "Techno-economic study of CO₂ capture and storage in coal fired oxygen fed entrained flow IGCC power plants.," *Fuel Processing Technology*, vol. 89, no. 9, p. 916–925, 2008.
- [134] L. W. Lake and M. P. Walsh, "Enhanced oil recovery (EOR) Field data literature results," Department of Petroleum and Geosystems Engineering University of Texas at Austin , Austin, Texas, 2008.
- [135] Chemicalogic, "Molier charts," Chemicalogic, [Online]. Available: <http://www.chemicalogic.com/Pages/DownloadMollierCharts.aspx>. [Accessed 20 Februari 2015b].
- [136] S. Rehman and L. M. Al-Hadhrami, "Study of a solar PVdieselebattery hybrid power system for a remotely located population near Rafha, Saudi Arabia," *Energy*, vol. 35, pp. 4986-4995, 2010.
- [137] J. J. Dooley, R. T. Dahowski and D. H. Davidson, "CO₂-driven Enhanced Oil Recovery as a Stepping Stone to What?," U.S. department of energy, 2010.
- [138] B. M. Adams, T. H. Kuehn, J. M. Bielicki, J. B. Randolph and M. O. Saar, "A comparison of electric power output of CO₂ Plume Geothermal (CPG) and brine geothermal systems for

- varying reservoir conditions," *Applied Energy*, vol. 140, pp. 365 - 377, 2015.
- [139] J. Gale and P. Freund, "Coal-bed methane enhancement with co2 sequestration worldwide potential," *environmental geosciences*, vol. 8, no. 3, pp. 210-217, 2001.
- [140] C. M. Oldenburg, S. H. Stevens and S. Benson, "Economic feasibility of carbon sequestration with enhanced gas recovery (CSEGR)," *Energy*, vol. 29, p. 1413–1422, 2004.
- [141] NETL, "Carbon Dioxide Enhanced Oil Recovery - Untapped Domestic Energy Supply and Long Term Carbon Storage Solution," 2010.
- [142] G. Moritis, "SPECIAL REPORT: More US EOR projects start but EOR production continues," *oil and gas journal*, 2008.
- [143] M. Godec, V. Kuuskraa, L. S. Melzer and N. Wildgust, "CO₂ Storage in Depleted Oil Fields: The Worldwide Potential for Carbon Dioxide Enhanced Oil Recovery," *Energy procedia*, vol. 4, pp. 2162-2169, 2011.
- [144] V. Alvarado and E. Manrique, "Enhanced Oil Recovery: An Update Review," *Energies*, pp. 1529-1575, 2010.
- [145] NETL, "Mobility and Conformance Control for Carbon Dioxide Enhanced Oil Recovery (CO₂-EOR) via Thickeners, Foams, and Gels – A Detailed Literature Review of 40 Years of Research," US department of energy, 2012.
- [146] J. R. Friedrich, G. R. List and A. J. Heakin, "Petroleum-Free Extraction of Oil from Soybeans with Supercritical CO₂," *JAOCs*, pp. 288-292, 1982.
- [147] J. Wang, H. Cui, S. Wei, S. Zhuo, L. Wang, Z. Li and W. Yi, "Separation of Biomass Pyrolysis Oil by Supercritical CO₂ Extraction," *Smart Grid and Renewable Energy*, pp. 98-107, 2010.
- [148] B. Metz, O. Davidson, H. de Coninck, M. Loos and M. Meyer, "IPCC: special report on carbon capture and storage," Cambridge University Press, 2005.
- [149] S. Gilfillan, B. Lollar, G. Holland, D. Blagburn and S. S. M. Stevens, "solubility trapping in formation water as dominant CO₂ sink in natural gas fields," *Nature*, no. 458, pp. 614-618, 2009.
- [150] M. Wilkinson, R. Haszeldine, A. Fallick, N. Odling, S. Stoker and R. Gatliff, "CO₂-mineral reaction in a natural analogue for CO₂ storage — implications for modeling," *Journal of Sedimentary Research*, vol. 79, pp. 486-494, 2009.
- [151] I. s. r. o. C. D. c. a. storage, "Metz, B.; Davidson, O.; de Coninck, H.; Loos, M.; Meyer, M.," Cambridge University Press, 2005.
- [152] phywe, "Nikhef," [Online]. Available: http://www.nikhef.nl/~h73/kn1c/praktikum/phywe/LEP/Experim/3_2_06.pdf. [Accessed 16

December 2014].

- [153] L. Andre, P. Audigane, M. Azaroual and A. Menjoz, "Numerical modeling of fluid–rock chemical interactions at the supercritical CO₂–liquid interface during CO₂ injection into a carbonate reservoir, the Dogger aquifer (Paris Basin, France)," *Energy conversion and management*, vol. 33, p. 1782–1797, 2007b.
- [154] C. M. Oldenburg, "Joule-Thomson cooling due to CO₂ injection into natural gas reservoirs," *Energy Conversion and Management*, vol. 48, p. 1808–1815, 2007.
- [155] IEA, "caprock systems for CO₂ geological storage," 2011.
- [156] J. Rutqvist, "The Geomechanics of CO₂ Storage in Deep Sedimentary Formations," *geotechnical geology and engineering*, no. 30, p. 525–551.
- [157] J. Inglese, "Capturing Carbon emissions," Allianz, [Online]. Available: <http://www.agcs.allianz.com/assets/PDFs/riskfeatures/Capturing-carbon-emissions-GRD-engl.pdf>. [Accessed 12 01 2015].
- [158] Chemical logic, [Online]. Available: http://www.chemicallogic.com/documents/co2_mollier_chart_met.pdf. [Accessed 13 Januari 2015].
- [159] NCSU, "public lecture on real gas calculations," [Online]. Available: http://www4.ncsu.edu/~franzen/public_html/CH433/lecture/Imperfect_Gases_Detail.pdf. [Accessed 3 Februari 2015].

Appendix I: main Matlab script

```

clc; close all;

global Par % allows all the functions to access the input
parameters
output = zeros(5,9); % for functionality
CPGcosts = zeros(5,5); % for functionality
depletion = zeros(25,1);
Deprate = zeros(25,3);
EORcosts = zeros(21,9);
permeability = zeros(21,3);
COE=zeros(3,4);
Par = zeros(24,1); % generates a matrix for the parameters

%% to import reservoir data from excell
% for i = 1:1 % predefined reservoir parameters
%     if i < 2; Range='E8:E28';
%     else
%         if i <3; Range='F8:F28';
%         else     Range='G8:G28' ;
%         end
%     end
%     end
%     Par = xlsread('input.xls','Sheet1',Range);
for g = 1:4;
for i = 6:21; % to iterate over a range of input parameters
    for p = 1:3;
        Par(9,1) = 800+200*i; %2500; %The reservoir depth (m)
        Par(1,1) = 120; %40 +(20*i); %output mass flow in kg/s
        Par(2,1) = Par(9,1)*0.01; % initial reservoir pressure
(Mpa)
        Par(4,1) = 707.1; %distance between the production and
injection well
        Par(5,1) = 15; %ambient temperature degC
        Par(6,1) = 1; %darcy flow channel cross-sectional area
(m^2)
        Par(7,1) = 25+5*g; %thermal gradient in degC per km
        Par(3,1) = (Par(9,1)/1000)*Par(7,1)+Par(5,1); %
Temperature of the hot rocks reservoir, oK
        Par(10,1) = 0.25-0.03*(Par(9,1)/1000); % porosity of the
reservoir (%)
        Par(8,1) = 5E-13*((Par(10,1)/0.25)^3)*((1-0.25)/(1-
Par(10,1)))^2;%permeability in m^2 (x10^-15 for md)
        Par(11,1) = 300; % height of the reservoir (m)
        Par(12,1) = 0.005; % loss factor of the system

        % well parameters
        Par(13,1) = 0.23125; %The injection well diameter, m
        Par(14,1) = 0.23125; %The production well diameter, m
        Par(15,1) = 1; % number of injection wells
        Par(16,1) = 4; % number of production wells
    end
end
end

```

The joint potential of CO₂-EOR with CPG| By Roland Vernooij

```

% Oil parameters
Par(17,1) = 32; % API gravity degree of the oil
Par(18,1) = 0.60; % fraction of the Pore volume occupied
by oil
Par(19,1) =
1000*1000*Par(11,1)*Par(10,1)*Par(18,1)*6.2898105697751;%
Original oil in place
Par(20,1) = 2.5; % ratio of bbl oil/t CO2 injected
Par(21,1) = 0.15; %0.1; %0.15 % recovery factor of the
OOIP recovered by EOR

% Thermal parameters
Par(22,1) = 920; % rock specific heat of the formation
(sandstone)J/kg/k
Par(23,1) = 2.1; % thermal conductivity W/m/k
Par(24,1) = 2650; % Rock grain density kg/m^3
Par(25,1) = 50000+40*Par(9,1); % Salinity of the brine
(ppm)

% incoming CO2 parameters[pressure (Mpa), Temperature (K),
density (kg/m^3)
vin = [9.65,273.15+Par(5,1),848.98,0,0,0,0,0]; % based on
CO2 from the sheep mountain reservoir
vin = co2eqofstate('PTL', vin);
CO2comp = [97.0, 0.6, 2.4, 0]; % composition of the gas
[%CO2, %N2, %CH4, %H2O]
Oilcomp = [0.96, 0.58, 0.3, 4.49, 2.99, 4.75, 2.73, 3.46];
% composition of the light oilf [N2, CO2, H2S, CH4,C2H6, C3H8,
C4H10]
PCO2 = 45; % costs for natural CO2 ($/tonne)
Prec = 13.45; % costs for recycled CO2 ($/tonne)
Poil = 60; % $/bbl
Pdisp = 1.801E-4; % costs of water disposal

% to calculate the effect of Carbon taxes

ETS = zeros(1,20); PCO2= ones(1,20)*45;
for t = 1:20;
if p==1; option = 'low-ETS'; end
if p==2; option = 'high-ETS'; end
if p==3; option = 'base-ETS'; end
% prediction
switch option
case 'low-ETS'
ETS(t) = 11+1.65*t;
if ETS(t)>60; PCO2(t)= (60-ETS(t))/3;
else PCO2(t)= 60-ETS(t);end
case 'base-ETS'
ETS(t) = 16.5+2.48*t;
if ETS(t)>45; PCO2(t)= (45-ETS(t))/3;
else PCO2(t)= 45-ETS(t); end

```

```

        case 'high-ETS'
            ETS(t) = 27.5+3.60*t;
            if ETS(t)>30; PCO2(t) = (30-ETS(t))/3;
            else PCO2(t) = 30-ETS(t);end
        end
    end

    if p ==1; Pinject = co2calibration;
    injstore(i) = Pinject;
    else
    Pinject = injstore(i);

    if Pinject < 7.38;
    PinjectEOR = 7.38; % to make sure CO2 is in supercritical
state at the point of injection
    else PinjectEOR = Pinject;
    end
    [Pr,v1,v2,v3,v,sweptarea] = co2(PinjectEOR,Par(3,1));
%determines the properties at the base of the production well
    Par(26,1)=Par(10,1)*sweptarea;
    %% calculate the oil displacement
    % to check miscibility
    capEOR2 = 0;
    T1 = 25; % Initial T1 (will change in function)
    [MMP_pure,EORtype, MMP_imp] =
reservoirmisc(CO2comp,Oilcomp); % determines whether
displacement is miscible
    [FCO2,EOR,Wpump,OPEXeor,T1,CO2sto1]=
CO2EOR(v,v2,v3,vin,PCO2,Prec,Poil,PinjectEOR,capEOR2,T1);
    if MMP_imp < Par(2,1);
        E=1; else E=0;
    end
%     if E==0;
%         continue
%     end

    %% calculate the reservoir drying time
    CO2inject=Par(1,1)*86.4*365;
    Threshold=0.99;
    Mwater = 18.01528E-3; % molar mass of H2O (kg/mol)
    Mco2 = 44.0095E-3; % molar mass of CO2 (kg/mol)
    densh2o = 1230; %H2Odensity(Par(3,1),Par(2,1)); %density
of H2O at res P and T (kg/m^3)
    densco2 = v2(3); % density of CO2 at the bottom of the
production well (Kg/m^3)
    CO2volthreshold=(Threshold*(Mwater/densh2o))/((1-
Threshold)*(Mco2/densco2)+(Threshold*(Mwater/densh2o))); % to
calculate the CO2 threshold volume fraction
    mir = CO2inject*1000; %mass injection rate at the
reservoir (kg/year)

```

The joint potential of CO₂-EOR with CPG| By Roland Vernooij

```

    vir = mir/(v2(3)); %volumetric injection rate at the
reservoir (m^3/year)
    vm = 0.1*vir;
    T2 = 20; % Initial T2 (will change in function)
    dry = zeros(T2,4);
    for t=1:T2
    [FCO2,dry] = Drying(t,v2,v3,FCO2,CO2inject,T2,dry);
    EORrat= lognpdf(T1+t-2.0,1.59,0.40)*Par(20,1)*10;
    %out(t,i)=FCO2;
    oildry(t,i)=EORrat*CO2inject;
    if FCO2 > CO2volthreshold;
    T2 = t;
    break
    end
    end
    Tdry=T2;
    water = [EOR(1:T1,6);dry(1:T2,4)];
    Maxw = max(water);

    Recload = [EOR(1:T1,3);dry(1:T2,5)]; % creates a vector
with the rec facility throughput
    Maxrec = max(max(Recload/1000000))*51.813; % calculates
the maximum anual throughput of the recycling facility MMcfd

    [capEOR,Cwell,Crecfac,Cpump,Cdisp,capEOR2,debug] =
capitalEOR(Maxrec,Wpump,Maxw);
    [dpdry1,qinj,k1,rdry1]= injectivity(v,Tdry);
    presdrop(1:Tdry,1)=transpose(dpdry1);
    presdrop(1:Tdry,2)=transpose(qinj);
    presdrop(1:Tdry,3)=transpose(rdry1);

    permeability(i,1)= Par(8,1);
    permeability(i,2)= k1;
    permeability(i,3)= (k1-Par(8,1))/Par(8,1)*100;

%% calculate the CPG phase
    % to calculate the surface processing and costs
    Par(8,1) = k1;
    Tres = Par(3,1); % set initial reservoir temperature
    replate = 80E-3; % thermal replenishment rate for the
reservoir
    Lifetime = 25; % lifetime in years
    for t = 1:Lifetime; type = 'CPG';
    [Pr,v1,v2,v3,v,sweptarea,Downhole] = co2(Pinject,Tres);
%determines the properties at the base of the production well
    Heatflux = Par(1,1)*31556926*((v(3,2)-
v(2,2))*(v(2,7)+v(3,7))/2)-(replate*(10^3)*31556926);
%heatflow in kJ/year
    Cp_rock = (Par(24,1)*Par(22,1)*(Par(11,1)*10E6*(1-
Par(10,1))))/1000; % heat capacity of the formation section
(kJ/K)

```

The joint potential of CO₂-EOR with CPG| By Roland Vernooij

```

Tres = Tres - (Heatflux/Cp_rock); %calculates the average
temperature depletion of the reservoir
depletion(t,1)= Tres;
[v4, Uphole,upflow] = uphole(v3); % determines the
properties at the production wellhead
DeltaP = (v(2,1)-v(3,1)); % calculates the pressure
difference over the reservoir
[Power,CO2bought3] = co2turbine(v,vin); % calculates the
output and system efficiency based on a turbine isentropic
efficiency of 0.85
[capitalCPG,Cturbine,piping,Cheatex,Fp,Qheatex] =
capitalcosts(v,Power(3)); %calculates the capital costs of the
CPG system
generation(t,1)=Power(3); % power generation (kWh/year)
CO2sto3(t,1)=CO2bought3; % CO2 stored in the CPG phase
(tonne/year)
end

Deprate(1:Lifetime,i)= depletion;

%% collate output data
output(i,1) = Par(9,1); % depth
output(i,2) = E; % injection pressure
output(i,3) = v4(1); % production pressure
output(i,4) = MMP_pure ; % MMP pure co2
output(i,5) = MMP_imp ; % MMP impure CO2
output(i,6) = Power(2) ; % Turbine work = h4-h5*mdotg*eff
output(i,7) = Power(8) ; % binary Turbine work = h5-
h6*mdotg*eff*carnot
output(i,8) = Power(3) ; % Net turbine work
output(i,9) = Qheatex ; % heat flow through the heat
exchanger
output(i,10) = Power(4) ; %total heat flux from reservoir
output(i,11) = Par(2,1) ; %initial reservoir pressure MPa
output(i,12) = DeltaP ;

[LCEEOR,costsCO2EOR,costsdisp,LCEEOR2] =
LCEeor(T1,OPEXeor, capEOR, PCO2, Prec, Pdisp, EOR, capEOR2) ;
EORper(i,1:6)=[Par(9,1),LCEEOR,LCEEOR2,sum(EOR(1:T1,5))*E-
6,(sum(EOR(1:T1,11))-sum(EOR(1:T1,3)))*E-6,EOR(T1,2)];

[LCECPGdry,LCECPG,Cdry,CPGOPEX,CPGOPEX2] =
LCEgeothermal(Tdry,
capitalCPG,CO2bought3,PCO2,dry,Pdisp,Prec,generation,oildry,ca
pEOR);
CO2Price(1:20,p) = PCO2;
COE(p,1) = Cdry;
COE(p,2) = LCECPG;
COE(p,3) = LCECPGdry;
COE(p,4) = LCEEOR2;
end

```

```

EORcosts(i,1) = Par(9,1);
EORcosts(i,2) = capEOR;
EORcosts(i,3) = Cwell;
EORcosts(i,4) = Crecfac;
EORcosts(i,5) = Cdisp+costsdisp;
EORcosts(i,6) = Cpump;
EORcosts(i,7) = costsCO2EOR;
EORcosts(i,8) = sum(OPEXeor);
EORcosts(i,9) = LCEEOR;
EORcosts(i,10) = LCEEOR2;

CPGcosts(i,1) = Par(9,1);
CPGcosts(i,2) = capitalCPG;
CPGcosts(i,3) = Cturbine;
CPGcosts(i,4) = piping;
CPGcosts(i,5) = Cheatex;
CPGcosts(i,6) = Cdry;
CPGcosts(i,7) = CPGOPEX;
CPGcosts(i,8) = CPGOPEX2;
CPGcosts(i,9) = LCECPGdry;
CPGcosts(i,10) = LCECPG;

time = transpose(0:1:T1+T2+Lifetime);
CO2sto =
[Par(9,1);transpose(CO2sto1);dry(1:T2,3)/1000;CO2sto3];
storage(1:numel(time),1) = time;
storage(1:numel(time),i+1) = CO2sto;
storage(numel(time)+1,i+1) = sum(dry(1:T2,3))/1000;

% To generate an excell file with the results
% For the economic performance
if g==4;
xlswrite('Results2.xlsx',CPGcosts,'Economics','B14');
if i==1; xlswrite('Results2.xlsx',COE,'Economics','L13');
xlswrite('Results2.xlsx',Par(9,1),'Economics','L12'); end
if i==2; xlswrite('Results2.xlsx',COE,'Economics','L21');
xlswrite('Results2.xlsx',Par(9,1),'Economics','L20'); end
if i==3; xlswrite('Results2.xlsx',COE,'Economics','L29');
xlswrite('Results2.xlsx',Par(9,1),'Economics','L28'); end
if i==4; xlswrite('Results2.xlsx',COE,'Economics','L37');
xlswrite('Results2.xlsx',Par(9,1),'Economics','L36'); end
if i==5; xlswrite('Results2.xlsx',COE,'Economics','L45');
xlswrite('Results2.xlsx',Par(9,1),'Economics','L44'); end
if i==6; xlswrite('Results2.xlsx',COE,'Economics','L53');
xlswrite('Results2.xlsx',Par(9,1),'Economics','L52'); end
if i==7; xlswrite('Results2.xlsx',COE,'Economics','L61');
xlswrite('Results2.xlsx',Par(9,1),'Economics','L60'); end
if i==8; xlswrite('Results2.xlsx',COE,'Economics','L69');
xlswrite('Results2.xlsx',Par(9,1),'Economics','L68'); end

```

```

    if i==9;  xlswrite('Results2.xlsx',COE,'Economics','L77');
xlswrite('Results2.xlsx',Par(9,1),'Economics','L76'); end
    if i==10; xlswrite('Results2.xlsx',COE,'Economics','L85');
xlswrite('Results2.xlsx',Par(9,1),'Economics','L84'); end
    if i==11;
xlswrite('Results2.xlsx',COE,'Economics','Q13');
xlswrite('Results2.xlsx',Par(9,1),'Economics','Q12'); end
    if i==12;
xlswrite('Results2.xlsx',COE,'Economics','Q21');
xlswrite('Results2.xlsx',Par(9,1),'Economics','Q20'); end
    if i==13;
xlswrite('Results2.xlsx',COE,'Economics','Q29');
xlswrite('Results2.xlsx',Par(9,1),'Economics','Q28'); end
    if i==14;
xlswrite('Results2.xlsx',COE,'Economics','Q37');
xlswrite('Results2.xlsx',Par(9,1),'Economics','Q36'); end
    if i==15;
xlswrite('Results2.xlsx',COE,'Economics','Q45');
xlswrite('Results2.xlsx',Par(9,1),'Economics','Q44'); end
    if i==16;
xlswrite('Results2.xlsx',COE,'Economics','Q53');
xlswrite('Results2.xlsx',Par(9,1),'Economics','Q52'); end
    if i==17;
xlswrite('Results2.xlsx',COE,'Economics','Q61');
xlswrite('Results2.xlsx',Par(9,1),'Economics','Q60'); end
    if i==18;
xlswrite('Results2.xlsx',COE,'Economics','Q69');
xlswrite('Results2.xlsx',Par(9,1),'Economics','Q68'); end
    if i==19;
xlswrite('Results2.xlsx',COE,'Economics','Q77');
xlswrite('Results2.xlsx',Par(9,1),'Economics','Q76'); end
    if i==20;
xlswrite('Results2.xlsx',COE,'Economics','Q85');
xlswrite('Results2.xlsx',Par(9,1),'Economics','Q84'); end
    if i==21;
xlswrite('Results2.xlsx',COE,'Economics','Q93');
xlswrite('Results2.xlsx',Par(9,1),'Economics','Q92'); end
end

    if i==1;  xlswrite('Results2.xlsx',Downhole,'Wells','B8');
xlswrite('Results2.xlsx',Uphole,'wells','B109'); end
    if i==2;  xlswrite('Results2.xlsx',Downhole,'wells','F8');
xlswrite('Results2.xlsx',Uphole,'wells','F109'); end
    if i==3;  xlswrite('Results2.xlsx',Downhole,'wells','J8');
xlswrite('Results2.xlsx',Uphole,'wells','J109'); end
    if i==4;  xlswrite('Results2.xlsx',Downhole,'wells','N8');
xlswrite('Results2.xlsx',Uphole,'wells','N109'); end
    if i==5;  xlswrite('Results2.xlsx',Downhole,'wells','R8');
xlswrite('Results2.xlsx',Uphole,'wells','R109'); end
    if i==6;  xlswrite('Results2.xlsx',Downhole,'wells','V8');
xlswrite('Results2.xlsx',Uphole,'wells','V109'); end

```

```

    if i==7;    xlswrite('Results2.xlsx',Downhole,'Wells','Z8');
xlswrite('Results2.xlsx',Uphole,'wells','Z109'); end
    if i==8;
xlswrite('Results2.xlsx',Downhole,'wells','AD8');
xlswrite('Results2.xlsx',Uphole,'wells','AD109'); end
    if i==9;
xlswrite('Results2.xlsx',Downhole,'wells','AH8');
xlswrite('Results2.xlsx',Uphole,'wells','AH109'); end
    if i==10;
xlswrite('Results2.xlsx',Downhole,'wells','AL8');
xlswrite('Results2.xlsx',Uphole,'wells','AL109'); end
    if i==11;
xlswrite('Results2.xlsx',Downhole,'wells','AP8');
xlswrite('Results2.xlsx',Uphole,'wells','AP109'); end
    if i==12;
xlswrite('Results2.xlsx',Downhole,'wells','AT8');
xlswrite('Results2.xlsx',Uphole,'wells','AT109'); end
    if i==13;
xlswrite('Results2.xlsx',Downhole,'Wells','AX8');
xlswrite('Results2.xlsx',Uphole,'wells','AX109'); end
    if i==14;
xlswrite('Results2.xlsx',Downhole,'wells','BB8');
xlswrite('Results2.xlsx',Uphole,'wells','BB109'); end
    if i==15;
xlswrite('Results2.xlsx',Downhole,'wells','BF8');
xlswrite('Results2.xlsx',Uphole,'wells','BF109'); end
    if i==16;
xlswrite('Results2.xlsx',Downhole,'wells','BJ8');
xlswrite('Results2.xlsx',Uphole,'wells','BJ109'); end
    if i==17;
xlswrite('Results2.xlsx',Downhole,'wells','BN8');
xlswrite('Results2.xlsx',Uphole,'wells','BN109'); end
    if i==18;
xlswrite('Results2.xlsx',Downhole,'wells','BR8');
xlswrite('Results2.xlsx',Uphole,'wells','BR109'); end
    if i==19;
xlswrite('Results2.xlsx',Downhole,'Wells','BV8');
xlswrite('Results2.xlsx',Uphole,'wells','BV109'); end
    if i==20;
xlswrite('Results2.xlsx',Downhole,'wells','BZ8');
xlswrite('Results2.xlsx',Uphole,'wells','BZ109'); end
    if i==21;
xlswrite('Results2.xlsx',Downhole,'wells','CD8');
xlswrite('Results2.xlsx',Uphole,'wells','CD109'); end
end

xlswrite('Results2.xlsx',permeability,'Performance','B149');
    if i==1;
xlswrite('Results.xlsx',presdrop,'pressuredrop','A8'); end
    if i==2;
xlswrite('Results.xlsx',presdrop,'pressuredrop','F8'); end

```

The joint potential of CO₂-EOR with CPG| By Roland Vernooij

```
    if i==3;
xlswrite('Results.xlsx',presdrop,'pressuredrop','K8'); end
    if i==4;
xlswrite('Results.xlsx',presdrop,'pressuredrop','P8'); end
    if i==5;
xlswrite('Results.xlsx',presdrop,'pressuredrop','U8'); end
    if i==6;
xlswrite('Results.xlsx',presdrop,'pressuredrop','A8'); end
    if i==7;
xlswrite('Results.xlsx',presdrop,'pressuredrop','F8'); end
    if i==8;
xlswrite('Results.xlsx',presdrop,'pressuredrop','K8'); end
    if i==9;
xlswrite('Results.xlsx',presdrop,'pressuredrop','P8'); end
    if i==10;
xlswrite('Results.xlsx',presdrop,'pressuredrop','U8'); end
    if i==11;
xlswrite('Results.xlsx',presdrop,'pressuredrop','A8'); end
    if i==12;
xlswrite('Results.xlsx',presdrop,'pressuredrop','F8'); end
    if i==13;
xlswrite('Results.xlsx',presdrop,'pressuredrop','K8'); end
    if i==14;
xlswrite('Results.xlsx',presdrop,'pressuredrop','P8'); end
    if i==15;
xlswrite('Results.xlsx',presdrop,'pressuredrop','U8'); end
    if i==16;
xlswrite('Results.xlsx',presdrop,'pressuredrop','A8'); end
    if i==17;
xlswrite('Results.xlsx',presdrop,'pressuredrop','F8'); end
    if i==18;
xlswrite('Results.xlsx',presdrop,'pressuredrop','K8'); end
    if i==19;
xlswrite('Results.xlsx',presdrop,'pressuredrop','P8'); end
    if i==20;
xlswrite('Results.xlsx',presdrop,'pressuredrop','U8'); end
    if i==21;
xlswrite('Results.xlsx',presdrop,'pressuredrop','U8'); end

xlswrite('Results2.xlsx',EORcosts,'Economics','B14');
xlswrite('Results2.xlsx',CPGcosts,'Economics','B50');

% For the input parameters of the system:
xlswrite('Results2.xlsx',Par,'Parameters','E8')

% For the thermodynamics over the different stages of the
system:
xlswrite('Results2.xlsx',v,'Thermodynamics','C9');
xlswrite('Results2.xlsx',vin,'Thermodynamics','C8');

% For the EOR performance
```

```

xlswrite('Results2.xlsx',EOR,'EOR','A8');
xlswrite('Results2.xlsx',EORper,'EOR','A40');

% For the CPG system performance
if g == 1;
xlswrite('Results2.xlsx',output,'Performance','B8'); end
if g == 2;
xlswrite('Results2.xlsx',output,'Performance','B30'); end
if g == 3;
xlswrite('Results2.xlsx',output,'Performance','B52'); end
if g == 4;
xlswrite('Results2.xlsx',output,'Performance','B74'); end
if g == 5;
xlswrite('Results2.xlsx',output,'Performance','B96'); end
xlswrite('Results2.xlsx',Deprate,'Performance','B175');
% xlswrite('Results2.xlsx',out,'Performance','M37');
end
end

% FOr the CO2 storage
xlswrite('Results2.xlsx',storage,'storage','A8');
xlswrite('Results2.xlsx',CO2Price,'storage','A70');

if LCECPGdry < 0.30;
url = 'https://www.youtube.com/watch?v=dQw4w9WgXcQ';
else url = 'https://www.youtube.com/watch?v=6dOwHzCHfgA';
end
web(url,'-browser');

```

Appendix II: CO₂-calibration

```
function Pinject=co2calibration
```

```
global Par;
```

```
mass = Par(1,1);
```

```
Ptarget = Par(2,1);
```

```
%Qtarget=20000; %target kW of heat from reservoir (kW)
```

```
Pinject = fminsearch(@(Pinject) co2_error(mass, Ptarget,Pinject), 10.347, ...
```

```
optimset('Display','iter','MaxFunEvals',50,'TolX',1e-1));
```

```
fprintf(1,'mass flow = %.1f\n',mass);
```

```
function retval=co2_error(mass,Ptarget,Pinject)
```

```
P = co2(Pinject);
```

```
retval=(Ptarget-P)^2;
```

Appendix III: CO₂ (thermodynamics)

```
% This function serves to calculate the properties of CO2 in
the various
```

```
% stages in the system
```

The joint potential of CO₂-EOR with CPG| By Roland Vernooij

```

function [Pr,v1,v2,v3,v,sweptarea,Downhole] =
co2(Pinject,Tres)
    global Par
    mdotg=Par(1,1); %mass flowrate (kg/s)
    Pinj=Pinject;%12; %injection pressure
    depth = Par(9,1); %well depth (m)
    length = Par(4,1); %distance between wells (m)
    height = Par(11,1); %hieght of the reservoir (m)
    K= Par(8,1)%permeability in m^2 (x10^-15 for md)
    Di = Par(13,1); %well diameter (m)
    Dp = Par(14,1); %well diameter (m)
    Trock = 273.15+Tres; % Temperature of the hot rocks
reservoir, oK
    %Tc = 304.1282; %critical temperature

% Create the vectors to hold the properties at each point
v = zeros(6, 8); % allows the model to run more smooth

% Point #1 - Assume the same state Pruess assumed for the
starting point
v(1,1) = Pinj; v(1,2) = 273.15+(Par(5,1));
v1 = co2eqofstate('PTL', v(1,:));
v(1,:)=v1;

% Point #2 - Bottom of Injection Hole
[v2,Downhole]=downhole(v1, depth, Di, mdotg);
v(2,:)=v2;

% Point #3 - Bottom of Production Hole
[v3,sweptarea]=reservoir(v2, length, height, mdotg/4, 100, K,
Trock);
v(3,:)=v3;
Pr = v(3,1);

% Point #4 - Top of production hole
[v4]=uphole(v3, depth, Dp, mdotg);
v(4,:)=v4;

% Point %5 - After turbine
v(5,6) = v(4, 6);
v(5,1) = v(1, 1);
v(5,2) = v(1, 2); % Trial value for temperature
%v(5,3) = co2prop('DV',v(5,2)); % Trial value for density
v5 = co2eqofstate('PTG', v(5,:));
v(5,3) = v5(3); % Trial value for density
v5 = co2eqofstate('PS', v(5,:)); % Find the rest for given
(p, s)
v(5, :)=v5;
% figure(1); putpoint(v(5,6),v(5,2),'5');

cycle_option = 'supercritical-loop';

```

```

% Point #6
switch cycle_option
    case 'condensing-loop'
        v(6,1) = v(5,1);
        v6 = co2eqofstate('PSATG', v(6,:));
    case 'supercritical-loop'
        v(6,:) = (v(1,:));
        v6 = v(6,:);
end
v(6,:) = v6;

```

Appendix IV: reservoir miscibility

% Calculates the miscibility of CO₂ and oil in a reservoir
 % Based on: M. Dong, S. Huang, S. B. Dyer en F. M. Mourits,
 % „A comparison of CO minimum miscibility pressure determinations for Weyburn
 crude oil,”
 % Journal of Petroleum Science and Engineering, vol. 31, pp. 13-22, 2001.

```

function [MMP_pure, EORtype, MMP_imp] = reservoirmisc(CO2comp,Oilcomp)
global Par
API = Par(17,1);
MWC5 = (7864.9/API)^(1/1.0386); %calculates the molar weight of the C5+ fraction
from the API gravity

```

% species present in injected CO₂ (based on sheep mountain)

```

FCO2 = CO2comp(1)/100;
FN2 = CO2comp(2)/100;
FCH4 = CO2comp(3)/100;
FH2O = CO2comp(4)/100;

```

% species present in the oil (Based on weyburn oil)

```

OFN2 = Oilcomp(1);
OFCO2 = Oilcomp(2);
OFH2S = Oilcomp(3);
OFCH4 = Oilcomp(4);
OFC2H6 = Oilcomp(5);
OFC3H8 = Oilcomp(6);
OFC4H10 = Oilcomp(7);
volrat = (OFN2+OFCH4)/(OFH2S+OFCO2+OFC2H6+OFC3H8+OFC4H10);%Xvol/Xint;
%ratio of volatile to intermediate oil fractions

```

% critical Temperature of species in K

```

TCCO2 = 304.25;
TCN2 = 126.2;
TCCH4 = 190.8;
TH2O = 647;

```

```

TPC = (FCO2*TCCO2)+(FN2*TCN2)+(FCH4*TCCH4)+(FH2O*TH2O);% the pseudocritical
temperature of the injected mixture

```

```

MMP_pure = 6.05E-6*((1.8*Par(3,1)+32)^1.06)*(MWC5^1.78)*(volrat)^0.136; %
calculates the MMP for pure CO2
Fimp = 1-0.0213*(TPC-304.2)+2.51E-4*((TPC-304.2)^2)-2.35E-7*((TPC-304.2)^3); %
impurity factor
MMP_imp = MMP_pure*Fimp; % MMP for impure CO2

if Par(2,1) > MMP_imp,
    EORtype = 'Miscible';
    fprintf(1, 'Miscible\n');
else
    EORtype = 'Immiscible';
    fprintf(1, 'Immiscible\n');
end

```

Appendix V: CO₂-EOR

```

% estimates the oil production using CO2-EOR over time
% Methodology based on: Element Energy,
% „Economic impacts of CO2-enhanced oil recovery for
Scotland,“
% Scottish Enterprise, London, 2012.

function[FCO2,EOR,Wpump,OPEX,T1,CO2sto1]=
CO2EOR(v,v2,v3,vin,PCO2,Prec,Poil,PinjectEOR,capEOR,T1)
global Par

EOR = zeros(T1,11);
OOIP = Par(19,1); % original oil in place in the reservoir
FCO2=0; %initial amount of CO2 in the reservoir
% operatinject = 12;% operational costs for co2 compression
and injection ($/tCO2 injected)
% operatrec = 0; %7.15;% operational costs for co2 recycling
($/tCO2 recycled)
% operatoil = 16.65; % operational costs for oil treatment
($/Bbl produced)
mean = 1.59; % mean oil production
std = 0.40; %standard deviation of the lognormal curve
delay = 2.0; % time after injection before oil production
starts
RecF = Par(21,1); % recovery factor of the OOIP produced with
EOR
ScaleF = OOIP*RecF;
EORavg = Par(20,1); % ratio of bbl produced to tonne CO2
injected
% benop=0.01;
% cosop=0;

for t = 1:T1
    if t >= T1
        break
    end
end

```

```

end
OPEX(t) = 13930185.60;
if t <= delay
    oilproduction = 0;
    CO2inject = 442252.3057;
    cumCO2inject=442252.3057*t;
    [FCO2,dry] = Drying(t,v2,v3,FCO2,CO2inject);
%     CO2rec=dry(t,5); % CO2 recycled in tonne/year
%     Oilrevenue = oilproduction*Poil;
    EORrat=0;

else
    % to calculate the injection and production profiles
    cumoilproduction = logncdf(t-delay,mean,std)*ScaleF; %
calculates the cumulative oil production at time t
    oilproduction = lognpdf(t-delay,mean,std)*ScaleF; %
calculates the oil production at time t
    EORrat= lognpdf(t-delay,mean,std)*EORavg*10;
    CO2inject = oilproduction/EORrat; % CO2 injection rate
(tonne/year)
    cumCO2inject = cumoilproduction/EORrat; % cumulative CO2
injected
    [FCO2,dry] = Drying(t,v2,v3,FCO2,CO2inject);
end

% to calculate the recycled CO2 from the reservoir
CO2rec= dry(t,5); % CO2 recycled in tonne/year
CO2stol(t)=(CO2inject-CO2rec);
CO2costs(t) =(CO2stol(t)*PCO2(t)+CO2rec*Prec); % costs for
CO2

% to calculate te operational costs and benefits
Oilrevenue = oilproduction*Poil;
%OPEXeor(t) =
operatinject*CO2inject+oilproduction*operatoil+CO2rec*operatre
c;
    benop = Oilrevenue+(CO2rec*(PCO2(t)-Prec));
    cosop = CO2costs(t)+OPEX(t);

EOR(t,1) = t;
EOR(t,2) = FCO2;
EOR(t,3) = CO2rec;
EOR(t,4) = cosop;
EOR(t,5) = oilproduction;
EOR(t,6) = dry(t,4);
EOR(t,7) = Oilrevenue;
EOR(t,8) = EORrat;
EOR(t,9) = cumCO2inject;
EOR(t,10) = benop;
EOR(t,11) = CO2inject;
EOR(t,12) = PCO2(t);

```

```

if t >= mean+delay && benop <= cosop
    T1=t ;
end
end
    effpump = 0.85; % isentropic efficiency of the pump
    Wpump = ((1000*10)/(365*24*36))*(CO2inject*(PinjectEOR-
vin(1)))/(v(1,3)*effpump);
    if Wpump <0 ; Wpump = 0; end

```

Appendix VI: Capital costs EOR

```

% this function serves to calculate the costs of the CPG
system
% Based on A. D. Atrens, H. Curgenci en V. Rudolph,
% „Economic analysis of a CO2 thermosiphon,“
% in World Geothermal Congress , Bali, 2010.

function [capEOR,Cwell,Crecfac,Cpump,Cdisp, capEOR2, debug] =
capitalEOR(Maxrec,Wpump,Maxw)
global Par
depth = Par(9,1);
Di = Par(13,1);
Dp = Par(14,1);
injwells = Par(15,1);
prowells = 1;% Par(16,1);

% to calculate the costs of wells
K = 0.554; % costant based on Atrens
b = 0.000613; % costant based on Atrens
sigma = 0.25; % costant based on Atrens
Cwell = (injwells*(K*(exp(b*depth))*(1-
sigma)+(Di/0.2313)*sigma*K*(exp(b*depth)))+ prowells
*(K*(exp(b*depth))*(1-
sigma)+(Dp/0.2313)*sigma*K*(exp(b*depth))))*1000000;

rho_brine = 1230*0.0624279606; %density of brine in pounds per
square feet
W = Maxw*2.20462262/7866; % maximum brine injection rate in
lb/hour
D = 0.0254*(2.2*(W^0.41))/(rho_brine^0.31); % diameter of the
disposal well
L = 1500; % depth of the disposal reservoir
Cdisp = (K*(exp(b*L))*(1-
sigma)+(D/0.2313)*sigma*K*(exp(b*L)))*1000000; % costs of
the disposal well

% for the recycling facility
if Maxrec < 30;
    Crecfac = 1200000*Maxrec;
else

```

The joint potential of CO₂-EOR with CPG| By Roland Vernooij

```
Crecfac = 36000000+(Maxrec-30)*750000;
end
% Crecfac= Maxrec*32110000;

% for the pump
if Wpump>0; Cpump = (1.11E6*Wpump/1000)+0.07E6; else Cpump =
0; end

% to calculate the Total capital costs
capEOR = Cwell+Crecfac+Cpump+Cdisp;

% if calculated based on Heddle et al.
capEOR2 = 232539.09+58816.84+54.38*depth;
```

Appendix VII: Drying

```
% to calculate the time needed to 'dry' the reservoir to the
required purity
% Calculations based on: A. Atrens, H. Curgency en V. Rudolph,
% „Removal of water from a carbon dioxide based EGS system,“
% in Thirty-Sixth Workshop on Geothermal Reservoir Engineering
Stanford University,
% Stanford, 2011.

function [FCO2, dry] = Drying(t,v2,v3,FCO2,CO2inject,T2,dry)
%if nargin<6, Threshold=0.06; end
if nargin<6, T2=t; end

% to calculate the threshold volume fraction for the reservoir
global Par
Lossf = Par(12,1); %fraction stored in reservoir
mir = CO2inject*1000; %mass injection rate at the reservoir
(kg/year)
vir = mir/(v2(3)); %volumetric injection rate at the reservoir
(m^3/year)
densh2o = 1230;%H2Odensity(Par(3,1),Par(2,1)); %density of H2O
at res P and T (kg/m^3)
volR=Par(26,1);

% to calculate the losses from the reservoir
vl = vir*Lossf; % volumetric loss rate
vp = vir*(1-Lossf); % production rate
vm = 0.0*vir; % mixing rate
%calculates the in years necessary to dry the reservoir to
threshold

% to calculate the drainage/imbibition from the reservoir
% FCO2 = (vir/(vm+vir))*(1-exp(-(vir/volR)*t)); %Volume
fraction of the pores occupied by CO2
DvCO2 = vir-FCO2*vl-FCO2*vp-FCO2*vm; % change in CO2 volume in
the reservoir
```

```

%Dvother = vm-(1-FCO2)*vl-(1-FCO2)*vp-(1-FCO2)*vm; %change in
other volume in the reservoir
FCO2 = FCO2+(DvCO2/volR);
mp = FCO2*vp*v3(3); % mass of CO2 kg/year
mwater(t,1) = (1-FCO2)*(1-Par(18,1))*vp*densh2o; % mass other
produced (kg/year)

% to calculate the recycled CO2 from the reservoir
CO2rec = (mp/1000)*0.90; % CO2 recycled in tonne/year with rec
efficiency of 90%
CO2bought2 = mir/1000-CO2rec; % amount of CO2 bought for the
drying phase (tonnes)

mCO2inj = mir*T2; % cumulative mass injected CO2

% to model the drying values
dry(t,1) = t; % volume fraction
dry(t,2) = FCO2; % volume fraction
dry(t,3) = CO2bought2; % amount of CO2 bought for the drying
phase kg/year
dry(t,4) = mwater(t); % amount of water that has to be
disposed off kg/year
dry(t,5) = CO2rec;
dry(t,6) = mCO2inj;

```

Appendix VIII: Downhole (injection well)

```

% function vbottom=downhole(vtop, L, D, mdot, N)
% Both "vtop" and "vbottom" are 8-element vectors (see co2eqofstate for
% definitions).
% Only two elements in vtop need to be specified in calling this function:
% vtop(1) = Pressure, MPa
% vtop(3) = Density, kg/m3
% The other input arguments are
% L = The well depth, m (default=5000 m)
% D = The well diameter, m (default=0.5 m)
% mdot= The mass flow rate, kg/s (default=100 kg/s)
% N = The number of integration elements along the well (default=100)
function [s,Downhole]=downhole(vtop, L, D, mdot, e, N)
% Set the defaults if necessary
if nargin<6, N=100; end
if nargin<5, e=0.0004; end
if nargin<4, mdot=100; end
if nargin<3, D=0.23125; end
if nargin<2, L=5000; end
% Set up the working parameters
dz = L/N;
g = 9.81;
s = vtop;

```

```

%recording vectors
p = zeros(N,1);
V = zeros(N,1);
T = zeros(N,1);
rho = zeros(N,1);
dP1 = zeros(N,1);
dP2 = zeros(N,1);
% Start calculating

% Start integrating
for i=1:N
    V(i)= mdot/(s(3)*pi*D*D/4);    % The velocity (m/s) in this segment
    dP1(i) = s(3)*g*dz/1e6;        % Pressure increment from PE in MPa
    mu = co2visc(s(2),s(3));      % viscosity in this segment
    Re = s(3)*V(i)*D/mu;          % Reynolds number in this segment
    f = (-1.8*log10(6.9/Re+(e/D/3.7)^1.11))^2; %friction factor
    dP2(i) = (f*dz/D*s(3)*V(i)^2/2)/1e6; % Frictional Pressure drop in this segment
    s(1) = s(1)+dP1(i)-dP2(i);
    s(5) = s(5)+g*dz/1000;
    s = co2eqofstate('PH', s);
    p(i)= s(1);
    T(i)= s(2);
    rho(i)=s(3);
%   if Re < 2300
%       Flowtype = 'Laminar';
%   if Re > 2300 && Re < 4000
%       Flowtype = 'Transient';
%   else Flowtype = 'Turbulent';
%   end
% end
    Downhole(i,1) = Re;
    Downhole(i,2) = p(i);
    Downhole(i,3) = T(i);
end

```

Appendix IX: reservoir flow

```

% calculates the flow through the reservoir and the
thermodynamics
% in the different sections of the reservoir

function [v,sweptarea]=reservoir(vbottom, L, height, mdot, N,
K, Tres)

% Set up the working parameters
dx = L/N;
%g = 9.81;

```

```

v    = vbottom;
H    = ones(N,1).*height;
W    = ones(N,1);
p    = zeros(N,1);
dP   = zeros(N,1);
V    = zeros(N,1);
T    = zeros(N,1);
dT   = zeros(N,1);
A    = zeros(N,1);
% x = zeros(N,1);
Cp   = zeros(N,1);
%dT(N/5*3:N/5*4) = (Tres-v(2))/(N/5);
mu   = zeros(N,1);
d    = zeros(N,1);
ent  = zeros(N,1);
% Start integrating
% a = L/2;
b    = L/2;

dT(1:N) = (Tres-v(2))/N;
% % generate non-constant cross-section
W(1) = 0.4*3.14;
for i=2:N/2
%     x(i) = i*L/N-L/2-L/N/2;
%     W(i) = 2*(b^2*(1-(x(i).^2)./(a^2)))^0.5;
    W(i) = W(i-1)+b/(N/2);
end
W(N/2+1) = W(N/2);
for i=N/2+2:N
    W(i) = W(i-1)-b/(N/2);
end

%integrate across reservoir
for i=1:N
%     x(i) = i*L/N-L/2-L/N/2;
    A(i) = H(i).*W(i);
    V(i) = mdot/(v(3).*A(i));           % The velocity (m/s)
in this segment
    mu(i) = co2visc(v(2), v(3));       % calls viscosity
calculation
    %mu(i) = 2.4073082940333514e-5;    % co2 viscosity at 235
degC in kg/m/s
    dP(i) = -V(i)*mu(i)*dx/K/1e6;      % Pressure increment in
MPa
    v(2) = v(2)+dT(i);                 % Temperature (K) in
the next segment
    v(1) = v(1)+dP(i);                 % Pressure in the next
segment, MPa
    v    = co2eqofstate('PTG', v);
    p(i) = v(1);

```

```

T(i)= v(2);
d(i)= v(3);
ent(i)= v(6);
Cp(i)=v(8);
end
sweptarea=sum((A(1:N)*L/N)); %calculates the total swept
area of the reservoir

```

Appendix X: CO₂ viscosity

```

% function vresexit=co2visc(v, L, A, mdot, N)
% CO2 viscosities based on:
% A. Fenghour, A. Wakeham en V. Vesovic, „The viscoscity of
carbon dioxide,“
% Journal of physical and chemical reference data, vol. 27,
nr. 1, pp. 31-44, 1998.

function mu=co2visc(T, d)

escale= 251.196;      % energy scaling factor
Tr=T/escale;        % reduced temperature

%%-----calculation of zero-density viscosity-----
-----%%
%coefficients for calculation of zero-density viscosity
a0=0.235156;
a1=-0.491266;
a2=5.211155e-2;
a3=5.347906e-2;
a4=-1.537102e-2;

%calculation of reduced effective cross-section
G=exp(a0+a1*(log(Tr))+a2*(log(Tr)^2)+a3*(log(Tr)^3)+a4*(log(Tr)
)^4));

eta0=(1.00697*T^0.5)/G;      %zero density viscosity

%%-----calculation of excess viscosity-----
-----%%
%coefficients for calculation of excess viscosity
d11=0.4071119e-2;
d21=0.7198037e-4;
d64=0.2411697e-16;
d81=0.2971072e-22;
d82=-0.1627888e-22;

deta=d11*d+d21*d^2+d64*d^6/Tr^3+d81*d^8+d82*d^8/Tr;
mu=(eta0+deta)/1000000; %outputs viscosity in Pa.s

```

Appendix XI: Uphole (production well)

```

% function vbottom=downhole(vtop, L, D, mdot, N)
% Both "vtop" and "vbottom" are 8-element vectors (see co2eqofstate for
% definitions).
% Only two elements in vtop need to be specified in calling this function:
% vtop(1) = Pressure, MPa
% vtop(3) = Density, kg/m3

function [s,Uphole]=uphole(vbottom, L, D, mdot, e, N)
% Set the defaults if necessary
global Par
if nargin<6, N=100; end % The number of integration elements along the well
(default=100)
if nargin<5, e=0.0004; end
if nargin<4, mdot=Par(1,1)/4; end
if nargin<3, D= Par(14,1); end
if nargin<2, L=Par(9,1); end
% Set up the working parameters
dz = L/N;
g = 9.81;
s = vbottom;

%recording vectors
p = zeros(N,1);
V = zeros(N,1);
T = zeros(N,1);
rho = zeros(N,1);
dP1 = zeros(N,1);
dP2 = zeros(N,1);
% Start calculating

% Start integrating
for i=1:N
    V(i)= mdot/(s(3)*pi*D*D/4); % The velocity (m/s) in this segment
    dP1(i) = s(3)*g*dz/1e6; % Pressure increment from PE in MPa
    mu = co2visc(s(2),s(3)); % viscosity in this segment
    Re = s(3)*V(i)*D/mu; % Reynolds number in this segment
    f = (-1.8*log10(6.9/Re+(e/D/3.7)^1.11))^-2; %friction factor
    dP2(i) = (f*dz/D*s(3)*V(i)^2/2)/1e6; % Frictional Pressure drop in this segment
    s(1) = s(1)-dP1(i)-dP2(i);
    s(5) = s(5)-g*dz/1000;
    s = co2eqofstate('PH', s);
    p(i)= s(1);
    T(i)= s(2);
    rho(i)=s(3);
    if p(i)<6.4
        fprintf(1, 'PRESSURES TOO LOW\n');
    end
end

```

```

% if Re < 2300
%   Flow = 'Laminar';
%   if Re > 2300 && Re < 4000
%     Flow = 'Transient';
%   else Flow = 'Turbulent';
%   end
% end
% end
Uphole(i,1) = Re;
Uphole(i,2) = p(i);
Uphole(i,3) = T(i);

```

end

Appendix XII: CO₂ turbine

```

% To calculate the efficiency and output of a turbine from the
reservoir conditions
% based on: A. Athrens, H. Curgency en V. Rudolph, „Exergy
analysis of a CO2 thermosiphon,“
% in Thirty-Fourth Workshop on Geothermal Reservoir
Engineering Stanford University ,
% Stanford, 2009.

```

```

function [Power,CO2bought3] = co2turbine(v,vin)
% cycle_option = 'supercritical-loop';
global Par
mdotg = Par(1,1); %100*3.05;
effturb = 0.85; % isentropic efficiency of the turbine
effpump = 0.90; % isentropic efficiency of the pump
Lossf = Par(12,1);
CO2bought3=mdotg*Lossf; % to compensate for the stored CO2
in the reservoir

% Calculate the cycle efficiency for a direct system
qh = (v(4,5)-v(2,5));
%qc = v(6,2)*(v(6,6)-v(1,6))+(v(5,6)-
v(6,6))*(v(5,2)+v(6,2))/2;
wt = (v(4,5)-v(5,5))*mdotg*effturb; % Turbine work = h4-h5
QT = (v(3,5)-v(2,5))*mdotg; %total heat flux from reservoir
Ptarg = v(3,1);
Pinit = v(1,1);

if(v(1,5)-vin(5))*CO2bought3 > 0
    wp1 = (v(1,5)-vin(5))*CO2bought3; % Pump work for new CO2
else wp1 = 0;
end
wp2 = 0; % pump work for recycled CO2
wp = (wp1+wp2)/effpump; % total pump work parasitic load
wh = 0.0189*(v(5,5)-v(6,5))*mdotg; % work delivered by forced
air heat exchanger

```

```

% % To calculate the efficiency of a binary system
% based on B. M. Adams, T. H. Kuehn, J. M. Bielick, J. B.
Randolph en M. O. Saar,
% „On the importance of the thermosiphon effect in CPG (CO2
plume geothermal) power systems,“
% Energy, vol. 69, pp. 409 - 418, 2014.

Binary_eff=0.5; % binary system efficiency
carnot_eff=(1-v(1,2)/v(5,2)); %calculates the carnot
efficiency
Pbin=Par(1,1)*Binary_eff*carnot_eff*(v(5,5)-v(6,5)); % power
from a binary system
Pout = (wt-wp-wh); % output power of the turbine
eff= (Pout+Pbin)/QT*100; % efficiency of the CPG system
Power = [eff, wt, Pout, QT, qh, Ptarg, Pinit, Pbin];
%generates a vector of outputs

```

Appendix XIII: Hemholz free energy CO₂ Equation of state

```

% Calculates the thermodynamic properties of CO2 at the
various stages of
% the system from some properties in input vector (v).
% from: R. Span and W. Wagner, "A new equation of state for
carbon dioxide
% covering the fluid region from the Triple-point Temperature
to 1100 K at pressures up to 800 Mpa,"
% Journal of physical and chemical reference data,
% vol. 25, no. 6, pp. 1509-1590, 1996. vR.

% v(1) = Pressure, MPa
% v(2) = Temperature, K
% v(3) = Density, kg/m3
% v(4) = Internal energy, kJ/kg
% v(5) = Enthalpy, kJ/kg
% v(6) = Entropy, kJ/(kg-K)
% v(7) = Constant-volume specific heat, kJ/(kg-k)
% v(8) = Constant-property specific heat, kJ/(kg-k)

function v=co2eqofstate(mode, v0, debugging)
global pt Tt pc Tc dc
if nargin<3, debugging=0; end
pt = 0.51795; % Triple-point pressure, MPa
Tt = 216.592; % Triple-point, oK
Tc = 304.1282; % Critical point oK
pc = 7.3773; % Critical point MPa
dc = 467.6; % Critical point kg/m3
R = 0.1889241; % Ideal gas constant for CO2 kJ/kg-oK
v = zeros(1,7);
mode = upper(mode);
switch(mode)

```

```

case 'TD'
    T = v0(2);
    d = v0(3);
    v(2) = T;
    v(3) = d;
    tau = Tc/T;
    delta=d/dc;
    % First check if it is saturated or not
    if (T<Tc)
        df = co2prop('DL', T);
        dg = co2prop('DV', T);
    end
    if (T<Tc && d<df && d>dg) % if it is a saturated
mixture
        x = (df-d)/(df-dg)*dg/d; % Quality
        vf = co2eqofstate(mode, [0 T df+0.001]);
        vg = co2eqofstate(mode, [0 T dg-0.001]);
        v(1) = (vf(1)+vg(1))/2;
        for i=4:8
            v(i) = vf(i)+x*(vg(i)-vf(i));
        end
        fprintf(1, 'Saturated Mixture\n');
    else
        phi0=co2prop('phi0', T, d);
        phir=co2prop('phir', T, d);
        v(1)=(1+delta*phir(2))*d*R*T/1000;
        v(4)=R*T*tau*(phi0(3)+phir(3));
        v(5)=R*T*(1+tau*(phi0(3)+phir(3))+delta*phir(2));
        v(6)=R*( tau*(phi0(3)+phir(3)) - phi0(1) -
phir(1) );
        v(7)=-R*tau^2*(phi0(5)+phir(5));
        v(8)=R*(-tau*tau*(phi0(5)+phir(5)) ...
            +(1+delta*phir(2)-delta*tau*phir(6))^2 ...
            /(1+2*delta*phir(2)+delta*delta*phir(4)));
    end
case 'PH' % Find the rest of the state given (p,h)
    x0 = v0(2:3);
    p = v0(1);
    h = v0(5);
    x = fminsearch(@(x) ph_error(x, p, h), x0, ...
        optimset('Display', 'off', 'MaxFunEvals', 500));
    %fprintf(1, 'Final P-h Error = %.6g\n',
ph_error(x,p,h));
    v = v0;
    v(2) = x(1);
    v(3) = x(2);
    v = co2eqofstate('TD', v);
case 'PS' % Find the rest of the state given (p,s)
    x0 = v0(2:3);
    p = v0(1);
    s = v0(6);

```

```

x = fminsearch(@(x) ps_error(x, p, s, debugging), x0,
...
    optimset('Display', 'off', 'MaxFunEvals', 500));
v = v0;
v(2) = x(1);
v(3) = x(2);
v = co2eqofstate('TD', v);

case 'PTL' % Find the rest given (p,T) for compressed
liquid
p = v0(1);
T = v0(2);
x1 = co2prop('DL', T)+1;
x2 = 10*x1;
x = fminbnd(@(x) PTL_error(x, p, T, debugging),
x1,x2, ...
    optimset('Display', 'off', 'MaxFunEvals', 500));
v = v0;
v(3) = x;
v = co2eqofstate('TD',v);
case 'PTG' % Find the rest given (p,T) for
superheated/supercritical
p = v0(1);
T = v0(2);
if (T<Tc)
x2 = co2prop('DV', T);
x1 = x2/20;
else
x1 = 1;
x2 = 1500;
end
x = fminbnd(@(x) PTL_error(x, p, T, debugging),
x1,x2, ...
    optimset('Display', 'off', 'MaxFunEvals', 500));
v = v0;
v(3) = x;
v = co2eqofstate('TD',v);
case 'PSATG' % Find the rest given (p) for saturated
vapour
p = v0(1);
x1 = 200;
x2 = Tc;
x = fminbnd(@(x) PSATG_error(x, p), x1,x2, ...
    optimset('Display', 'off', 'MaxFunEvals',
500));
v = v0;
v(2)= x;
v(3)= co2prop('DV', x);
v = co2eqofstate('TD',v);
case 'PSATF' % Find the rest given (p) for saturated
liquid

```

The joint potential of CO₂-EOR with CPG| By Roland Vernooij

```

p    = v0(1);
x1   = 200;
x2   = Tc;
x    = fminbnd(@(x) PSATG_error(x, p), x1,x2, ...
              optimset('Display', 'off', 'MaxFunEvals',
500));
v    = v0;
v(2) = x;
v(3) = co2prop('DL', x);
v    = co2eqofstate('TD',v);
end

% x(1) and x(2) : Temperature and density that need to be
determined to
% minimise the value of this function
% p, h      : The pressure and enthalpy that are known
function retval=ph_error(x, p, h)
hx=co2prop('H', x(1), x(2));
px=co2prop('P', x(1), x(2));
retval = (p-px)^2+(h-hx)^2;
fprintf('(%1f %2f)-> (%1f %2f)\n', x(1), x(2), px, hx);

% x : The density to be determined to minimise the value of
this function
% p, T      : The given pressure and temperature
function retval=PTL_error(x, p, T,debugging)
px=co2prop('P', T, x);
retval = (p-px)^2;
if debugging
    fprintf('PTL_error(%1f, %1f, %1f)-> px=%1f and
retval=%5f\n', ...
        x, p, T, px, retval);
end

% x(1) and x(2) : Temperature and density that need to be
determined to
% minimise the value of this function
% p, s      : The pressure and entropy that are known
function retval=ps_error(x, p, s, debugging)
sx=co2prop('S', x(1), x(2));
px=co2prop('P', x(1), x(2));
retval = (p-px)^2+(s-sx)^2;
if debugging
    fprintf('Ps_error - (%1f %2f)-> (%1f %2f) and
error=%5g\n', ...
        x(1), x(2), px, sx, retval);
end

% x : The temperature to be determined
% p : The given pressure for the saturated vapour
function retval=PSATG_error(x, p)

```

```
px=co2prop('PV', x);
retval = (p-px)^2;
fprintf('(%0.1f)-> (%0.1f) = %0.5f\n', x, px, retval);
```

Appendix XIV: Capital costs of the CPG system

```
% this function serves to calculate the costs of the CPG
system
% Based on A. D. Atrens, H. Curgenci en V. Rudolph,
% „Economic analysis of a CO2 thermosiphon,“
% in World Geothermal Congress , Bali, 2010.

function [capitalCPG,Cturbine,piping, Cheatex, Fp, Qheatex] =
capitalcosts(v,wt)
global Par
mdotg = Par(1,1);

% to calculate the costs of the turbine
alpha = 1.066;
beta = 0.5439;
gamma = -0.1472;
Cturbine = alpha*(wt^beta)*(v(5,3)^gamma)*1000000;

% % to calculate the size of the heat exchanger
U = 10; % the overall heat transfer coefficient in W/m2K
Qheatex = mdotg*((v(5,5)-v(6,5))+(1-0.85)*v(4,5)-v(5,5));
areahx = Qheatex/(U*10^(v(5,2)-v(6,2)));

% to calculate the costs of the heat exchanger
K1 = 4.0336;
K2 = 0.2341;
K3 = 0.0497;
Cp = 10^(K1+K2*areahx+K3*(areahx)^2);% for making the heatex
in carbon steel
C1 = -0.1250;
C2 = 0.15361;
C3 = -0.02861;
Fp = 10^(C1+C2*(v(6,1))+C3*(v(6,1))^2);
B1 = 0.96;
B2 = 1.21;
Fm = 2.9;
Cheatex = (B1+B2*Fm*Fp)*Cp;

% to calculate the Total capital costs
lambda = 1.4; % 2.4 % factor to take into account additional
piping etc.
piping = (lambda*Cturbine)-Cturbine; % Costs of dditional
piping and facility
capitalCPG = Cheatex+Cturbine+piping;%+Cwell;
```

Appendix XV: LCE CO₂ plume geothermal

```

function
[LCECPGdry,LCECPG,Cdry,CPGOPEX,CPGOPEX2]=LCEgeothermal(T2,capitalCPG,CO2bought3,PCO2,dry,Pdisp,Prec,generation,oildry,capEOR)

Lifetime = 25;
n = Lifetime;
exp = zeros(Lifetime,1);
r = 0.05; % discount rate
Poil = 60;
% operatinject = 12;% operational costs for co2 compression
and injection ($/tCO2 injected)
% operatrec = 0; %7.15;% operational costs for co2 recycling
($/tCO2 recycled)
% operatoil = 16.65; % operational costs for oil treatment
($/BBL produced)

for t=1:T2
%if round(t/365)<8; A = round(t/365); else A = 8; end
OPEXdry(t) = 13930185.60;
Cdry(t,1) = (dry(t,4)*Pdisp+(dry(t,3)*PCO2(12+t)))+OPEXdry(t)-
oildry(t)*Poil/(1+r)^t;
end

Cdry = sum(Cdry);
investment = (capitalCPG+Cdry)*0.9;
for t= 1:n
OPEX(t) = (0.9*capitalCPG*0.05-((generation(t,1)/1000)*21.5));
OPEX2(t) = (0.01*generation(t,1)*8766)*1.01^t;
CCO2(t) = CO2bought3*PCO2(20);
exp(t) = (OPEX2(t)+ CCO2(t))/((1+r)^(t+T2));
pro(t) = (0.9*(generation(t,1)*8766))/((1+r)^(t+T2));
end

Totexp = investment+sum(exp);
Totpro = sum(pro);
LCECPGdry = Totexp/Totpro;

investment = capitalCPG;
for t= 1:n
OPEX(t) = capitalCPG*0.05;
OPEX2(t) = (0.01*generation(t,1)*8766)*1.01^t;
CCO2(t) = CO2bought3*PCO2(20);
exp(t) = (OPEX2(t)+ CCO2(t))/((1+r)^(t));
pro(t) = 0.9*(generation(t,1)*8766)/((1+r)^(t));
end
Totexp = investment+sum(exp);
Totpro = sum(pro);
LCECPG = Totexp/Totpro;

```

```
CPGOPEX = sum(OPEX);
CPGOPEX2 = sum(OPEX2);
```

Appendix XVI: LCE CO₂-EOR

```
% Calculates the levelised costs of oil production
```

```
function
```

```
[LCEEOR, costsCO2EOR, costsdisp, LCEEOR2]=LCEeor(T1, OPEXeor, capit
alEOR, PCO2, Prec, Pdisp, EOR, capEOR2)
investment = capitaleOR;
r = 0.05; % discount rate
```

```
for t= 1:T1
```

```
CCO2(t) = ((EOR(t,11)-EOR(t,3))*PCO2(t)+EOR(t,3)*Prec);
exp(t) = (OPEXeor(t) + CCO2(t))+EOR(t,6)*Pdisp/((1+r)^t);
pro(t) = (EOR(t,5)*0.775)/((1+r)^t);
wd(t,1) = EOR(t,6)*Pdisp/((1+r)^t);
```

```
end
```

```
Totexp = investment+sum(exp);
Totpro = sum(pro);
LCEEOR = Totexp/Totpro;
costsCO2EOR=sum(CCO2);
costsdisp=sum(wd);
```

```
% to calculate the costs for oil production based on heddle et
al.
```

```
OPEX = 13930185.60;
```

```
for t= 1:T1
```

```
CCO2(t) = ((EOR(t,11)-EOR(t,3))*PCO2(t)+EOR(t,3)*Prec);
exp(t) = (OPEX + CCO2(t))/((1+r)^t);
pro(t) = ((EOR(t,5))*0.775)/((1+r)^t);
```

```
end
```

```
Totexp = capEOR2+sum(exp);
Totpro = sum(pro);
LCEEOR2 = Totexp/Totpro;
costsCO2EOR=sum(CCO2);
```

Appendix XVII: Injectivity reduction through salt precipitation

```
% Injectivity decline due to salt precipitation
% Based on: M. Burton, N. Kumar en S. Bryant,
% Time-Dependent Injectivity During CO2 Storage in Aquifers
% The University of Texas, Austin, 2008.
```

```
function [dpdry1, qinj, k1, rdry1]= injectivity(v, T2)
```

```
global Par
```

```
rw= Par(13,1)/2; % wellbore radius [m]
```

```

k01=Par(8,1);
por0_1=0.1;

muw=1*10^-3; %viscosity water [pa s]
h= Par(11,1); % height reservoir [m]
df_dS=0.3; % defined with welge construction from curve.
sal=Par(25,1); % salinity [ppm]
rhob_salt=2170; % density salt [kg/m3]
rhob_sol=1230 ; % density solution [kg/m3]
rhob_gas=v(2,3); % density CO2 [kg/m3]
mug=co2visc(v(3,2),v(2,3)); % viscosity [Pa s]
Vfsalt=(sal*rhob_sol)/(10^6*rhob_salt) ;
qinj= (Par(1,1)/rhob_gas)*86400; % Injection rate m3/day
t=linspace(1,T2,T2);

krl=0.85;

fg=(muw*krl)/(krl*muw+(1-krl)*mug);
df=1.2-fg; % welge construction
por1=0.095; % Por0=10%

Sgdry1=((por1-por0_1)/(por0_1*Vfsalt))+1;
df_dS1=df/(1-Sgdry1);
k1=k01*((por1/por0_1)^3)*((1-por0_1)/(1-por1))^2;

for i=1:T2;
rdry1(i)=sqrt(qinj/(por1*pi()*h)*df_dS1*t(i)+(rw^2));
SF1(i)=(k01/k1-1)*log(rdry1(i)/rw);
dpdry1(i)=(qinj*mug)/(2*pi()*h*(k1^2/k01))*(log(rdry1(i)/rw)*S
F1(i));
end

```

Appendix XIIX: Properties of CO₂

% CO2 properties based on
 % R.Span and W Wagner, J.Phys.Chem.Ref.Data, 25(6), 1509-1596 (1996)

```

function xx=co2prop(mode, T, d)
global pt Tt pc Tc dc
pt = 0.51795; % Triple-point pressure, MPa
Tt = 216.592; % Triple-point, oK
Tc = 304.1282; % Critical point oK
pc = 7.3773; % Critical point MPa
dc = 467.6; % Critical point kg/m3
R = 0.1889241; % Ideal gas constant for CO2 kJ/kg-oK
tau = Tc/T;
if nargin>2, delta=d/dc; end
mode = upper(mode);
switch(mode)

```

```

case 'DL' % Saturated liquid density at T
    xx=liquid_density(T);
case 'DV' % Saturated vapour density at T
    xx=vapour_density(T);
case 'P' % The pressure at (T,d)
    phir=he_residual(tau, delta);
    xx = (1+delta*phir(2))*d*R*T; % This will in kPa
    xx = xx/1000; % Convert to MPa
case 'S' % Entropy at (T,d)
    phi0=he_idealgas(tau, delta);
    phir=he_residual(tau, delta);
    xx = R*( tau*(phi0(3)+phir(3)) - phi0(1) - phir(1) );
%    xx = tau*((phi0(3)+phir(3))-phi0(1)-phir(1))*R;
case 'U' % Internal Energy at (T,d)
    phi0=he_idealgas(tau, delta);
    phir=he_residual(tau, delta);
    xx = R*T*tau*(phi0(3)+phir(3));
case 'H' % Enthalpy at (T,d)
    phi0=he_idealgas(tau, delta);
    phir=he_residual(tau, delta);
    xx = R*T*(1+tau*(phi0(3)+phir(3))+delta*phir(2));
case 'PM' % Melting pressure at T
    xx=melting_pressure(T);
case 'PS' % Sublimation pressure at T
    xx=sublim_pressure(T);
case 'PV' % Vapour pressure at T
    xx=vapour_pressure(T);
case 'PHI0'
    xx=he_idealgas(tau, delta);
case 'PHIR'
    xx=he_residual(tau, delta);
case 'TRIPLEPOINT'
    figure(1); clf;
    T=Tt:0.01:Tt+2; pm=melting_pressure(T);
    plot(T,pm, 'k', 'LineWidth', 2);
    hold on;
    T=180:0.01:Tt; ps=sublim_pressure(T);
    plot(T, ps, 'b', 'LineWidth', 2);
    T=Tt:0.01:Tc; pv=vapour_pressure(T);
    plot(T, pv, 'r', 'LineWidth', 2);
    axis([210 310 0 12]);
    xx=1;
end
end

function pm=melting_pressure(T)
global pt Tt
x = T/Tt-1;
if (x<0), pm = -1;

```

```
else    pm = pt*(1+1955.5390*x+2055.4593*x.*x);
end
end
```

```
function ps=sublim_pressure(T)
global pt Tt
x = 1-T/Tt;
a1 = -14.740846;
a2 = 2.4327015;
a3 = -5.3061778;
if (x<0), ps=-1;
else
    z = (Tt./T).*(a1*x+a2*x.^1.9+a3*x.^2.9);
    ps=pt*exp(z);
end
end
```

```
function pv=vapour_pressure(T)
global pc Tc
x=1-T/Tc;
a=[-7.0602087; 1.9391218; -1.6463597; -3.2995634];
t=[1; 1.5; 2; 4];
if T>Tc, pv=-1;
else
    z=zeros(size(T));
for k=1:4
    z=z+a(k)*x.^t(k);
end
pv = pc*exp((Tc./T).*z);
end
end
```

% Saturated liquid density

```
function dl=liquid_density(T)
global dc Tc
z = zeros(size(T));
x = 1-T/Tc;
a = [1.9245108; -0.62385555; -0.32731127; 0.39245142];
t = [0.34; 0.5; 10/6; 11/6];
for k=1:4
    z=z+a(k)*x.^t(k);
end
dl = dc*exp(z);
end
```

% Saturated vapour density

```
function dv=vapour_density(T, d)
global dc Tc
z = zeros(size(T));
```

```

x = 1-T/Tc;
a = [-1.7074879; -0.82274670; -4.6008549; -10.111178; -29.742252];
t = [0.340; 0.5; 1; 7/3; 14/3];
for k=1:5
    z=z+a(k)*x.^t(k);
end
dv = dc*exp(z);
end

% The ideal gas part of the dimensionless Helmholtz Energy (Fo)
% Section 6.1 Span & Wagner
% The returned variable is a vector:
% phi0(1) = Fo
% phi0(2) = Fo_delta
% phi0(3) = Fo_tau
% phi0(4) = F0_delta+delta
% phi0(5) = F0_tau+tau
% phi0(6) = F0_delta_tau
function phi0 = he_idealgas(tau, delta)
a    = [8.37304456; -3.70454304; 2.50000000; 1.99427042; ...
        0.62105248; 0.41195293; 1.04028922; 0.08327678]; %checked
teta = [0;      0;      0;      3.15163;...
        6.11190; 6.77708; 11.32384; 27.08792]; %checked
phi0(1) = log(delta) + a(1) + a(2)*tau + a(3)*log(tau); %Fo
phi0(2) = 1/delta; % Fo_delta
phi0(3) = a(2) + a(3)/tau;
phi0(4) = -1/delta/delta;
phi0(5) = -a(3)/tau/tau;
phi0(6) = 0;
for i=4:8
    ett = exp(-tau*teta(i));
    z = 1-ett;
    phi0(1) = phi0(1) + a(i)*log(z); % Fo
    phi0(3) = phi0(3) + a(i)*teta(i)*(1/z-1); % Fo_tau
    phi0(5) = phi0(5) - a(i)*teta(i)^2*ett*z^(-2);
end
end

% The residual part of the dimensionless Helmholtz Energy (Fr)
% Table 32. Span & Wagner
% The returned variable is a vector:
% phir(1) = Fr
% phir(2) = Fr_delta
% phir(3) = Fr_tau
% phir(4) = Fr_delta+delta
% phir(5) = Fr_tau+tau
% phir(6) = Fr_delta_tau
function phir = he_residual(tau, delta)

```

```

n = [ 0.38856823203161; 2.9385475942740; -5.5867188534934;...
      -0.76753199592477; 0.31729005580416; 0.54803315897767;...
      0.12279411220335; 2.1658961543220; 1.5841735109724;...
      -0.23132705405503; 0.058116916431436; -0.55369137205382;...
      0.48946615909422; -0.024275739843501; 0.062494790501678;...
      -0.12175860225246; -0.37055685270086; -0.016775879700426;...
      -0.11960736637987; -0.045619362508778; 0.035612789270346;...
      -0.0074427727132052; -0.0017395704902432;-0.021810121289527;...
      0.024332166559236; -0.037440133423463; 0.14338715756878;...
      -0.13491969083286; -0.023151225053480; 0.012363125492901;...
      0.0021058321972940;-0.00033958519026368; 0.0055993651771592;...
      -0.00030335118055646; -213.65488688320; 26641.569149272;...
      -24027.212204557; -283.41603423999; 212.47284400179;...
      -0.66642276540751; 0.72608632349897; 0.055068668612842]; %checked
%
d = [1; 1; 1; 1; 2; 2; 3; ...
     1; 2; 4; 5; 5; 5; 6; 6; 6; 1; 1; 4; 4; 4; 7; 8; ...
     2; 3; 3; 5; 5; 6; 7; 8; 10; 4; 8; ...
     2; 2; 2; 3; 3]; %checked
%
t = [0; 0.75; 1; 2; 0.75; 2; 0.75; ...
     1.5; 1.5; 2.5; 0; 1.5; 2; 0; 1; 2; 3; 6; 3; 6; 8; ...
     6; 0; 7; 12; 16; 22; 24; 16; 24; 8; 2; 28; 14; ...
     1; 0; 1; 3; 3]; %checked
%
c = zeros(34,1);
c(8:34) = [1; 1; 1; 1; 1; 1; 1; 1; 2; 2; 2; 2; 2; 2; 3; 3; 3; ...
           4; 4; 4; 4; 4; 4; 5; 6];
%
alfa = zeros(39,1);
alfa(35:39) = [25; 25; 25; 15; 20];
%
beta = zeros(42,1);
beta(35:42) = [325; 300; 300; 275; 275; 0.3; 0.3; 0.3];
%
gama = zeros(39,1);
gama(35:39) = [1.16; 1.19; 1.19; 1.25; 1.22];
%
eps = zeros(39,1);
eps(35:39) = [1; 1; 1; 1; 1];
%
a = zeros(42,1);
a(40:42) = [3.5; 3.5; 3];
b = zeros(42,1);
b(40:42) = [0.875; 0.925; 0.875];
A = zeros(42,1);
A(40:42) = [0.7; 0.7; 0.7];
B = zeros(42,1);
B(40:42) = [0.3; 0.3; 1.0];

```

```

C = zeros(42,1);
C(40:42)= [10; 10; 12.5];
D = zeros(42,1);
D(40:42)= [275; 275; 275];
%
phir=zeros(1, 6);
for i= 1: 7
    ddi = delta^d(i);
    tti = tau^t(i);
    phir(1) = phir(1) + n(i)*(ddi)*(tti);
    phir(2) = phir(2) + n(i)*d(i)*delta^(d(i)-1)*tti;
    phir(3) = phir(3) + n(i)*t(i)*ddi*tau^(t(i)-1);
    phir(4) = phir(4) + n(i)*d(i)*(d(i)-1)*delta^(d(i)-2)*tti;
    phir(5) = phir(5) + n(i)*t(i)*(t(i)-1)*ddi*tau^(t(i)-2);
    phir(6) = phir(6) + n(i)*d(i)*t(i)*delta^(d(i)-1)*tau^(t(i)-1);
end

for i= 8:34
    ddi = delta^d(i);
    dci = delta^c(i);
    edci= exp(-dci);
    tti = tau^t(i);
    phir(1)=phir(1) + n(i)*(ddi)*(tti)*edci;
    phir(2)=phir(2) + n(i)*edci*(delta^(d(i)-1)*tti*(d(i)-c(i)*dci));
    phir(3)=phir(3) + n(i)*t(i)*ddi*tau^(t(i)-1)*edci;
    phir(4)=phir(4)+n(i)*edci*(delta^(d(i)-2)*tti*((d(i)-c(i)*dci)*...
        (d(i)-1-c(i)*dci)-c(i)^2*dci));
    phir(5)=phir(5)+n(i)*t(i)*(t(i)-1)*ddi*tau^(t(i)-2)*edci;
    phir(6)=phir(6)+n(i)*edci*delta^(d(i)-1)*t(i)*tau^(t(i)-1)...
        *(d(i)-c(i)*dci);
end

for i=35:39
    ddi = delta^d(i);
    tti = tau^t(i);
    de2 = (delta-eps(i))^2;
    ea = exp(-alfa(i)*de2-beta(i)*(tau-gama(i))^2);
    phir(1)=phir(1) + n(i)*(ddi)*(tti)*ea;
    phir(2)=phir(2)+n(i)*ddi*tti*ea*(d(i)/delta-2*alfa(i)*(delta-eps(i)));
    phir(3)=phir(3)+n(i)*ddi*tti*ea*(t(i)/tau -2*beta(i)*(tau-gama(i)));
    phir(4)=phir(4)+n(i)*tti*ea*(-2*alfa(i)*ddi+4*alfa(i)^2*ddi*de2...
        -4*d(i)*alfa(i)*delta^(d(i)-1)*(delta-eps(i))...
        +d(i)*(d(i)-1)*delta^(d(i)-2));
    phir(5)=phir(5)+n(i)*ddi*tti*ea*...
        ((t(i)/tau-2*beta(i)*(tau-gama(i)))^2-t(i)/tau/tau-2*beta(i));
    phir(6)=phir(6)+n(i)*ddi*tti*ea*...
        (d(i)/delta-2*alfa(i)*(delta-eps(i)))*(t(i)/tau-2*beta(i)*(tau-gama(i)));
end

```

```

for i=40:42
    teta = (1-tau)+A(i)*(((delta-1)^2)^(1/2/beta(i))); %checked
    ksi = exp(-C(i)*((delta-1)^2)-D(i)*((tau-1)^2)); %checked
    DELTA= teta^2 + B(i)*(((delta-1)^2)^a(i)); %checked
    Dbi = DELTA^b(i);
    Dbim1= DELTA^(b(i)-1);
    Dbim2= DELTA^(b(i)-2);
    Dm1bm1 = ((delta-1)^2)^(1/2/beta(i)-1);
    dKSId = -2*C(i)*(delta-1)*ksi; % del KSI/ del delta

    phir(1) = phir(1) + n(i)*(Dbi)*delta*ksi;

    dDELTAAd = (delta-1)*(A(i)*teta*2/beta(i)*...
    (Dm1bm1+2*B(i)*a(i)*((delta-1)^2)^(a(i)-1)));
    dDELTAAbd = b(i)*Dbim1*dDELTAAd; % del DELTA^bi/del delta

%   phir(2)=phir(2)+n(i)*(Dbi*(ksi+delta*(-2*C(i)*(delta-1)*ksi)...
%       +dDELTAAbd*delta*ksi)); %25/12/2007
    phir(2)=phir(2)+n(i)*(Dbi*(ksi+delta*dKSId)+dDELTAAbd*delta*ksi);
    dDELTAAbt = -2*teta*b(i)*Dbim1; % del DELTA^bi/del tau
    dKSIt = -2*D(i)*(tau-1)*ksi; % del KSI/del tau
    phir(3)=phir(3)+n(i)*delta*(dDELTAAbt*ksi+Dbi*dKSIt);
%
    d2KSId= (-2*C(i)*(delta-1)^2-1)*2*C(i)*ksi; % del^2 KSI/del delta^2
    d2KSIt= (2*D(i)*(tau-1)^2-1)*2*D(i)*ksi; % del^2 KSI/del tau^2
    d2KSIdt=4*C(i)*D(i)*(delta-1)*(tau-1)*ksi; % del^2 KSI/deldelta+deltau
    d2DELTAAd= 1/(delta-1)*dDELTAAd+(delta-1)^2*...
    ( 4*B(i)*a(i)*(a(i)-1)*((delta-1)^2)^(a(i)-2)...
    +2*A(i)^2*(1/beta(i))^2*(Dm1bm1)^2 ...
    +A(i)*teta*4/beta(i)*(1/2/beta(i)-1)*...
    ((delta-1)^2)^(1/2/beta(i)-2)); % del^2DELTA/del delta^2
    d2DELTAAbd = b(i)*(Dbim1*d2DELTAAd+(b(i)-1)*Dbim2*dDELTAAd^2);
    % del^2 DELTA^bi / del delta^2
    d2DELTAAbt = 2*b(i)*Dbim1+4*teta^2*b(i)*(b(i)-1)*Dbim2;
    % del^2DELTA^bi / del tau^2
    d2DELTAAbdt= -A(i)*b(i)*2/beta(i)*Dbim1*(delta-1)*Dm1bm1...
    -2*teta*b(i)*(b(i)-1)*Dbim2*dDELTAAd;
    % del^2DELTA^bi / del_delta del_tau
    phir(4)=phir(4)+n(i)*( Dbi*(2*dKSId+delta*d2KSId)...
    +2*dDELTAAbd*(ksi+delta*dKSId)...
    +d2DELTAAbd*delta*ksi);
    phir(5)=phir(5)+n(i)*delta*(d2DELTAAbt*ksi+2*dDELTAAbt*dKSIt+Dbi*d2KSIt);
    phir(6)=phir(6)+n(i)*(Dbi*(dKSIt+delta*d2KSIdt)...
    +delta*dDELTAAbd*dKSIt...
    +dDELTAAbt*(ksi+delta*dKSId)...
    +d2DELTAAbdt*delta*ksi);

end
end

```